TAMPEREEN TEKNILLINEN YLIOPISTO
TAMPERE UNIVERSITY OF TECHNOLOGY

Karol Bzdawka

Optimization of Office Building Frame with Semi-Rigid Joints in Normal and Fire Conditions

Julkaisu 1038 • Publication 1038

Tampere 2012

Tampereen teknillinen yliopisto. Julkaisu 1038
Tampere University of Technology. Publication 1038

Karol Bzdawka

Optimization of Office Building Frame with Semi-Rigid Joints in Normal and Fire Conditions

Thesis for the degree of Doctor of Science in Technology to be presented with due permission for public examination and criticism in Rakennustalo Building, Auditorium RN201, at Tampere University of Technology, on the 26th of April 2012, at 12 noon.

Tampereen teknillinen yliopisto - Tampere University of Technology
Tampere 2012

ISBN 978-952-15-2808-8 (printed)
ISBN 978-952-15-2812-5 (PDF)
ISSN 1459-2045

ABSTRACT

There are many framing systems for buildings. This thesis considers one particularly popular system for office buildings in the Nordic countries. The frame consists of welded steel box beams (WQ-beams) and composite square concrete-filled hollow section columns (CFHS). The frame is non-sway – in the horizontal direction it is supported by lift shafts, staircases or shear walls. In this thesis, only the vertical load bearing system is considered. The only imposed load is the live load for office buildings – 3.0 kN/m^2. The live load is transferred to the beams via hollow core (HC) slabs. The optimization of a structure consisting of the three elements: slabs, beams and columns is the subject of this thesis.

Several different layouts of the structure are optimized using Particle Swarm Optimization (PSO). The objective function of the optimization is the structure cost. The cost is calculated based on data available in the literature.

The investigated structures differ in static layouts, dimensions and dimension proportions and complexity. The variables of the optimization are the cross-sections of the members. The semi-rigid joints are assumed in order to investigate the influence of joint rigidity on the optimum solution. The joint stiffness is either fixed or variable in the optimization. The joint design is not part of this thesis so the true rotational stiffness of the joint is not used but rather its proportion to the beam bending stiffness.

The feasibility of each solution is verified following Eurocodes (with Finnish national annexes) and Eurocode-based Finnish guidelines for structural design. The requirements of ULS are verified in both normal and fire-design situations. The beams and joints are insulated from fire conditions so that the beam resistance and stiffness do not change because of temperature increase.

The data obtained from the optimization is presented and analysed. It was found that due to their high cost, the HC slabs determine the building's shape. The relatively low cost CFHS columns have considerable reserve of capacity in ambient conditions allowing the use of semi-rigid joints. A semi-rigid beam-column joint reduces the sagging moment in the beam and increases the moment in the column. However, the column cross-section does not get much bigger since the moment increase in a fire situation is low due to the low column stiffness. The use of semi-rigid joints reduces the structure cost by ~10 % and the frame cost by ~20 %. The use of semi-rigid joints is recommended.

The thesis proposes modifications to the current frame solution and indicates the direction for future studies.

The PSO algorithm is found to be suitable for these kinds of problems due to its ease of use and good convergence towards the minimum.

PREFACE

The research presented in this thesis was performed in 2009-2011 in the Department of Built Environment. I would like to thank all the employees of Tampere University of Technology for the pleasant working atmosphere and their help.

My greatest gratitude goes to my mentor professor Markku Heinisuo. His guidance and enthusiasm are invaluable. Every single discussion that we had was very fruitful and gave me better understanding of steel structures.

The reviewers of the thesis professor Kuldeep Virdi and Jussi Jalkanen are acknowledged for their valuable comments which helped improving this manuscript.

The financial support was one of the most crucial components that allowed this research to be carried out. I wish to take the opportunity to thank the three contributors: Rautaruukki Corporation, HAMK University of Applied Science and Hämeenlinnan Kaupunki for financing my studies.

The whole team of Sheet Metal Development Centre where most of the research took place earns my warmest thanks for their niceness and help whenever it was needed.

Thanks go also to Adrian Benfield for the verification of the English language.

I would like to thank my girlfriend Joanna for the warmth and support she gave me. Also for her help with processing the pictures for this manuscript.

Last but not least I would like to thank my parents Tomasz and Grażyna for their love and faith in me.

Tampere, March 2012

Karol Bzdawka

CONTENTS

NOMENCLATURE

Latin upper case letters

A_a	cross-sectional area of the column tube
A_{an}	area of steel tube cross-section within the h_n distance from the centre-line of the column cross-section
A_c	cross-sectional area of the column filling
A_c	unreduced cross-sectional area of the plate
A_{cn}	area of concrete cross-section within the h_n distance from the centre-line of the column cross-section
A_{con}	cross-section of concrete filling around the WQ-beam
A_d	additional indirect action caused by the fire
A_{fc}	cross-sectional area of the flange in compression
A_{floor}	floor area of a single storey
A_{hc}	cross-sectional area of the hollow core slab
A_s	cross-sectional area of the column reinforcement
$A_{section}$	cross-sectional area of the beam
A_{sn}	area of reinforcement cross-section within h_n distance from the centreline of the column cross-section
A_v	shear area of the cross-section
A_w	cross-sectional area of the web
E	Young's modulus
K_o	calibration factor
E_a	Young's modulus of the column tube
$E_{c.eff}$	effective Young's modulus for column filling
E_{cm}	Young's modulus of the column filling
K_e	correction factor
$K_{e.II}$	correction factor
K_{ea}	correction factor for column tube
K_{ec}	correction factor for concrete filling
K_{es}	correction factor for reinforcement
$E_{fi.d}$	design value of effect of actions in fire situation

E_s	Young's modulus of the column reinforcement
G	Shear modulus
G_k	characteristic value of dead load distributed over beam length
$G_{k.j}$	characteristic value of dead load
H	storey height
I	second moment of area
I_a	second moment of area of the column tube
I_c	second moment of area of the column filling
I_{hc}	second moment of area of the hollow core slab
I_s	second moment of area of the column reinforcement
L	total length of the beam – measured between the column axes
L_0	length of the beam accounting for the joint stiffness
$M_{c.Rd}$	design value of the resistance to bending
$M_{Ed.col}$	design moment from eccentric column loading
$M_{el.Rd.y}$	design value of elastic resistance to bending
$M_{max.Rd}$	maximal design bending resistance of the column cross-section
$M_{p.Ed}$	design bending moment in the WQ-beam bottom flange
$M_{pl.Rd}$	design plastic bending resistance of the column cross-section
$M_{pl.Rd.y}$	design value of plastic resistance to bending in y direction
$M_{p.pl.Rd}$	design bending resistance of the WQ-beam bottom flange
N_{Ed}	design axial force
N_{cr}	Euler critical force
$N_{cr.eff}$	effective critical force
$N_{g.Sd}$	part of axial force that is caused by permanent loads
N_{plR}	characteristic plastic axial resistance
N_{plRd}	design plastic axial resistance
N_{Rd}	design axial resistance
P_k	characteric value of prestressing action
Q	desing value of live load distributed on beam length
Q_{30kg}	characteristic value of live load used in dynamic analysis
Q_k	characteristic value of live load distributed over beam length

Q_{k1} characteristic value of leading variable action

Q_{ki} characteristic value of accompanying variable action

$Q_{k.1}$ characteristic value of main live load

$Q_{k.i}$ characteristic value of the accompanying live loads

R reaction transferred from the beam to the column console

$R_{fi,d,t}$ design resistance in fire situation after time t

S relative joint stiffness (end fixity ratio)

S_{ini} initial rotational joint stiffness

$V_{b.Rd}$ design shear resistance of a cross-section with unstiffened webs

$V_{bf.Rd}$ flange contribution in design shear resistance

$V_{bw.Rd}$ web contribution in design shear resistance

V_{Ed} design shear force

V_{plaRds} design plastic shear resistance of the column

$V_{pl.Rd}$ design plastic shear resistance of the cross-section

V_{Rdc} shear resistance of the concrete core

V_{Rdcmin} minimum shear resistance of the concrete core

W_{el} elastic section modulus

W_{pa} plastic section modulus of the steel tube

W_{pan} section modulus of steel tube cross-section within the h_n distance from the centreline of the column cross-section

W_{pc} plastic section modulus of the concrete filling

W_{pcn} section modulus of concrete cross-section within the h_n distance from the centreline of the column cross-section

W_{pl} plastic section modulus

W_{ps} plastic section modulus of the reinforcement

W_{psn} section modulus of reinforcement cross-section within h_n distance from the centreline of the column cross-section

$W_{pl.eff}$ plastic section modulus of the effective cross-section

X width of the building

Y column spacing in the direction along the building

Latin lower case letters

a	stiffener interval
b	width of the plate of the WQ-beam top flange
$\overline{b}$	width of the considered element
b_{f1}	width of the WQ-beam top flange
$b_{f2.eff}$	effective width of the WQ-beam bottom flange
b_{nom}	nominal width of WQ-beam
b_w	width of the concrete core
c	short cantilever of the bottom flange of WQ-beam
c_1	cognitive behaviour factor
c_2	collective behaviour factor
c_a	specific heat of steel
col	size of the column tube
d	console eccentricity
d	depth of the concrete core
e	eccentricity
f_0	fundamental frequency of the slim floor
$f_{0.b}$	fundamental frequency of the WQ-beam
$f_{0.s}$	fundamental frequency of the HC slab
f_a	characteristic yield strength of the column tube
f_{ad}	design yield strength of the column tube
f_{cd}	design compressive resistance of the column filling
f_{ck}	characteristic compressive resistance of the column filling
f_{sd}	design strength of the column reinforcement
f_{sk}	characteristic strength of the column reinforcement
f_{yf}	yield strength of the flange in compression
g	gravitational acceleration
g_{slab}	self weight of HC slab
h	total height of WQ-beam
h_n	distance between the centreline of the column cross-section and the neutral axis
h_{nom}	nominal height of WQ-beam
$\dot{h}_{net}$	heat flux to the surface of the member

$\dot{h}_{net,c}$	convective component of the heat flux
$\dot{h}_{net,d}$	design value of the net heat flux
$\dot{h}_{net,r}$	radiative component of the heat flux
h_w	height of the WQ-beam web
k	factor
k	iteration number
k	number of natural frequency
k_1	coefficient
$k_{Ea.\theta}$	reduction factor of Young's modulus for the column tubes
$k_{Es.\theta}$	Young's modulus reduction factor for reinforcement at elevated temperature
k_{shadow}	correction factor for shadow effect
$k_{c.\theta}$	strength reduction factor for concrete at elevated temperature
$k_{s.\theta}$	strength reduction factor for reinforcement at elevated temperature
$k_{y.\theta}$	yield strength reduction factor for steel tube at elevated temperature
k_σ	buckling factor
l_e	buckling length of column
m	number of storeys
n	number of longitudinal reinforcing bars
$\mathbf{p}_k^g$	best location for the swarm at iteration k
$\mathbf{p}_k^i$	best location for particle i at iteration k
q_k	characteristic value of the live load distributed over the floor area
r_1	random factor
r_2	random factor
s	spacing of the stirrups
t	column tube wall thickness
t_{f1}	thickness of the WQ-beam top flange
t_{f2}	thickness of the WQ-beam bottom flange
t_w	web thickness of the WQ-beam
u_s	distance between the inner surface of the steel tube and the outer surface of longitudinal reinforcement
v	member temperature in fire situation
$v_{critical}$	critical member temperature in fire situation

$\mathbf{v}_{k+1}^{i}$ velocity of particle i at iteration $k+1$

w particle's inertia

x length of the cantilever beam as proportion of X

y distance between the beam-column joint and the beam hinge as a proportion of X

$y_{f2.eff}$ effective yield strength of the WQ-beam bottom flange

z_0 elastic neutral axis

z_{pl} plastic neutral axis of the cross-section

Greek letters

α portion of a part of the cross-section in compression

α_A reduction factor of imposed loads on floors and accessible rooftops

α_c coefficient of heat transfer by convection

α_M coefficient

α_n reduction factor of total imposed loads from several storeys

β equivalent moment factor

γ_a material safety factor for the steel tube

γ_c material safety factor for concrete

γ_{con} density of concrete

γ_G partial safety factor for dead load

γ_{GA} partial safety factor for the dead load in accidental design situation

$\gamma_{G.j}$ partial safety factor for the dead load

γ_Q partial safety factor for live load

$\gamma_{Q.1}$ partial safety factor for the main live load

$\gamma_{Q.i}$ partial safety factor for the accompanying live loads

γ_s material safety factor for reinforcement

δ steel tube contribution ratio

$\Delta\theta_{a,t}$ heating rate

ε coefficient depending on f_y

$\varepsilon_{cu.\theta}$ reduction factor for concrete at elevated temperature

ε_f emissivity of the fire

ε_m surface emissivity of the member

η	factor for shear area
Θ_g	gas temperature in the vicinity of the exposed member
Θ_m	surface temperature of the member
Θ_r	effective radiation temperature of the environment
$\bar{\lambda}$	dimensionless column slenderness
λ_{vert}	comparative column slenderness
$\bar{\lambda}_w$	slenderness parameter for webs
μ	coefficient accounting for the influence of axial force on the bending resistance
μ	uniformly distributed mass
ν	Poisson's ratio
ρ	reduction factor for plate buckling
ρ_a	unit mass of steel
σ	Stephan Boltzmann constant
σ_{cp}	compressive stress in concrete due to axial load
σ_E	elastic critical buckling stress
τ_{cr}	elastic shear buckling stress
φ_i	unit rotation
ϕ	diameter of longitudinal reinforcing bars
ϕ_t	creep coefficient for concrete
ϕ_s	diameter of the stirrup
$\boldsymbol{\Phi}$	configuration factor
χ	reduction factor for the relevant buckling curve
χ_w	shear buckling factor
Ψ	stress ratio
$\Psi_{0.i}$	combination factor for the accompanying live loads
Ψ_1	factor for frequent value of a variable action
Ψ_2	factor for quasi-permanent value of a variable action
$\Psi_{2.1}$	combinatorial factor for the main live load
$\Psi_{2.i}$	combinatorial factor for the accompanying live load

Acronyms

ACS	ant colony system
CFHS	concrete-filled hollow section
CHS	circular hollow section
FEM	finite element method
GA	genetic algorithm
HC	hollow core
HS	harmony search
HSS	high strength steel
ISO	International Organization for Standardization
NFL	“no free lunch” theorem
PSO	particle swarm optimization
SA	simulated annealing
SHS	square hollow section
SLS	serviceability limit state
S-R	semi-rigid
TS	tabu search
TSP	travelling salesman problem
ULS	ultimate limit state

1 INTRODUCTION

Economic factors have always been important in building design. Designers have always been drawn towards finding inexpensive and simple solutions for structures. Ease of construction is possible thanks to the high level of prefabrication which can be carried out in workshops. Figure 1 presents an example of a building that is erected using this technology. The other way to lower the cost is optimization. Nowadays, the availability of computers allows us to optimise almost everything – from small parts like joints to whole buildings. The easiest objective is mass minimisation, although increasingly nowadays, designers minimise the cost of a structure, particularly for structures composed of different materials, as in this case, where a steel-concrete structure is optimized.

In contrast with the above is the fact that the safety of building structures is of primary importance. Modern design codes ensure that new structures are safe for people – not only in normal situation but also in accidental ones. The effects of earthquakes, fires or explosions are extensively studied nowadays, largely due to the use of computers that enable simulations of a structure's behaviour under different conditions and in a variety of accident scenarios. Assuming fire as a case in point, this could start anywhere in the building. The temperature increase changes the stiffness of the structural elements and leads to a different distribution of forces. In statically indeterminate structures this is where the engineer's intuition ends. In cases with multiple static layouts to investigate, it is impossible to say which solution is the best for the given structure. The inclusion of semi-rigid joints in the mix makes the problem even more complex.

This thesis considers one type of load-bearing system for a building in order to find the optimum solution for it. It considers both normal and fire design situations and takes advantage of semi-rigid joint behaviour in the search for the answer to this "stiffness riddle". This chapter presents current progress in this field and also introduces the topic of the thesis.

Figure 1. Construction of a hospital using prefabricated elements [Ruukki, 2011]

1.1 Literature review

Optimization, fire design and semi-rigid joints are the three main points of interest in this thesis. This chapter briefly presents the development of research that has been conducted in each of these three fields.

1.1.1 Optimization Algorithms

This subchapter deals with optimization algorithms. A historical draft of optimization procedures is presented, followed by a more focused and detailed review of recently popular direct search methods. The third subchapter introduces the concept of particle swarm optimization, and the chapter ends with a presentation of "no free lunch" theorems.

1.1.1.1 Historical review

The first optimization method was presented by Cauchy in 1847. He used a gradient to find the minimum of a function. Courant's paper on penalty functions is regarded as the beginning of modern optimization methods. This was followed by Danzig's simplex method for linear programming and the "KKT" optimality conditions for constrained problems. In the 1960s several methods for non-linear optimization problems were created. Mixed integer programming combined algorithms created by Land and Doig with Gomory's cutting plate method. The conjugate gradient method (by Fletcher and Reeves) and the variable metric method (by Davidon, Fletcher, Powell) were developed for unconstrained minimization. Rosen's Gradient Projection Method, the Method of Feasible Directions by Zoutendiik, the generalized Reduced Gradient Method of Adabie, Carpentier and Hensgen, and the Sequential Unconstrained Minimization Technique of Fiacco and McCormick were the pioneer methods for constrained optimization [Belegundu & Chandrupatla, 1999].

1.1.1.2 Direct search methods

There are two main groups of optimization algorithms: gradient based and non-gradient methods. Gradient based methods were first described in the middle of 19th century and have been constantly developed ever since. They are widely described in the existing literature. More recently another family of algorithms is under development. The so-called "direct methods" (also called non-gradient) that do not need to derive the objective function in the search for the optimum. Particle Swarm Optimization that was used in the study presented in this thesis belongs to that group.

Since gradient based algorithms are better known already and there are not used in this study they will not be presented here. Instead the focus of this chapter will be on direct methods. Some early examples of these methods come from the 1960s. These are: the Method of Orthogonal Directions by Rosenbrock, the Pattern Search Method by Hooke and Jeeves, the Method of Conjugate Directions by Powell, the Simplex Method by Nelder and Meade and the Method of Box. The most novel are: Simulated Annealing (SA) [Kirkpatrick et al., 1983], Genetic Algorithm (GA) [Holland, 1992], Particle Swarm Optimization (PSO) [Kennedy & Eberhart, 1995] and Ant Colony System (ACS) [Dorigo & Gambardella, 1997].

The Simulated Annealing optimization algorithm was first proposed by Kirkpatrick et al. [Kirkpatrick et al., 1983]. It uses an algorithm proposed by Metropolis [Metropolis, 1953] that simulates the physical process of annealing. In the process, the annealed material is

heated to a certain temperature and then cooled down slowly to relieve stresses. If the cooling is too rapid the particles will not reach the required minimum of energy. This principle is applied in looking for the minimum of the objective function.

In Holland's book, "Adaptation in Natural and Artificial Systems" [Holland, 1992] the basis of genetic algorithms (GA) is considered. The idea of GA is to simulate evolution. A population of candidate solutions is created and their properties are encoded into binary strings called chromosomes, from which individual's fitness function can be evaluated. In each iteration of the GA, only the fittest survive. The probability that an individual will be used to create the next generation is proportional to the value of its fitness function. A new generation is created by crossover: two parents are randomly split into pieces from which two children are made. The probability of crossover is usually 60-80 % [Jalkanen, 2007]. The remaining 20-40 % of the parents is copied directly to the new generation. This method of creating a new generation produces an increasingly homogenous population at each step, finally leading to stagnation. Therefore, a process of mutation is incorporated. This introduces minor, random changes to the individuals in order to bring diversity to the population, which results in a better solution. Usually, the probability of a mutation is in the range of 0.5 to 5.0 % [Jalkanen, 2007]. The algorithm is terminated either when a certain number of iterations have been performed, when the objective function does not improve after a certain number of iterations, or when the individuals become too similar.

Gero at al. [Gero et al., 2006] compared a self-developed genetic algorithm with commercial solutions available on the open market for complex structural optimization. After the algorithm had been validated on a 2 dimensional structure it was tuned and improved to analyze 3D structures. The mass of the structure was the objective function and the constraints were the ultimate limit states for the structures that can be found in the building codes. A comparison of the weight and the cost of structures optimized with GA and those optimized with commercial programs showed that GA obtains improved results but the computational costs are higher.

The Ant Colony System (ACS) was introduced by Dorigo and Gambardella [Dorigo & Gambardella, 1997]. This algorithm was applied to the Travelling Salesmen Problem (TSP), in which the length of a route connecting a certain number of cities depends on the order in which the cities are visited. The idea was inspired by real ants, who can find the shortest path from their nest to a food source. When exploring the nest's surroundings, each ant leaves a pheromone trail which attracts other ants to follow it. When food is found it is brought back to the nest. The shorter the path, the higher the frequency of the ants taking it. Thus, the pheromone trail on the path gets stronger and stronger and so more and more ants follow it. However, some of the ants still tend to wander in search of other food sources, and in doing so they sometimes chance on finding a new, shorter path to the already-discovered food source. When the older path has not been in use for some time the pheromone trail grows steadily weaker and over time it disappears. When applied to TSP, the ACS was found to outperform algorithms such as simulated annealing and evolutionary computing, both in terms of the found solution and the computation time.

1.1.1.3 Particle Swarm Optimization - PSO

Particle Swarm Optimization (PSO) was first introduced by Kennedy and Eberhart [Kennedy & Eberhart, 1995]. The work presented the concept of non-linear function optimization and described the evolution of several paradigms. The authors acknowledged the work of their predecessors in the field. Reynolds [Reynolds, 1987] and Heppner and Grenander [Heppner & Grenander, 1990] were the first to simulate a flock of birds based on the observation that flocking birds try to maintain an optimum distance from each other. This idea was further developed by Wilson who suggested how a school of fish benefits from schooling [Wilson, 1975]. The advantage that the fish gain from learning about food sources found by other members of the school is greater than the drawbacks of competition for food. The first bird flock simulation was easy to write. At each iteration, the velocity of an individual was related to the velocity of the individual nearest to it. In this way, the flock quickly settled into a uniform group moving in one static direction at a constant speed. To make the simulation more lifelike "craziness" was introduced, so at each iteration one particle changed direction and speed randomly. The craziness was removed when the "cornfield vector" was introduced. This vector described an individual's distance from the source of food, i.e. the position in the design space that was attracting the birds. The location of the food source was unknown but the birds knew which of them was the closest. This information was shared by the whole group. Moreover, each bird remembered its own best location. The velocity of each individual was calculated using its distance from the global best solution and its own best location. These values were multiplied by some random numbers and local and global increments. When the global increment was set to a high value, compared to the personal increment, the birds were rapidly sucked into the cornfield. When both increments were set low the birds circled around the solution for a longer time before approaching it, thus exploring a larger area. It became clear from this that this method could be used to search for a function's extremes. When the requirement regarding the distances between the particles was removed the simulation no longer resembled a flock of birds but was more like a swarm of bees, although it was still able to locate the source of food. Both the increments, personal and global, were set to the value of 2.0. This value was selected for the global increment in order to make the particles overfly the target about half of the time. The authors [Kennedy & Eberhart, 1995] also set the personal increment at the value of 2, although they suggest that more research is needed to determine whether this is the best possible value. Tests of the PSO algorithm showed that it can train feed-forward multilayer perceptron neural network weights just as well as the error back-propagation method that is usually used. Tests on training a neural network to classify the Fisher Iris Data Set [Fisher, 1936] yielded similar results. PSO was also tested on the Schaffer f6 function [Davis, 1991] and found the optimum in each run. In conclusion, the authors [Kennedy & Eberhart, 1995] highlight the fact that although the PSO algorithm is extremely simple (only a few lines of code) it produces good results. The stochastic factors allow for an extensive search of the design space without premature rushing to the local optimum, while at the same time avoiding overshooting the global optimum.

1.1.1.4 No Free Lunch theorems

In 1997, Wolpert and Macready presented their “no free lunch” (NFL) theorems for optimization. The authors [Wolpert & Macready, 1997] proved that comparing the performance of optimization algorithms based on a small sample of problems may lead to incorrect conclusions. A geometric interpretation was given showing what is required for an algorithm to be well suited for a certain type of problem. The final conclusion was that there is no single best algorithm for all problems and that the algorithm best suited for solving one particular problem may not be the best one for seemingly similar problems.

In his dissertation, Jalkanen [Jalkanen, 2007] compares four heuristic optimization algorithms, taking the mass of a tubular truss as the problem to be minimized. Heuristic algorithms such as Tabu Search (TS), Simulated Annealing (SA), Genetic Algorithm (GA) and Particle Swarm Optimization (PSO) were tested. The first two (TS, SA) are local search algorithms while the latter two (GA, PSO) are population based. The author highlights the advantages of heuristic algorithms, which are mainly their flexibility and ease of implementation. Their suitability for computationally difficult discrete problems, their ability to avoid weak local minima and the ease of use of parallel processing are also noted. The main disadvantages are the need for a large number of function evaluations (FEM analysis) and uncertainty about the quality of the results.

All of the algorithms in question were found to be useful tools for optimizing tubular trusses. The rules of steel design place awkward constraints on the function, but these did not pose any problems for the heuristic optimizers. The disadvantage is that, since the optimization procedure is stochastic, several runs of the algorithm are needed to reduce the risk of finding a local minimum. In addition, the quality of the final result is unknown. No single one of the tested algorithms was found to give the best results for all the structures under consideration. However, PSO was found to be the easiest one to implement, also for mixed integer problems.

1.1.2 Fire design of frames

This subchapter presents a brief review of the fire design of frames. A short history of the origins of fire design is followed by a review of more recent studies of the basic frame elements: steel beams and steel and composite columns. The final two sections describe the results of studies on joints and whole frames in fire.

1.1.2.1 History of fire design

The aim of the first standard fire-temperature curve, developed in 1918, was to evaluate the performance of constructional elements in fire situation. This was based on a concept introduced in 1916 and used in early *ad hoc* testing of temperature development in fire [Babrauskas & Williamson, 1978]. The concept of “fire load” was established in the classic work of Ingberg [Ingberg, 1928], in which he proposed that the fire resistance requirement is dependent on the fire load. Nowadays, fire codes around the world still use this system. Subsequent tests have shown that the degree of fire exposure is affected by the properties of the furnace, especially the emissivity of its walls [Paulsen & Hadvig, 1977], [Malhotra, 1982]. In 1982, specifications of a furnace’s thermal properties were proposed by Bohm [Bohm, 1982].

As well as this, the development of fires in buildings was also studied. The amount of prone to fire material in buildings was investigated in a number of surveys [Pettersson et al., 1976], [Law and Arnault, 1972], [Bolwin et al., 1970], [Culver, 1976]. The concept of the wood equivalent was established, which is the amount of wood needed to produce the same amount of heat as the combustible materials found in a building. Kawagoe [Kawagoe, 1958] analyzed a number of test results and noted that the wood combustion was greatly influenced by the airflow within the compartment. He proposed a formula to describe the burning rate as a function of the ventilation factor. Today, we know that his equation omitted one factor, namely the function of the compartment size [Ove Arup & Partners, 1977].

Fire grading in the building codes is specified as R 30, R 60, R 90, etc. This is determined by the severity of the fire in a building [Ma & Mäkelainen, 2007]. The fire severity is classified based on occupancy type and is derived from the wood equivalent. The meaning of the fire resistance is that if a structural compartment can retain a standard fire, it will also be able to retain a natural fire. In 1967, the probability factor for fire was introduced into the Swedish building code [SBN, 1967]. Nowadays the Eurocodes take a similar approach. The Eurocode regarding the fire safety design of structures allows active fire precautions such as sprinklers to be taken into account [EN 1991-1-2, 2003]. This means that the fire load density may be reduced by as much as 40 % and may result in natural fires with maximum gas temperatures of only 400 ˚C [Ma & Mäkelainen, 2007].

1.1.2.2 Beams in fire

There are many kinds of analyses of beams in fire. The following subchapter presents some of the floor beam analyses which also take column behaviour into consideration, and represent the most recent findings in this field.

Bailey [Bailey, 1999] studied the behaviour of asymmetric, slim floor beams in fire. The author developed computer software to simulate beams supporting composite concrete floor slabs on deep profiled steel decking. After ensuring that the program yielded accurate results for simply supported beams when compared to test results, the rotational stiffness of the beam-column joint was introduced. Since this type of joint is fully encased in concrete it retains most of its stiffness. Such joints may increase the fire resistance of a beam from 60 to 90 minutes. The author noted that this is beneficial as long as the external columns can resist the beam moment that is transferred to them. A frame analysis of the asymmetric slim floor system with simply supported beams showed that the temperature of the beam's bottom flange, at a distance span/20 from the support, was 780 ˚C when failure occurred. By including joint stiffness, this temperature was raised to 990 ˚C. This analysis also considered the columns and it was found that they would not fail as long as the column temperature was kept below 60% of the temperature of the bottom flange of the beam. This means that the columns also require fire protection.

Mäkelainen and Ma [Mäkelainen & Ma, 2000] studied the fire resistance of slim floor beams by investigating the thermal and structural performance of a new slim floor beam. A numerical analysis program was used to simulate the floor behaviour in fire situation, using the standard ISO fire [EN 1991-1-2, 2003] and natural fires. The dependency of the fire resistance time on the load ratio under ISO fire was analyzed. It was found that without any enhanced fire protection, a fire resistance of 60 minutes can be achieved for a simply

supported beam if the load ratio between the mechanical loads in fire and in normal situation is under 0.47. However, the beam-column joint has to be designed properly to bear the catenary force developed in the beam. The analysis of natural fires showed that without enhanced fire protection the new slim floor beam can be used if the fire load density is lower than 1100 MJ/m^2.

Yin and Wang [Yin & Wang, 2005, Parts 1 and 2] analyzed the catenary action in steel beams using a simplified method of manual calculation. They presented the theory, which they validated with computer simulations, for uniform distribution of the temperature [Yin & Wang, 2005, Part 1] and for non-uniform temperature distribution [Yin & Wang, 2005, Part 2]. The goal of the two papers was to develop a simple analysis method of the development of catenary action in a steel beam in fire situation. The analysis was carried out on beams with uniform and non-uniform temperature distribution as well as uniformly distributed and point loads, and a variety of beam end-restraints. The beams in question had various combinations of rotational and axial restraints. Validation of the results was done with ABAQUS software [ABAQUS, 2010]. It was found that the deformation mode assumed for the beam plays a key role in the analysis.

For a uniformly heated beam [Yin & Wang, 2005, Part 1] with uniformly distributed load and no rotational restraints a polynomial that satisfies the boundary conditions for displacements can be chosen. For a point loaded beam the deformation mode that was chosen was similar in shape to the moment diagram. For a full bending restraint beam deflection mode, a polynomial that satisfies the boundary conditions for the displacements has to be chosen. For semi-rigid joints the deflection mode is interpolated as a function of the ratio of the rotational restraint to the beam bending stiffness.

For a beam with non-uniform temperature [Yin & Wang, 2005, Part 2], the distribution of the deflection mode is a combination of its mechanical deflection and thermal deflection. The mechanical deflection is the same as for uniform temperature while the thermal deflection depends on the rotational restraints. With full rotational restraints, there is no thermal deflection – the beam does not “bow away”, but with only partial restraint, interpolation is necessary.

The manual calculation method indicates higher catenary forces in the beams than those produced in the simulations. This is due to the fact that the catenary force can increase until it reaches the beam’s full axial load-bearing capacity. At this point the beam no longer has any bending resistance. However, this is not how the true stresses and strains in a beam develop. In a simulation, a beam will always have some bending resistance and so the maximum catenary force will be lower. Although the simplified method gives higher catenary forces, especially for beams with high rotational restraint levels, it is still valid since they are on the safe side. This method allows designers to estimate the catenary action in fire situation. However, the resistance of the joints and adjacent structures to the forces induced by the catenary action have to be verified. Thus, any decisions about a beam’s critical temperature come only from the maximum deflection in fire situation. In their report, [TNO, 2002] the authors propose increasing that limit from L/20 to L/10, or L^2/400h, where h is the height of the profile and L is the span of the beam.

For a beam with a non-uniform temperature due to bowing deflection, the catenary force doesn't usually reach the beam's axial resistance. The exact temperature distribution profile has very little influence on the catenary force. For non-uniform temperature distribution there is even better agreement between the simplified method and the computer simulation.

1.1.2.3 Steel columns

This and the next subchapter present some recent studies concerning steel columns in fire and composite columns in both ambient and fire conditions respectively.

Wang and Davies [Wang & Davies, 2003] carried out experiments on non-sway loaded and rotationally restrained steel column assemblies in fire conditions. Eighteen columns were tested in two series of tests. The objective was to analyze in detail the tests results and to focus on the variations in the bending moment and the effective length of the columns. It was found that the bending moment in a column in fire situation changes in a complicated manner. However, a comparison of the failure temperatures measured in tests revealed that the initial bending moment applied to the column and the joint type has negligible effect on the failure temperature. Another conclusion drawn by the authors [Wang & Davies, 2003] is that using both BS-5950 Part 8 [BS 5950, 1990] and Eurocode 3, Part 1-2 [EN 1993-1-2, 2005] the agreement between the calculation and the test results was closer when the bending moment was omitted from the calculation and the effective length of the column was taken to be 0.7 of the total length.

In another paper, Wang et al. [Wang et al., 2010] presented a practical method for the design of restrained steel columns in fire. The proposed method is used to calculate the buckling and failure temperatures for columns. It is based on the results of numerical parametric studies using ABAQUS software. It covers restrained columns with an axial load or with a combined axial load and bending moment. The axial force from the restrained thermal elongation is included and the equation for an unrestrained column is used when calculating the buckling temperature of the restrained column. The failure criterion for columns under combined axial force and bending moment is the temperature at which the axial force returns to its initial value. The failure temperatures obtained by the authors [Wang et al., 2010] for both axial-only and axial-bending loaded columns agree closely with those of the ABAQUS simulations [ABAQUS, 2010]. The condition is that the bending moment compared to the axial force should have realistic values.

1.1.2.4 Composite columns

Wang [Wang, 2000] presents a simple method for calculating the fire resistance of concrete-filled circular hollow sections. He presents an equation for calculating the squash load and bending stiffness of a column, which is suitable for calculating the column's capacity in fire situation. Eurocode 4, Part 1-2 [EN 1994-1-2, 2004] gives only the principles of the temperature analysis. The method presented by Wang only has a few more equations than the one for ambient situation. This new method doesn't require the non-uniform temperature distribution in the column to be evaluated. The structural calculation is also simpler than the one in Eurocode 4 and may encourage practicing engineers to use circular CFHS. The author [Wang, 2000] also presented a validation of the simple method for protected, non-reinforced columns. These results were then compared to the ones obtained using Eurocode 4. For realistic column sizes and steel temperatures, the simple

method was shown to be accurate within 10 %. Inaccuracies higher than 20 % were found for columns that are unlikely to be used in real life. For example, small sized profiles with steel temperature greater than 800 ˚C and a load ratio (fire/ambient) of less than 30 %. The studies went on to validate the methods used for calculation of the steel temperature. For the time being, it is assumed that this is known.

Han et al. [Han, Yang, Xu, 2003] investigated the resistance of concrete-filled SHS and RHS columns. They carried out 11 tests on composite columns in fire, with and without fire protection. The columns were loaded with axial and eccentric loadings. The results of the tests allowed for the study of the influence of certain parameters, such as fire duration time, dimensions of the cross-section, column slenderness, load eccentricity and the strength of the used materials on the residual strength index (RSI). Using the obtained data the authors [Han, Yang, Xu, 2003] developed formulas for both the fire resistance of columns and fire protection thickness.

One finding was that columns in standard fire behaved in a relatively ductile manner, meaning the testing was well controlled. It was found that the fire protection can be reduced by 25-70 % of the recommended value in GB50045-95 [GB50045-95, 2001]. The developed formulas show reasonable consistency with the tests, and are within the safety margin. The findings of [Han, Yang, Xu, 2003] were used in the Shangye Building in Hangzhou, China.

Han et al. [Han et al., 2005] investigated the compressive and flexural behaviour of concrete filled steel tubes after fire exposure. The tested columns were firstly subjected to standard ISO-834 fire [ISO-834, 1975]. Then, the axial and bending resistances of the columns were determined experimentally. The results were in close agreement with the load versus deformation curves that were predicted. The calculation method developed earlier was used to investigate a number of parameters influencing the ultimate strength and flexural stiffness of the column sections. It was found that the columns behaved in a ductile manner and the test proceeded smoothly. This was the result of the composite action between the steel tube and the concrete filling. The mathematical model developed by Han and Huo [Han & Huo, 2003] was again demonstrated as being in close agreement with the tests. The above-mentioned model [Han & Huo, 2003] was next extended [Han et al., 2005] to calculate the residual bending moment resistance. It was found that the use of ambient bending resistance (according to Eurocode 4 Part 1-1 [EN 1994-1-1, 2004]) gave the best predictions. The predicted residual moment resistance was 26% lower than the moment obtained in the tests.

Another method for calculating the fire resistance of circular and square CFHS is presented in a paper by Kodur [Kodur, 1999]. The design method is performance-based. It is expressed in terms of design parameters and thus can be easily adopted to find the most optimal solution in terms of cost if the required resistance is given. Using this method, the author found that the columns' fire resistance is 60 to 180 minutes, depending on the type of filling, compared to about 20 minutes for empty hollow sections. The author noted that the concrete filling is an effective alternative to other methods of fire protection for hollow steel section columns. It was also recommended that when the required fire resistance was greater than 2 hours, the columns should be eccentrically loaded or very slender, bar-

reinforced or fiber-reinforced concrete should be used. When the column is under very high axial compression, the concrete should be bar-reinforced.

A recent study by Nyman and Virdi [Nyman & Virdi, 2011] highlights the drawbacks of the Eurocode [1994-1-2, 2006] calculation for CFHS columns. The simple method given in the code requires reduction factors that are not specified clearly. So, it is easier to use the iterative method presented in Annex H of [1994-1-2, 2006]. On the other hand, some countries, such as Finland, prohibit the use of the Annex H method since it is not fully validated. The authors [Nyman & Virdi, 2011] looked for an alternative method for designing CFHS columns. They compared the results obtained using the Annex H method with advanced calculations done with the SAFIR and SOSMEF programs, and with tests. Both programs gave safe predictions for the resistance time and their results were very consistent. The Annex H method produced up to 50 % too high capacity for slender columns. Since there are a great number of factors influencing column behaviour, simple methods are not able to estimate the capacity for all cases. Advanced methods are becoming easier to use because of the increase in computational power. The authors [Nyman & Virdi, 2011] believe that programs such as SAFIR or SOSMEF may be used in column design, especially in view of the fact that the Annex H method is iterative and therefore quite time consuming for a designer anyway.

1.1.2.5 Steel joints

The behaviour of the joints in fire situation is of particular interest. It is not only a question of the joint resistance at elevated temperatures but also about the temperature increase in fire situation. The joint temperature depends on whether the joint is exposed to fire, specially fire protected or simply “hidden” from fire - for example in a slim floor. The joint behaviour in fire greatly influences the behaviour of the adjoining members. For this reason the following two subchapters will briefly present some recent research on the behaviour of steel joints in fire and their influence on the behaviour of frames in fire. The greatest emphasis is on temperature development in a variety of protected and unprotected joints.

Ding and Wang [Ding & Wang, 2009] investigated the temperatures in fire situation for unprotected steel joints between steel beams and concrete filled tubular columns. In their paper, the authors presented experimental, numerical and analytical results for four types of joints: fin plate, end plate, reverse channel and T-stub. Experiments showed that the temperatures of the joint components that are in the same region are the same. This allows the use of the lumped mass temperature equation of Eurocode 3, Part 1-2 [EN 1993-1-2, 2004] using the equivalent sectional factor for all the components in a region of the same temperature. Suitable expressions for sectional factors were developed for all the joints in question. Authors [Ding & Wang, 2009] also compared the simple temperature calculation method of Eurocode 3, Part 1-2 [EN 1993-1-2, 2004], Annex D with the experimental results, and it was found that this method gives grossly inaccurate results.

In another paper Ding and Wang [Ding & Wang, 2007] presented the results of experiments made to study the structural behaviour of different beam-column joints. Four types of joints (fin plate, end plate, T-stub and reverse channel) were exposed to fire conditions in ten tests. The assembly consisted of two composite concrete filled tubular columns and one I-section beam, creating a “rugby goalpost” layout. The assembly was first loaded and then

exposed to temperature increase. Eight out of ten tests terminated at the failure of the joint and with the beam being in catenary action. In the other two tests a cooling phase took place, starting when the beam was near pure bending and just about to go into the catenary action. It was found that even the simplest joints were able to allow substantial catenary action in the beam, thus allowing the temperature to increase over the limit calculated by assuming only pure bending in the beams. The failure always occurred in the joints, even though beam deflection at that point was L/5. The authors [Ding & Wang, 2009] concluded that higher resistance of the joints would allow the catenary force in the beam to reach even higher level.

One of the tests [Ding & Wang, 2007] in which forced cooling took place was conducted for a reversed channel joint. The joint was found to have high stiffness and strength and, at the same time, high rotational capacity and ductility. All in all, these tests provided a better understanding of joint behaviour and assembly behaviour in fire.

The effect of partial fire protection on the temperature in steel joints was studied by Dai et al. [Dai et al., 2010]. Their paper presents the results of experiments on the temperature increase in composite steel-concrete joints. Four types of joints were considered. Three partial fire protection layouts were studied: protection of the whole assembly except for the bolts, protection of a segment of the beam and protection of the column only. The results of the tests with partial fire protection were then compared with the results of tests with complete fire protection and no protection. Unprotected bolts in a protected joint had a higher temperature than in a totally protected joint but much lower than that of the bolts in a totally unprotected assembly. With regard to the temperatures in the joint, it was found that fire protection on a 400 mm segment of the beam is sufficient. On the other hand, when only the columns are fire painted, only those elements closest to the columns have temperatures significantly lower than the rest of the unprotected assembly. Moreover, the column temperatures in the vicinity of the unprotected joints were significantly higher than in those parts of the column which were further away from the joint.

Dai et al. [Dai et al., 2010] investigated different beam-column assemblies in fire using numerical modelling. The paper presents a simulation methodology used to provide numerical stability for the model, as well as joint structural behaviour, and compares the results of the analyses to the experimental results. The close agreement between the simulation and the test results demonstrates that the developed model is suitable for joint simulation in fire situation. This includes beams with restrained thermal expansion and beams in catenary action. It has been found that the element mesh of the model has to be very fine because of severe local deformations. Also, rapid transitions of the behaviour mode (the compression in the beam changes to tension) cause a convergence problem. This can be solved by introducing pseudo-damping to the model. In the end the experimental results were reproduced accurately and the validated model may be used to develop the understanding of joint behaviour in fire.

Al-Jabri et al. [Al-Jabri et al., 1998] conducted experiments to investigate the behaviour of steel and composite beam-column joints in fire. They summarized tests performed on five joints: 3 bare steel joints and 2 composite joints. It was found that the failure mode was similar to the one observed at ambient temperature. The bare steel joints suffered from end-plate deformation and fracture while the composite joints experienced separation of the

shear studs from the concrete and fracture of the reinforcement mesh. The degradation of the joints in fire was determined. In all cases, the degradation was low at temperatures up to ~400 ˚C, after which a significant increase in degradation was observed. Due to the insulation and heat sink effects of the concrete slab, the degradation of the composite joint was slower than that of the bare steel joints. The data obtained allowed the moment-rotation relationship for joints under constant load and in conditions of increasing temperature to be derived.

Al-Jabri et al. [Al-Jabri et al., 2005] conducted a series of tests on the behaviour of beam-column, semi-rigid joints in fire situation. For a variety of joints, including flush end-plates and flexible end-plates of various thicknesses, moment-rotation-temperature curves were developed to assess other researchers' studies of semi-rigid joint fire behaviour.

Mao et al. [Mao et al., 2009] investigated a semi-rigid, moment-resistant beam-column joint in fire using an H cross-section beam, heated from all four sides. The authors proposed a method for calculating the stiffness of the joint and verified their results using ASNYS. For constant temperature and increasing vertical loading of the beam, the results are consistent. For constant load and increasing beam temperature, the method is found to be conservative. The authors also conducted research into three-sided heating of the beam, since in real structures the top surface of the beam is protected by the floor.

1.1.2.6 Frames in fire

Al-Jabri et al. [Al-Jabri et al., 2001] conducted parametric studies to investigate the influence of joint characteristics on the behaviour of beams in fire. They adopted Ramberg-Osgood expressions for the moment-rotation function in fire and used the finite element program VULCAN [Vulcan Solutions Limited, 2011] to perform the analyses. Bare steel and composite sub-frames with both flush and flexible end-plate joints were analyzed. It was observed that a flush end-plate joint provided a 70 ˚C higher failure temperature for the bare steel beam than the flexible end-plate joint, showing that the joint type has considerable influence on the performance of a steel member in fire. The behaviour of bare steel and composite beams was only slightly different, depending on whether the joint was made with a flexible end-plate or if it was pinned. Therefore, connected beams may be regarded as simply supported. It was also found that the thickness of the end-plate and the joint temperature had little effect on the beam failure temperature for flexible end-plate joints. For bare-steel flush end-plates, the joint stiffness had a greater influence on the beam response. The survival time of the beam was not improved by contact between the beam flange and the face of the column. On the other hand, load ratio in fire was found to have a great influence on the beam's critical temperature for all the joints in question. It was found [Al-Jabri et al., 2001] that the true characteristics of the joint can be beneficial for beam design in fire situation.

El-Rimawi et al. [El-Rimawi et al., 1999] studied the behaviour of a "rugby-post" steel subframe in fire. The frame had semi-rigid joints. They found that heat expansion, thermal bowing due to uneven heating of the beam, and the axial loads in the columns all affect the forces in the individual elements and that the failure mode is the result of their combined effects. The thermal expansion of the beam in the studied substructure was the main reason for column failure, as this was found to produce large bending moments in the outer

columns. On the other hand, semi-rigid beam-column joints lowered the sagging moment in the beams, resulting in higher failure temperatures for the beams. The authors studied all-steel frames without concrete slabs. However, they pointed out that the slab would decrease the temperatures of the upper part of the beam cross-section and also provide some restraint to the bowing deformation, as well as giving some additional stiffness and resistance to the hogging moment. Thus, it would seem that this topic merits further study.

There is a simplified approach which assumes that, at the temperature of 550 ˚C, steel's resistance drops to about 60 % of its value at 20 ˚C, and the safety margin of the normal structural design is evened out. However, this concept of the load ratio of the bending moment and the axial force from the normal design situation is questionable [El-Rimawi et al., 1999] since the failure mode obtained in fire situation corresponds to the column bending caused by beam expansion.

1.1.3 Frame optimization

This subchapter describes recent research into frame optimization and presents some newly-developed simplified methods for frame analysis. This is followed by studies dealing with frame optimization under ambient conditions. The subchapter concludes with one example of optimization of a steel frame in fire conditions.

1.1.3.1 Simple methods of frame analysis

Anderson [Anderson, 2006] has presented a very simple method for a design to limit sway in unbraced multi-storey frames with semi-rigid joints. The method can be used to generate the initial section sizes and joint details. However, the paper questions the further use and development of simple approximate methods for these kinds of frames. The author [Anderson, 2006] notes that nowadays there is plenty of software available capable of running second-order analyses. In the future, these methods will also include non-linear analysis of the joints and creep and cracking of the concrete. It is noted that rigorous second-order analysis is more suitable for future use than the rough manual calculation methods of limited scope.

In their paper, Wong et al. [Wong et al., 2007] propose a modified Muto's method for analysis of composite, unbraced frames. The effect of the semi-rigid beam-column joints is incorporated using equivalent beam stiffness and the difference between beam bending stiffness in hogging and sagging areas. The fitness of the method has been validated using rigorous FEM analysis, also showing that some semi-rigid unbraced frames may satisfy the inter-storey drift limit of h/500 when subjected to lateral loads.

1.1.3.2 Flexibly jointed frame optimization in ambient conditions

Machaly [Machaly, 1986] was the first to apply optimization in order to minimize the weight of a semi-rigid steel frame. The design variables were the flange width and the web height of the W-shape profiles used for the beams and columns. The analysis covered only the vertical loads distributed on the beams and the P-Δ effect was not taken into account. The constraints were the normal and shear stresses and the nodal displacements of the frame together with the cross-section dimensions. A direct search method was used to find the optimum, and the optimization procedure was performed for all joint stiffness ratios [Monforton, 1963] in the range 0.0 to 1.0 at steps of 0.1. Machaly's studies showed that

significant reductions in weight can be obtained, mostly through reduction of the beam's cross-section with the use of semi-rigid joints.

Juang [Juang, 1989] analyzed a three-storey, two-bay, unbraced frame with semi-rigid joints. He considered both static and seismic loads. The stresses, displacements, inter-storey drifts and minimal cross-sections were the design constraints and the cross-section area of the members was the only design variable. The displacement method, both with and without the P-Δ effect, was incorporated into the system motion equation. Non-linearity of the joints was not adopted in the optimized model. The joint stiffness varied within the range 0.0-1.0 with steps of 0.1 and the results confirmed the earlier findings of [Machaly, 1986] that the beam cross-section may be reduced when semi-rigid joints are used. However, for seismic design, rigid joints provided the lowest frame mass.

Al-Solloum and Almusallam [Al-Solloum & Almusallam, 1995] studied the optimality and safety of both rigidly and flexibly jointed steel frames. The simplified procedure they used is based on elastic analysis and allowable stress design as specified in AISC [AISC, 1989]. The joint stiffness is modelled as its secant stiffness. The optimum, for both flexibly and rigidly connected portal frames, is found using the predictor-corrector scheme. The authors [Al-Solloum & Almusallam, 1995] found that taking into account the joint flexibility in the optimization produces material savings but induces larger lateral drifts. The optimum design found for flexibly jointed frames is unfeasible when the joints are rigid. This means that the solution found for frames with flexible joints is unsafe for frames with rigid joints.

Simões [Simões, 1996] described a computer-based method for the optimization of steel frames. His proposed procedure took both the joints and the members into account. The joint stiffness was a continuous design variable while the member cross-section was discrete. With respect to displacement and stress limitation, the optimization algorithm minimized the cost of the joints and members for two example frames. One example was a 7.3 m wide, two-storey, one-bay frame. The other frame was 3-storeys high with two bays, each of 6.1 m. Both frames were loaded with vertical loads distributed on the beams, and concentrated horizontal loads applied to the beam-column joints. It was found that the use of semi-rigid joints in Frame 1 gave 14 % savings in the mass of the frame while the corresponding value for Frame 2 was 12 %. In his conclusions, the author suggests that the use of semi-rigid joints rather than idealized hinged or fully rigid joints is both economical and realistic. The moment redistribution in a semi-rigid frame makes better utilization of the material used to resist the loads that are applied to the frame.

Tahir [Tahir, 1997], in his doctoral thesis, studied the structural and economic aspects of the use of semi-rigid joints in steel frames. The author considered a variety of frame parameters, such as the number of bays, the beam span and the cross-section, as well as different types of joints. The grade of steel remained the same and was set as S 355. It was found that a framing system with semi-rigid joints gives considerable savings in terms of both costs and material. Both the ultimate limit state (ULS) and the serviceability limit state (SLS) were checked, with high emphasis on stability and deflections. The author proposed rules for increasing stability and stiffness. His investigation showed that the frames should be limited to four storeys, and the extended joint study showed that the proposed semi-rigid joints were not suitable for unbraced wind-moment frames.

Kameshki and Saka [Kameshki & Saka, 2001] used semi-rigid joints to minimize the mass of a steel frame. They used a genetic algorithm due to its ease of implementation and its effectiveness for discrete problems. The imposed constraints were the strength constraints specified in the British structural steel specification [BS5950, 1990], lateral and inter-storey drift, and dimensional constraints. Non-linearity was considered for the semi-rigid joints, as well as the P-Δ effect for the whole frame. Because of that, and the fact that a genetic algorithm analyses several solutions at each iteration, the amount of computational work required was found to be large. It was found that the semi-rigid joint produced a lower total mass for the frame when the P-Δ effects were not taken into account and a higher one when the P-Δ effects were considered.

In their paper, Wang and Li [Wang & Li, 2008] present a practical design method for composite frames with semi-rigid joints. The proposed method takes into account the semi-rigidity of the joints while at the same time being easy to use for a practicing engineer. The authors considered a composite floor and a non-symmetric I-section steel beam, together with part of the concrete slab. The columns were steel I-sections. They presented a simple method for calculating beams subjected to hogging and sagging moments, and they also determined those moments and the beam bending stiffness. The distribution of the bending moment exerted on the columns from the beams is also shown. The formulas for checking the joints for both serviceability and ultimate limit states are also presented. The proposed method has been verified in two full-scale tests and a cost estimation was also carried out. It was shown that the semi-rigid frame system has advantages over traditional ones. The authors highlighted that semi-rigid joints could be used in optimizing the moment distribution in columns.

Poitras et al. [Poitras et al., 2011] performed an optimization on a steel floor conforming to the Canadian S16 design standard. The variables taken into account were girder size, the number and the dimensions of the beams, the number of the studs per beam, the steel deck profile and the thickness of the concrete cover. Both composite and non-composite floor systems were analyzed. The results showed that the Particle Swarm Optimization (PSO) algorithm finds consistent results for both steel mass minimization and cost minimization.

1.1.3.3 Frame optimization in fire

Jármai et al. [Jármai et al., 2005] performed an optimization on the supporting frame for a steel pressure vessel. They used particle swarm optimization (PSO) in order to minimize the total mass of the frame. There was no fire protection for the steel frame and its fire resistance could only be improved by increasing the amount of material. Optimization was performed for a number of specified, increasingly long fire resistance times. The cross-sections of the beams and columns were square hollow sections (SHS) and rectangular hollow sections (RHS) and they were increased in line with the time requirement. It was found that a fire resistance time of about one hour requires three times more material in the structure. It was also found that the PSO algorithm was very robust. The authors propose to continue their research in this field by taking into account the fire paint and optimizing the frame cost.

1.2 Topic of the thesis

There are many framing systems for office buildings to choose from. One of them is especially popular in Nordic countries. It consists of beams and columns which transfer all the vertical loads to the foundations and specific support structures which bear all the horizontal loads. These support structures are usually concrete lift shafts, shear walls and staircases. The mechanical behaviour of such a vertical load-bearing structure may vary greatly. In Sweden, single-storey columns with multi-span beams are popular, while in Finland, multi-storey columns with single-span beams with hinged joints are more common. In seismic regions, frames with rigid joints are often used.

In this study, pre-stressed concrete hollow core slabs (HC slabs) are used. They transfer the vertical loads from the floors to the welded box beams via a wide bottom flange that supports the slabs. In Finland, these beams are called *WQ-beams*. *W* stands for *welded* and *Q* comes from the shape of the cross-section of a beam that supports a slab only on one side. The floors are slim floors, meaning that only the bottom flange of the beam is not hidden in the floor. The manufacturing technology of the beams allows large pre-cambers to be made. Therefore, the deflection constraint is usually not the governing one in the design of WQ-beams.

The columns in question are cold formed hollow sections filled with concrete (CFHS). The concrete can be reinforced or not. The concrete filling is injected into the column on site, which means that in erection design situation it is necessary to provide sufficient support for the columns.

This kind of solution is very economical due to the small amount of wet work that has to be done on site and the high level of prefabrication. Most of the elements are prefabricated and then merely put into place. This solution is also safe as in fire conditions only the bottom and side surfaces of the bottom flange are exposed to fire. The rest of the beam is encased in concrete which not only prevents direct heating of other beam elements but, due to the heat transfer from the bottom flange, it also works as a heat sink for the beam's web. The beam's bottom flange is usually fire protected by intumescent paint or protective boards.

The concrete filling of the column gives the required resistance in fire situation – especially if it's reinforced. The concrete filled columns are recently also studied for their performance under seismic loading [Mamaghani, 2011].

This study focuses on the load carrying system for vertical loads, meaning fully steel beams and steel-concrete composite columns. Therefore, neither the lift shafts, shear walls, staircases, foundations nor the cladding structures are not taken into account in the optimization procedure. However, to find the optimum column layout for the structure, concrete slabs are included in the load calculation and also the cost calculation. The structure will be optimized for two design cases: normal and fire. The effect of the stiffness of the joints between the beam and the column on the optimum solution is the other objective of this study. The joints are considered theoretically – the beam-column joints are hinged, rigid, or semi-rigid while the column base joints are either hinged or rigid. The rotational stiffness varies without taking into account the details of the joint. It is believed

that in the future, with small modifications, the joint that is currently in use can reach the required rotational stiffness.

Figure 2 shows examples of the three elements considered in this study, HC slabs, WQ-beams and CFHS columns while Figure 3 shows the layout of the current hinged beam-column joint.

Figure 2. Examples of HC slabs (left), WQ-beams (middle) and CFHS columns (right) [Ruukki, 2011].

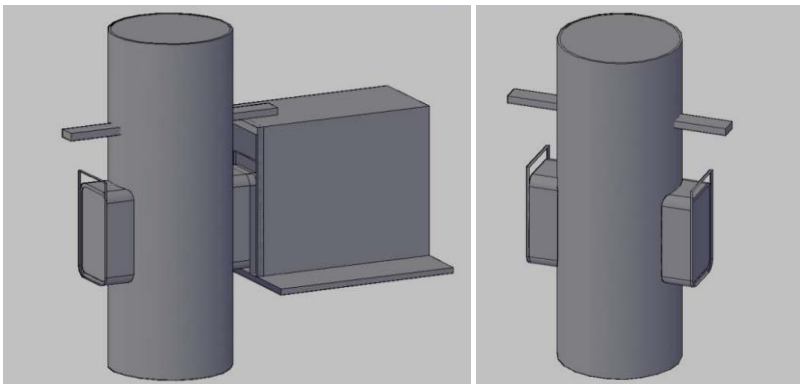

Figure 3. Console joint of a circular CFHS column [Hömmö, 2008]

1.3 Goal and outline of the study

The goal of this study is to find the most cost effective solution for the framing systems in question. The task is not only to find the most economical solution, but also to investigate what are the main factors that determine the structure's cost and how these change with changes in the static layout, building dimensions, required fire classes, material unit prices, material grades and joint stiffness. One of the main points of interest in this study is the use of semi-rigid beam-column joints. Joints of this type are known to enhance the performance of the frame in the normal design situation. However, their influence on the frame behaviour in both ambient and fire situation, and their effect on the cost function have not been studied for a non-sway frame.

This thesis tries to fill that gap.

Most probably it is impossible to solve current problem in arbitrary case i.e. to find the global optimum. However the use of stochastic methods for similar mixed integer problems have been found to be reliable and provided reasonable results in earlier studies [Jalkanen, 2007].

Chapter 2 of the thesis presents the details of the structure under consideration. The load-bearing system for the vertical loads is composed of three elements: slabs, beams and columns, and these are described in subchapter one. The semi-rigid joints are only considered theoretically. Their design is not studied in detail, and in the cost calculation they are implemented into the beam cost to get a better approximation. Subchapter two presents the principles of the fire calculation in accordance with Eurocodes, since this is the method used in this study. The following subchapter presents an example of the calculations performed for each of the structures in the optimization process. The variables are the structural dimensions and the material properties while the loads are fixed. Aside from the dead load, only the vertical live load is considered, 3.0 kN/m^2, as that is the most common value used for office buildings in Finland. The resistance checks for the elements follow Eurocodes and Eurocode-based Finnish design guidelines. The idea of subchapter 2.3 is to give the reader an insight into the design procedure used. The numerical calculations presented in the appendices show the amount of calculation needed to evaluate the feasibility and the value of the objective function in the optimization.

The Particle Swarm Optimization (PSO) algorithm was used in this study due to its suitability for the kinds of problems described in Chapter Three. The data used in the optimization procedure is also presented in that chapter.

Chapter Four present the results of the analyses. These analyses were performed for 1, 3 and 6-storey buildings. Subchapters 1-3 present the details of the analysis for each of the buildings, together with their results. The specification of each analysis is described and the results are presented and discussed. Short descriptions of the analyses are given below.

- The 1-storey building is analysed in normal design situation with several different static layouts and different building proportions. Semi-rigid joints are not considered at this point.

- The 3-storey building is considered for one set of building dimensions and one static layout. Semi-rigid joints are used here, and the structure is analysed in normal and fire conditions. The first floor of the building is engulfed in R 60 fire and a variety of joint stiffnesses are investigated.

- The 6-storey building analysis is done to determine the influence of the required fire class on the cost. Fires of classes R 30 to R 120 are considered on the 1^{st}, 3^{rd} or 6^{th} floor. In the 6-storey building analysis the joints are either hinged or with variable stiffness.

A sensitivity study is performed for the 3-storey building to investigate the influence of the material price variation on the optimum structure. The use of high strength steel (HSS) is considered for a selected type of 1-storey building to determine the building size above which the use of HSS becomes economically justified.

Due to the initial beam pre-cambers, only ULS is considered in the optimization. The SLS is verified for one structure to determine if it has any effect on the optimum solution.

Chapter Five summarizes the study and the obtained results and also gives some guidelines for future research.

1.4 Limitations

The problem considered in this thesis is very complex. Due to large time necessary for the optimization of a whole load bearing structure of a building some simplifications have been made to make the problem easier to handle. This subchapter summarizes all the limitations of the presented problem.

The considered load bearing structure is carrying only the vertical loads. It is assumed that the wind load applied to the outer walls is transferred to the concrete lift shafts by rigid floors. The lift shafts are considered to be separate structures that have no influence on the chosen solution. The main focus of this thesis is the cost of steelwork which is influenced by only by the vertical loads – live loads and floor dead weigh. The live load is taken equal to 3.0 kN/m^2 which is the normative value for office buildings [EN 1991-1-1, 2002]. Moreover, due to the fact that whole frame was analysed at once, imposed load reduction factors α_A and α_n were omitted in this study.

Due to simplicity and the use of space frame program the stiffening effect of the floors was not taken into account. The floors generate only loads and costs. For the same reason also the envelope of the building and the foundations have been omitted in the optimization.

Structure is analysed only in final stage – erection is not considered.

Another simplification that was made was to omit the serviceability limit state. The maximum deflection of the beam was not investigated since the manufacturing technology of WQ-beams allows large pre-cambers to be made in workshop. The vibration limit state was also not considered. Usually it is not a problem for this type of floors but, as is presented later, the optimized floor turned out to be very shallow in which case the vibration limit state will determine the design. Taking it into account is one of the recommendations for future research.

In this study the connections also were not modelled. Relative joint stiffness was used instead. At this moment the solution for semi-rigid joint for these types of structures is not proposed and the aim of this thesis is to investigate the possible savings in the structural members if such connections are to be developed.

In fire situation only the columns are influence by the temperature increase. The beams are assumed to be fire protected sufficiently so that the beams' yield strength and Young's modulus remain the same as in normal situation. Because of that the effects of beams' thermal elongation are not taken into account. The joint stiffness also remains the same in fire as in ambient since it is hidden in the floor and no temperature increase occurs. The fire is always assumed on the whole area of one single floor and its temperature is uniform – column heating does not depend on the distance from the floor. Thermal expansion of the column is considered to be uniform and thus does not cause any increase in the internal forces.

2 THE STRUCTURE

The type of structure considered in this study is very popular for office buildings in Scandinavian countries. The structure bearing the vertical loads is composed of three basic elements: slabs, beam and columns. All three of them have to retain the ability to bear the loads in fire conditions. This chapter gives some more information about the framing system and its elements. The principles of fire calculation used by Eurocodes are also briefly described. The third subchapter presents the design procedure used in the optimisation. The explanation is given for an example structure for which the detailed numerical calculations can be found in the appendices.

The example calculations shows in detail the feasibility checks for the beams and columns according to Eurocodes and Finnish guidelines. These are shown in order to demonstrate the feasibility checks that have to be conducted repeatedly during the optimization procedure. All the checks are programmed in Matlab [Matlab, 2009] to perform all the required analyses with the use of a frame program (*frame3D*) and the PSO algorithm (*JJPSO*) [Jalkanen, 2007].

2.1 General information on the structure and elements

Several static layouts for the frame were considered in this study. In general, there are two types of structures. TYPE 1 structures have two frames located in the walls on the longer sides of the building. TYPE 2 structures have two or more smaller frames that are located at right angles to the longer side of the building. TYPE 1 structures are presented in Figure 4 and TYPE 2 structures in Figure 5.

The main dimensions of the building used in this research were taken from the most popular structure in Finland at the moment, TYPE 1A. Dimension X, the width of the building, is determined by the minimal and maximal lengths of the hollow core (HC) slabs that are available on the market. The manufacturer Parma [Parma, 2009] has been chosen in this study as the slab provider. The slab lengths provided by Parma [Parma, 2009] are between 10 and 20 meters, and thus dimensions within this range are chosen for the building width. The other dimension, Y, is a multiple of 2.7 m. This type of building usually has parking spaces on the lowest floor. The Finnish practice is to take the width of a single parking space as equal to 2.7 meters. The number of parking spaces in this study is between 2 and 5, giving a Y dimension of between 5.4 m and 13.5 m. The height of a single storey of an office building also follows Finnish practice, and is equal to 3.6 m. The number of cells (the number of Y dimensions that fit in the building length) is 2. The other main dimensions of the building, such as x and y, are proportional to the building width. The dimension x is the length of the cantilever part of the beam for TYPE 2 structures while y is the distance between the column and the hinge in the beam in TYPE 2C. The proportion ranges used in the optimization are given in subchapter 4.1.

TYPE 1

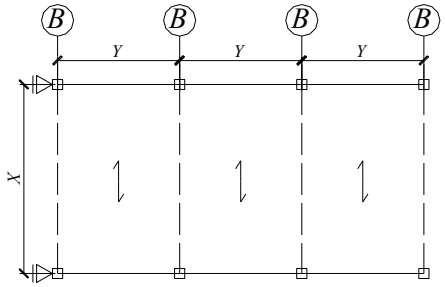

TYPE 1A

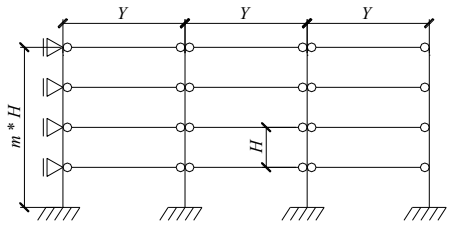

TYPE 1C

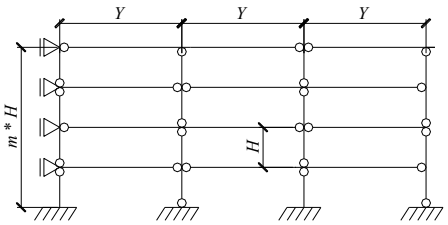

TYPE 1B

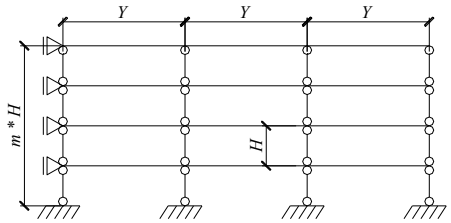

TYPE 1D

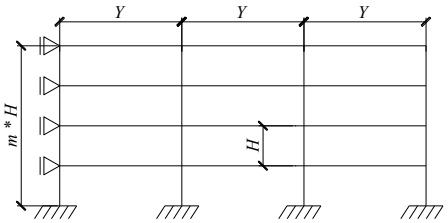

Figure 4. Static layout of TYPE 1 structures

TYPE 2

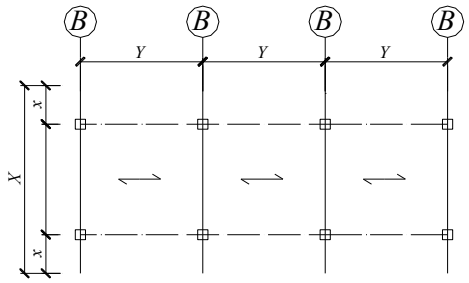

TYPE 2A

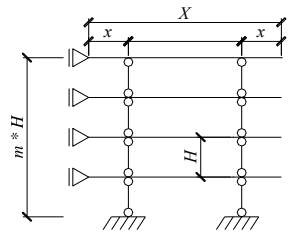

TYPE 2B

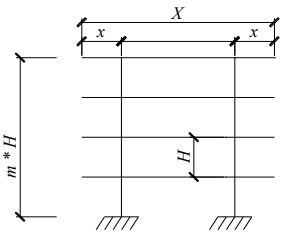

TYPE 2C

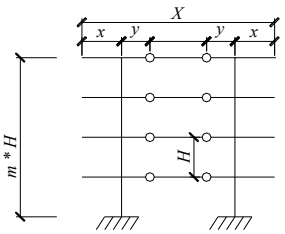

Figure 5. Static layout of TYPE 2 structures

Depending on the X or Y dimension (for TYPE 1 and 2 respectively) a proper HC slab is chosen from the producer's catalogue [Parma, 2009] for a live load of 3.0 kN/m^2. The available slabs are presented in Table 1. Unit prices presented in Table 1 are taken from [Haahtela, 2005].

Table 1. Hollow core slab data

	Nominal height	Maximum span	Concrete cover	Support width	Self weight	Unit price
Slab symbol	[mm]	[m]	[mm]	[mm]	[kg/m^2]	[€/m^2]
P20	200	10.0	60	60	260	46
P27	265	12.0	60	60	380	54
P32	320	14.0	60	60	400	55
P40	400	17.0	100	100	465	63
P50	500	20.0	100	100	600	90

A graphic representation of the available HC slabs for different building dimensions can be seen in Figure 6.

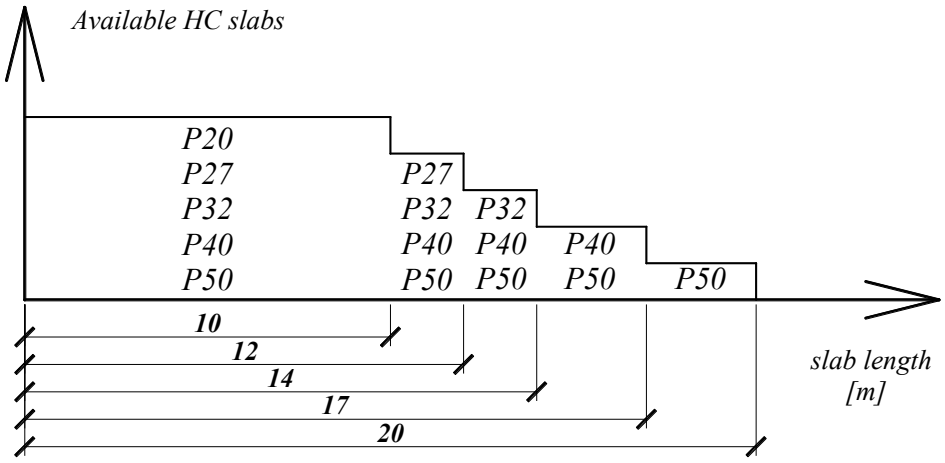

Figure 6. Available slabs depending on required length

Figure 6 shows that for a slab span of, say, 16 m, either slab P40 or P50 could be used. However, using thicker slabs when a shallower one could be used cannot be justified economically. In all cases, the nominal height of the beam is tied to the thickness of slab. This means that shallow beams should be used for shallow slabs, which would result in thick plates being used for the beam. It was originally thought that perhaps choosing a thicker slab would result in thinner plates for the beam and thus produce a more economical structure. However, due to the large differences in the unit costs of the slabs, together with the fact that the slabs constitute more than 50 % of the structure's cost, this idea was later discarded. Thus, the thinnest slab available is always used. It should be noted that the displacement constraint is not taken into account, so thin slabs with shallow beams can be chosen. The beams have initial pre-cambers made in the workshop and this takes care of the deflection limitation.

The WQ-beam is welded from plates available on the market. The nominal beam height is equal to the slab height (Figure 7). Beams that are higher than the slab and stick out from the ceiling are sometimes used, but in this study they are not considered in order to limit the

number of variables. The nominal width (b_{f1}) of the beam is a design variable, while the width of the bottom flange is directly dependent on b_{f1} and the width of the support required for the slab or slabs (see Table 1), which in turn depends on whether it is an edge or middle beam (see Figures 4 and 5). The space between the beam web and the slab is always 50 mm and this is filled with concrete (Figure 7). The only cross-sectional dimensions of the beam that are left are the thicknesses of the top and bottom flanges, and the webs. These are the design variables in the optimization and the values from which they can be chosen are taken from [TRY, 2009]:

- Top flange t_{f1} = 10, 12, 15, 18, 20, 22, 25, 30, 35 or 40 mm,
- Bottom flange t_{f2} = 10, 12, 15, 18, 20, 22, 25, 30 or 35 mm,
- Both webs t_w = 5, 6, 8 or 10 mm.

The beams and joints are sufficiently fire protected to ensure that they do not lose any resistance or rigidity. This means that the temperature of the beam's bottom flange does not exceed 100 ˚C up to the required resistance time. For example, the average gas temperature of ISO standard fire [EN 1991-1-2, 2003] for the first 60 minutes of the fire's duration is approximately 800 ˚C. Let us take that to be the temperature of the outer surface of a fibre insulating board that covers the beam. The thermal conductivity ($t_w = 0.041\ \mathrm{W/m^2K}$), specific heat ($c_p = 2090\ \mathrm{J/kgK}$) and density ($\rho = 229\ \mathrm{kg/m^3}$) of the board conform to [Drysdale, 2004]. If the temperature of the inner surface of the insulation is required to remain below 100 ˚C after one hour of fire, the minimum insulation thickness of 80 mm can be calculated using [Hagentoft, 2001]. If the required resistance is 2 hours, and the average gas temperature is assumed to be equal to 900˚C, then the minimum insulation thickness is about 115 mm. Assuming that the beams are sufficiently protected against temperature increase in fire situation, their resistance can be calculated as it is in ambient temperature.

Fire protection is not part of this research, so it is not calculated precisely in the optimization procedure, but some estimation of the fire protection cost is included in the cost function.

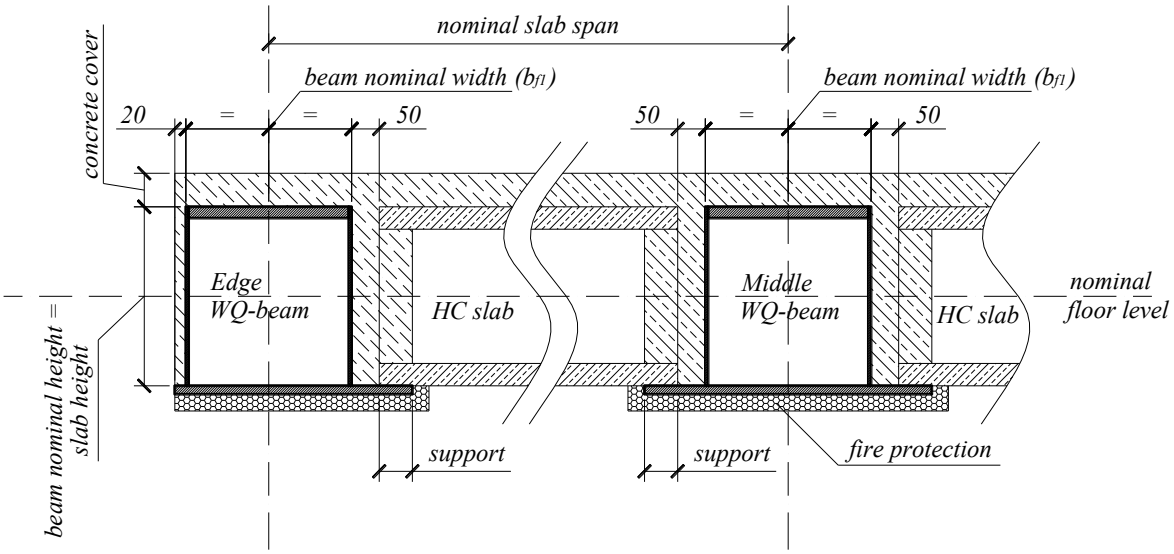

Figure 7. HC slabs resting on WQ-beams

The columns used in this structure are square concrete-filled hollow sections. These are composite sections consisting of three materials: the steel tube, the concrete filling and the reinforcement for the filling. The design procedure for the column follows the Finnish guide manual [TRY, 2004], which is an extension of the Eurocodes and includes tabulated temperatures for fire calculations. The columns used in this research are mostly taken from [TRY, 2004], but due to the use of rigid and semi-rigid joints in some structures the set of columns had to be increased to include larger columns with greater bending stiffness and resistance. The columns that have been used are shown in Table 2. The columns with reinforcing bars thicker than 32 mm actually have bundles of bars, but to simplify the calculations substitute bars of a corresponding cross-sectional area are used:

- 3 bars of 20 mm have the same cross-sectional area as a single 34.6 mm bar,
- 3 bars of 25 mm have the same cross-sectional area as a single 43.3 mm bar,
- 3 bars of 32 mm have the same cross-sectional area as a single 55.4 mm bar,

Table 2. Column cross-sectional data

Origin	no.	Column cross section	Cross-section dimensions				Aditional dimensions	
			size of the steel tube (col)	steel tube wall thickness (t)	number of reinforcing bars (n)	longitudinal reinforcement diameter (ϕ)	Stirrups diameter (ϕ_s)	Stirrups spacing (s)
			[mm]	[mm]	[1]	[mm]	[mm]	[mm]
Betonitäytteisen teräsliittopilarin suunnitteluohje [TRY, 2004]	1	150x150x5 0T00	150.0	5.0	0	0.0	0.0	0
	2	150x150x5 4T12	150.0	5.0	4	12.0	6.0	180
	3	150x150x5 4T16	150.0	5.0	4	16.0	6.0	240
	4	180x180x5 0T00	180.0	5.0	0	0.0	0.0	0
	5	180x180x5 4T12	180.0	5.0	4	12.0	6.0	180
	6	180x180x5 4T16	180.0	5.0	4	16.0	6.0	240
	7	180x180x5 4T20	180.0	5.0	4	20.0	6.0	300
	8	180x180x5 4T25	180.0	5.0	4	25.0	8.0	375
	9	200x200x5 0T00	200.0	5.0	0	0.0	0.0	0
	10	200x200x5 4T16	200.0	5.0	4	16.0	6.0	240
	11	200x200x5 4T20	200.0	5.0	4	20.0	6.0	300
	12	200x200x5 4T25	200.0	5.0	4	25.0	8.0	375
	13	200x200x6 0T00	200.0	6.0	0	0.0	0.0	0
	14	200x200x6 4T16	200.0	6.0	4	16.0	6.0	240
	15	200x200x6 4T20	200.0	6.0	4	20.0	6.0	300
	16	200x200x6 4T25	200.0	6.0	4	25.0	8.0	375
	17	220x220x6 0T00	220.0	6.0	0	0.0	0.0	0
	18	220x220x6 4T16	220.0	6.0	4	16.0	6.0	240
	19	220x220x6 4T20	220.0	6.0	4	20.0	6.0	300
	20	220x220x6 4T25	220.0	6.0	4	25.0	8.0	375
	21	250x250x6 0T00	250.0	6.0	0	0.0	0.0	0
	22	250x250x6 4T16	250.0	6.0	4	16.0	6.0	240
	23	250x250x6 4T20	250.0	6.0	4	20.0	6.0	300
	24	250x250x6 4T25	250.0	6.0	4	25.0	8.0	375
	25	250x250x6 8T20	250.0	6.0	8	20.0	6.0	300
	26	250x250x6 8T25	250.0	6.0	8	25.0	8.0	375
	27	300x300x8 0T00	300.0	8.0	0	0.0	0.0	0
	28	300x300x8 4T20	300.0	8.0	4	20.0	6.0	300
	29	300x300x8 4T25	300.0	8.0	4	25.0	8.0	375
	30	300x300x8 4T32	300.0	8.0	4	32.0	8.0	450
	31	300x300x8 8T25	300.0	8.0	8	25.0	8.0	375
	32	300x300x8 8T32	300.0	8.0	8	32.0	8.0	450
	33	350x350x10 0T00	350.0	10.0	0	0.0	0.0	0
	34	350x350x10 4T20	350.0	10.0	4	20.0	6.0	300
	35	350x350x10 4T25	350.0	10.0	4	25.0	8.0	375
	36	350x350x10 4T32	350.0	10.0	4	32.0	8.0	450
	37	350x350x10 8T25	350.0	10.0	8	25.0	8.0	375
	38	350x350x10 8T32	350.0	10.0	8	32.0	8.0	450
	39	400x400x10 0T00	400.0	10.0	0	0.0	0.0	0
	40	400x400x10 4T20	400.0	10.0	4	20.0	6.0	300
	41	400x400x10 4T25	400.0	10.0	4	25.0	8.0	375
	42	400x400x10 4T32	400.0	10.0	4	32.0	8.0	450
	43	400x400x10 8T20	400.0	10.0	8	20.0	6.0	300
	44	400x400x10 8T25	400.0	10.0	8	25.0	8.0	375
	45	400x400x10 8T32	400.0	10.0	8	32.0	8.0	450
ADDITIONAL	46	450x450x12 0T00	450.0	12.5	0	0.0	0.0	0
	47	450x450x12 4T20	450.0	12.5	4	20.0	6.0	300
	48	450x450x12 4T25	450.0	12.5	4	25.0	8.0	375
	49	450x450x12 4T32	450.0	12.5	4	32.0	8.0	450
	50	450x450x12 8T25	450.0	12.5	8	25.0	8.0	375
	51	450x450x12 8T32	450.0	12.5	8	32.0	8.0	450
	52	500x500x12 0T00	500.0	12.5	0	0.0	0.0	0
	53	500x500x12 4T20	500.0	12.5	4	20.0	6.0	300
	54	500x500x12 4T25	500.0	12.5	4	25.0	8.0	375
	55	500x500x12 4T32	500.0	12.5	4	32.0	8.0	450
	56	500x500x12 8T25	500.0	12.5	8	25.0	8.0	375
	57	500x500x12 8T32	500.0	12.5	8	32.0	8.0	450
	58	500x500x12 4T35	500.0	12.5	4	34.6	8.0	450
	59	500x500x12 4T43	500.0	12.5	4	43.3	8.0	450
	60	550x550x16 0T00	550.0	16.0	0	0.0	0.0	0
	61	550x550x16 4T20	550.0	16.0	4	20.0	6.0	300
	62	550x550x16 4T25	550.0	16.0	4	25.0	8.0	375
	63	550x550x16 4T32	550.0	16.0	4	32.0	8.0	450
	64	550x550x16 8T25	550.0	16.0	8	25.0	8.0	375
	65	550x550x16 8T32	550.0	16.0	8	32.0	8.0	450
	66	550x550x16 4T35	550.0	16.0	4	34.6	8.0	450
	67	550x550x16 4T43	550.0	16.0	4	43.3	8.0	450
	68	550x550x16 4T55	550.0	16.0	4	55.4	8.0	450

There are no temperature data for columns bigger than 400 mm. Therefore, the temperatures used in the calculations are taken to be the same as for 400 mm. This is the best approximation so far. The bigger, more massive columns will have lower core temperatures in fire than slender ones, so this solution is on the safe side.

As shown in Table 2, the columns seem to have many factors determining the cross-section (col, t, n, ϕ) but these are all dependent on each other. Wall thickness t is in most cases fixed to the tube size (except for a $col = 200\text{mm}$ tube that can have either 5 or 6 mm wall thickness). The number and diameter of the reinforcement bars is such that the reinforcement level is kept within a reasonable range. Because of this, only one variable for the column cross-section was used in the optimization process – its number being as presented in Table 2.

The column cross-sections change with the floor number; the lower the floor the greater the axial force and the larger the columns which are required. Frames with semi-rigid joints require larger (stiffer) columns on the top floors where there are larger bending moments. In most of the types of structures considered here, the column cross-sections change every few floors, all at once. The exception is structure TYPE 1C, in which the columns are two-storey and change alternately as presented in Figure 8.

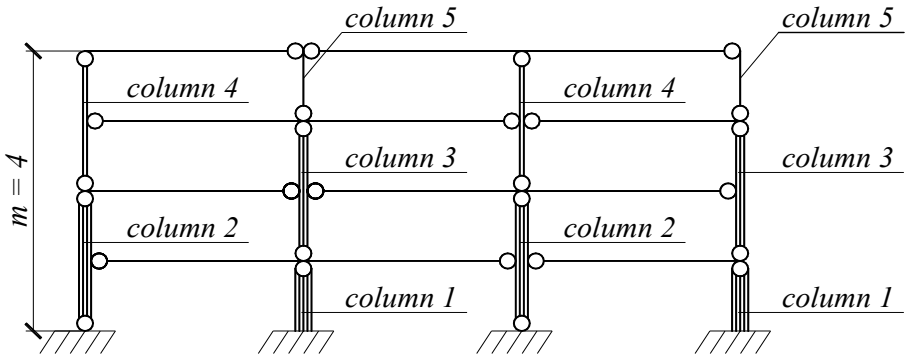

Figure 8. Column arrangement scheme for TYPE 1C structures

The design procedure for the columns is presented in subchapter 2.3.4. Numerical example can be found in Appendix C or [Bzdawka, 2010].

All the mechanical material data used in this study adheres to the Eurocodes [EN 1993-1-1, 2005], [EN 1994-1-1, 2004]. There are four materials used: hot-rolled flat products for the beams [EN 1993-1-1, 2005], cold-rolled steel tubes for the columns [EN 1994-1-1, 2004], concrete cast on site as the column filling, and column reinforcement [EN 1994-1-1, 2004]. Only one material is used for the beams, which means that hybrid beams – beams with flanges or webs made of a different class of steel than the rest of the beam, are not considered in this study. The material data and material safety factors in normal design situation conform to the Finnish National Annexes of the Eurocodes. Material mechanical and cost data used in the optimization are presented in Tables 3 and 4.

Table 3. Material data for all the steel elements of the structure

Steels used for WQ-beam

Steel grade	Young modulus [GPa]	Poissons ratio [1]	Density [kg/m^3]	Yield strength [MPa]	Ultimate strength [MPa]	Safety factor [1]	Price factor [1]
S 355 JR	210.0	0.3	7850	355.0	510.0	1.00	1.00
S 460 M	210.0	0.3	7850	460.0	540.0	1.00	1.17
S 700 MC	210.0	0.3	7850	680.0	750.0	1.00	1.43

Steels used for square hollow section

Steel grade	Young modulus [GPa]	Poissons ratio [1]	Density [kg/m^3]	Yield strength [MPa]	Ultimate strength [MPa]	Safety factor [1]	Price factor [1]
S 355 J2H	210.0	0.3	7850	355.0	510.0	1.10	1.00
S 460 MH/MLH	210.0	0.3	7850	460.0	540.0	1.10	1.17
S 700 MC	210.0	0.3	7850	680.0	750.0	1.10	1.43

Steels used for concrete reinforcement

Steel grade	Young modulus [GPa]	Poissons ratio [1]	Density [kg/m^3]	Yield strength [MPa]	Ultimate strength [MPa]	Safety factor [1]	Price factor [1]
A 500 HW	210.0	0.3	7850	-	500.0	1.15	1.00
A 700 HW	210.0	0.3	7850	-	700.0	1.15	1.10

Table 4. Material data used for the concrete filling of the columns

Concrete used for column filling

Concrete grade	Young modulus [GPa]	Density [kg/m^3]	Strength [MPa]	Safety factor [1]	Price factor [1]
C40/50	210.0	7850	400.0	1.35	1.00

The fire calculation of the structure only considered the vertical loads in fire conditions and the reduction in the stiffness and resistance of the elements, so no indirect actions from the temperature increase are taken into account (see subchapter 2.2). Because of this, the thermal expansion coefficient is not necessary for the design procedure used in the optimization and thus is not shown in the tables above.

The values for the price factor are used to increase the cost of members made of high strength steels. The values are read from Figure 9 and are found in the literature [Johansson, 2005] and then rescaled to fit the S 355 grade for the constructional steel and A 500 HW for reinforcement. This conforms to the corresponding default values in Johansson [2005] from where the prices for the cost calculation have been taken (see subchapter 2.3.5).

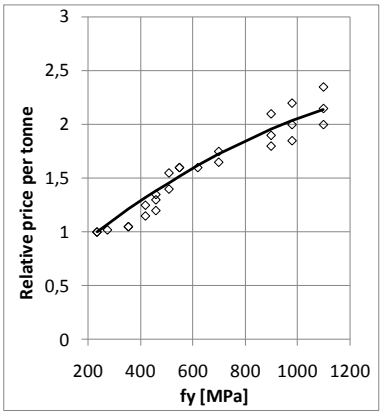

Figure 9. Relative steel price as a function of yield strength [Johansson, 2005]

2.2 The principles of Eurocode fire calculation.

The study presented in this thesis considered the frame in both ambient and fire conditions. The fire design calculation is conducted according to Eurocodes. The principles of Eurocode fire calculation are briefly presented below.

The fire analysis method for steel structures described in Eurocodes consists of several steps. Different parts of the Eurocode cover different steps in the design process. Eurocode 0 [EN 1990, 2002] presents the basis of design with definitions of accidental actions and their combinations. Eurocode 2, Part 1-2 [EN 1991-1-2, 2003] presents the mechanical actions on structures in fire. The rules on determining material temperatures and member resistances in fire for both steel and composite members are presented in Eurocode 3, Part 1-2 [EN 1993-1-2, 2005] and Eurocode 4, Part 1-2 [EN 1994-1-2, 2006] respectively.

Eurocodes are based on the concept of limit states. There are two limit states distinguished, the Ultimate Limit State (ULS) and the Serviceability Limit State (SLS). ULS corresponds to ensuring that the structure is safe and there is no loss of stability or the formation of any mechanism that might cause the structure to collapse. SLS defines the state of usability of the structure, meaning that these are the requirements that have to be met in order for the structure to perform its designed function well. The fire situation is considered to be an accidental one and thus only the ultimate limit state is verified. The idea of resistance verification for the members is that the design member resistance is greater than the effect of the design mechanical actions on the member. The effects of the actions are calculated using the design values of the actions, and the resistances are calculated using the design values for the material properties. The design values of both arise from the semi-probabilistic approach to the problem. It is impossible to give the structure zero probability of failure using the specified safety factors, but this can be reduced to an acceptable level. Another purpose of the safety factors is to cover all the uncertainties in the method of calculation for the effects of the actions, and the resistances and variations in the assumed data.

The Eurocode considers 4 loads in the fire design situation:

- Design value of a permanent action – design value,
- Accidental action – design value,
- Dominant variable action – frequent value,
- Other variable actions – quasi-permanent values.

In most cases it is difficult to determine which of the variable actions is dominant, and usually all of them are analysed in turns. The Eurocode expression for that is:

$$E_{fi.d} = G_k + P_k + \Psi_{1,1} Q_{k1} + \sum_{i>1} \Psi_{2,i} Q_{ki} \quad (2.1)$$

where Q_{k1} is the variable action that is considered to be dominant at that moment. The coefficients of the load combination factors can be found in the national annex of Eurocode 0 [EN 1990, 2002] in table A1.1. The table from the Finnish national annex is shown below in Table 5.

Table 5. Coefficients for load combinations following Finnish NA to EN 1990

Load	ψ_0	ψ_1	ψ_2
Imposed loads in buildings, category (see EN 1991-1-1)			
Category A: areas in residential buildings	0.7	0.5	0.3
Category B: office areas	0.7	0.5	0.3
Category C: congregation areas	0.7	0.7	0.3
Category D: shopping areas	0.7	0.7	0.6
Category E: storage areas	1.0	0.9	0.8
Category F: traffic area, vehicle weight ≤ 30 kN	0.7	0.7	0.6
Category G: traffic area, 30 kN < vehicle weight ≤ 160 kN	0.7	0.5	0.3
Category H: roofs	0.0	0.0	0.0
Snow loads on buildings (see EN 1991-1-3), when			
s_k < 2.75 kN/m²	0.7	0.4	0.2
s_k ≥ 2.75 kN/m²	0.7	0.5	0.3
Ice loads	0.7	0.3	0.0
Wind loads on buildings (see EN 1991-1-4)	0.6	0.2	0.0
Temperature (non-fire) in buildings (see EN 1991-1-5)	0.6	0.5	0.0

At this stage it should be noted that there is no accidental action in the equation presented in Eq. 2.1. Fire actions are indirect and come from the restrained thermal expansion. Therefore, this is taken into account when the fire resistance is calculated. The effects of these actions can be calculated at time t=0, which is the starting point of the fire. In some cases, these actions can either be considered negligible a priori, or taken into account via conservative fire safety requirements.

THERMAL ACTIONS ON TEMPERATURE ANALYSIS

Eurocode 1, Part 1-2, Section 3.1 [EN 1991-1-2, 2003] defines thermal actions as being caused by the heat flux to the surface of the member. The heat flux ($\dot{h}_{net}$) consists of two parts:

$$\dot{h}_{net} = \dot{h}_{net,c} + \dot{h}_{net,r} \quad (2.2)$$

where:

$\dot{h}_{net,c}$ is the convective component,

$$\dot{h}_{net,c} = \alpha_c(\Theta_g - \Theta_m), \quad (2.3)$$

where:

α_c is the coefficient of heat transfer by convection [W/m^{2}K],

Θ_g is the gas temperature in the vicinity of the exposed member [˚C],

Θ_m is the surface temperature of the member [˚C].

$\dot{h}_{net,r}$ is the radiative component,

$$\dot{h}_{net,r} = \boldsymbol{\Phi} * \varepsilon_m * \varepsilon_f * \sigma * [(\Theta_r + 273)^4 - (\Theta_m + 273)^4], \quad (2.4)$$

where:

$\boldsymbol{\Phi}$ is the configuration factor,

ε_m is the surface emissivity of the member (for steel $\varepsilon_m = 0.7$),

ε_f is the emissivity of the fire,

σ is the Stephan Boltzmann constant ($\sigma = 5.67 * 10^{-8}\,\mathrm{W/m^2K^4}$),

Θ_r is the effective radiation temperature of the environment [°C]. For fully engulfed members it is the same as the gas temperature,

Θ_m is the surface temperature of the member [°C].

TEMPERATURE-TIME RELATIONSHIP

The temperature–time curve equations presented in [EN 1991-1-2, 2003] are used in the case of a fully developed fire. They describe the temperature in which the member is located. It can either be the compartment temperature (standard and hydrocarbon curves) or the temperature in the vicinity of the member (external curve). The equations describing all three curves in [EN 1991-1-2, 2003] are presented below.

- Standard ISO fire as a function of time (t) given in minutes:

$$\Theta_g = 20 + 345\log_{10}(8t + 1). \tag{2.5}$$

- External fire as a function of time (t) given in minutes:

$$\Theta_g = 660(1 - 0.687e^{-0.32t} - 0.313e^{-3.8t}) + 20. \tag{2.6}$$

- Hydrocarbon fire as a function of time (t) given in minutes:

$$\Theta_g = 1080(1 - 0.325e^{-0.167t} - 0.675e^{-2.5t}) + 20. \tag{2.7}$$

Additionally, Annex A1 of [EN 1991-1-2, 2003] presents another calculation method that corresponds more closely to the conditions of a specific structure. This is called the “parametric temperature – time curve”.

In addition to the temperature - time relationship related fire calculation, [EN 1991-1-2, 2003] allows the use of other calculation models. One of these is the zone model, which can be either the one-zone model, assuming uniform temperature distribution in a compartment or the two-zone model, assuming an upper, hotter zone of uniform temperature and a lower, cooler one. The thicknesses of the zones are also a function of time. The difference between zone models and parametric fire models is that the temperature development is a function of all the physical quantities (of walls and openings, etc.) and not only one parameter representing them all.

In the case of localised fires (where flash-over is unlikely to occur) the thermal actions of a localised fire should be taken into account. The method for calculating actions caused by localised fires is presented in Annex C (national) of [EN 1991-1-2, 2003].

[EN 1991-1-2, 2003] also allows Computational Fluid Dynamics models. These define the evolution of temperature in fire as being space and time dependent. This is the most accurate method to date, but it is also the most time consuming.

MATERIAL TEMPERATURE

As the temperature of steel and concrete increases, the mechanical properties degrade, i.e. the stiffness (Young's modulus) and resistance of the materials decrease. Determining the steel temperature is of the utmost importance when calculating the design resistance in fire situation. In some cases, the Eurocode allows the use of a critical temperature failure criterion. In most cases, the steel temperature is a differential of time. For an unprotected steel member with uniform temperature distribution the heating rate as defined in Eurocode 3, Part 1-2, Section 4.2.5.1 [EN 1993-1-2, 2005] is:

$$\Delta\theta_{a,t} = 0.9 k_{shadow} \frac{a_m/V}{c_a \rho_a} \dot{h}_{net,d} \Delta t \qquad (2.8)$$

where:

$\Delta\theta_{a,t}$ is the heat change over time Δt [°C],

k_{shadow} is the correction factor for the shadow effect, dependent on the shape of the cross-section.

a_m/V is the section (massivity) factor for the unprotected steel members [1/m]. This is the proportion of the surface area of the member per unit length to the volume of the member per unit length,

c_a is the specific heat of steel [J/kgK] (temperature dependent),

ρ_a is the unit mass of steel [W/m^2] (temperature dependent, but the change is negligible),

$\dot{h}_{net,d}$ is the design value of the net heat flux [W/m^2],

Δt is the time interval [s].

The above equation is just another form of conservation of energy between the amount penetrating the section and the amount modifying the temperature.

The Eurocode also covers the temperature calculation for members that are fire protected. However, practicing engineers generally use tabulated data provided by the manufacturer of the fire protection. This causes some legislative difficulties since all the fire protection systems need the appropriate approval.

In this study it is assumed that the beams and joints are sufficiently protected against fire for the beam resistance and stiffness not to drop. The resistances and stiffness of the beams and the joints remain unchanged compared to those in ambient temperature. Thermal elongations of the beams can be discounted. As shown in subchapter 2.3.5, the fire protection for the beams has little effect on the total cost of the structure, so the exact thickness of the fire protection is not calculated in this study. The columns, on the other hand, are assumed to be unprotected. Temperature distributions are taken from [TRY, 2004]. A more advanced method for determining the column temperatures in fire is

presented in, for example, [Nyman & Virdi, 2011] based on the Eurocode equations and the SAFIR program.

In this study only standard ISO fire is used.

MECHANICAL ANALYSIS

Listed below are the three levels for the analysis of the fire resistance of a structure.

- Whole structure. This is the most exact method, but since it requires a great deal of computational time and sophisticated tools it is usually only used for small structures.
- Isolated member. At this level, each member of the structure is analysed separately. In this case, each member is located between supports (foundations or joints). The fire resistance time for each member is calculated and the resistance time for the whole structure is the minimum time for any of its members.
- Substructure analysis. This lies somewhere between the above two methods and involves an analysis of a substructure composed of several elements.

The decision about which method to use rests with the designer. In this study the isolated member analysis is used.

CALCULATION MODELS

There are three calculation models used for the mechanical analyses. These models are dependent on the analysis method and they are:

- tabulated data; used for member analysis only,
- simple calculation models; used for members and substructures,
- advanced calculation models; mainly used for substructures and structures.

Tabulated data is based on tests. It is collected in tables, and as such can be used to get the closest fit to the given parameters. This study uses tabulated data for the column [TRY, 2004] temperatures in fire situation.

Simple calculation models are the most common. Eurocode 3, Part 1-2 [EN 1993-1-2, 2005] defines the criterion for a member's load-bearing function after time t using Eq. 2.9.

$$E_{fi,d} \leq R_{fi,d,t} \tag{2.9}$$

where:

$E_{fi,d}$ is the effect of actions,

$R_{fi,d,t}$ is the corresponding resistance after time t.

Indirect actions are not taken into account. The bending and axial stiffness used in the linear frame analysis is reduced due to the elevated temperature. The resistances of materials used in the calculation of $R_{fi,d,t}$ are also functions of temperature. This is the model used in this study.

Advanced calculation models are basically computer simulations of the structure in fire conditions, based on fundamental mechanics. The calculations for the thermal response and structural behaviour of the structure are usually done separately.

There are three different approaches to the calculation for determining the fire resistance of a member:

- the required resistance time is lower than the failure time:

$$t_{required} \leq t_{failure}, \tag{2.10}$$

- the effects of actions after the required time is lower than the resistance after the required time:

$$E_{fi.d} \leq R_{fi.d.t_{required}}, \tag{2.11}$$

- the temperature of the member after the required time is lower than the critical temperature:

$$\theta \leq \theta_{critical}, \tag{2.12}$$

In this study, the beams are assumed to comply with the first fire resistance criterion due to the provision of sufficient fire insulation. The columns are calculated according to the second criterion. The column resistance for the specified resistance class is calculated based on temperatures from tests and analyses collected in [TRY, 2004]. The temperatures presented in [TRY, 2004] correspond to specific times: 30 min, 60 min, 90 min or 120 min in ISO standard fire conditions [EN 1991-1-2, 2003].

2.3 Design procedure

This subchapter presents the main points of the design procedure for all the framing systems under consideration. It consists of load calculations, load combinations and the determination of load cases, preparation of the model for the static analysis performed with *frame3D* by Jussi Jalkanen [Jalkanen, 2007], the results of the static analysis, code verification of the members and, finally, cost estimations for the structure. The procedure is presented in here based on an example structure, however due to limited space only the principles are presented in the main text. The detailed numerical calculations can be found in corresponding appendices. The purpose of this subchapter is to show the principles of the feasibility checks that are performed for every structure in the optimization process.

2.3.1 Input data for the example

This subchapter presents the preparation of the input data for the *frame3D* program [Jalkanen, 2007] used for the linear frame analysis.

2.3.1.1 Main dimensions

The example building has two frames along the building axis (Figure 10). The frames are three storeys high and have two bays. The middle columns have different cross-sections than the edge columns. Both have one cross-section through all 3-storeys. Each storey is 3.6 m high. The beams spanning between the columns (Y) are 12 m long – measured

between the column axes. There is a hollow-core slab between the beams. The slab (X) is 14 m long, measured between the beam axes. The HC slab is chosen from manufacturer's catalogue [Parma, 2009]. The minimum slab thickness for a 14 m span is 320 mm (P32) with 60 mm of covering concrete. The chosen slab can carry 3.0 kN/m^2 imposed live loads, which is typical for an office building according to Eurocode 2, Part 1-1, Section 6.3.1.2(1) [EN 1992-1-1, 2004].

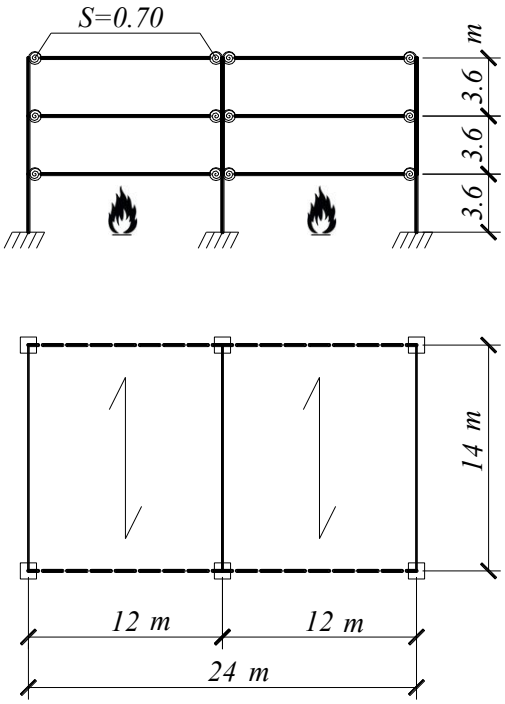

Figure 10. Layout of the example frame (TYPE 1A with semi-rigid joints)

2.3.1.2 Beams

The beams of the frame are welded Q-beams of the "EDGE" type (Figure 11). The beam material is grade S 355 steel. The nominal beam height (in this case 320 mm) is the height of the HC slab and was fixed in the analysis. The projecting parts of the bottom flange are 20 mm on the left for welding purposes (Figure 11), and 110 mm on the right. The right side of the projecting bottom flange is there to support the HC slab; 60 mm is needed to support a P32 HC slab (Table 1) and 50 mm is needed for the concrete filling between the slab and the beam web [TRY, 2009]. The point where the load from the slab is applied to the WQ-beam is shown in Figure 11 with an arrow. The point of loading is in the middle of the support width. The dimensions of the outer parts of the bottom flange are fixed, so the width of the bottom flange depends directly on the nominal beam width, in this case 300 mm. The dimensions of the beams and the columns were defined by the optimization, as is explained in the following chapters.

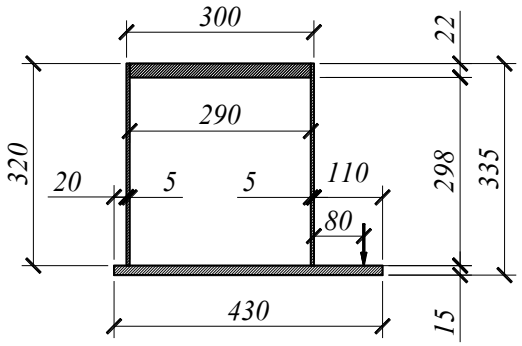

Figure 11. Dimensions of the cross-section of the example beam [mm]

The end fixity ratio (relative rotational joint stiffness S) of the beam elements is $S = 0.70$. For more details on the fixity ratio see subchapter 4.2.

2.3.1.3 Columns

Both column cross-sections – edge and middle – are concrete-filled square hollow sections. The concrete is grade C40/50, additionally reinforced with A500HW grade bars, and the steel tube is made of S 355 J2H. The dimensions of the optimized column cross-sections are shown in Figure 12.

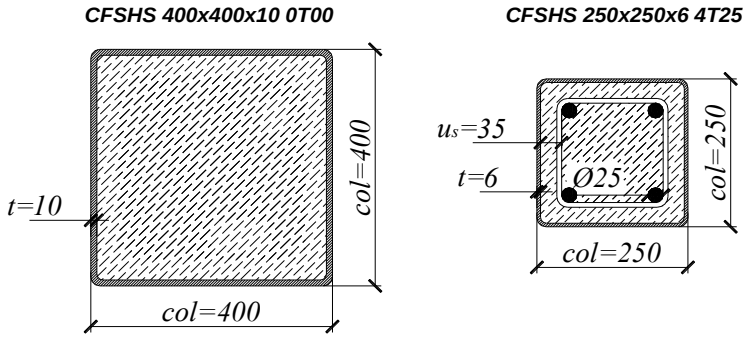

Figure 12. Cross-section dimensions of the edge (left) and middle (right) columns of the example structure [mm]

2.3.2 Data preparation for the static analysis

The linear static analysis is performed using the *frame3D* program by Jussi Jalkanen [Jalkanen, 2007] written in Matlab [Matlab, 2009]. The program can perform static, dynamic and stability analyses for three-dimensional frames. All the members are modelled as beam elements with 12 degrees of freedom at each node. This allows the use of semi-rigid joints for any degree of freedom for the element. The nodes are required as input data for *frame3D,* so for the purposes of the optimization the node matrix has to be automatically prepared for each analysed structure. This matrix is created in a slightly different way for each TYPE, but always using the main dimensions of the building: X, Y, x, y, H, m (See Figures 4 and 5). The structure is “growing”, meaning that the node numbers increase from the bottom up. After a two-dimensional grid has been created for the ground level, it is then duplicated and moved up a distance equal to the height of one storey (H). Following that, the top layer of nodes is duplicated and moved upwards, the whole process being repeated the required number of times, i.e. the number of storeys (Figure 13). This means that the

nodes of the columns are only located on the floor levels. The length of each column is equal to the height of a single storey. Each plane pattern of nodes is created from the characteristic points in the beams: ends, joints to columns, and intermediate hinges.

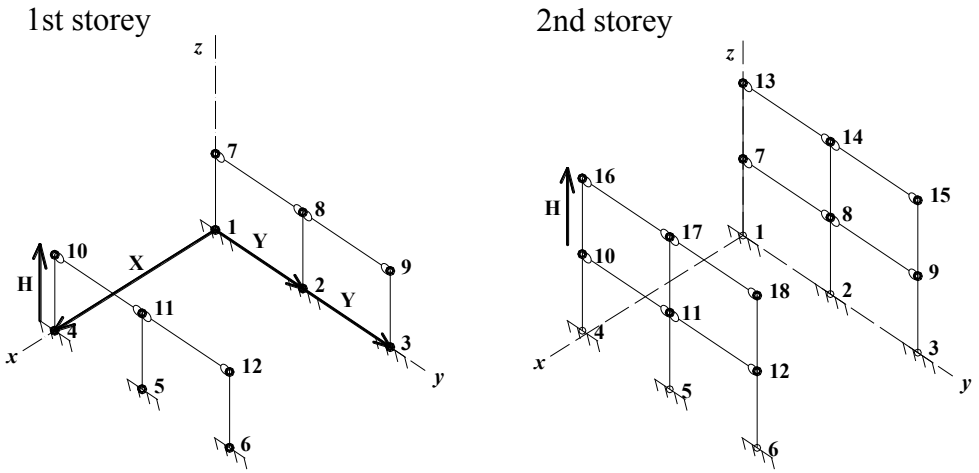

Figure 13. Node matrix creation

The beam elements in the structure always run along the *y*-axis, for both structure TYPES 1 and 2, meaning that the longitudinal axis of the building is along the *y*-axis for TYPE 1 and along the *x*-axis for TYPE 2. Each beam connecting two characteristic points is a single element. The elements are located so that they represent the centre of the rectangular part of the beam – point A – see Figure 14. Beam torsion occurring from the load applied to the bottom flange is prevented by the compression in the concrete filling between the beam web and the slab, and the tension in the reinforcement that goes through the beam and is anchored in the slab. This simplification could be made since the erection stage is not considered in this study.

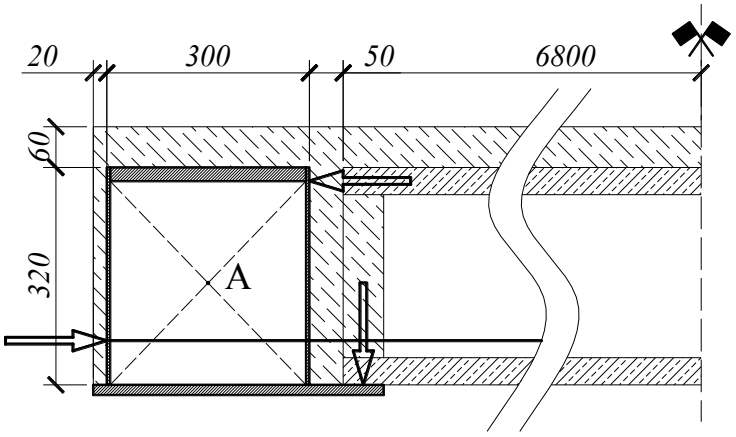

Figure 14. Main forces acting on the WQ-beam

The column elements always go up and the starting point of an element is always at its base.

In most of the structures in this study, the columns are fully fixed at the bottom. Since the horizontal loads are suppressed by concrete shafts, it is possible to use the requisite hinged joints for TYPES 1B and 2A. To ensure the stability of these structures, additional supports

in the horizontal direction were used at each floor level. Rotation in the plane perpendicular to the frame plane is always suppressed.

The input requires specification of the distributed and concentrated loads for all the members; the self weight of the members being calculated automatically based on the cross-section area and material properties. In order to simplify the calculations, the slabs (together with the covering concrete) are omitted in the static analysis. It is assumed that they collect loads from the floors and transfer them to the beams. The stiffening effect of the slab is not taken into account. Now, since the WQ-beams are modelled using only beam elements, it is impossible to apply the loads from the slab onto the bottom flange, so the beam is loaded along its axis, which is point A in Figure 14. The lateral bending of the bottom flange is checked separately, using the same load that is used for the loading of the beam. This also includes the live load and the covering concrete on the beam itself since the difference in the value is negligible. The torsion of the beam is not taken into account since, in the final design situation, the concrete filling between the beam web and the HC slab together with the reinforcement going through the beam and anchored in the slab (see Figure 14) prevent the beam from rotating. Therefore, the simplification of the beam loading position is safe and only the vertical loads on the beam are needed for the static analyses.

The *frame3D* program was originally written for steel members only. However, it also allows individual members to be defined using their stiffness. The axial and bending stiffnesses in both directions have to be provided for the static analysis. The torsional stiffness of all the elements is set to a high value, although this does not have any influence on the structure's statics since there are no loads causing torsion in any of the members.

2.3.2.1 Loads

DISTRIBUTED LOADS

As stated above, only the vertical loads on the beams are considered in this study. The calculation of the loads conforms to Eurocode 1, Part 1-1 [EN 1991-1-1, 2004] for the normal design situation and Eurocode 1, Part 1-2 [EN 1991-1-2, 2002] for the fire design situation. The imposed load on the floor is $q_k = 3.0\ \mathrm{kN/m^2}$ as in table 6.2 of [EN 1991-1-1, 2004] for a category B building, i.e. office areas. Detailed calculation of the live and dead loads applied to the frame is presented in Appendix A. The characteristic values of the loads obtained are:

- $Q_k = 21.51\ \mathrm{kN/m}$;
- $G_k = 38.00\ \mathrm{kN/m}$.

LOAD COMBINATIONS AND LOAD CASES FOR THE AMBIENT DESIGN SITUATION

For static calculations at ambient temperature the load combinations are made according to Eurocode 0, Annex A1 [EN 1990, 2002]. The load combinations are expressed in Eq. 2.13.

$$\Sigma\gamma_{G.j} * G_{k.j} + \gamma_{Q.1} * Q_{k.1} + \Sigma\gamma_{Q.i} * \Psi_{0.i} * Q_{k.i} \quad (2.13)$$

Detailed explanation of the used symbols is presented in Appendix A.

Since there is only one live load considered in this study, there will be only one upper and one lower load combination. The values of the favourable and unfavourable safety factors are presented in Table 6.

Table 6. Partial safety factors following EN 1990, Finnish National Annex A1, Table A1.2(B)

load	live	dead
unfavourable	1.50	1.15
favourable	0.00	0.90

Using the above factors, the upper and lower values of the design loads are calculated. The results for the example case are:

$$Sup = Q_{sup} + G_{sup} = 32.3\,\mathrm{kN/m} + 43.7\,\mathrm{kN/m} = 76.0\,\mathrm{kN/m} \quad (2.14)$$

$$Inf = Q_{inf} + G_{inf} = 0.0\,\mathrm{kN/m} + 34.2\,\mathrm{kN/m} = 34.2\,\mathrm{kN/m} \quad (2.15)$$

Depending on the structure type, there are 3 to 5 load cases considered in fire design situation. The load cases at ambient temperature cover different arrangements for the upper and lower loads on the beams in order to obtain the following effects of the loads:

- Load case 1 - greatest axial force in columns,
- Load cases 2-3 - greatest bending moment in beam span and in columns,
- Load cases 4-5 - greatest bending moment at the beam support.

Figure 15 presents all the load cases that have been used for **all types** of structures considered in this research. Because the number of beam spans for TYPE 1 structures is not fixed the form of *[0, 1]* vectors have been introduced to describe the loading patterns. Number *1* in the vector means the upper value of the load while number *0* means the lower one. Figure 15 presents the loads applied on the first floor of the building. The load on each consecutive floor has exactly opposite scheme. For example, if the load on the 1st floor is *[1, 0, 1, 0, 1]*, on the 2nd floor the load will be *[0, 1, 0, 1, 0]*. An example load case created using alternating vectors, for a structure with two bays, can be seen later in Figure 17. The only exception to this rule is the case *[1, 1, 1, 1, 1]* in which the load case vector stays the same on each floor to give maximum axial forces in the columns.

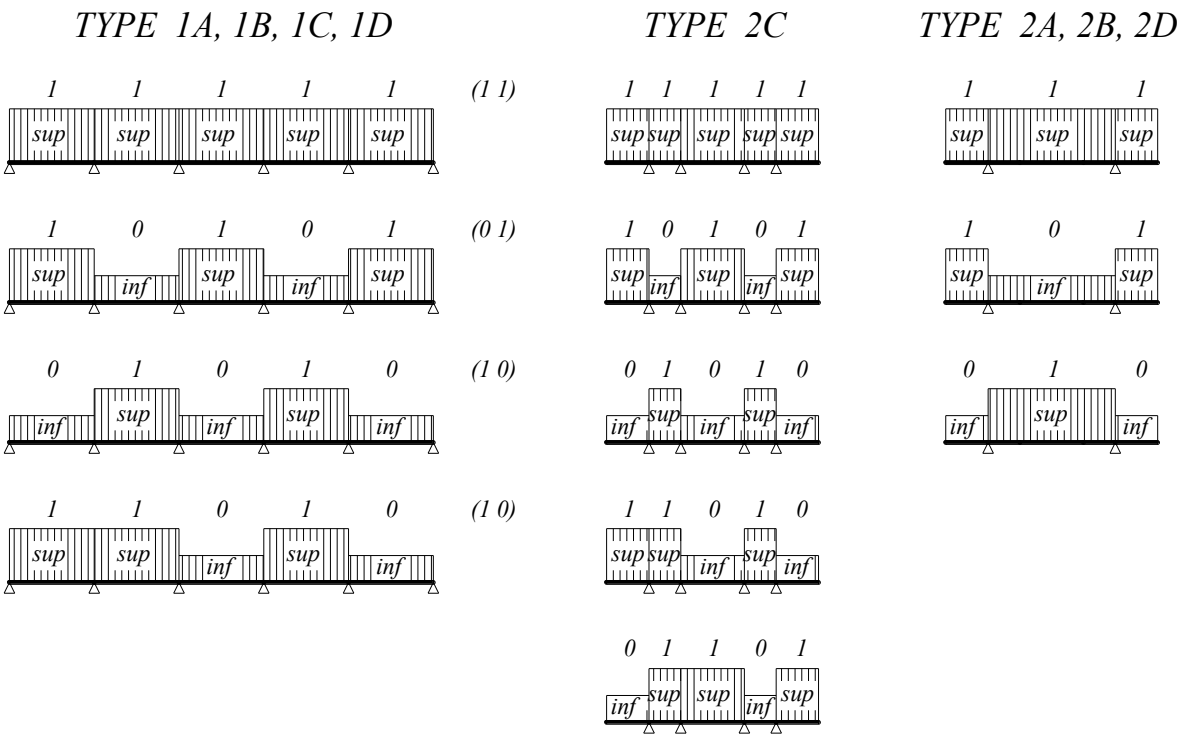

Figure 15. Scheme of load cases on ground floor beam for different structure types

LOAD COMBINATIONS FOR FIRE DESIGN SITUATION

For static calculations in fire design situation the load combinations are made according to Eurocode 0, Annex A1 [EN 1990, 2002]. In this case the load in fire has only one value as presented in Eq. 2.16. For of details fire load calculation please see Appendix A.

$$Fire = 44.5\,\mathrm{kN/m} \tag{2.16}$$

Unlike in the ambient situation, in fire there is only one load case. However, there are different locations for the fire. Since fire affects the stiffness of a member and thus the distribution of forces in the frame, this one load case in fire situation is used for the analysis of several “fire cases”. More details about the different stiffnesses for individual fire cases are presented later.

The influence of thermal expansion in fire situation is not taken into account in this study for the following reasons:

1. It is assumed that one whole storey is on fire at one time. It is typical in office buildings that one storey is one fire compartment. Because of this, it is assumed that the columns can elongate freely and at a uniform rate, thus not generating any internal forces in the frame.

2. In this study it is assumed that the beams and the joints are protected so that the beam elongation in fire is negligible, and the resistances and stiffness of the beams and joints in fire situation remain the same as in the ambient one.

3. The influence of fire on the WQ-beam and the moment distribution in a 3-storey, 2-bay frame was investigated in [Salminen & Bzdawka, 2011]. The studies showed that when the frames were designed according to assumptions 1 and 2 above, the frames could resist long times in fire even without fire protection for the WQ-beams. For more details see subchapter 4.2.3.

As mentioned earlier, the self weight of the frame elements was taken into account automatically in *frame3D.* Self weight of the composite column per meter is calculated from the cross-sectional areas of all three elements. The density of steel for the tube and reinforcement is 7850 kg/m^3 and the weight of normal density concrete without reinforcement is taken to be 2400 kg/m^3 as in [EN-1991-1-1, 2002]. The safety factor for the dead load of all three materials is 1.15. The weight of the beam is calculated using the density of 7850 kg/m^3.

CONCENTRATED LOADS

The console of the column on which the beam is resting causes eccentric loading for the column. The *frame3D* program doesn't account for eccentricities in the joints, so this effect has to be artificially implemented in the form of additional concentrated bending moment on top of the column. The eccentricity of the load on the column is the column width increased by a clearance of 20 mm [Hömmö, 2008]. However, the inaccuracies of the assembly also have to be taken into account. It has been assumed that the imperfection e is 5 mm [TRY, 2004]. On one side of the column the inaccuracy increases the eccentricity, while on the other it decreases it (see Figure 16). This means the eccentricity is $col/2$ + 15 or 25 mm. Due to the different load cases, it is difficult to say which case is the most unfavourable, the one with the 15 mm addition to the eccentricity or the one with 25 mm.

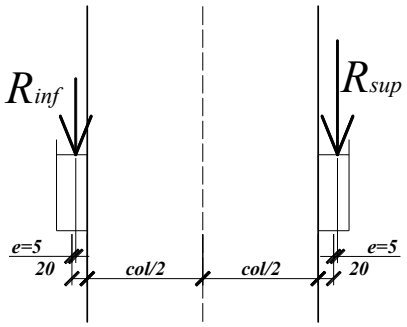

Figure 16. Eccentricities of column loading

This study does not consider the details of different joints in terms of their stiffness. It is assumed that all hinged and semi-rigid joints have a similar structure and the problem of eccentricity is only considered for those beam-column joints that aren't fully rigid. Thus, the problem of eccentric loading occurs only in TYPE 1A and TYPE 1C frames. Detailed explanation of how the bending moment for each column top is calculated is presented in Appendix A.

SUMMARY

The loads applied to the example structure in case 2 are presented in Figure 17. Vertical loads distributed on the beams are represented by the green colour, while the red vectors, with values in frames, represent concentrated moments applied to the column tops.

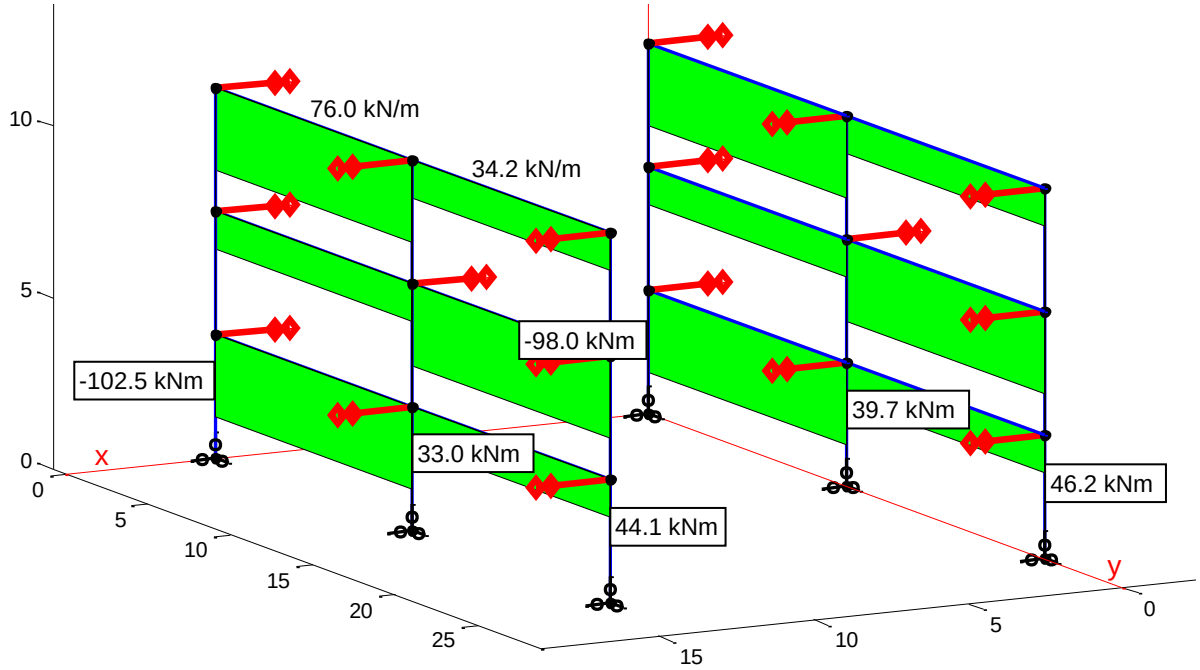

Figure 17. Scheme of forces applied to the model of the example structure – loading case 2 (concentrated moment values are given for the bottom column)

The concentrated bending moments in fire situation are calculated in a similar way but only using the loads of the one load combination that occurs in fire situation. The concentrated moment's values are 60.0 kNm and 57.4 kNm for the edge columns with 25 and 15 mm addition to the eccentricity respectively. The moment at the top of the middle column is 2.7 kNm.

Applying the pre-calculated moments to the tops of the columns allowed the use of a simplified static model where there are no eccentricities of the beam-column joints. All of the joints in the static model are in the axis of the column.

In the case of composite column design, the value of the permanent part of the load is required for the resistance calculation. Due to the large number of load cases considered in this study, and the varying number of columns in the different types of structures, instead of calculating the exact values for all the columns, a mean ratio of permanent load to total load is used. The ratio is 64 % - more details can be found in Appendix A.

One thing should be mentioned at this stage. Eurocode 1, Part 1-1, Section 6.3.1.2 [EN 1991-1-1, 2002] allows the use of reduction factors for imposed loads. The reduction factor α_A presented in point (10) [EN 1991-1-1, 2002] may be applied to live loads on floors and accessible rooftops. The α_n reduction factor – presented in point (11) of the referred section of [EN 1991-1-1, 2002] may be applied to all the imposed loads from several storeys for columns. These factors are mutually exclusive and they cannot be used simultaneously.

When the whole frame is analysed, as in this case, the lower live loads on the beams would cause lower axial forces in the columns, which would be incorrect. Thus the imposed load reduction factors α_A and α_n were omitted in this study.

2.3.2.2 Stiffness

To run the static analysis *frame3D* program, the stiffnesses of the individual members are required. *frame3D* was originally written for steel members only and was able to calculate the stiffness automatically for all the predetermined sections, such as welded I-sections. Since the beams in this study are welded box beams with a wide bottom flange, and the columns are composite, their stiffness has to be evaluated before the analysis and provided for the *frame3D* as input.

The stiffnesses calculation for the beams can be found in Appendix B and for the columns in Appendix C. Since the beam is fire protected and the beam temperature in fire situation is assumed not to increase significantly, the beam stiffness calculated for ambient temperature is used in static analysis in both normal and fire design situation.

As mentioned earlier, the column stiffness changes along with the change in temperature in fire situation. In this example, the fire resistance class of the structure is R 60, meaning that the structure is required to withstand 60 minutes of ISO fire [EN 1991-1-2, 2003]. The distribution of temperature in the column cross-section is taken from [TRY, 2004]. Depending on the temperature, the Young's modulus of all three materials of which the column is composed is reduced following tables 3.2-3.4 of Eurocode 4, Part 1-2 [EN 1994-1-2, 2006] – the tables and the stiffness calculation are presented in Appendix C.

It should be noted that due to the nature of Table 3.3 of [EN 1994-1-2, 2006] Young's modulus for the concrete is not the same for 20 ˚C in fire situation as it is in the ambient one. Because of this, and also the fact that in fire situation only parts of the columns are subjected to temperature increase, there are three different column stiffnesses that need to be calculated in order to run the static analysis. These are:

1. the column in normal situation, at 20 ˚C,
2. the column in fire situation, at elevated temperature,
3. the column in fire situation, at 20 ˚C.

2.3.3 Static analysis results

Static analysis is performed by the *frame3D* program. The results of the calculations used for the feasibility check are normal force, shear force and bending in plane of the frame.

The cross-sectional forces used for the resistance check of the example beams and columns can be found in Appendices B and C respectively.

Just to show how different are the bending moment distributions in the frame in normal and fire situations their plots are presented in following Figures. Figure 18 presents the bending moments in normal design situation while Figure 19 presents the bending moments in fire design situation with the fire on the bottom floor.

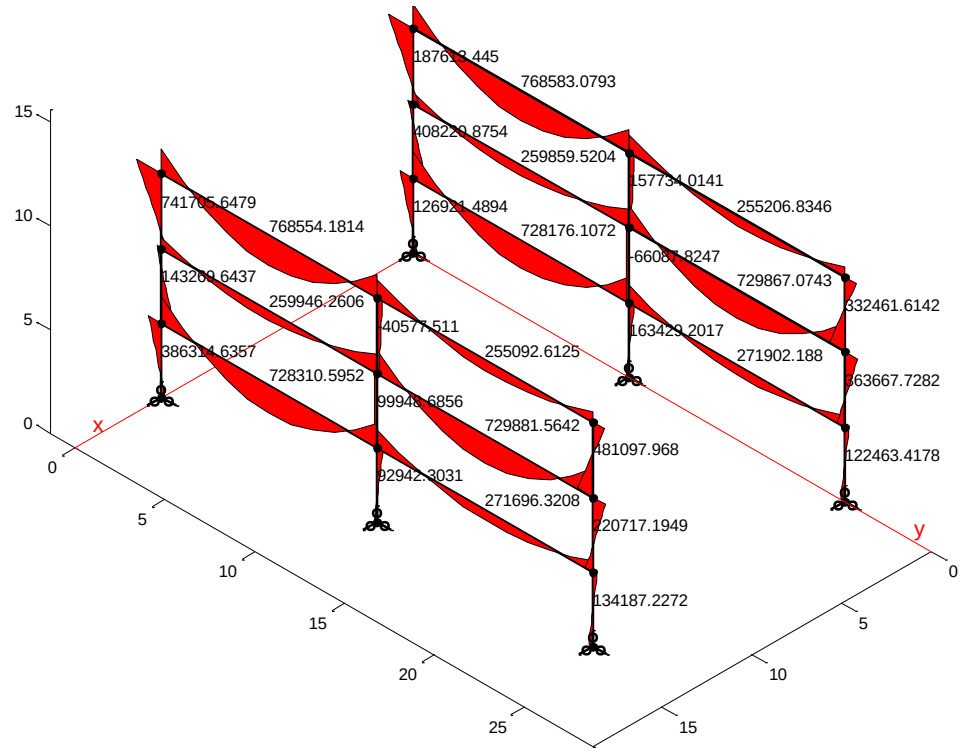

Figure 18. Bending moments [Nm] in the elements at ambient temperature for load case 2

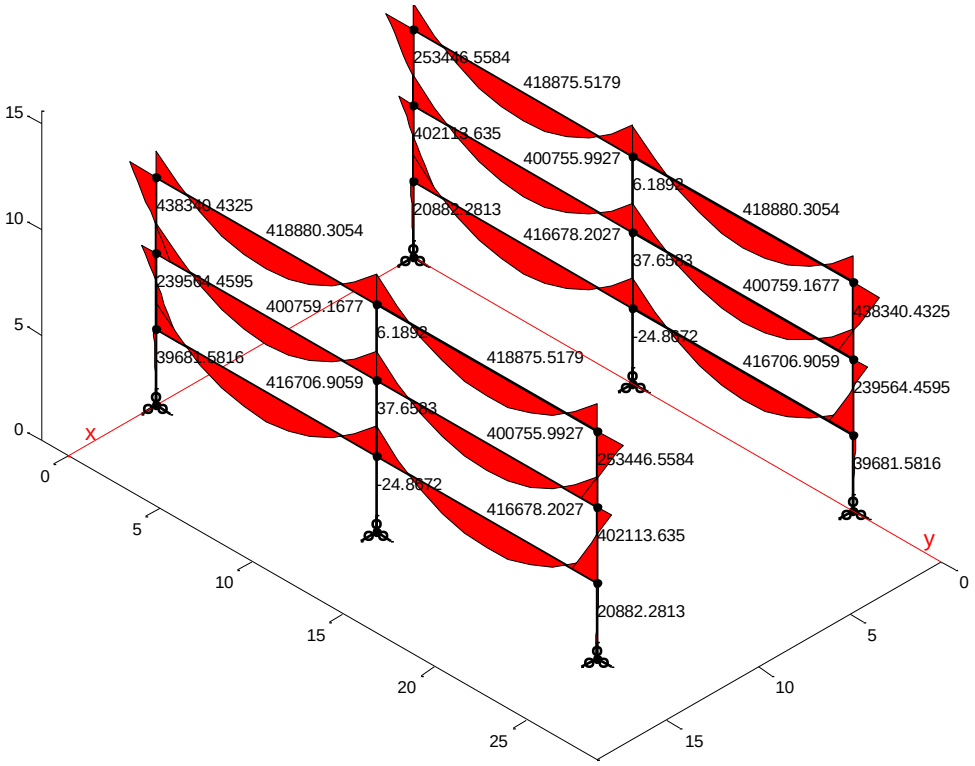

Figure 19. Bending moments [Nm] in the elements in fire for fire on the ground floor

2.3.4 Code verification

The structure's resistance is verified according to Eurocodes. The check is done for all the load cases for the normal design situation and for all the considered fire locations for the fire design situation. Since the columns have extreme bending moments at their ends and the shear force is constant, and the axial compression is maximal at the base, the code verification is performed only for the values at the column ends. In the beams there is interaction between the bending moment and the shear force. Because of the semi-rigid joints at the beam ends which are used in some of the structures, and the consequent variety in the distribution of the bending moment, it is difficult to determine where the most severe combination is. Therefore, the resistance check is performed in 11 cross-sections along the beam. It has been concluded that dividing the beam into 10 segments for which resistance will be verified is sufficient.

2.3.4.1 WQ-beam design

The evaluation of the beam's resistance is conducted separately for each element, cross-section and load case. The verification of the beam's resistance considers following aspects:

- resistance of bottom flange in lateral bending;
- shear resistance;
- bending resistance – together with moment increase caused by axial force;
- axial resistance;
- flange induced buckling.

For the sake of optimization some additional requirements regarding beams' shape are also considered. One of the requirements imposed on the WQ-beam is that the webs are at least class 3. The requirement is taken from Eurocode 3, Part 1-1 [EN 1993-1-1, 2005] and named $Class_{requirement}$.

All the requirements are collected in a $utility$ vector following Eq. 2.17.

$$utility = \left[Class_{requirement}, \frac{M_{p.Ed}}{M_{p.pl.Rd}}, \frac{\mathrm{V_{Ed}}}{V_{pl.Rd}}, \frac{\mathrm{V_{Ed}}}{V_{b.Rd}}, \frac{N_{Ed}}{N_{Rd}}, \frac{M_{Edy_{span}}}{M_{plRdy_{span}}}, \frac{N_{Ed}}{N_{Rd}} + \frac{M_{Edy_{span}}}{M_{plRdy_{span}}}, \frac{\frac{h_w}{t_w}}{k\frac{E}{f_{yf}}\sqrt{\frac{A_w}{A_{fc}}}} \right] \leq 1.0 \tag{2.17}$$

Appendix B presents the details of the resistance check for one example beam. The results of that check are briefly presented below. For the example beam at the end and in the middle of the span the $utility$ vectors are:

$utility_{sup} = [0.00,\ 0.304,\ 0.637,\ 0.780,\ 0.049,\ 0.793,\ 0.842,\ 0.371] \leq 1.0,$

$utility_{span} = [0.00,\ 0.304,\ 0.004,\ 0.005,\ 0.049,\ 0.948,\ 0.997,\ 0.371] \leq 1.0.$

For each beam element the highest utilities of the cross-section are recorded. For the example beam in load case 2 the utility vector describing the whole beam would be:

$$utility_2 = [0.00,\ 0.304,\ 0.637,\ 0.780,\ 0.049,\ 0.948,\ 0.997,\ 0.371] \leq 1.0.$$

The maximal utility ratios for the example beam in load case 1 are:

$$utility_1 = [0.00,\ 0.304,\ 0.647,\ 0.792,\ 0.062,\ 0.930,\ 0.992,\ 0.371] \leq 1.0.$$

The above shows that the beam profile that has been found is used very effectively. The utility ratios in both sagging and hogging moment are very high: 99.7% in the span in case 2 and 99.2% at the middle support in case 1.

2.3.4.2 CFHS column design

The column calculation follows Eurocode 4, Part 1-1 [EN 1994-1-1, 2004] for the normal design situation and Eurocode 4, Part 1-2 [EN 1994-1-2, 2006] for fire design situation. Based on those two codes *Betonitäytteisen teräsliittopilarin suunnitteluohje* [TRY, 2004] was written. [TRY, 2004] is the design manual for the CFHS columns written by the Finnish TRY association. It conforms to the Eurocodes but also supplements the data necessary for the calculation, such as the temperatures of the column cross-section in fire. [TRY, 2004] is in Finnish, but some examples of column calculations following [TRY, 2004] can be found in [Bzdawka, 2010].

Detailed calculations of the resistances of columns 1 and 13 (Figure 20) are presented in Appendix C. This chapter only highlights the requirements that have to be met and gives the final utilisation results for columns: 1, 2, 13.

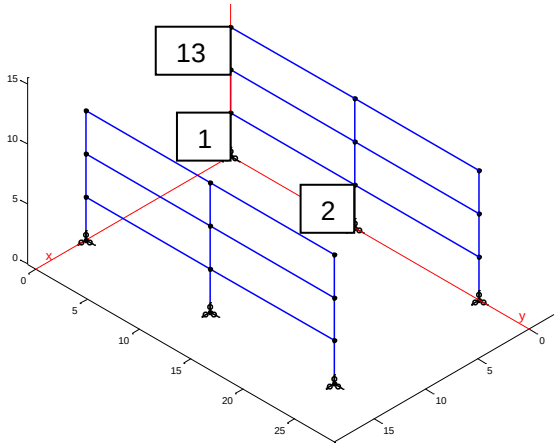

Figure 20. Notations of the example columns

In ambient temperature the maximum design bending resistance of the cross-section is given by the equation:

$$M_{max.Rd} = W_{pa} * f_{ad} + W_{ps} * f_{sd} + 0.5 * W_{pc} * f_{cd} \qquad (2.18)$$

In this case the forces in the cross section are not in equilibrium. An additional force from outside has to be exerted for the cross-section to achieve its full resistance. In a situation when the column is under pure bending. In that case, it is necessary to find the neutral axis of the cross-section as shown in Figure 21.

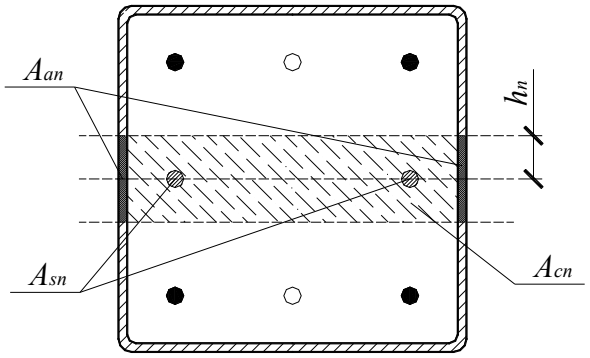

Figure 21. Symbols used in calculation of the neutral axis for column in pure bending

The distance between the neutral axis and the centreline of the cross-section is h_n. According to [TRY, 2004] the difference between the maximum plastic bending resistance and the plastic resistance in pure bending is equal to the plastic resistance of the material that is within h_n distance from the centre-line. Thus, the bending resistance of the cross-section is calculated from 2.19.

$$M_{pl.Rd} = M_{max.Rd} - W_{pan} * f_{ad} - W_{psn} * f_{sd} - 0.5 * W_{pcn} * f_{cd} \quad (2.19)$$

Where W_{pan}, W_{pcn}, W_{psn} are the section modules for steel, concrete and reinforcement, of areas A_{an}, A_{cn}, A_{sn}, respectively.

The axial resistance of the column is calculated in accordance with Eurocode 1994, Part 1-1, Section 6.7.3.5 [EN 1994-1-1, 2004]. A numerical calculation is presented in Appendix C.

Shear resistance is not normally the factor that determines the size of this type of column. In the most popular layout in Finland – continuous columns and simply supported beams, the bending moments in the columns only come from eccentric column loading. The bending moments are usually small and the corresponding shear forces are omitted in the resistance verification. [TRY, 2004] does not provide any information about the shear resistance calculation for CFHS columns. In this study, because rigid and semi-rigid joints are used, the bending moments and shear forces in the columns are considerably greater. The shear resistance of the column cross-section is calculated as the sum of the resistance of the steel tube and the reinforced concrete core. The shear calculation for the steel tube follows Eurocode 3, Part 1-1 [1993-1-1, 2005] and the shear calculation for the core follows Eurocode 2, Part 1-1 [EN 1992-1-1, 2004]. No composite action has been taken into account. A limitation has been imposed on the utilization of shear resistance so that it stays below 0.9. The influence of shear on the axial and bending resistance is not taken into account. In “normal” CFHS column design, shear resistance is not calculated. The stirrups that are used in the construction are only to keep the bars of longitudinal reinforcement in their designed position. In this study, their resistance in shear is taken into account. It is assumed that compression and bending are the drivers for the sizing of the cross-section, and if higher shear resistance is required, additional shear reinforcement would be used. The 0.9 limitation on the utility factor for shear was used in order to maintain some margin of safety. The numerical calculation of the column’s shear resistance can be found in Appendix C.

The second order effects can be accounted for, in accordance with Eurocode 3, Part 1-1, Section 6.7.3.4 [EN 1993-1-1, 2005]. In this example case $k = 1.0$ so the bending moment, including second order effects, is unchanged. For the detailed numerical calculation see Appendix C.

The calculation of the column bending resistance under axial load follows Eurocode 4, Part 1-1, Section 6.7.3.3 [1994-1-1, 2004]. The bending resistance is calculated from Eq. 2.20.

$$M_{Rd} = \alpha_M * \mu * M_{plRd} \tag{2.20}$$

where:

α_M is a coefficient dependent on steel grade

μ is a coefficient accounting for the influence of the axial force on the bending resistance. The coefficient is calculated using the graphical method presented in Appendix C.

The $utility$ vector for the column in normal design situation is written in a form of a vector presented in Eq. 2.21.

$$utility = \left[\frac{N_{Sd}}{N_{Rd}}, \frac{M_{Sd}}{M_{Rd}}, \frac{V_{Sd}}{0.9*V_{Rd}}\right] \leq 1.0 \tag{2.21}$$

For the example edge column on the top floor (column 13 in Figure 20), in load case 2, it is equal to:

$utility_2 = [0.052,\ 0.958,\ 0.184] \leq 1.0.$

The fire design description considers columns on the bottom floor, since this is where the fire is assumed to be. The stiffness and resistance of the materials, and thus the whole column, are lowered due to the temperature increase. The temperatures used in this study have been determined in tests for standard ISO fire conditions. They are collected in [TRY, 2004], and as such can be used for fire design in Finland. For instance the temperatures for the 400x400x10 0T00 column after 60 minutes taken from [TRY, 2004] are 889 ˚C for the steel tube and 335 ˚C for the concrete filling. Based on the tabulated temperatures the reduction factors for stress-strain relation for all three materials used in the columns are taken from tables 3.2-3.4 of Eurocode 4, Part 1-2 [EN 1994-1-2, 2006]. The numerical calculations for the example columns are presented in detail in Appendix C.

Most of the characteristics and resistances of the cross-section are the same as in the ambient design situation but calculated using the reduced material properties. One exception from this rule are the different values of the correction factors used in the calculation of bending stiffness. It should be also noted that the difference between maximal bending resistance and the resistance in pure bending is much greater than in normal design situation. For more detailed explanations see Appendix C.

For the example edge column (1) on the bottom floor the utility vector in fire situation it is:

$$utility_{fire} = \left[\frac{N_{Sd.\theta}}{N_{Rd.\theta}}, \frac{M_{Sd.\theta}}{M_{Rd.\theta}}, \frac{V_{Sd.\theta}}{0.9*V_{Rd.\theta}}\right] = [0.173,\ 0.340,\ 0.083] \leq 1.0. \tag{2.22}$$

The reserve in the bending resistance of the proposed cross-section is large. Even without taking the effect of the axial force into account, the pure bending resistance of the column is still greater than the bending moment in the column. This is due to the fact that the size of the edge column cross-section is determined in the normal design situation. At an ambient temperature, the bending moment in the column is much higher than in fire due to the higher bending stiffness of the column. Thus, the cross-section found in normal design situation is also sufficient in fire.

The columns that are not directly fire affected are also considered. Due to the lower rigidity of the ground floor columns, the bending moment distribution changes in the whole semi-rigidly jointed frame. The stiffness and resistance of the members that are not exposed to fire are different in fire situation than in ambient situation. The reason for the changed resistance values is the fact that material safety factors are 1.0 in fire design. This leads to higher member resistance. The stiffness of the column is lower than in the normal design situation due to the specific characteristics of concrete in fire, as defined in Eurocode 4, Part 1-2, Section 3.2.2 [EN 1994-1-2, 2006]. This, together with the low stiffness of the columns on the ground floor leads to different sectional force distribution and necessitates the verification of the members' resistance in fire design situation at 20 ˚C.

For the example edge column on the top floor (number 13 in Figure 20), the utility vector in fire situation is:

$$utility_{fire.20} = \left[\frac{N_{Sd.\theta.20}}{N_{Rd.\theta.20}}, \frac{M_{Sd.\theta.20}}{M_{Rd.\theta.20}}, \frac{V_{Sd.\theta.20}}{0.9{*}V_{Rd.\theta.20}}\right] = [0.026,\ 0.510,\ 0.132] \leq 1.0. \quad (2.23)$$

To summarise the design of the three example columns critical utilities are shown below.

For the edge column on the top floor (no. 13), for case 2 and fire respectively are:

$$utility_2 = [0.052,\ 0.957,\ 0.184] \qquad utility_{fire} = [0.026,\ 0.510,\ 0.132].$$

For the edge column on the bottom floor (no. 1), for case 1 and fire respectively are:

$$utility_1 = [0.152,\ 0.437,\ 0.101] \qquad utility_{fire} = [0.173,\ 0.340,\ 0.083].$$

For the middle column on the bottom floor (no. 2), for case 1 and fire respectively are:

$$utility_1 = [0.823,\ 0.011,\ 0.000] \qquad utility_{fire} = [0.862,\ 0.002,\ 0.000].$$

This short description, together with the detailed calculations in appendices, presents only some of the load and fire cases. The ambient design, as presented here, is performed for all the members in all the load cases. The fire design is performed for all the members, either at elevated temperature or at 20 ˚C, for all the fire cases. In this example structure, only one fire case has been considered, but for the 6-storey building (see subchapter 4.3) three different fire locations were considered. This illustrates the huge amount of calculations required to check the feasibility of a single particle. All the presented calculations are performed for all the individuals in the swarm at each iteration.

2.3.5 Cost calculation

The following subchapter will briefly present the principles of objective function calculation – structure cost. The more detailed presentation can be found in Appendix D.

A simplified method has been used to perform the cost calculation in this study. The unit prices for all the main elements are taken from a Finnish building construction cost data book [Haahtela, 2005] and these constitute the overall cost of the structure in question. The considered elements are widely used, and for all of them the unit price given in [Haahtela, 2005] accounts for manufacturing, transportation and erection on site. All the costs used in the calculation are taken at price level "75" – corresponding to the Helsinki region.

The cost of a WQ-beam consists of two elements: the welded steel beam and fire protection. The column cost consists of: steel tube, concrete filling and reinforcement. If steel of a grade other than S 355 is used (either for beams or columns) the calculated cost of the pure steel elements is multiplied by a factor corresponding to the difference between the prices of the steel. The proportions used in this calculation are presented in Table 11 (Chapter 4.1.1). When summarised, all the above give what is referred to as "frame cost". On top of that is the cost of floor elements – hollow core slabs and reinforced topping concrete. Frame cost together with floor cost gives "Structure cost".

The costs of the example structure are collected in Table 7. The costs of the individual elements are written in the column "Price per piece". The next column shows the number of pieces. For the columns and beams, this is the number of them in the structure; for the floors, this is the number of storeys, since the cost of the floor is calculated for the whole area of a single storey (Appendix D). Table 7 also shows how much of the total cost is accounted for by the elements. A similar cost analysis is presented in Table 8, but this covers only the cost of the frame and omits the cost of the floors. Figure 22 collects the results from both tables to present them more clearly. The left pie chart shows how much of the structure cost is due to the frame and the floors, while the one on the right divides the frame costs according to the materials that were used.

Table 7. Analysis of the costs of the structure

Structure cost analysis			Price per piece [€]	no. of pcs. [1]	Total structure cost [€]			Part of Total [%]	
Column	Steel tube	edge	733.05	12	8797	10973	12376	10.0 %	8.8 %
		middle	362.69	6	2176				
	Concrete filling	edge	66.05	12	793	943			0.8 %
		middle	25.01	6	150				
	Reinforcement	edge	0.00	12	0	460			0.4 %
		middle	76.73	6	460				
Beam	Steel beam		2963.80	12	35566		36570	29.4 %	28.6 %
	Paint		83.68	12	1004				0.8 %
Floor	HC slab		18850.00	3	56550		75396	60.6 %	45.5 %
	Concrete cover		2760.10	3	8280				6.7 %
	Reinforcement		3521.90	3	10566				8.5 %
					SUM:	124342			

Table 8. Analysis of the costs of the frame

Frame cost analysis			Price per piece [€]	no. of pcs. [1]	Total frame cost [€]			Part of Total [%]	
Column	Steel tube	edge	733.05	12	8797	10973	12376	25.3 %	22.4 %
		middle	362.69	6	2176				
	Concrete filling	edge	66.05	12	793	943			1.9 %
		middle	25.01	6	150				
	Reinforcement	edge	0.00	12	0	460			0.9 %
		middle	76.73	6	460				
Beam	Steel beam		2963.80	12		35566	36570	74.7 %	72.7 %
	Paint		83.68	12		1004			2.1 %
						SUM:	48946		

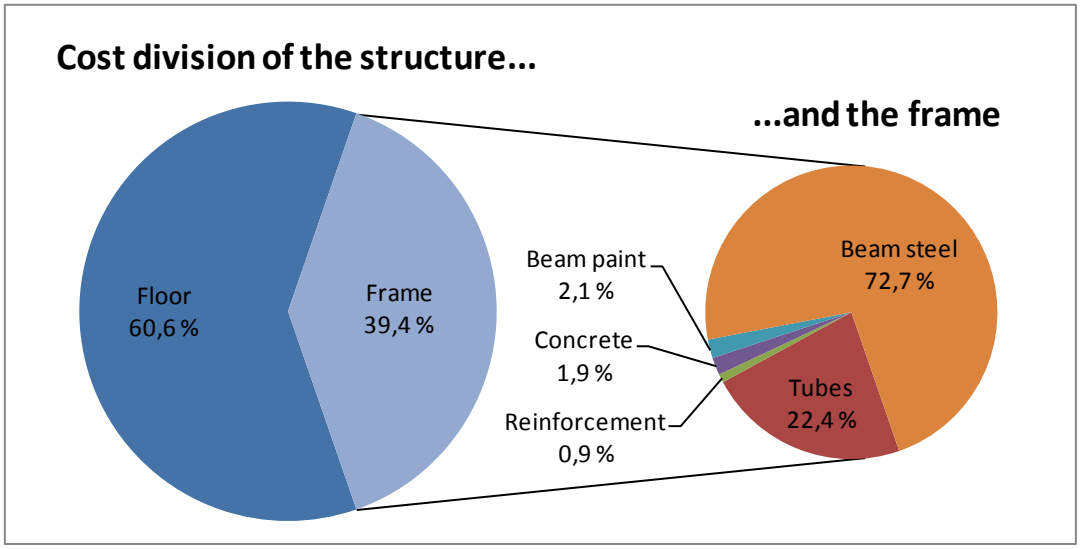

Figure 22. Division of costs

Figure 22 shows how great part of the total structure cost is constituted by the HC slab floor. This is the first indicator that the objective function of the optimization will be governed by the slabs. Another notable feature is that the beams constitute about 3/4 of the frame cost. In an optimization, this will lead to a solution that favours lighter beams over lighter columns.

3 OPTIMIZATION

The first part of this chapter presents the algorithm for Particle Swarm Optimization. The aim of this part is to give the reader an insight into how the PSO algorithm proceeds in the search for an optimum solution and what are the parameters that influence that process. The first part of this chapter shows the basic PSO algorithm while the second part shows what the objective function, design space, constraints etc. are in this specific case. The chapter ends with an example of performance of the algorithm.

3.1 Particle Swarm Optimization algorithm

The idea behind Particle Swarm Optimization (PSO) is to simulate a group of animals (swarm of bees, school of fish, flock of birds) in their search for food. Each individual in the group knows its best location so far. It also "sees" where the individual that has found the most food is. Based on these two directions, and the direction in which it is already moving, the individual looks for a better food source. Thanks to the information they all have and share, the swarm gains a lot of advantages in this search compared to a lone individual.

Taking that principle into an optimization algorithm we get a number of particles i that move in turns (iterations). The number of current iteration is k. Each particle has a current location in the design space $\mathbf{x}_k^i$, and at each step it moves to a new location $\mathbf{x}_{k+1}^i$ with a velocity of $\mathbf{v}_{k+1}^i$. As mentioned earlier, the speed vector consists of 3 factors as shown in Eq. 3.1.

$$\mathbf{v}_{k+1}^i = w\mathbf{v}_k^i + c_1 r_1\left(\mathbf{p}_k^i - \mathbf{x}_k^i\right) + c_2 r_2\left(\mathbf{p}_k^g - \mathbf{x}_k^i\right) \tag{3.1}$$

where:

w is inertia. This controls how wide the search of the design space is, usually between 0.8 and 1.4 [Jalkanen, 2007]. This value can be changed dynamically to explore a bigger area at the beginning of the optimization and to focus on the most promising in the end,

c_1 is a factor controlling cognitive behaviour, indicating how much the particle trusts itself,

r_1 is a random factor (between 0 and 1) for the cognitive part of the velocity vector,

$\mathbf{p}_k^i$ is the best location so far for the particle i,

c_2 is the factor controlling collective behaviour, indicating how much the particle trusts the group,

r_2 is a random factor (between 0 and 1) for the collective part of the velocity vector,

$\mathbf{p}_k^g$ is the best location so far for the whole swarm.

A graphical representation of the position updating is shown in Figure 23.

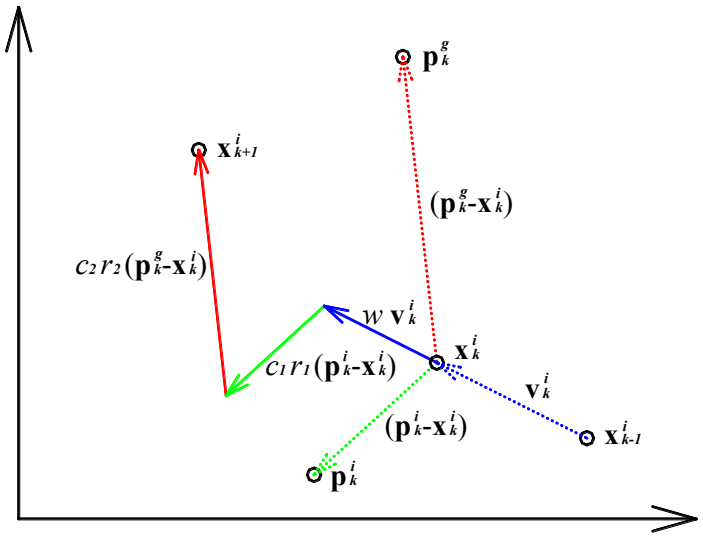

Figure 23. Calculation of the new position of particle i

This kind of position calculation is good for a continuous design space. However, in this study discrete values are used for all the design variables (see chapter 3.2). Therefore, the new locations of the particles, calculated in the manner shown in Figure 23, have to be rounded up or down to the closest permitted value.

In this study, the evaluation of the found position consists of a feasibility check and a cost calculation. The feasibility of the solution is verified in accordance with the requirements for structures laid down in Eurocodes – as presented in subchapter 2.3.4. These are the resistances of the members in normal and fire conditions, and also include the requirements for the cross-section classes, etc. A more detailed explanation of the imposed constraints is presented below in subchapter 3.2. If the constraints are validated, the result of the cost function calculated for the particle gets penalized. Each constraint that has a value greater than 0 is multiplied by the penalty factor and added to the total value of the penalty. The starting value of the penalty is 1. The cost of a solution is then multiplied by the total penalty.

At each step of the iteration, local and global optima are updated. For a minimisation function, if the value of the objective function for particle i in point $\mathbf{x}_{k+1}^i$ is lower than the minimum that has been found so far (f_k^i) for that particle, then the particle location becomes the new local minimum and the objective function value is kept for future searches (Esq. 3.2 – 3.3).

If $$f\left(\mathbf{x}_{k+1}^i\right) < f_k^i \tag{3.2}$$

then $$\mathbf{p}_{k+1}^i = \mathbf{x}_{k+1}^i \quad \text{and} \quad f_{k+1}^i = f\left(\mathbf{x}_{k+1}^i\right). \tag{3.3}$$

Similarly, the global optimum is calculated for $\mathbf{p}_{k+1}^i$ that gives the lowest f_{k+1}^i. The lowest objective function is for argument $\mathbf{y}$ and is calculated using Eq. 3.4.

$$\mathbf{y} = \arg min\left(f\left(\mathbf{p}_{k+1}^i\right)\right) \tag{3.4}$$

If $$f_k^g > f(\mathbf{y}) \tag{3.5}$$

then $$\mathbf{p}_{k+1}^g = \mathbf{y} \quad \text{and} \quad f_k^g = f(\mathbf{y}). \tag{3.6}$$

After the local and global optima are updated, the iteration number k gets increased by 1 and the next iteration takes place. The flowchart of PSO is presented in Figure 24.

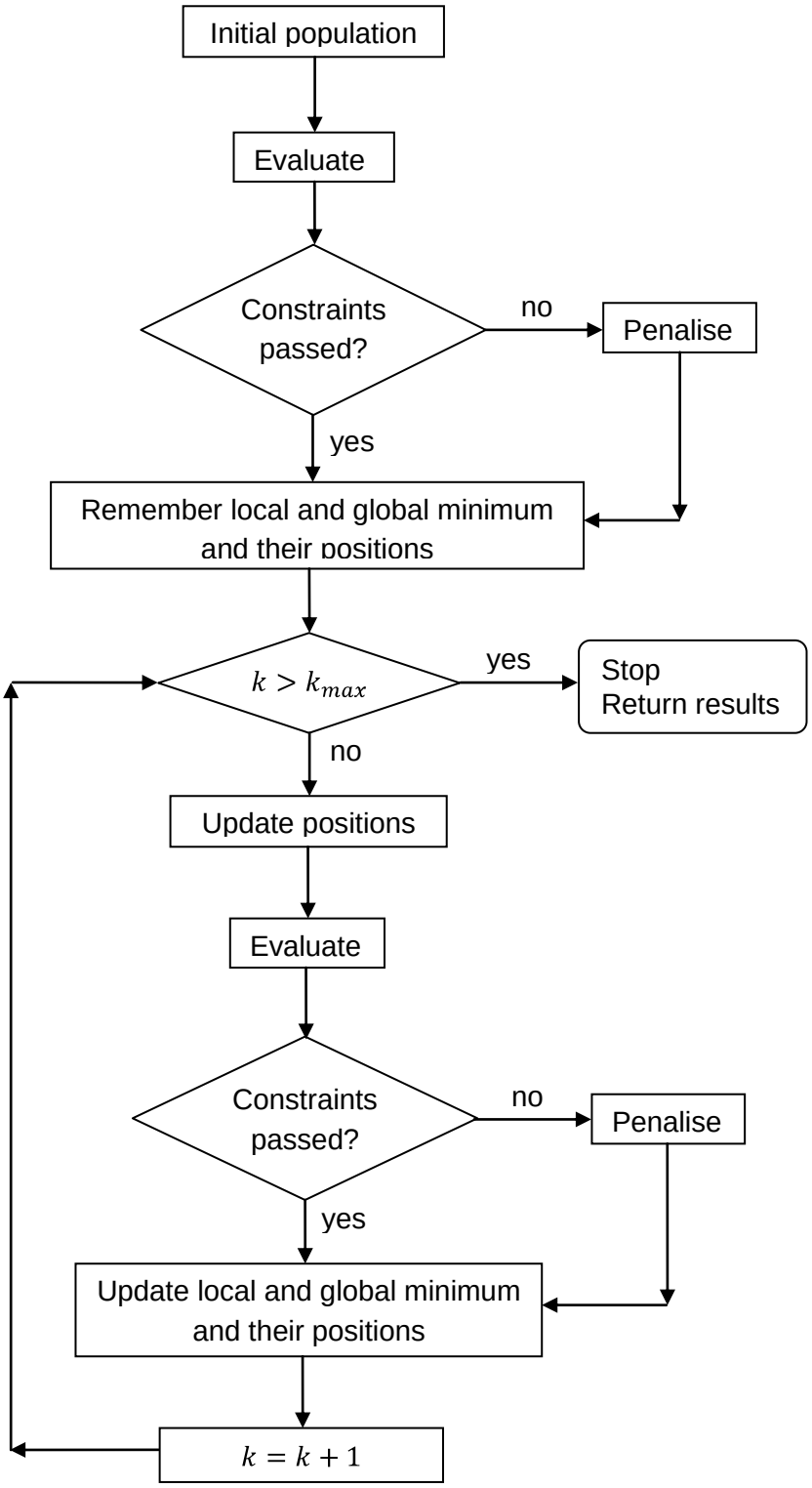

Figure 24. Particle swarm optimization flowchart.

The PSO procedure can be stopped when the convergence with certain accuracy has been reached or when a predetermined number of iterations have been completed. Because in this study there are very many cases considered in the optimization, to limit the time required for the optimization, the condition of the number of iterations was used. The risk of convergence not being reached and the minimum not being found was reduced thanks to a number of PSO runs that were performed. Since PSO is a stochastic algorithm the risk that a local minimum has been found is too great when considering only a single run.

3.2 Data for optimization

The following subchapter presents the main parameters of the optimization. In the light of what was presented in the previous chapter, this one describes what the design space for the optimization is, what the constraints that limit it are, and what the objective function is.

3.2.1 Space

In general, the design space is the different plate thicknesses for the WQ-beam, the width of the beam and the different columns. The dimensions of the building are always fixed, and if a set of different building sizes are considered it means that all of them are optimized separately. For the structures with semi-rigid joints the joint stiffness can be a variable or it can be fixed.

The other main dimensions or characteristics of the building are fixed in the optimization process. Some of these are constant for all the analyses, while others vary for the different PSO runs that are performed. The design data that are fixed all the time and those that vary are listed in Table 9.

Table 9. Fixed data in the PSO procedure.

Fixed all the time	Number of bays	2				
	Storey height	3.6 m				
	Live load	3.0 kN/m^2				
Varying for different analasyses	Number of storeys	1	3	6		
	HC slab	P20	P27	P32	P40	P50
	Material grade combination	S 355	S 460	S 700		
	Fire resistance class	R 30	R 60	R 90	R 120	

Defining the design space varies greatly depending on the specific case considered. The smallest space considered was 280 800 and the biggest was ~10^{12}. More details about the design space for each analysis conducted are shown in chapter 4, where the results are presented.

3.2.2 Constraints

All the constraints used in the optimization come from the Eurocode requirements together with the Finnish design guidelines for the beams and columns. All of them must be met for all the ambient and fire design situations. All the code requirements are collected in the form of $utility$ vectors (see subchapter 2.3). In this form, all the utilities below 1.0 mean that the requirement has been met and the solution is feasible. All those greater than 1.0 have not been met and indicate an unfeasible solution. However, the PSO program *JJPSO* by Jussi Jalkanen [Jalkanen, 2007] requires the constraints in such a form that the feasible

ones are lower than zero and the unfeasible ones are higher than zero. Thus all the utility vectors are decreased by 1.0 and used in this form in this optimization algorithm to verify whether the individual is feasible or not.

3.2.3 Objective function

There are two main points of interest in this study: the cost of the whole structure – slabs, beams, and columns, and the cost of just the frame, i.e. beams and columns. The slabs account for more than 50 % of the total structure cost (see subchapter 2.3.5). The cost of a slab is dependent mostly on its height and the thickness of the covering concrete, and these are the functions of the slab span. If we consider the cost of the structure per square meter of floor, there will be a different number of columns per one meter, so the ratio between structure cost and frame cost will keep changing. As long as the building dimensions keep changing there will be different optimum solutions found, depending on which is the objective function, i.e. the structure or the frame cost. When the building dimensions are fixed then it no longer makes a difference what the objective function is. The primary objective of this study is to minimise the total structure cost. The optimal solution for the structure is not always optimal for the frame, (see subchapter 4.1). When the building dimensions do not change, the solution found is optimal simultaneously for both costs (subchapters 4.2 and 4.3).

3.2.4 Governing factors

Usually PSO can offer good results when used in discrete or mixed integer problems. However the quality of the results is unknown and it may happen that it is sometimes far from the global optimum. There is no certainty that global minimum will be found. If the governing parameters are chosen improperly it may be also happen that even local minimum is not found. For example if inertia is too great and the particles keep overshooting the solution they are approaching. Fortunately the risk of not finding the global minimum can be reduced: large number of particles in the population and large initial inertia assure that the design space is combed thoroughly. Factor responsible for collective behaviour directs the procedure toward promising areas while factor responsible for cognitive behaviour ensures careful search through that area. Decreasing inertia helps avoiding overshooting the minimum in latter stage of optimization. In the end a number of PSO runs is performed to reduce the risk even further. From an engineer's point of view even if the global optimum is not found but the result is very close to it the solution can be considered good enough. This is one of the reasons why PSO is increasingly popular in structural optimization.

Table 10 presents the guiding parameters used in the optimizations of 1, 3 and 6-storey buildings. The values for the population size were tuned for the size of the design space. The number of feasible solutions depended on how difficult it was to get them in a randomly created population. Values given in Table 10 come from a number of trials. These are the ones that gave the fastest convergence.

The last two lines of Table 10 present also the total number of function evaluations for each considered structure compared to the approximate size of the design space. More details of the design space, together with the exact numbers, can be found in Chapter 4.

Table 10. Governing factors of PSO for different population sizes

	1-storey building	3-storey building	6-storey building
Population size	20-30	50	50
No. of feasible solutions in initial population	20	20	5-10
Number of iterations	50	50	100
Initial inertia	1.4	1.4	1.2
Inertia reduction coefficient	0.8	0.8	0.8
No. of iterations after which the inertia is reduced if the goal function is not improving	5	5	5
Cognitive behaviour factor	2.0	2.0	2.0
Collective behaviour factor	2.0	2.0	2.0
Penalty factor for unfeasible solutions	2.0	2.0	2.0
Total number of function evaluations	5,000 - 7,500	50,000	100,000
Approximate size of the desing space	280,000 - 65 mln	4.3 mln - 380 mln	1,5 bln - 10^12

3.3 PSO performance

The plot presented in Figure 25 shows the improvement of structure cost per square meter as a function of iteration number. The plot was made for the case of 3-storey building with varying joint stiffness. The design space was 380 millions – for more details see chapter 4.2.

Figure 25 also shows that the mean of the cost function decreases rapidly in the first stage of optimization and flattens out in the later. The number of feasible solutions in the randomly created initial population was set to 20. This gave quite good initial guess and thus the improvement in the initial stage is not as rapid as in examples found in the literature [Jalkanen, 2007].

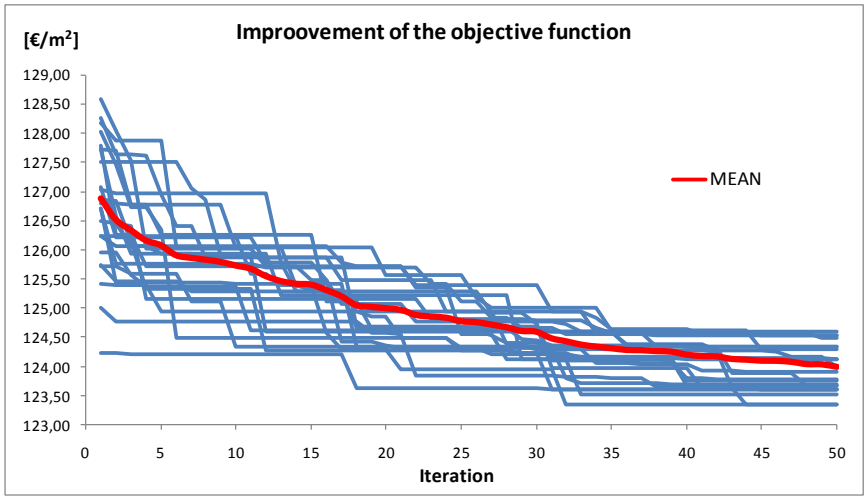

Figure 25. PSO performance – 3-storey building with variable joint stiffness and R60 class.

4 RESULTS

The conducted study investigated all 7 static layouts presented in Figures 4 and 5 in search of the most economical one. First, one-storey buildings were investigated to compare the cost effectiveness of different building dimensions for different layouts without taking fire conditions into account. Based on the initial results, one of the layouts was chosen for further analyses of multi-storey frames. 3 and 6-storey buildings with semi-rigid joints were analysed. The smaller, 3-storey, building was investigated for a wide range of joint stiffnesses and to determine their influence on the behaviour of the WQ-beam in fire. A sensitivity study of the solution with regard to changing unit prices was also investigated. The larger, 6-storey building was studied for the use of semi-rigid joints in more complex structures; this building had different column cross-sections for the bottom three and the top three floors, and different beam cross-sections on the top floor than on the other floors. This chapter presents the result of the analyses of the 1, 3 and 6-storey buildings.

4.1 1-storey building

The layouts of the structures considered in this part are presented in Figure 26.

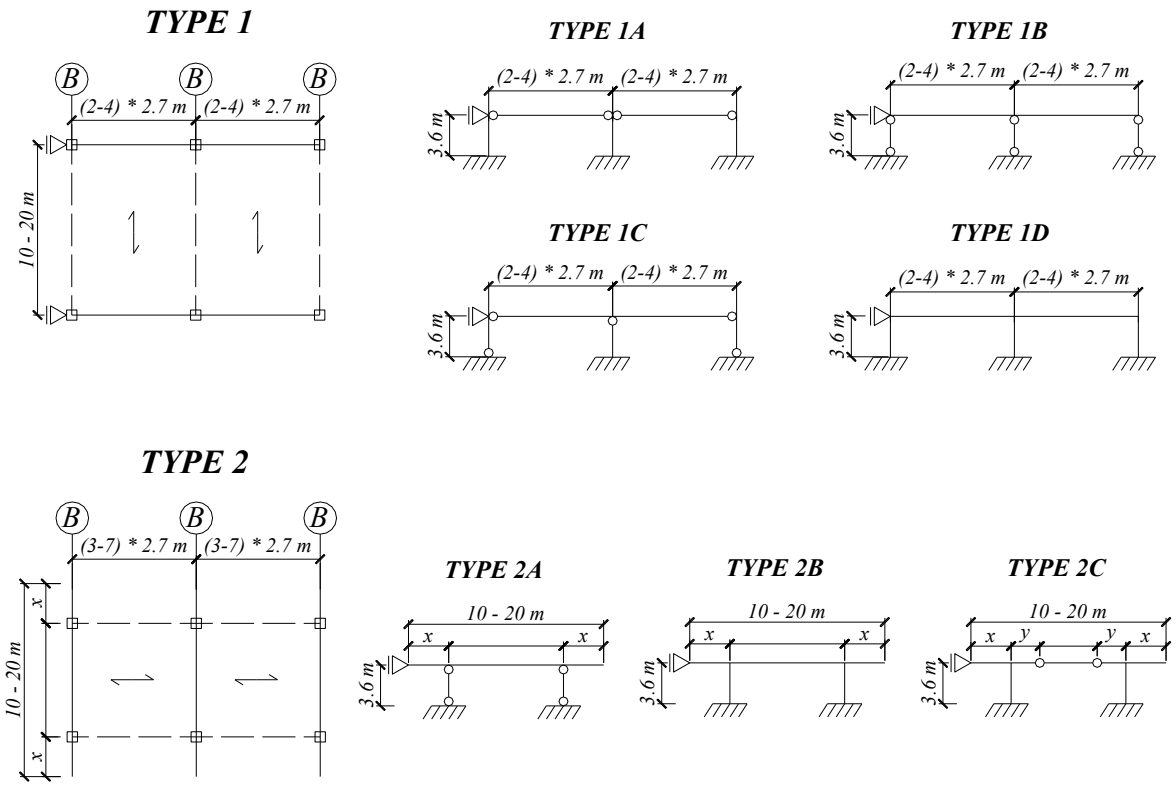

Figure 26. The analyzed one-storey buildings

All the buildings are single-storey and have two bays. The height of a single floor was set at 3.6 m. Each building was investigated for a number of varying dimensions. The width of the building varied from 10 to 20 meters in steps of 0.5 meters. This dimension was one of those referred to as grid dimensions. The other was the column spacing along the building. It was the width of a single parking space times a natural number (k). The width of a parking place is 2.7 m, and the number k ranged from 2 to 4 for TYPE 1 structures and

from 3 to 7 for TYPE 2 structures. In other words, the column spacing along the building was 5.4 to 10.8 m in 2.7 m steps for TYPE 1, and 8.1 to 18.9 m in 2.7 m steps for TYPE 2. The building width and the column spacing along the building are referred to as grid dimensions. The optimization was performed for 63 different dimension combinations for TYPE 1A-1D and 2B-2C, and 105 for TYPE 2A. The HC slab dimensions were a direct function of the building dimensions (see subchapter 2.1). The dimensions that are listed below were the variables in the optimization.

x – is the cantilever part of the beam in proportion to the length of the whole beam (building width). This variable was only used for TYPE 2 structures. It is in the range of 10-30 % and the step is 1 %.

y – is the distance between the inner node of the beam and the column in proportion to the length of the whole beam (building width). This variable was only used for TYPE 2C structures. It is in the range of 5-15 % and the step is 1 %.

b_{f1} – is the nominal beam width and varies between 200 and 390 mm with a 10 mm step.

t_{f1} – is the thickness of the beam's top flange. The whole range of plate thicknesses shown in chapter 2.1: $t_{f1} = \{10,\ 12,\ 15,\ 18,\ 20,\ 22,\ 25,\ 30,\ 35,\ 40\}\ \mathrm{mm}$.

t_{f2} – is the thickness of the beam's bottom flange. The whole range of plate thicknesses shown in chapter 2.1 is in use: $t_{f2} = \{10,\ 12,\ 15,\ 18,\ 20,\ 22,\ 25,\ 30,\ 35\}\ \mathrm{mm}$.

t_w – is the thickness of the beam's web. The whole range of plate thicknesses shown in chapter 2.1 is in use: $t_w = \{5,\ 6,\ 8,\ 10\}\ \mathrm{mm}$.

col_num - is the number of column cross-section chosen from Table 2. At this stage only the original columns of [TRY, 2004] are in use: $col\_num = \{1 : 45\}$.

At this stage, only ambient temperature analysis was conducted. The dimension u_s, which is the distance between the inside surface of the steel tube and the outer surface of the longitudinal reinforcing bars, meets the requirements of [TRY, 2004] for fire class R 60.

The number of variables depends on the structure type. The design space for TYPE 1A, 1B, 1C and 1D structures is 280,800 options, for TYPE 2A and 2B it is 5,896,800 and for TYPE 2C it is 64,864,800.

For each set of dimensions, there were 5 PSO runs completed. It should be noted at this stage that the analyses made for 1-storey building were only preliminary and the task was to choose one of the layouts for further investigation. 5 runs is usually not enough for stochastic algorithms but in this case the lines that were drawn based on the results are used only to show the trend of the cost function. Because of that even if one of the results is far from the optimum (the point in the plot is far from neighbouring points) it is singled out and simply not taken into account.

For TYPE 1 structures the number of particles was set to 20 (all feasible in the initial population) and for TYPE 2, due to the larger design space, it was 30 (20 feasible). The initial population was created randomly. Each PSO run had 50 iterations.

Figures 27 to 30 present the results of the analyses of all the considered types and building dimensions.

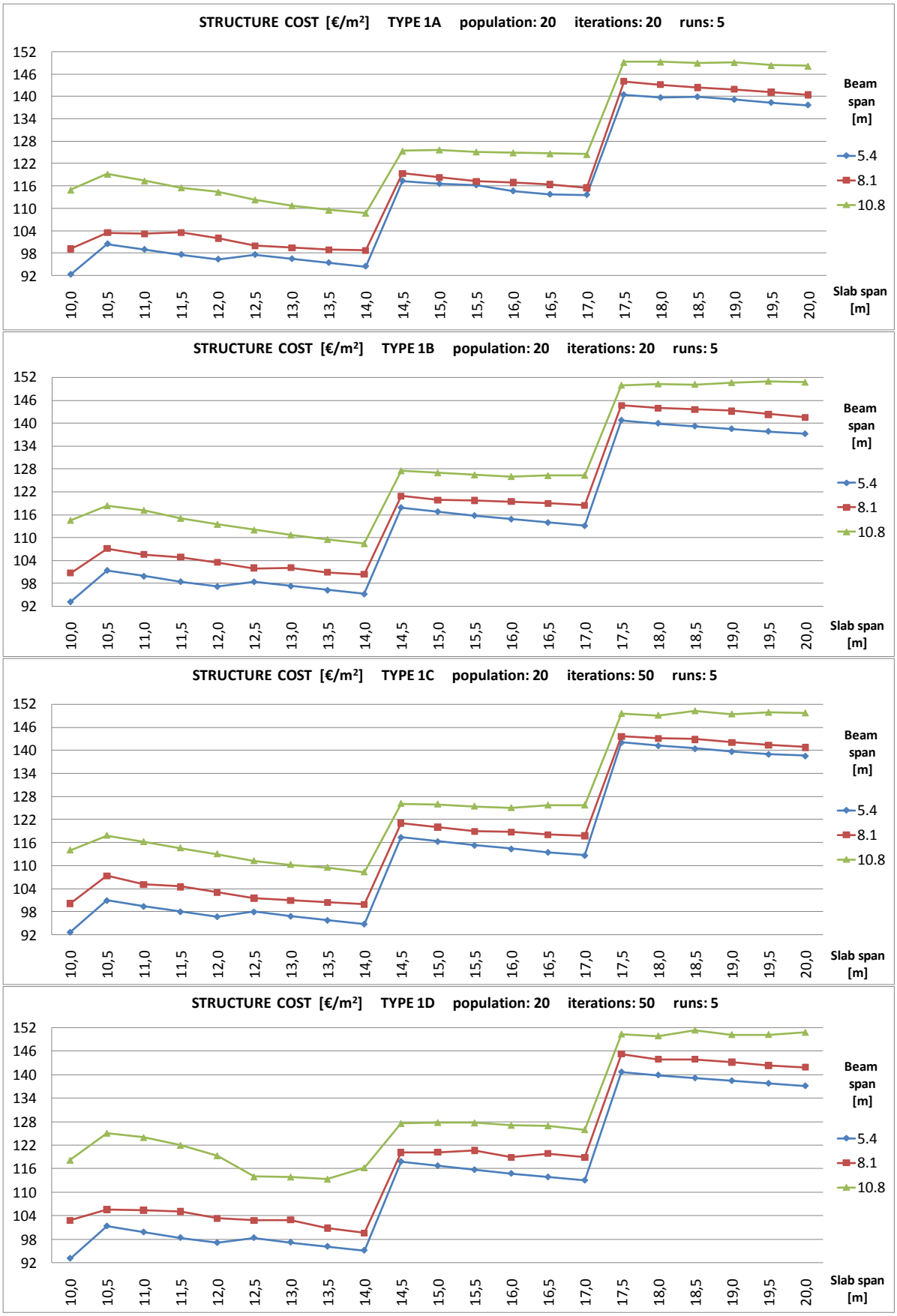

Figure 27. Total structure costs for structure of TYPE 1.

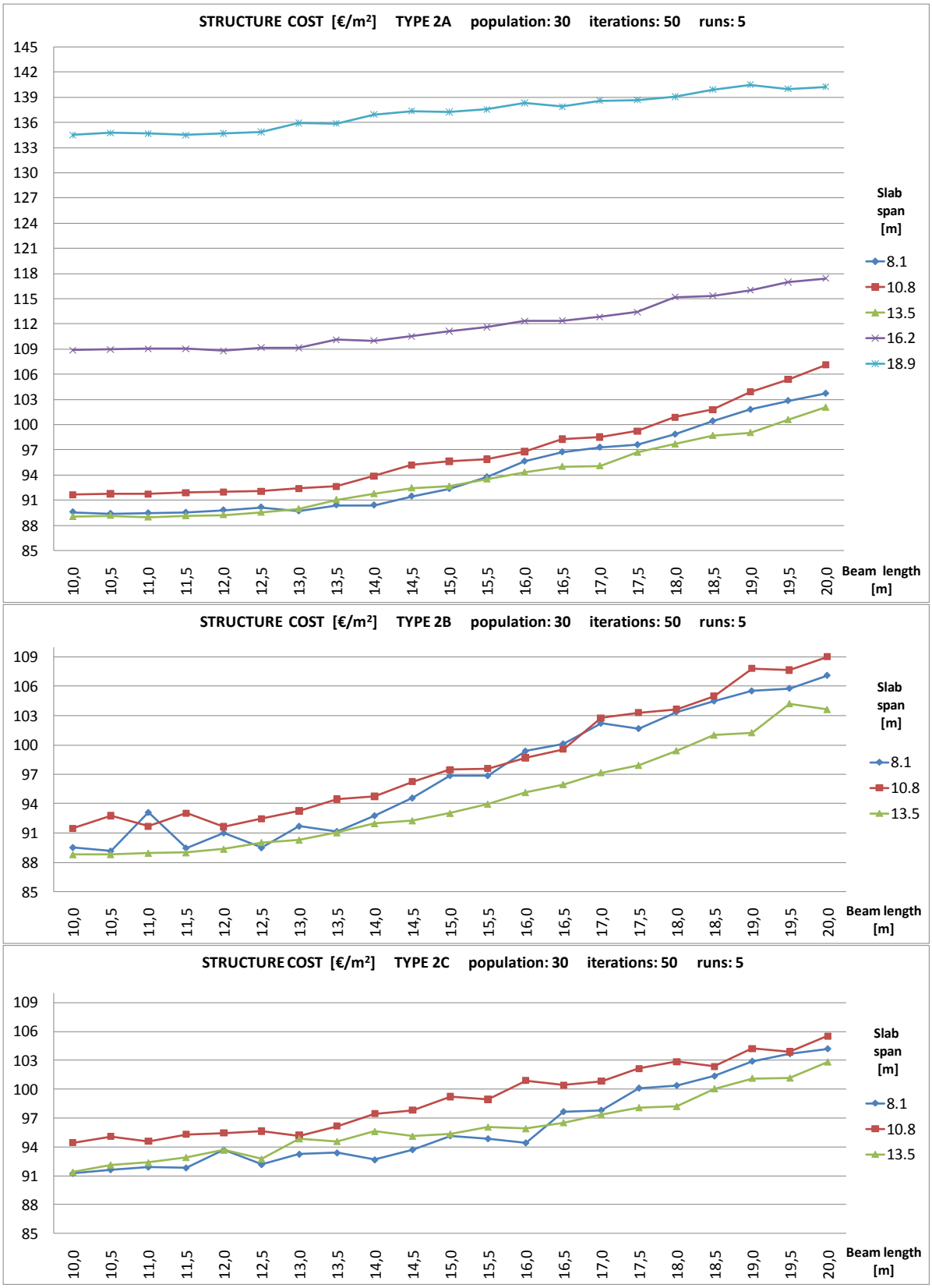

Figure 28. Total structure costs for structure of TYPE 2.

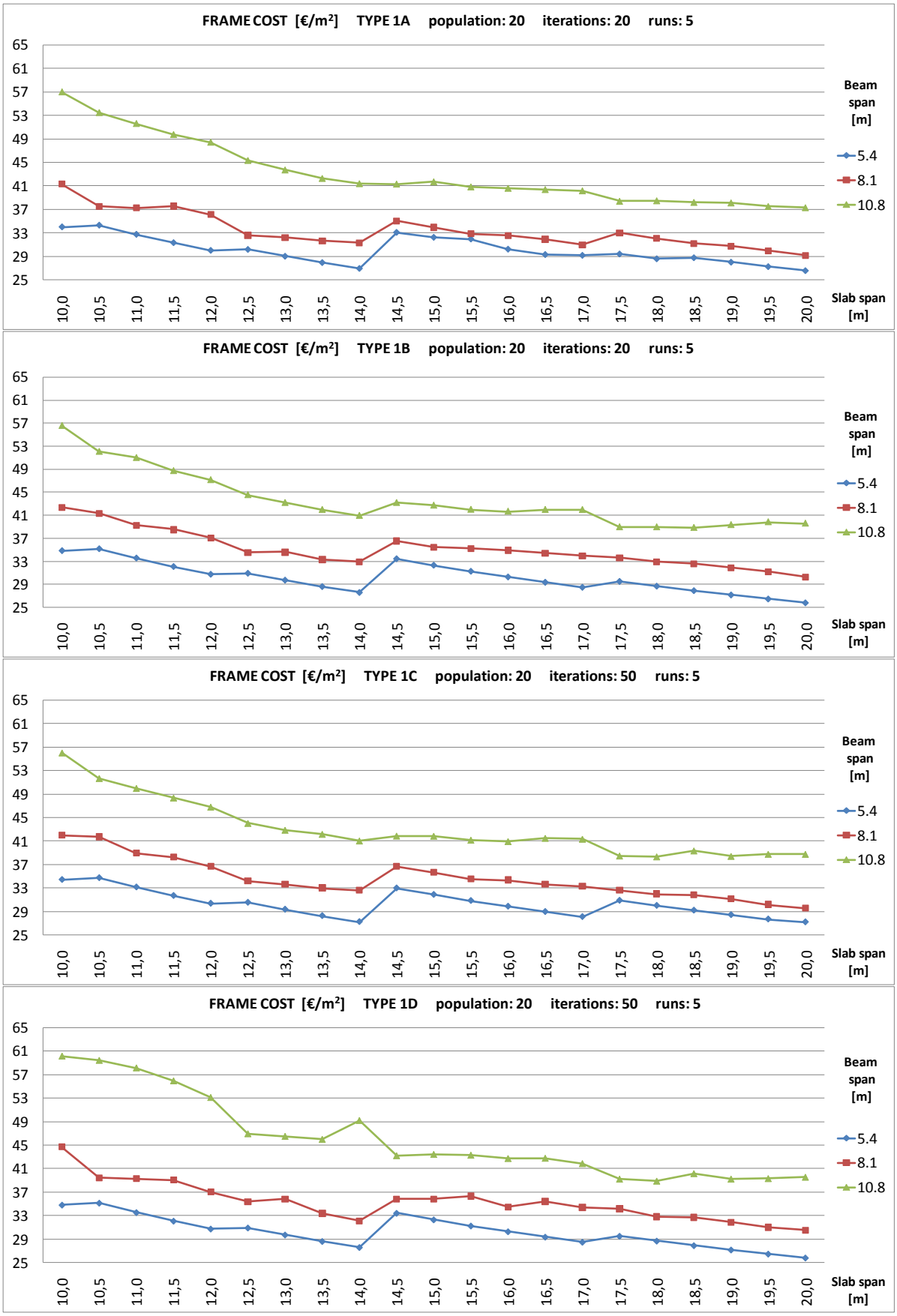

Figure 29. Frame costs for TYPE 1 structures.

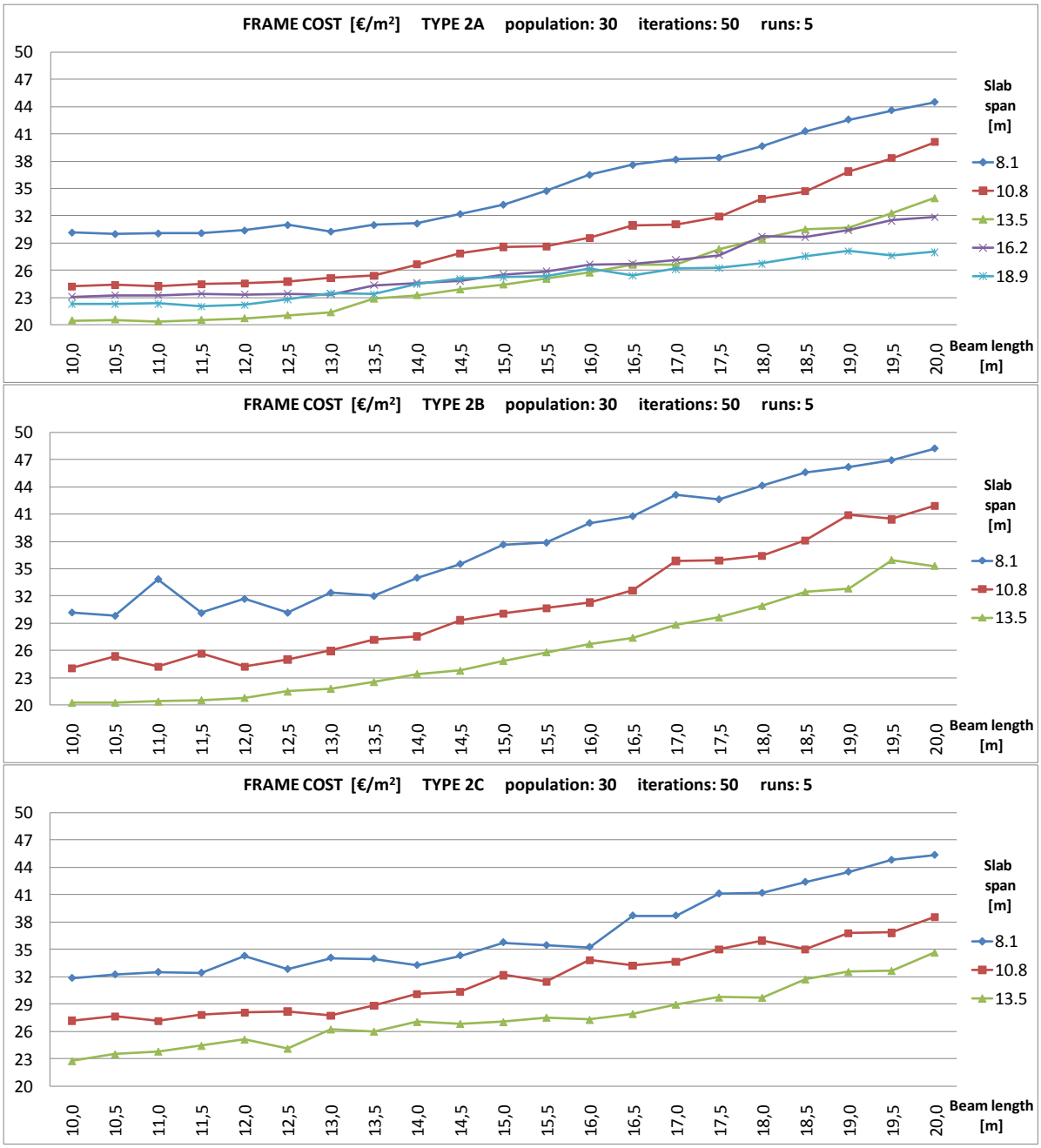

Figure 30. Frame costs for TYPE 2 structures.

The first thing that can be noticed from the graphs (in Figures 27-30) is that the results appear to be consistent. There are some small bumps in the plots, but the main trends can be clearly seen, which confirmed that the number of particles, iterations, runs and values of the governing factors were chosen properly.

Another feature is the large steps present in the plots of the costs for all the TYPE 1 structures. These steps indicate where the slab height changes. The 400 and 500 mm thick HC slabs are very expensive in comparison to the thinner slabs (see Table 6). Due to the fact that slab cost constitutes more than 50 % of the structure cost, this leads to significant changes in the cost of the structure. However, the difference between the prices of the 265 mm and the 320 mm slabs are smaller, and when the slab goes from 265 to 320 mm the

structure cost actually goes down (Figure 27) for the 8.1 and 10.8 m beam spans. The beam cross-section for the 5.4 m beam and 12.0 m slab is the minimum allowed in the optimization. For the 5.4 m beam and the 12.5 m slab it is still minimal, although the structure cost goes up due to the higher slab price. For the 8.1 and 10.8 beams with slab spans ranging from 12.0 to 12.5 the cost goes down, since for those beam spans the beam cross-section is no longer minimal and it is more economical to use higher beams, even though the slab cost goes up slightly.

Let us take a look at the cost of frame 1A (Figure 29). For a certain slab height the cost goes down slightly with the increase in the beam span. The reason for this is that the same number of columns and beams are "distributed" over an increasingly large cell area, giving a lower cost per square meter. This reduction gets smaller as the grid dimensions increase. This shows that for larger dimensions (more than 14.5 x 10.8 m) the capacity of the frame is utilised better. For frames 1B-1D, which are bigger than 14.5 x 10.8 m, the cost starts going up. In contrast to this, the blue lines in all the plots in Figure 29 are exactly the same because, independently on the static layout, the beam and column cross-sections are the lowest available. This means that the utility ratio is very low for the smallest grid dimensions.

The analysis showed that the for larger slab spans (16.2 and 18.9 m) the structure cost for 2A is very high due to the high HC slab price (Figure 28). But, as the beam length increases and the structure cost goes up, the cost for the structures with large slab spans (16.2 and 18.9 m) grows slower than for structures with shorter slab spans (8.1-13.5 m). Because of the huge cost difference, the two biggest slab spans were not analysed for TYPE 2B and TYPE 2C.

There are no major differences in the costs of the TYPE 2 structures except that for TYPE 2C the costs for small beam lengths are greater than for the other two types (Figure 28). The frame cost for structure 2A with long beams (> 16 m) is lowest when the slab span is 18.9 m. But the frames with long beams are more expensive than the ones with short beams, which is yet another reason to omit the structures with 16.2 and 18.9 m slabs in the analysis of TYPE 2B and TYPE 2C.

The lowest structure cost for TYPE 2 was 88.95 €/m^2 found for TYPE 2A (Figure 28). The corresponding frame cost was 20.40 €/m^2, which is close to the lowest found (Figure 30).

For TYPE 1, the lowest structure cost was found for 1A with 5.4 x 10.0 grid dimensions. However, all the cross-sections are minimal for all TYPE 1 structures with these dimensions. The lowest cost for 1A was achieved because the joint stiffness was taken into account when calculating the costs (see subchapter 2.3.5). On the other hand, the lowest structure cost (Figure 27) does not correspond to the lowest frame cost (Figure 29). The lowest frame cost was found for long slab spans and short beams, meaning large structure costs. The most interesting result, in this sense, is the one with a 14.0 m slab and a 5.4 m beam, where both the structure and the frame costs are close to the lowest that was found. For TYPE 1A the structure and frame costs are 94.48 €/m^2 (Figure 27) and 26.95 €/m^2 (Figure 29) respectively.

The difference between the minimums of 1A and 2A solutions is small – the most economical 1A solution is 5.6 % more expensive than the most economical 2A solution, so

the simpler TYPE 1A structure was chosen for further investigation. The TYPE 1A structure is most commonly used in Finland at the moment. The present beam-column joints used in Finland in TYPE 1A frames (Figure 3) can be changed relatively easily to a type that can be considered semi-rigid. This should motivate further studies of these frames.

The next point of interest is the use of semi-rigid joints in the 1A structure (with analyses conducted in both normal and fire conditions). The solution that was found to be the best for one-storey building is still made of the minimal sections. To fully investigate the influence of joint rigidity on the structure cost, larger frame dimensions were proposed. This means the PSO will not get stuck on the upper or lower limits of the available cross-section library, and the limits will not influence the solution. For the same reason, the set of CFHS columns that can be used was increased over the original set specified in [TRY, 2004].

4.1.1 Use of high strength steel

Additional analyses were made for TYPE 1A structures to investigate the influence of the use of high strength steel on the total cost of the structure. The dimensions of the building are the same as before; the building is one-storey and analysed without taking into account fire conditions. One more building width was analysed for this purpose – 13.5 m ($k = 5$). The steel grade was not a variable in the optimization; the analyses were run separately for three "steel combinations". The steel grade used for all three structural elements (beam, column tube and reinforcement) varies for different steel combinations, while the concrete remains the same. The concrete is always C40/50 as in Table 4. The steel combinations, together with the price ratios used in the HSS analysis are presented in Table 11.

Table 11. Material combinations used for HSS analysis

Steel combination	Steel for the WQ-beam				Steel for column tube				Column reinforcement		
	Grade	Yield strength [MPa]	Ultimate strength [MPa]	Price ratio	Grade	Yield strength [MPa]	Ultimate strength [MPa]	Price ratio	Grade	Ultimate strength [MPa]	Price ratio
S 355	S 355 JR	355.0	510.0	1.00	S 355 J2H	355.0	510.0	1.00	A 500 HW	500.0	1.00
S 460	S 460 M	460.0	540.0	1.17	S 460 MH/MLH	460.0	540.0	1.17	A 500 HW	500.0	1.00
S 700	S 700 MC	680.0	750.0	1.43	S 700 MC	680.0	750.0	1.43	A 700 HW	700.0	1.10

All the optimization variables are exactly the same as earlier. The steel combination that was found to be the best for different grid dimensions is presented in Figure 31.

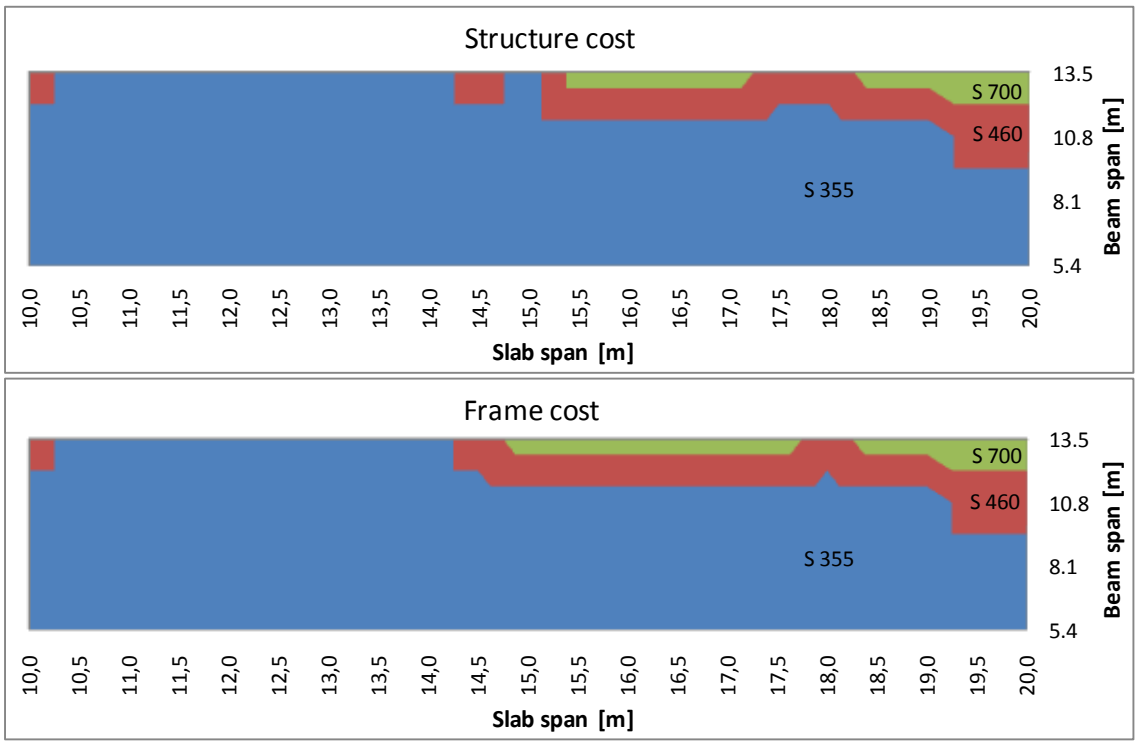

Figure 31. Best found steel combination in TYPE 1A structures – structure and frame costs

The plots in Figure 31 are created so that they are continuous. There are no jumps from steel combination S 355 to S 700. The method of generating the plot for structure cost is presented in Figure 32. For each grid combination the most cost-efficient steel grade is given in Figure 31.

Figure 32. Method of generating the plots shown in Figure 31

When using HSS, the minimal cross-sections of the beams could be used for larger dimensions of the building than when using normal steel. This means that for the smallest frames the HSS gave a larger cost. In the middle range of building dimensions, the lighter HSS beams were as economically viable as the heavier normal steel beams. It was only for the largest building dimensions that the structures made of HSS were found to be more economical than the same structures made of normal steel. This can be seen in Figure 31.

The use of HSS is only found to be economical for structures with beams longer than 12 m and slabs longer than 15 m. The largest cost difference was found for 16 m slabs and 13.5 m beams. In this case, the cost of the structure with S 700 steel was 3.2 % lower than with S 460. This conclusion is true for a one-storey building. It is believed that the building dimensions for which the use of HSS is justified will decrease for multi-storey structures due to the more effective utilisation of the CFHS columns.

A similar analysis was conducted for TYPE 2A frames. It was found that even for large frames of this type (20 m beam and 13.5 m slab) the cost of a structure made of normal steel is lower than for a structure made of HSS. However, the difference in the cost decreases as the dimensions increase. For 20 x 13.5 grid dimensions it is only 1.2 %. It seems likely that the use of HSS would be reasonable for even greater beam lengths.

4.2 3-storey building

This subchapter looks at a TYPE 1A structure, but instead of hinged joints at the ends of the beams the structure has semi-rigid joints. The column bases are assumed to be absolutely rigid. The layout of the structure considered in this subchapter is presented in Figure 33.

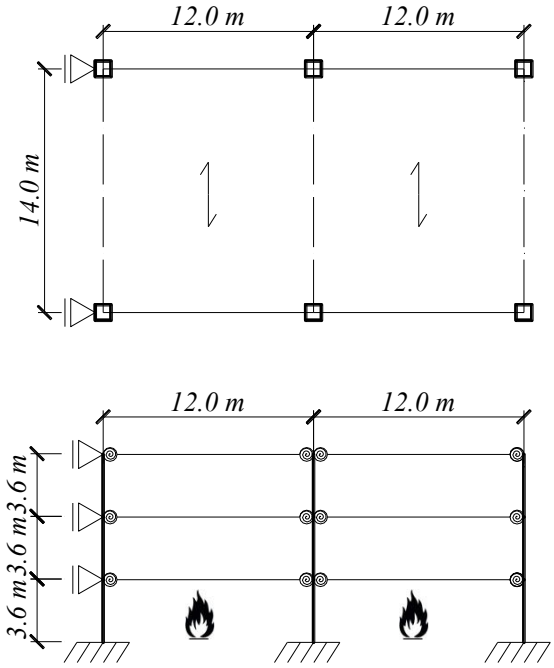

Figure 33. Analyzed TYPE 1A three-storey building with semi-rigid joints

All the buildings considered in this subchapter are three-storey and have two bays. The height of a single floor is 3.6 m. The building width is 14.0 m, which is the maximum span for the 320 mm slab that was found to give the best results for the one-storey building. To avoid "bouncing off" the boundaries of the design space and to investigate the influence of semi-rigid joints on the structure cost, the column spacing in the longitudinal direction (bay width) was set to 12.0 m. Several joint rigidities are investigated in the range of 0.0 to 1.0. The joint rigidity is expressed in terms of beam bending rigidity, following Eq. 4.1:

$$S = \frac{1}{1+\frac{3EI_y}{S_{j,ini}*L}} \quad \text{[Monforton, 1963],} \tag{4.1}$$

where:

EI_y is the strong axis bending stiffness of the beam,

$S_{j,ini}$ is the joint initial rotational stiffness in terms of Eurocode 3, Part 1-8 [EN 1993-1-8, 2005],

$L = 12$ m is the beam span.

In this study, the true stiffness based on the details of the joint is not determined. In the analysis, only the proportional joint stiffness is used. To find the general trend of the cost function in relation to the joint stiffness the optimization procedure was run for a number of values: $S = \{0.0,\ 0.2,\ 0.4,\ 0.6,\ 0.8,\ 1.0\}$. 0.0 means a fully hinged joint while 1.0 is fully rigid. Compared to the classification presented in Eurocode 3, Part 1-8, Section 5.2.2.5 [EN 1991-1-8, 2005] joints of relative stiffness lower than 0.143 can be considered as hinged and joints of stiffness higher than 0.727 can be considered as rigid (in non sway frame) independently of the beam's bending stiffness and length.

One more analysis was conducted where the joint stiffness was a design variable in the optimization. In this case the value differed from 0.01 to 0.90 with a step of 0.01. It should be noted here that due to the modelling of the frame, instead of value 0.00 the value 0.0001 is used for the joint stiffness S, in order to avoid numerical difficulties in the analysis. In structures with semi-rigid joints of high stiffness, a large bending moment will be transferred to the columns at the corners of the building, while the columns in the middle will carry mostly the axial force. For this reason there are two different cross-sections: one for the corner columns (referred to as *edge*) and one for the middle columns. These are the design variables in the optimization:

$col\_no._{edge}$ - the number of column cross-section chosen from Table 2:

$$col\_no._{edge} = \{10 : 57\},$$

$col\_no._{middle}$ - the number of column cross-section chosen from Table 2:

$$col\_no._{middle} = \{10 : 57\}.$$

All the beams in the structure have the same cross-section. The design variables defining their cross-section are:

b_{f1} – the nominal beam width, varying between 200 and 300 mm with a 10 mm step,

t_{f1} – the thickness of the beam's top flange: $t_{f1} = \{20,\ 22,\ 25,\ 30,\ 35,\ 40\}$ mm,

t_{f2} – the thickness of the beam's bottom flange: $t_{f2} = \{15,\ 18,\ 20,\ 22,\ 25,\ 30,\ 35\}$ mm,

t_w – the thickness of the beam's web: $t_w = \{5,\ 6,\ 8,\ 10\}$ mm.

The analysis of the three-storey frame considers both normal and fire design situations. There is only one fire design situation, the fire in question being located on the bottom floor. The fire analysis is conducted for fire resistance classes R 60 and R 120. The dimension u_s (see Figure 12) is different for those two classes and corresponds to their requirements. The lower limit for the cross-section dimension of the column was chosen as 250 mm since this is the required minimum for columns of fire class R 120. The upper limit is set high enough to give a reasonably big design space for the feasible solutions. The ranges of the beam dimensions were limited to increase the speed of optimization. The limits were established in the preliminary analyses performed for the whole range of plate thicknesses.

The number of variables is different for structures with predetermined joint stiffness and those with varying joint stiffness. For structures with given joint stiffness the design space is 4,257,792 options while for structures with variable joint stiffness it is 383,201,280 options.

The 14 different combinations of joint stiffness and fire class that have been analysed can be presented using matrices: $[var \quad 0.0 \quad 0.2 \quad 0.4 \quad 0.6 \quad 0.8 \quad 1.0] * [R\,60 \quad R\,120]$, where var denotes joint stiffness, which is a variable in the optimization. For each combination, 20 PSO runs were performed with 50 particles, of which 20 in the initial population are required to be feasible. The number of iterations in each run is 50.

Table 12 presents the results of the analyses for all the combinations. The objective function in the PSO was the structure cost.

The beams and columns analysed in detail in subchapter 2.3 are taken from the fifth line of Table 12 (variable joint stiffness and R 60 fire resistance class).

Table 12. Best found solutions for structures of the 3-storey building.

Imposed joint stiffness	Fire class	Frame cost/m2 [€/m^2]	Structure cost/m2 [€/m^2]	WQ-BEAM bf1 [mm]	tf1 [mm]	tf2 [mm]	tw [mm]	Weigth [kg/m]	Utility ratio	EDGE COLUMN Cross-section	Utility AMB	Utility FIRE	MIDDLE COLUMN Cross-section	Utility AMB	Utility FIRE	S
0.00	R 60	61.10	135.94	290	40	30	6	216.3	0.990	250x250x6 4T16	0.461	0.650	250x250x6 4T25	0.825	0.874	0.00
0.20		54.70	129.57	280	35	25	6	184.2	0.976	300x300x8 0T00	0.842	0.446	250x250x6 4T25	0.824	0.872	0.20
0.40		50.36	125.22	280	30	22	5	159.5	0.953	300x300x8 4T32	0.975	0.519	250x250x6 4T25	0.827	0.871	0.40
0.60		48.67	123.68	240	30	20	5	137.4	0.921	350x350x10 4T20	0.994	0.532	250x250x6 4T25	0.942	0.868	0.60
variable		48.55	123.35	300	22	15	5	125.8	0.941	400x400x10 0T00	0.957	0.511	250x250x6 4T25	0.982	0.862	**0.70**
0.80		50.34	125.17	290	25	18	5	139.4	0.930	400x400x10 4T20	0.942	0.502	250x250x6 4T25	0.964	0.867	0.80
1.00		56.11	130.94	290	30	22	5	163.6	0.956	450x450x12 0T00	0.785	0.419	250x250x6 4T25	0.856	0.870	1.00
0.00	R 120	62.54	137.37	290	40	30	6	216.3	0.990	250x250x6 8T20	0.405	0.889	300x300x8 4T25	0.461	0.917	0.00
0.20		55.38	130.25	280	35	25	5	179.8	0.979	300x300x8 0T00	0.839	0.682	400x400x10 0T00	0.309	0.544	0.20
0.40		50.88	125.86	250	35	22	5	156.7	0.947	350x350x10 0T00	0.848	0.452	300x300x8 4T25	0.460	0.909	0.40
0.60		49.62	124.52	270	25	20	5	138.9	0.944	350x350x10 4T20	0.998	0.536	300x300x8 4T25	0.534	0.909	0.60
variable		49.31	124.11	300	22	15	5	125.8	0.919	400x400x10 0T00	0.930	0.500	300x300x8 4T25	0.573	0.90	**0.68**
0.80		51.02	125.82	300	25	20	5	149.5	0.863	400x400x10 0T00	0.999	0.538	300x300x8 4T25	0.557	0.912	0.80
1.00		57.16	132.03	280	35	22	5	170.1	0.919	400x400x10 4T25	0.979	0.535	300x300x8 4T25	0.566	0.921	1.00

Table 12 shows that there is not much difference in the cost of the best found structure depending on the fire class. This comes from the fact that the most expensive elements, the slabs and beams, are not fire affected – as explained in subchapter 2.1.

Another noticeable thing is that the optimized joint stiffness, S, is almost the same in both fire resistance classes. When considering a simply supported beam with doubly

symmetrical cross-section and increasing rotational joint stiffness, the optimum, i.e. the lowest cross-section of the beam or the lowest bending moment in the beam, will be found when the joint stiffness is about 2/3 and the hogging and sagging moments have the same values [Haapio & Heinisuo, 2010]. The values obtained in the 3-storey building analysis are close to that. They are slightly larger, but this difference arises from the finite rigidity of the columns. Although stiffness is higher than 66 %, the sagging moment is larger than the hogging moment (see bending moments in the example case: Figures 18-19).

In almost all cases the middle column remains the same when the joint stiffness increases. What changes are the edge column and the beam cross-section. The beam gets lighter and lighter until the optimal joint-stiffness is reached. When the joint stiffness increases beyond the optimum, the beam weight starts to grow. At the best found joint stiffness, the beam weight is 58 % of its weight for S=0.0 and for S=1.0 it is 76-78 %.

When the joint stiffness is zero, the edge column is minimal. When the joint stiffness increases, ever larger columns are required to carry the bending moment coming from the beam and to give rotation resistant support to the beam. The size of the edge column is governed by the ambient design situation. In contrast, the size of the middle column is governed by the fire design situation, and this is particularly noticeable in the results of the analysis for the R 120 fire class.

Figures 34 and 35 present the frame and structure costs (respectively) as a function of joint rigidity. The line plots present the cost, expressed in Euros per square meter, and the column plots present the cost in relation to the cost of the solution with zero joint stiffness.

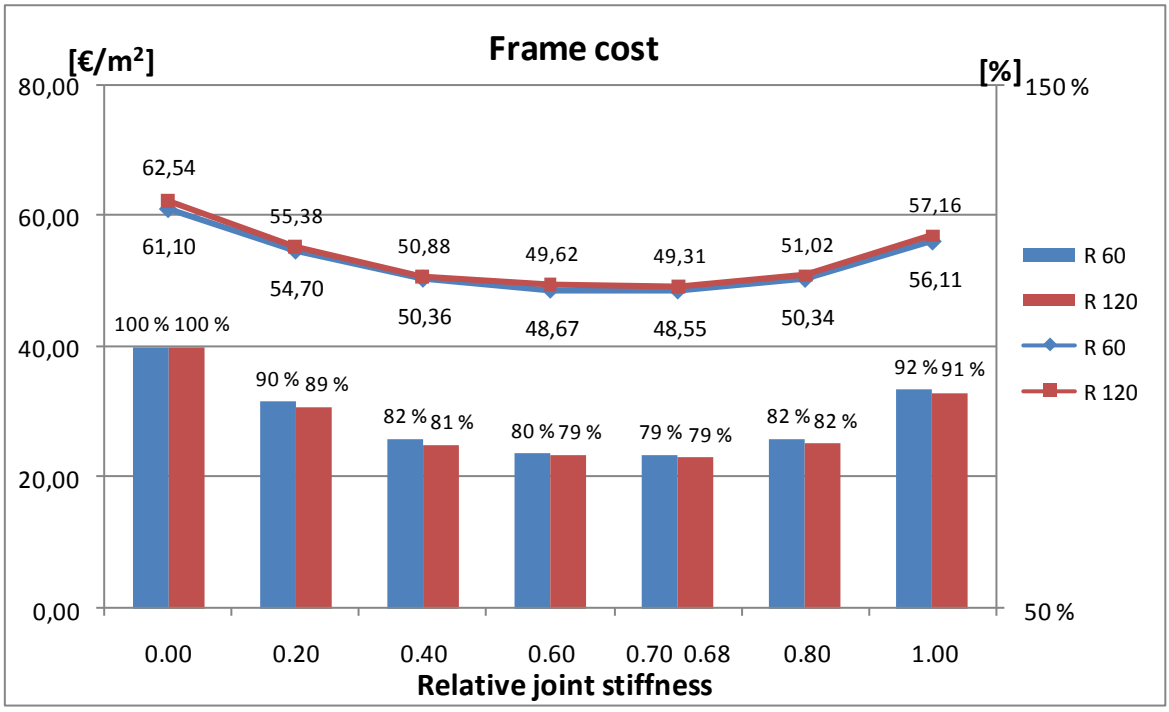

Figure 34. Frame cost for the 3-storey building as a function of joint stiffness

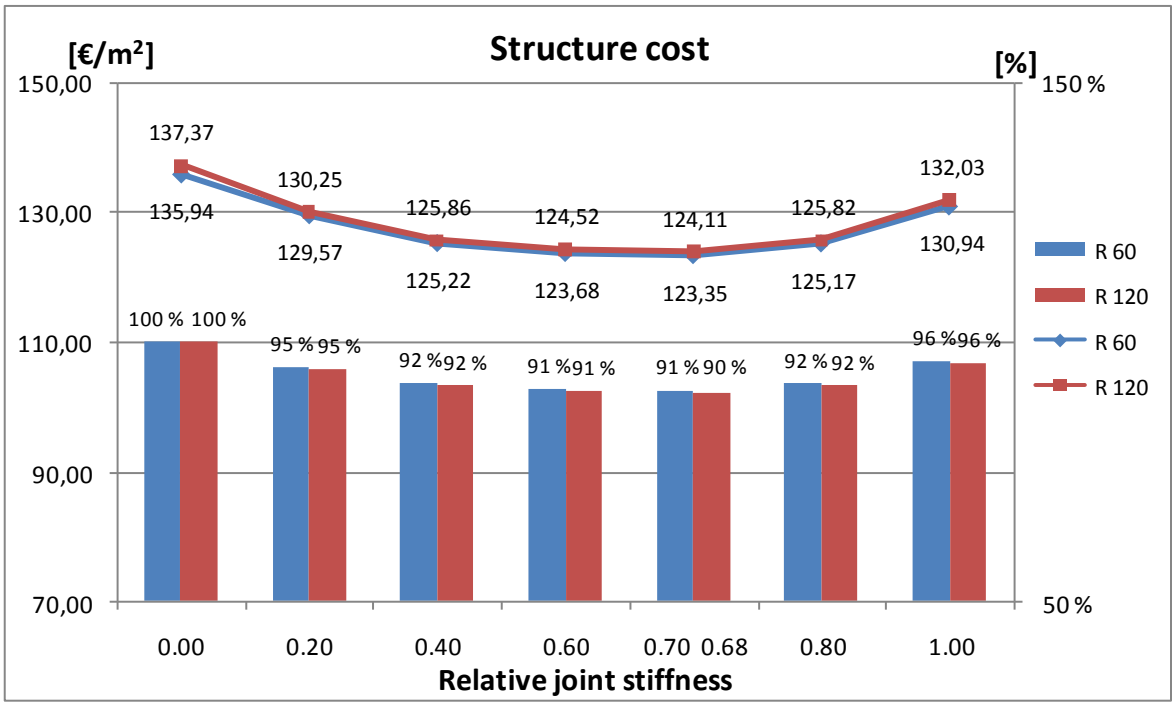

Figure 35. Structure cost for the 3-storey building as a function of joint stiffness

All the lines in the above plots are smooth and follow logically, without noise, the physical reality. This indicates that at each point the solution that was found for each case is close to the global minimum. Furthermore, the high utility ratios for all the constructional elements indicate a good solution. However, it should be noted that it is possible that all the found minima are local in which case the plot can be smooth but all the results are far from the global optima.

Both the structure cost and frame cost plots have the same shape since the slab is the same in all cases. The slab length only varies slightly with the variation of the beam width, but the effect of this on the overall structure cost is negligible. The cost difference between the R 60 and R 120 fire class is also very small – only about 1-2 % for the frame and 0.5-1.0 % for the structure. The joint stiffness has the biggest influence on the structure cost. At first it drops rapidly, 8 % as the joint stiffness goes from 0.0 to 0.4. It then stabilizes as the joint stiffness moves from 0.4 to 0.8 (2 % difference), with the lowest found at 0.68-0.70. Then it rises again (3-4 %) for joint stiffness between 0.8 and 1.0.

The main result of this example is that by using semi-rigid joints instead of hinged joints for TYPE 1A frames the following maximum savings can be obtained:

- Structure cost ~ 10 %,
- Frame cost ~ 20 %.

Such savings would be considered remarkable in real projects. It is recommended that the use of semi-rigid joints for these kinds of frames should be considered in the future in real projects, as they have also been recommended for pure steel sway frames in [Simões, 1996]. In this example, the savings are shown for non-sway frames.

4.2.1 Sensitivity study

Optimization of a structure or a constructional element in order to minimise its cost always has the drawback of the uncertainty of the unit prices. Unlike mass minimisation, it does not find a solution that is always true. The material prices change every day. The best that we can do is to use tabulated cost data found in the literature [Haahtela, 2005] for the optimization and verify the found results with some alternative cost data. The objective is to determine if the solution that is found to be the best is sensitive to price variations.

The prices used in this research are not perfect. [Haahtela, 2005] uses a number of simplifications for the costs of beams and steel tubes for columns. Plots of the prices given in [Haahtela, 2005] have large steps (Figures 36-37) and in general they are not smooth. The prices of the beam favour the heavier beams a lot, as can be seen in Figure 36. The beam unit price is 1.70 €/kg for beams lighter than 120 kg/m and only 1.40 €/kg for beams heavier than 150 kg/m.

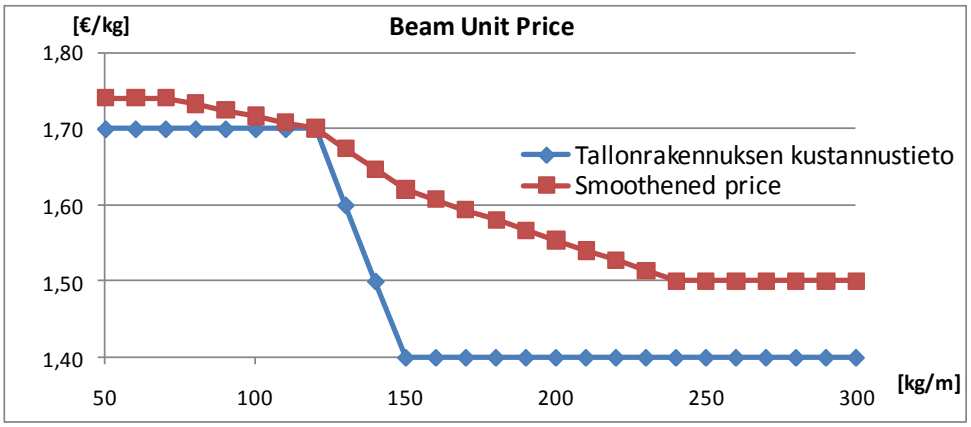

Figure 36. Beam unit prices used for sensitivity study

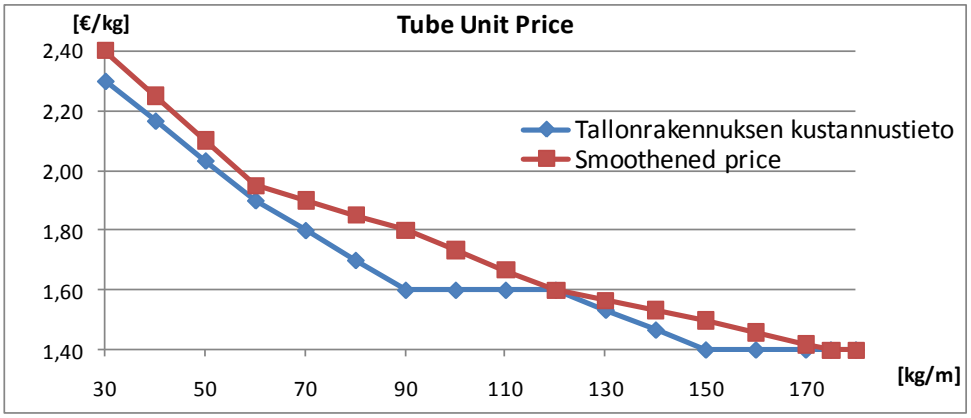

Figure 37. Tube unit prices used for the sensitivity study

For the sensitivity study, another set of prices for WQ-beams and SHS tubes has been used. These prices are based on author's previous experience; they are more smooth then the prices from [Haahtela, 2005]. Because of that they do not favour the heavy solutions so much. The smoothened prices are represented by the red plots in Figures 36-37.

The design variables of the optimization remain the same and all the combinations of joint stiffness and fire class are the same. The characteristics of the optimization are also the

same, i.e. 50 particles (20 feasible in the initial population), 50 iterations for each PSO run and 20 runs.

The comparison of structure costs for the new prices and the prices from the book [Haahtela, 2005] is presented with line plots in Figure 38. It can be seen that the new prices result in higher costs for the low joint stiffness due to the fact that they do not favour the heavier simply supported beams. At the same time, the costs for higher joint stiffness also increase due to the use of higher prices for both the beams and the columns.

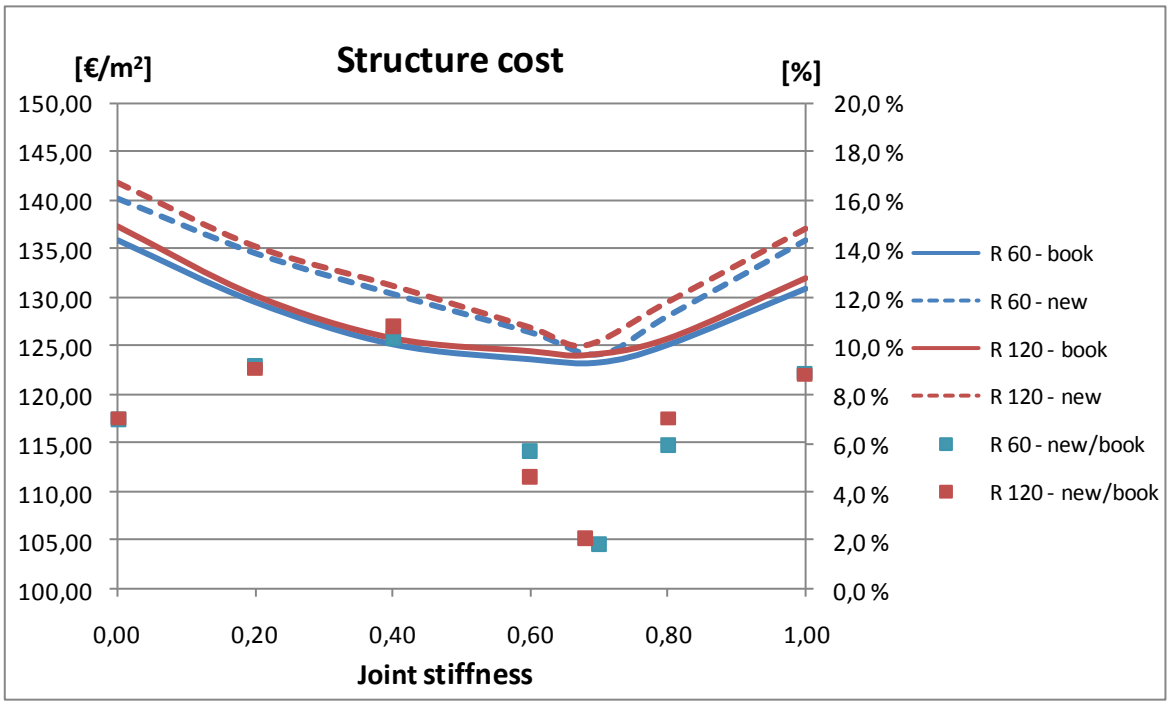

Figure 38. Results of sensitivity analysis

Although there is some difference in the shape of the plots, both analyses found the same joint stiffness to be the best and the solution that was found at that point was exactly the same. The blue and red squares in the graph show the percentage comparison of the solutions obtained using new and book prices. The blue and red squares correspond to the R 60 and R 120 fire classes respectively. The average difference between the frame cost obtained using the new set of prices and the book [Haahtela, 2005] prices is 7 %, for both R 60 and R 120. The maximum difference is 10.8 % - corresponding to a 4.3 % difference in structure cost. For the best found structure stiffness, the difference in frame cost is only 1.9 % for R 60 and 2.1 % for R 120. In terms of the structure cost, the difference falls to 0.7 and 0.8 % respectively.

It can be concluded from the above that the shape of the cost (structure or frame) as a function of joint stiffness is influenced by the variation in material prices. At the same time, the joint stiffness found by PSO was the same. The best found solution for that point was also the same, and the difference in the structure cost was very small – less than 1 %. This is due to the fact that the beam and tube unit prices for the cross-sections used in the best found solution are very close to each other (see Figures 36-37). The beam weight is 125.8 kg/m while the price plots meet at the 120 kg/m (Figure 36).

4.2.2 Vibration

In the analyses presented above the SLS was not considered because pre-cambering is frequently used for welded beams. Furthermore, large pre-cambers are possible, so that the final deflection in SLS can be set to acceptable limits defined in the codes. However, in the previous case the optimization resulted in a 12 m long beam with a height of 320 mm, meaning a very slender beam. Because of that additional check is performed for the vibration of the floor. For reasons of serviceability, the natural frequency of a structure is not permitted to have the same vibration frequency as the human body. The Finnish guidelines for the design of floors with respect to vibrations [TRY, 2005] state that the natural frequency of a building must be higher than 3 Hz. In most real-life projects the fundamental frequency of the structure is not this low but since such shallow floors are obtained in this study the vibration might pose a problem. Because of that the natural frequency of one of the solutions found in optimization (line 5 in Table 12) is investigated.

The fundamental natural frequency of the floor is calculated according to [TRY, 2005] and is expressed with Eq. 4.2:

$$f_0 = \frac{1}{\sqrt{\frac{1}{(f_{0,b})^2} + \frac{1}{(f_{0,s})^2}}} \tag{4.2}$$

where:

$f_{0,b}$ is the fundamental frequency of the WQ-beam,

$f_{0,s}$ is the fundamental frequency of the HC slab.

This gives fundamental frequency of the whole floor (numerical calculations can be found in Appendix E) as shown in Eq. 4.3:

$$f_0 = \frac{1}{\sqrt{\left(\frac{1}{3{,}112\text{Hz}}\right)^2 + \left(\frac{1}{3{,}763\text{Hz}}\right)^2}} = 2.398\text{Hz}. \tag{4.3}$$

The first natural frequency of the floor is lower than the acceptable 3 Hz limit. In practice, the WQ-beam and the hollow core slab work together, at least in SLS. This composite action means higher bending stiffness for the beam and a higher first natural frequency. However, in future studies of structures with semi-rigid joints it is recommended that the natural frequency be taken as one of the constraints in the optimization. The savings with semi-rigid joints compared to hinged joints may increase when vibrations are taken into account.

4.2.3 Beam in catenary action

In this thesis, a certain assumption regarding the fire design of beams and joints has been made. The WQ-beams are assumed to be completely protected from the temperature increase in fire situation. Most of the beam is hidden in the floor and only the bottom flange has to be fire protected. It is assumed that the bottom flange of the beam (see Figure 7) is covered with fire protection of sufficient thickness to limit the increase in beam temperature in a fire. It was assumed that both the beams and joints would retain their ambient resistance and stiffness in fire. The following will present a detailed study of the WQ-beam behaviour in a fire to get an idea of the limits within which the above assumption is safe. The idea is to study the beam behaviour using the temperature data available in [TRY, 2009] for paint protected and for unprotected beams. The joints are assumed to behave in fire as they do in ambient temperatures.

The traditional fire design of beams is a copy of the ambient temperature design. Like in the ambient design, the deflections are assumed to be small and the detailing of the beam is governed by the bending resistance. A new approach to the problem is shown [Yin & Wang, 2005] where large deflections of beams in fire are taken into consideration and the beam starts to behave more like a chain or a rope than a beam element. In this case, the beam's fire resistance is determined by its axial resistance and the resistance of the joints. This being so, the effect on the adjacent structure also has to be verified and the resistance to this type of loading needs to be determined. This approach typically results in higher survival times in fire.

The structure that is investigated in this study is the result of the optimization for fire class R 60 and the imposed relative joint stiffness of 0.2. The beam and column data for that solution can be found in Table 12, line 2. The structure is studied using ABAQUS [ABAQUS, 2010] FEM software.

The FEM model was constructed following the same principles as those described in [Salminen & Bzdawka, 2011]. The sub-structure that was analysed is shown in Figure 39. The edge column was modelled using brick elements and the ground floor beam was modelled using shell elements. The beam-column joint is not modelled in detail – it is a short cantilever with a linear rotational spring at the end. The beam on the upper floors and the middle column were modelled using beam elements. To speed up the calculations only half of the frame was modelled.

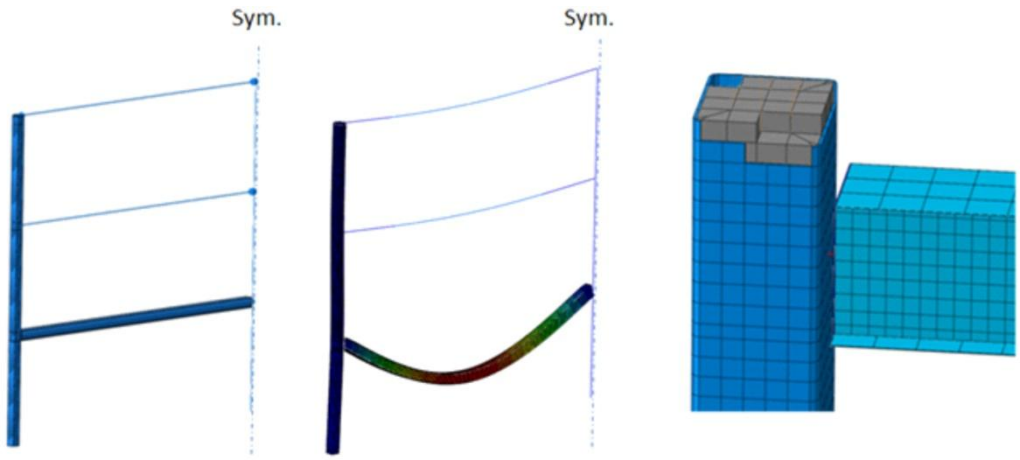

Figure 39. Sub-structure model in ABAQUS

Earlier studies [Salminen & Bzdawka, 2011] considered similar two-bay, three-storey frames with several different joint stiffnesses and both fire protected and unprotected WQ-beams. The beam and column cross-sections were, however, different since in [Salminen & Bzdawka, 2011] they were the result of an optimization using variable joint stiffnesses.

In both studies, [Salminen & Bzdawka, 2011] and the one presented here, the fire temperatures were taken from Finnish guidelines on WQ-beam design [TRY, 2009]. The temperatures used in both studies are the same, since the thickness of the bottom flange is the same, and these are presented in Table 13. These temperatures come from tests and in the form shown in Table 13 they can be used for WQ-beam design. All the intermediate values are interpolated from those that are given. The column temperatures in fire situation conform to [TRY, 2004]. The analysis has been conducted starting from zero time, the beginning of the fire, up to 90 or 120 minutes. For an unprotected WQ-beam the data in [TRY, 2009] covers the time up to 120 minutes and for a protected one up to 90 minutes. The non-linear material models have been taken from the Eurocodes. The steel data for the beams and column tubes was taken from Eurocode 3, Part 1-1 [EN 1993-1-1, 2005] and Part 1-2 [1993-1-2, 2005] and the steel data for the reinforcement was taken from Eurocode 2, Part 1-1 [EN 1994-1-1, 2004] and Part 1-2 [EN 1994-1-2, 2006]. For the concrete, a parabola-rectangle stress-strain relation was taken for compression (as in Eurocode 2, Part 1-1, Sections 3.17 and 3.18 [EN 1992-1-1, 2004]) and a bi-linear relation was taken for tension.

Table 13. Beam temperatures used in the ABAQUS analysis

Elapsed fire time [minutes]	Temperature of beam part [˚C]					
	Bottom flange		Webs		Top flange	
	Unprotected	Protected	Unprotected	Protected	Unprotected	Protected
0	20	20	20	20	20	20
30	546	327	88-546	50-327	101	52
60	735	524	223-735	115-524	246	122
90	829	656	358-829	202-656	392	216
120	911	NA	488-911	NA	533	NA

In the study presented in [Salminen & Bzdawka, 2011] several joint stiffnesses were investigated for the unprotected beam in the range from 0.00 to 0.30, while the protected

beam was also verified for stiffnesses of 0.00 and 0.30. The conducted analyses [Salminen & Bzdawka, 2011] showed that even unprotected beams can resist more than 60 minutes of ISO fire. The longest fire resistance time was found for a joint stiffness of 0.05. For lower values, the failure occurs in the columns that were pulled towards the inside the building. For a higher S value, the failure occurred in the beam when the lower (hotter) part of the beam web buckled near the support. The compression in the beam that was the result of thermal expansion (reaching its maximum at ~12 minutes) quickly changed into tension due to beam deflection (after ~15-25 minutes). The tensile forces in the beam were found to be much greater than the preceding compression, but the tensile resistance of the beam was never exceeded. Also, the tie force resistance of the joint, which is required for accidental loading (following Eurocode 1, Part 1-7 [EN 1991-1-7, 2007]) is larger than the axial force in the beam. The use of semi-rigid joints was also found to be useful in keeping the deflection below the limit for a longer time and keeping the strains of the bottom flange below 2 %, which is the limit for fire protection paint.

The use of semi-rigid joints had many positive outcomes in terms of frame behaviour in fire [Salminen & Bzdawka, 2011]. However, the biggest drawback was the buckling of the beam web at the support (Figure 40). The beam web buckling occurred for all beams with joint stiffness higher than 0.05 [Salminen & Bzdawka, 2011]. Therefore, in the study presented in this subchapter, the solution found in the optimization for S = 0.20 and fire class R 60 is investigated (Table 12). The results of the ABAQUS analyses for both fire protected and unprotected beams are presented in Table 14. To compare the resistance times of a frame with semi-rigid joints to a frame with hinges (which is the most popular nowadays) Table 14 also shows the results of the ABAQUS analysis using S = 0.00.

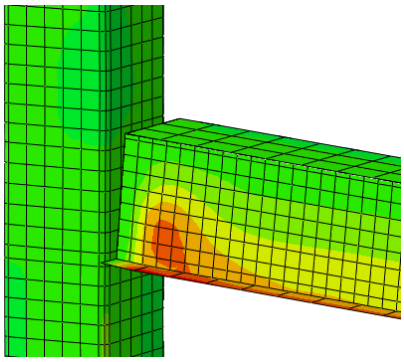

Figure 40. Web buckling in fire situation, for unprotected beam and S = 0.20.

Table 14. Fire resistance times and failures

Design criterion	Unprotected		Protected	
	S = 0.00	S = 0.20	S = 0.00	S = 0.20
Fire resistance in minutes	56	74	> 90	> 90
Beginning of web buckling in minutes	-	38	-	82
Failure occured in:	column	beam	-	-
Deflection limit (L/20) reached after:	39	68	65	> 90

The fire resistance times in Table 14 show the moment when no convergence was found using ABAQUS implicit. Table 14 shows that for the unprotected beam the fire resistance time is increased. The failure mode changes from column failure to beam failure when the

joint stiffness of an unprotected beam increases from 0.00 to 0.20. The time when the beam failure occurs increases from 56 to 74 minutes. It also takes more time before the beam reaches the limit deflection. The resistance time is increased by 18 minutes and the deflection limit time by 29 minutes. For a fire protected WQ-beam it is not possible to determine the resistance times precisely. The temperature data available in [TRY, 2009] ends at 90 minutes and we can only say that the resistance time for protected beams is more than that. The data that is available is the time after the deflection limit is reached. This is also found to be more than 90 minutes, whereas for a hinged beam it is only 65 minutes, so the increase is at least 25 minutes.

In conclusion, it can be said that the use of semi-rigid joints increases the fire resistance time and changes the mode of failure. On the other hand, buckling of the web is believed to take place earlier for beams with a joint stiffness higher than 0.20. If a joint with higher rotational stiffness is to be developed, this issue would need to be taken into account when designing the joint details. It is believed that changing the joint stiffness from 0.00 to 0.20 does not require many alterations to the joint details. The joint with a layout similar to the hinged joint that is in use today, and with a stiffness of 0.20, is found to be safe for fire resistance classes up to R 60. Even without any fire protection, the beam that is found using the presented optimization lasts for at least 74 minutes (Table 14).

An interesting observation arising from the completed ABAQUS analyses was that with large relative rotational joint stiffness the ABAQUS implicit could not go over the web lower part buckling mode to more complete catenary action in the beam. It is believed that the ABAQUS explicit model can go over the buckling phase, as has been shown in similar cases [Dai et al., 2010]. ABAQUS explicit analyses are beyond the scope of this study. They are recommended for future studies of this kind. Large rotational stiffness with high temperatures in the beams will be investigated in the future. The column failure should also be taken into account in any future research, since the high bending moment in the columns may lead to the development of plastic hinges, as has been found in [Salminen & Bzdawka, 2011].

4.3 6-storey building

This subchapter presents the results of the analysis of a 6-storey building. The structure in question is in many ways similar to the one presented in subchapter 4.2. It is a TYPE 1A structure with semi-rigid joints and two bays. Each floor is 3.6 m high. The difference is that it has 6 floors and the cross-sections of the beams and columns change depending on which floor they are located. Floors 1-3 have one set of column cross-section dimensions (different for the edge and middle columns) and floors 4-6 have another set. On almost all the floors the beam cross-section is the same, the exception being the beam on the top floor. In total, there are four different column cross-sections and two different beam cross-sections in the frame. In this study, the structures of two different grid dimensions were analysed, one with a 12 m beam and 14 m slab span, the other with a 10 m beam and 16.8 m slab span. The idea is to compare the minimised costs for structures with the same floor area (both grids give 168 m^2 per cell) but different HC slabs. The 10 x 16.8 meter grid requires thicker HC slabs, P40, while P32 is enough for the 12 x 14 m grid. The layouts of the structures are shown in Figure 41.

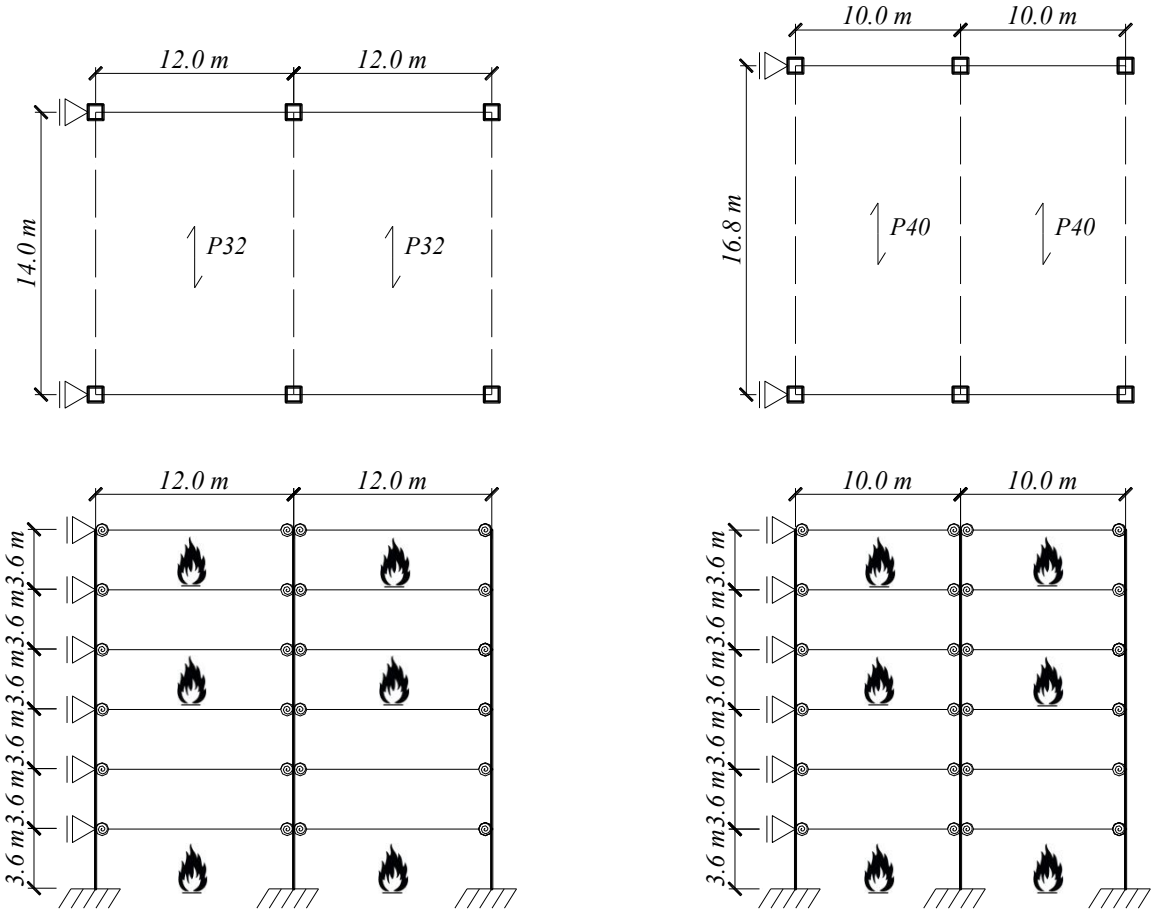

Figure 41. Analyzed six-storey building of TYPE 1A with semi-rigid joints

This study considers 3 fire cases. The fire is on the bottom floor, i.e. where the largest axial force is. The largest axial force for the upper columns is on the 4th floor and on the top floor is where the largest bending moments occur in the columns. Once again, the whole storey of the building is on fire and the columns are surrounded by it on all sides.

Both structures were analysed with hinged joints and semi-rigid joints. The stiffness of the semi-rigid joints was a variable in the optimization. The joint stiffness in the optimization was in the range 0.00-0.90 with a step of 0.01.

All the structures were analysed for fire resistance classes R 60 and R 120. The structure with grid dimensions 12 x 14 m and variable joint stiffness was also analysed for fire resistance classes R 30 and R 90. In addition, in order to be able to evaluate the influence of the fire resistance class on the structure cost and the optimum joint rigidity, the structure was also analysed in fire situation at the temperature equal to 20 ˚C, which corresponds to the beginning of the fire and in this thesis is referred to as “R 0”.

The design space is enormous due to the large range of column cross-sections available, and the fact that four different sections are used. The columns are in the range of 250x250x6, 4T16, and 500x500x16, 4T43. The largest columns were not actually used in any of the cases, but they were necessary to facilitate the creation of the starting population. While the web thickness of the beams was kept as before (5-10 mm) the range of the other beam dimensions differed depending on the case under consideration. For the beams with semi-rigid joint at the ends, the range of flange thicknesses and the beam’s nominal width were kept large:

$b_{f1} = 200 \div 300$ mm with 10 mm step

$t_{f1} = \{15,\ 18,\ 20,\ 22,\ 25,\ 30,\ 35,\ 40\}$ mm.

$t_{f2} = \{15,\ 18,\ 20,\ 22,\ 25,\ 30,\ 35\}$ mm.

For structures with hinged beams it is known that the beam has to take all the bending moment in the middle of the span. The bending is not “distributed” into sagging and hogging. Therefore, the variables that determine the beam’s bending resistance were limited to only the higher values:

$b_{f1} = 240 \div 300$ mm with 10 mm step

$t_{f1} = \{30,\ 35,\ 40\}$ mm.

$t_{f2} = \{22,\ 25,\ 30,\ 35\}$ mm.

This speeded up the creation of the initial population. The design space was also reduced; for the structure with hinged joints it was 1,504,425,216, while for the structure with semi-rigid joints it was 1.003953 *10^{12}. For each combination, 20 PSO runs were performed with 50 particles. It was extremely time consuming to find the initial population with the desired number of feasible solutions, since it was generated randomly. The number of feasible solutions was limited to 10 particles for the analysis with semi-rigid joints, and to 5 particles for the analysis with hinged joints. There were 100 iterations for both cases.

The frame costs and the structure costs found for all the considered fire classes, joint stiffnesses and grid dimensions are presented in Table 15.

Table 15. Cost results of the analysis of the 6-storey frame

Fire class	Frame geometry				Frame cost		Structure cost	
	Frame spacing [m]	Column spacing [m]	Relative joint stiffness		Total [€]	Per area [€/m^2]	Total [€]	Per area [€/m^2]
R 0	14.00	12.00	Optimized stiffness	0.66	95 842	47.54	246 776	122.41
R 30	14.00	12.00		0.62	96 250	47.74	247 040	122.54
R 60	14.00	12.00		0.62	97 393	48.31	248 183	123.11
R 90	14.00	12.00		0.66	97 592	48.41	248 599	123.31
R 120	14.00	12.00		0.68	97 850	48.54	248 857	123.44
R 60	14.00	12.00	S = 0.00	0.00	125 651	62.33	276 514	137.16
R 120	14.00	12.00		0.00	129 081	64.03	279 943	138.86
R 60	16.80	10.00	Optimized stiffness	0.65	82 628	40.99	261 377	129.65
R 120	16.80	10.00		0.63	81 343	40.35	260 284	129.11
R 60	16.80	10.00	S = 0.00	0.00	90 723	45.00	269 024	133.44
R 120	16.80	10.00		0.00	95 633	47.44	273 934	135.88

To better show the influence of the required fire class on the best found solution the data from Table 15 is summarised in the plot presented in Figure 42. The plot presents the frame cost for the building with 14 x 12 m grid dimensions and optimized joint stiffness.

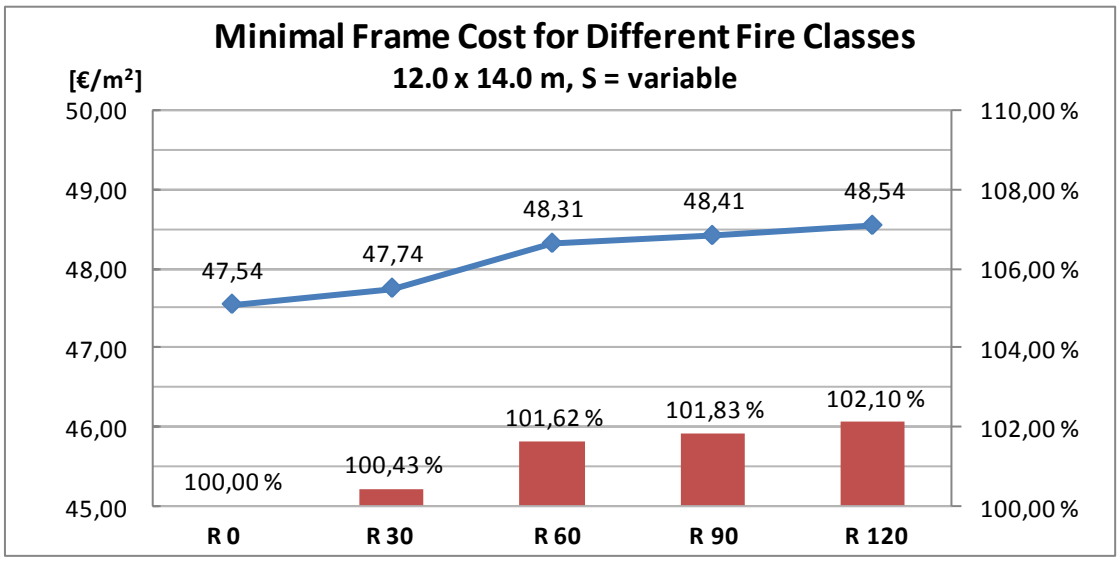

Figure 42. Frame cost as a function of fire class

The frame cost does not change much with the increase in the required fire resistance class. Between R 0 and R 30 there is only a 0.43% difference, the result of the fact that there is a relatively small temperature increase during the first period of the fire. After a larger jump between R 30 and R 60, 1.19 %, the frame cost stabilises and between R 60 and R 120 it only increases by 0.48 %. The difference in structure cost is even lower than that. The cost for R 120 is only 0.84 % higher than the cost for R 0. One reason for this is that only the columns change with the increase in fire class, and they constitute only a small part of the total cost. The other factor is that the use of semi-rigid joints requires stiffer edge columns. Their size is determined by the normal design situation as they are required to transfer the bending moment from the beam. In fire situation their stiffness is reduced, so the bending moment in the columns is reduced and the columns mainly have to take only the axial load. Therefore, the edge columns have a lot of reserve of capacity in a fire

situation. In both cases, the middle column carries mainly the axial load. However, there is a reduction in the applied loads (characteristic values are used in fire situation, the live load is lower) and a reduction of the material safety factors (they are equal 1.0). For this reason, the size of the middle column for fire classes R 0 and R 30 is determined in the normal design situation. A comparison of the utility ratios of the columns in 14 x 12 m solution with semi-rigid joints is presented in Figure 43.

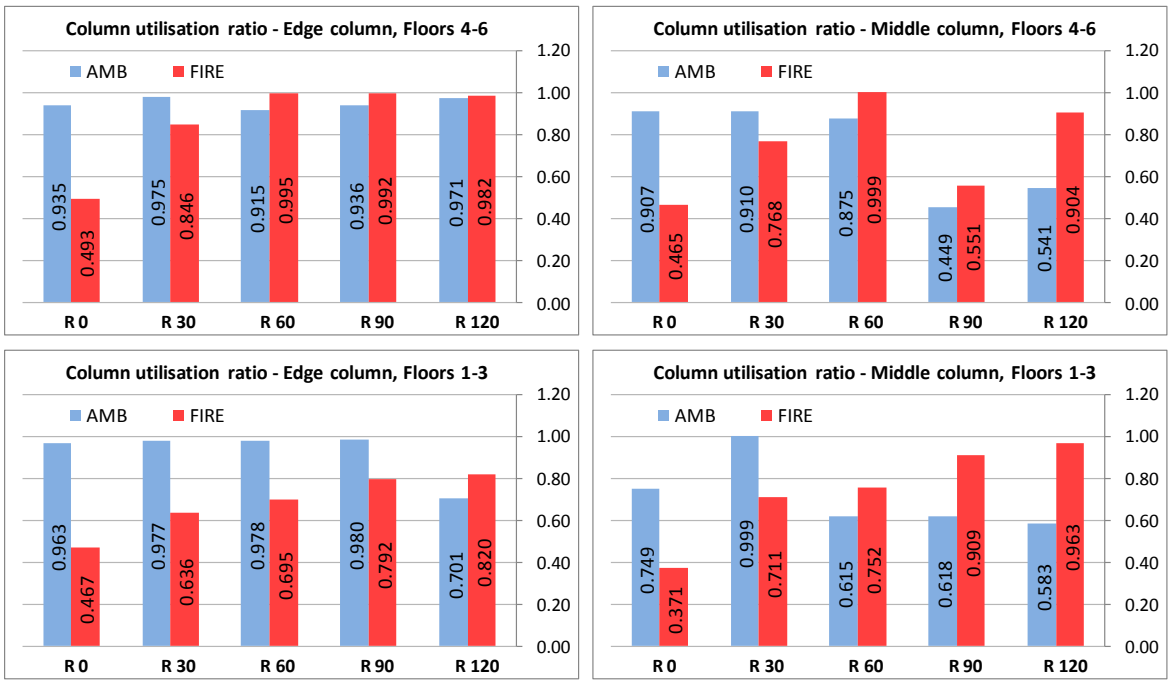

Figure 43. Column utilities for different fire cases

The cross-sections of the columns used for all the considered cases are presented in Tables 16-17. Table 16 shows that in all the cases with semi-rigid joints the edge column has a larger cross-section on the upper 3 floors than on the lower 3 floors. This is not acceptable in real structures, so in future, research constraints should be imposed to avoid such solutions.

Table 16. Edge column cross-sections for 6-storey building

Fire class	Grid dimensions [m]	Relative joint stiffness		Edge columns					
				Floors 1-3			Floors 4-6		
				Section	AMB	FIRE	Section	AMB	FIRE
R 0	14.0 x 12.0	Optimized stiffness	0.660	300x300x8 4T25	0.963	0.467	400x400x10 0T00	0.935	0.493
R 30	14.0 x 12.0		0.620	300x300x8 4T20	0.977	0.636	350x350x10 4T25	0.975	0.846
R 60	14.0 x 12.0		0.620	300x300x8 4T20	0.978	0.695	350x350x10 4T32	0.915	0.995
R 90	14.0 x 12.0		0.660	300x300x8 4T25	0.980	0.792	350x350x10 8T25	0.936	0.992
R 120	14.0 x 12.0		0.680	350x350x10 0T00	0.701	0.820	350x350x10 4T32	0.971	0.982
R 60	14.0 x 12.0	S = 0.00	0.000	250x250x6 4T25	0.832	0.886	250x250x6 4T20	0.352	0.612
R 120	14.0 x 12.0		0.000	300x300x8 4T25	0.465	0.928	250x250x6 8T20	0.405	0.916
R 60	16.8 x 10.0	Optimized stiffness	0.650	300x300x8 4T25	0.976	0.752	350x350x10 4T20	0.926	0.995
R 120	16.8 x 10.0		0.630	300x300x8 4T25	0.970	0.755	350x350x10 4T25	0.905	0.940
R 60	16.8 x 10.0	S = 0.00	0.000	250x250x6 8T25	0.835	0.807	250x250x6 4T20	0.511	0.743
R 120	16.8 x 10.0		0.000	350x350x10 4T20	0.411	0.869	250x250x6 8T25	0.426	0.952

Table 17. Middle column cross-sections for 6-storey building

Fire class	Grid dimensions [m]	Relative joint stiffness		Middle columns					
				Floors 1-3			Floors 4-6		
				Section	AMB	FIRE	Section	AMB	FIRE
R 0	14.0 x 12.0	Optimized stiffness	0.660	350x350x10 0T00	0.749	0.371	250x250x6 4T16	0.907	0.465
R 30	14.0 x 12.0		0.620	300x300x8 8T25	0.999	0.711	250x250x6 4T16	0.910	0.768
R 60	14.0 x 12.0		0.620	400x400x10 0T00	0.615	0.752	250x250x6 4T20	0.875	0.999
R 90	14.0 x 12.0		0.660	400x400x10 0T00	0.618	0.909	350x350x10 4T25	0.449	0.551
R 120	14.0 x 12.0		0.680	400x400x10 4T20	0.583	0.963	300x300x8 4T25	0.541	0.904
R 60	14.0 x 12.0	S = 0.00	0.000	400x400x10 0T00	0.615	0.757	250x250x6 4T25	0.825	0.874
R 120	14.0 x 12.0		0.000	400x400x10 4T25	0.568	0.892	300x300x8 4T25	0.461	0.955
R 60	16.8 x 10.0	Optimized stiffness	0.650	400x400x10 0T00	0.725	0.943	350x350x10 4T20	0.414	0.505
R 120	16.8 x 10.0		0.630	400x400x10 0T00	0.720	0.935	250x250x6 8T20	0.926	0.993
R 60	16.8 x 10.0	S = 0.00	0.000	400x400x10 0T00	0.711	0.996	250x250x6 8T25	0.829	0.798
R 120	16.8 x 10.0		0.000	400x400x10 8T25	0.608	0.948	300x300x8 8T25	0.564	0.878

The cross-sections of the beams are not much influenced by the fire requirement class (see Tables 18-19). On the other hand, the influence of joint rigidity is high. For the 14 x 12 m grid dimensions the intermediate beam with hinges at the ends is 72 % (R 60 class) and 85 % (R 120) more expensive than the beam with semi-rigid joints, (Table 18). The difference for the top floor beams is 60 % and 46 % for R 60 and R 120 fire classes respectively (Table 19). For the frame with the smaller beam span and thicker slabs this ratio is lower: 52 and 51 % for the intermediate floor beams (for R 60 and R 120 respectively) and 25 and 32 % for the top floor beams (for R 60 and R 120 respectively).

Table 19 also shows that the beam on the top floor in the structure with semi-rigid joints is much larger than the beam used on the intermediate floors. On average, the beam on the top floor is 17.5 % heavier than the beam on the intermediate floors. In a real structure, where the load on the top beam would be lower, (snow load may be below 3.0 kN/m^2) perhaps it would be possible to use the same beam cross-section on all the floors. In this study, where the loads are equal, cost minimisation requires the use of different beams.

Table 18. Beam dimensions for the intermediate floors of the 6-storey building

Fire class	Grid dimensions [m]	Relative joint stiffness		Intermediate floor beam							
				bf1 [mm]	bf2 [mm]	hnom [mm]	tf1 [mm]	tf2 [mm]	tw [mm]	Weigth [kg/m]	Utility ratio
R 0	14.0 x 12.0	Optimized stiffness	0.660	230	400	400	40	22	5	169.6	0.999
R 30	14.0 x 12.0		0.620	300	430	320	22	15	5	125.8	0.993
R 60	14.0 x 12.0		0.620	300	430	320	22	15	5	125.8	0.991
R 90	14.0 x 12.0		0.660	270	400	320	22	15	5	117.1	1.000
R 120	14.0 x 12.0		0.680	270	400	320	22	15	5	117.1	0.994
R 60	14.0 x 12.0	S = 0.00	0.000	290	420	320	40	30	6	216.3	0.990
R 120	14.0 x 12.0		0.000	290	420	320	40	30	6	216.3	0.990
R 60	16.8 x 10.0	Optimized stiffness	0.650	230	400	400	20	15	5	113.0	0.999
R 120	16.8 x 10.0		0.630	200	370	400	22	15	6	113.7	0.996
R 60	16.8 x 10.0	S = 0.00	0.000	300	470	400	30	18	6	171.9	1.000
R 120	16.8 x 10.0		0.000	300	470	400	30	18	6	171.9	1.000

Table 19. Beam dimensions for the top floor of the 6-storey building

Fire class	Grid dimensions [m]	Relative joint stiffness		Top floor beam							
				bf1 [mm]	bf2 [mm]	hnom [mm]	tf1 [mm]	tf2 [mm]	tw [mm]	Weigth [kg/m]	Utility ratio
R 0	14.0 x 12.0	Optimized stiffness	0.660	300	430	320	18	15	10	140.4	0.958
R 30	14.0 x 12.0		0.620	300	430	320	20	15	10	144.8	0.970
R 60	14.0 x 12.0		0.620	300	430	320	20	18	6	136.1	0.991
R 90	14.0 x 12.0		0.660	280	410	320	20	15	10	139.3	0.941
R 120	14.0 x 12.0		0.680	220	350	320	40	20	6	150.4	0.862
R 60	14.0 x 12.0	S = 0.00	0.000	300	430	320	40	30	5	217.4	0.980
R 120	14.0 x 12.0		0.000	280	410	320	40	30	8	219.6	0.995
R 60	16.8 x 10.0	Optimized stiffness	0.650	250	420	400	25	18	5	137.8	0.944
R 120	16.8 x 10.0		0.630	200	370	400	30	18	5	128.4	0.936
R 60	16.8 x 10.0	S = 0.00	0.000	250	420	400	40	20	5	172.7	0.997
R 120	16.8 x 10.0		0.000	230	400	400	40	22	5	169.6	0.999

The cost comparison of the 14 x 12 and the 16.8 x 10 m structures is presented in Table 20. The costs are compared to the cost of the frame/structure of a building with 14 x 12 m grid dimensions and semi-rigid joints. When only the frame cost is considered, in a structure with hinged joints, the use of longer and higher slabs together with shorter beams gives 26-28 % savings, depending on the fire class. This corresponds to only a 2-3 % saving in the structure cost. On the other hand, changing the joint from hinged to semi-rigid may save 22 % of the frame cost and 10-11 % of the structure cost. Changing the building dimensions reduces the frame cost more than switching to semi-rigid joints. However, when the structure cost is the object of interest, greater savings are achieved with the semi-rigid joint. The most cost effective solution in terms of the frame cost alone is the one with 16.8 x 10 m grid dimensions and semi-rigid joints, where the saving is 34 %, but when considering structure cost the saving is only 5-7 %, which is less than the savings for the 14 x 12 m building with S-R joints.

Table 20. Cost comparison of different solutions for the 6-storey building

Grid dimensions [m]	Fire class - R 60			
	FRAME		STRUCTURE	
	S=0.00	S=opt	S=0.00	S=opt
14.0 x 12.0	100%	78%	100%	90%
16.8 x 10.0	72%	66%	97%	95%
Grid dimensions [m]	Fire class - R 120			
	FRAME		STRUCTURE	
	S=0.00	S=opt	S=0.00	S=opt
14.0 x 12.0	100%	78%	100%	89%
16.8 x 10.0	74%	66%	98%	93%

5 CONCLUSIONS

Summary

The first objective of this study was to formulate the optimization problem for a certain structure for an office building. The structure in question was composed of pre-stressed concrete hollow core slabs, welded steel WQ-beams and composite concrete-filled square hollow section columns.

Particle Swarm Optimization was chosen for the optimisation algorithm. The current literature indicates that from an engineer's point of view it is the best optimization algorithm for this kind of problem. Being easy to implement, non-gradient and population based, this algorithm turned out to be suitable for this problem.

Feasibility check for each solution was done for both ambient and fire design situations using the most up-to-date European and Finnish building code standards and guidelines. The hollow core slabs for the calculation were chosen from the manufacturer's catalogue depending on the desired span. The beam in the normal design situation was calculated according to Eurocodes, and in fire situation the beam was assumed to be fully fire protected so that the resistance and stiffness of the beam stays ambient in fire. The composite hollow section columns are not fire protected, so their resistance was verified in both normal and fire situations according to the Eurocodes. The joints between the beams and columns are assumed to be semi-rigid and to maintain both their resistance and stiffness in fire.

The objective function of the optimization algorithm was the total cost of the structure composed of three elements: slabs, beams and columns. The cost function was written based on prices including the costs of manufacture, transport and erection that were found in the literature. The cost analysis of several examples shows that the costs of HC slabs vary greatly, depending on their thickness. The HC slab was found to be very expensive and the slab cost constitutes 50-80 % of the cost of the structure.

The static analyses of the frames were conducted using a linear space frame program. The HC slab was not modelled but only gave the loads for the frame analysis and the costs for the cost analysis of the structures. The column stiffness varied based on the temperatures in fire. The resistances of the beams and columns were checked according to the frame results. The resistance check also acted as a feasibility check for the solution. All the calculations, including the PSO algorithm, were completed using a program written in MATLAB. The goal was to see whether semi-rigid joints generated cost savings for these types of structures, which are used widely in Nordic countries, particularly for office buildings. The fire requirements for the structures (excluding slabs) in standard ISO fire were also the constraints of the optimization. There is no mention of this kind of study in the literature.

Results

Shape optimization of a one-storey, two-bay building conducted only in ambient design situation showed that the most promising solution is the one which is currently most commonly used, i.e. continuous columns with one span and simply supported beams

(TYPE 1A). The slab length that was found to be the best was 14 m, which is the maximum for the 320 mm thick slab used in that solution. The beam length that was found to be the best was only 5.4 m, the shortest length considered. The cost of this structure was 92.48 €/m^2. Another solution found an even lower structure cost of 89.57 €/m^2. This was for the TYPE 2A solution with frames perpendicular to the building and with partly cantilevered beams. In that solution the columns were not in the outer walls of the building, but instead they were taking up space inside the building. Another feature of that solution was that the lowest found structure cost didn't correspond to the lowest frame cost, unlike for the first mentioned solution where the frame cost was relatively low. Because the TYPE 1A structure was only slightly more expensive than the TYPE 2A, and because a solution could be found for 1A that kept both the structure and the frame costs low, the TYPE 1A was chosen for further and more detailed study.

Use of High Strength Steel was studied for one-storey TYPE 1A structures. The comparison of the lowest found cost for the solutions using normal steel (S 355) and high strength steel (S 460 – S 700) showed that the use of HSS is economically viable for frames with beam spans longer than 12 m and slab spans longer than 15 m. The use of S 700 was the most economical for the frame with 16 m slabs and 13.5 m beams. The S 700 solution gave a 3.2 % lower frame cost than the S 355 solution.

The use of semi-rigid joints for structures in different fire conditions was investigated in multi-storey buildings. A three-storey, two-bay structure with fixed dimensions (14 m slab and 12 m beam) was optimized in ambient and fire design situations. The fire case considered two fire resistance classes, R 60 and R 120, and the whole ground floor of the building was assumed to be on fire. The beams and joints in fire situation were protected by being encased in the concrete of the floor and by fire insulation underneath. The fire affected the columns from all four sides. The three-storey building analysis also took into account semi-rigid joints. These joints were not designed in detail but their end fixity ratio at the beam ends was used in the static analysis. A fixity ratio of zero corresponds to a hinged joint, while one means a fully rigid joint. The semi-rigid joints caused high bending moment in the columns at the corners of the building, resulting in the need for different cross-sections for the middle and edge columns. The edge column size was determined in ambient design situation while the middle column size came from fire design. For this reason the difference in the structure cost was almost independent of the fire class, being only 0.5-1.0 % of the structure cost and 1.0-2.3 % of the frame cost. The most cost effective solution was found for almost exactly the same joint stiffness, S = 0.70 and S = 0.68 for the R 60 and R 120 fire classes respectively. The solution found with joint stiffness S = 0.70 for R 60 gave 42 % lighter beams (compared to S = 0.00). The results obtained for all the joint stiffnesses analysed created a smooth plotline on the graph, indicating that the solutions that were found are close to minima. Also the PSO algorithm was found to be suitable for this type of problems. However, to achieve the smoothness of the curve many PSO runs had to be performed for each considered joint stiffness.

The main conclusion of this thesis is that the use of a TYPE 1A structure with semi-rigid joints yields significant savings compared to the use of the same structure with hinged joints. What may seem obvious when considering only the beams is actually more complicated when considering the whole structure. The semi-rigid connections decrease

the bending moment in the span of the beam but increase bending at the supports. Since the cross-section of the beam is not symmetric and shear resistance influences the bending resistance it is difficult to say beforehand what moment distribution yields the lowest beam cost. The use of semi-rigid joints also introduces rather high bending moments in the columns. This plays only a minor role in normal design situation but has much greater effects in fire design. It was found that the reduced stiffness of the fire affected column causes the most of the bending moment from the beam being transferred to the column on the floor above. In some cases it was the resistance of the column above the fire compartment that was determining the design. An exception to this rule was the case when the fire was considered on the top floor and the entire bending moment from the beam was transferred to the column in fire.

Some cost reductions could be obtained with the use of semi-rigid joints thanks to the mechanism presented above. The savings for the structure (slabs, beams, columns) are about 10 % and the savings for the frame (beams and columns) are about 20 %. This would make a remarkable difference in real-life projects. When hinged joints are used, the composite columns' size is determined in fire conditions. In normal design situation these columns have considerable capacity reserve. This reserve can be utilised in bending when semi-rigid joints are introduced at the ends of the beams. The bending moments in the columns subjected to temperature increase are moderately low because of the loss of stiffness and the redistribution of the moment to columns not affected by the fire. Consequently, it is recommended that semi-rigid joints should be used in these kinds of frames in the future.

Guidelines for future

PSO sensitivity to price variation had been performed for the three-storey building. It showed that the solution found in the optimisation is only moderately affected by material prices. Although the shape of the cost function changes with the changes of the prices of different materials and profiles, these minor changes do not have an influence on the convergence of the optimization algorithm. Moreover, the joint stiffness that was found to be the most economic is the same regardless of the prices used.

Vibration was found to pose problems in the very shallow floors obtained from the optimisation. The floor's fundamental frequency for one case was 2.4 Hz. It is recommended that in future studies, the natural frequencies should also be taken into account in the optimization algorithm. This requirement can be implemented as one of the constraints.

The details of a real-life semi-rigid joint were not studied. However, an additional FEM analysis showed that some problems with web buckling arise when joints of non-zero rigidity are used between the beam and the column. The FEM analysis was conducted using the ABAQUS program. The assumption that the beam is entirely insulated from fire was dropped. The beam was merely fire protected by paint or not fire protected at all. It was found that the resistance time of the beam in fire conditions increases due to the use of semi-rigid joints, but the failure mode changes. If the end fixity ratio is more than 0.05 the beam fails due to web buckling. The joint was not modelled in detail and neither was the concrete filling around the beam, which would prevent the web from buckling outwards. The

joint layout and its influence on the web buckling phenomenon is a topic for future research. What can be said at this point is that the fire requirement class R 60 is met for a structure with a joint stiffness S = 0.20, even without fire protection for the beams.

Limits for columns sizes on consecutive floors were found to be necessary. The six-storey building analysis again confirmed that the fire class requirement has little influence on the structure cost. The sizing of the edge columns is determined in the ambient design situation, and only the size of middle columns is affected by the fire class. The edge columns are designed to resist the bending moment that is transferred to them from the beams. Because of this, the top floor columns are bigger than the columns below them. This is not acceptable in real structures and should be taken into account in future when searching for optimum joint stiffness.

Solution for further development is suggested. The building structure with two frames located in the side wall of the building together with hollow core slab spanning between them is the most promising. The total structure cost is greatly affected by the cost of the slabs, so this should be the first criterion for selecting building proportions and dimensions. The use of semi-rigid joints offers great savings in the frame cost, typically about 20 % compared to the hinged solution. This is perhaps the most significant result of this study. The savings might be still greater if the SLS requirements are taken into account. In that case, a new type of joint should be developed, ideally one that would prevent the beam web near the support from buckling in fire situation. It is recommended that the first step would be to use an advanced FEM program, such as ABAQUS explicit, to study whether there is enough ductility to pass over the web buckling stage into the catenary action. The fact that semi-rigid joints transfer large bending moments to the columns at the corners of the building should be taken into account, as these columns, being designed for the ambient design situation, are often bigger than the columns below them. It was also found that if the beams are sufficiently fire protected, the structure cost varies only slightly with the change in the required fire class.

For the time being, the use of semi-rigid joints with an end fixity factor of 0.20 was found to be safe for fire resistance class R 60 when the requirement for fire protection for the beam is discounted. The author believes that the current solution of the hinged joint could easily be adapted to exhibit the required stiffness. Perhaps it already fulfils this requirement, since its rotation is prevented by the concrete in which it is embedded. Tests are recommended to determine the joint stiffness both in ambient and fire situations. Changing the joint stiffness from 0.00 to 0.20 gives ~5 % savings in the structure cost and ~10 % in the frame cost.

The use of high strength steel is economically viable when large span beam and slabs are required. The frame for the solution with 16 m slabs and 13.5 m beams would cost 3.2 % less with S 700 than it would with S 355 steel.

The next step in the optimization of this specific office building system is to take into account the outer envelope and the foundations.

REFERENCES:

ABAQUS 6.10/CAE User's Manual, Dassault Systemes, 2010

AISC, *Specification for Structural Steel Buildings-Allowable Stress Design and Plastic Design*, American Institute of Steel Construction, 9th Ed., Chicago, 1989

Al-Jabri K.S., Lennon T., Burgess I.W., Plank R.J., Behaviour of steel and composite beam-column joints in fire, *J. Constructional Steel Research*, 46, 308-309, 1998

Al-Jabri K.S., Burgess I.W., Lennon T., Plank R.J., Moment-rotation-temperature curves for semi rigid joints, *J. Constructional Steel Research*, 61, 281-303, 2005

Al-Jabri K.S., Burgess I.W., Plank R.J., The influence of joint characteristics on the behaviour of beams in fire, *Structural Engineering, Mechanics and Computation (Vol. 2)*, 1087-1094, 2001

Al-Solloum, Y.A., Almusallam, T.H. Optimality and safety of rigidly- and flexibly-jointed steel frames, *J. Constructional Steel Research*, 35, 189-215, 1995

Anderson D., Design of unbraced multi-storey steel frames, *J. Constructional Steel Research*, 62, 1171-1177, 2006

Babrauskas V., Williamson, R.B., The Historical Basis of Fire Resistance Testing, part II. *Fire Technology*, Vol. 14, No. 4, 304-316, 1978

Bailey C.G., The behaviour of asymmetric slim floor beams in fire, *J. Constructional Steel Research*, 50, 235-257, 1999

Belegundu A.D., Chandrupatla T.R.: *Optimization concepts and applications in engineering*, Upper Saddle River, New Jersey, 1999

Bohm B., *Calculated Thermal Exposure of Steel Structures in Fire Test Furnaces – a non-ε_{res} approach*, Tech. University Denmark, CIB W14/82/73 (DK), 1982

Bolwin R., Law M., Giffiths L.G., Survey of Fire Loads in Modern Office Buildings- Some Preliminary Results. *Fire Research Note No.808*, Joint Fire research Organization, England, 1970

BS-5950, *Structural Use of Steelworks in Buildings Part 1. Code of Practice for Dead and Imposed Loads.* British Standards Institution, London, 1990

Bzdawka K., *Composite Column – Calculation Examples,* Tampere University of Technology, Research Report 147, Tampere, 2010

Culver C.G., Survey results for Fire Loads in Office Buildings. *NBS, Building Science Series 85*, National Bureau of Standards, Washington D.C., 1976

Dai X.H., Wang Y.C., Bailei C.G., Effects of partial fire protection on temperature developments in steel joints protected by intumescent coating, *Fire Safety Journal*, 44, 376-386, 2009

Dai X.H., Wang Y.C., Bailey C.G., Numerical modeling of structural fire behaviour of restrained steel beam-column assemblies using typical joint types, *Engineering Structures*, 32, 2337-2351, 2010

Davis L., *Handbook of Genetic Algorithms*, Van Nostrand Reinhold, New York, 1991

Ding J., Wang Y.C., Experimental study of structural behaviour of steel beam to concrete filled tubular column assemblies with different types of joints, *Engineering Structures*, 29, 3485-3502, 2007

Ding J. Wang Y.C., Temperatures in unprotected joints between steel beams and concrete-filled tubular columns in fire, *Fire Safety Journal*, 44, 16-32, 2009

Dorigo M., Gambardella L.M., Ant colony system: a cooperative approach to the travelling salesman problem. *IEEE transactions on evolutionary computation,* Vol. 1, No. 1, 1997

Drysdale D., *An Introduction to Fire Dynamics*, John Wiley & Sons, 2004

El-Rimawi J.A., Burgess I.W., Plank R.J., Studies of the behaviour of steel subframes with semi-rigid joints in fire, *J. Constructional Steel Research*, 49, 83-98, 1999

EN 1990 – Eurocode 0: *Basis of structural design*, CEN, Brussels, 2002

EN 1991-1-1 – Eurocode 1: *Actions on structures – Part 1-1: General actions. Densities, self weight, imposed loads for buildings*, CEN, Brussels, 2002

EN 1991-1-2 – Eurocode 1: *Actions on structures – Part 1-2: General actions – Actions on structures exposed to fire*, CEN, Brussels, 2003

EN 1991-1-7 – Eurocode 1: *Actions on structures – Part 1-7: General actions. Accidental actions,* CEN, Brussels, 2007

EN 1992-1-1 – Eurocode 2: *Design of concrete structures – Part 1-1: General rules and rules for buildings,* CEN, Brussels, 2004

EN 1992-1-1 – Eurocode 2: *Design of concrete structures – Part 1-2: General rules – Structural fire design,* CEN, Brussels, 2004

EN 1993-1-1 – Eurocode 3: *Design of steel structures – Part 1-1: General rules and rules for buildings*, CEN, Brussels, 2005

EN 1993-1-2 – Eurocode 3: *Design of steel structures – Part 1-2: General rules: Structural fire design*, CEN, Brussels, 2005

EN 1993-1-5 – Eurocode 3: *Design of steel structures – Part 1-5: Plated structural elements*, CEN, Brussels, 2006

EN 1993-1-8 – Eurocode 3: *Design of steel structures – Part 1-8: Design of joints*, CEN, Brussels, 2005

EN 1993-1-12 – Eurocode 3: *Design of steel structures – Part 1-12: Additional rules for the extension of EN 1993 up to steel grades S 700*, CEN, Brussels, 2006

EN 1994-1-1 – Eurocode 4: *Design of composite steel and concrete structures – Part 1-1: General rules and rules for buildings*, CEN, Brussels, 2004

EN 1994-1-2 – Eurocode 4: *Design of composite steel and concrete structures – Part 1-2: Structural fire design*, CEN, Brussels, 2006

Fisher R.A., The use of multiple measurements in taxonomic problems, *Annals of Eugenics*, 7, 179-188, 1936

GB50045-95. Code for Fire Protection Design of Tall Buildings, Chinese Planning Press, Beijing (in Chinese), 2001

Gero M.B.P., Garcia A.B., del Coz Diaz J.J., Design optimization of 3D steel structures: Genetic algorithms vs. classical techniques, *J. Constructional Steel Research*, 62, 1303-1309, 2006

Haahtela Y., Kiiras J., Talonrakennuksen kustannustieto (in Finnish), Tammer Paino Oy, Tampere, 2005

Haapio J., Heinisuo M., Minimum cost steel beam using semi-rigid joints, *Rakenteiden Mekaniikka*, 43, 1-11, 2010

Hagentoft, Carl-Eric, *Introduction to Building Physics*, Sweden, 2001

Han L-H., Huo J-S., Concrete-filled HSS columns after exposure to ISO-834 fire standard, *J. Structural Engineering*, ASCE 2003:129(1), 68-78, 2003

Han L-H., Huo J-S., Wang Y-C., Compressive and flexural behaviour of concrete filled steel tubes after exposure to standard fire, *J. Constructional Steel Research*, 61, 882-901, 2005

Han L-H., Yang Y-F. Xu L., An experimental study and calculation on the fire resistance of concrete filled SHS and RHS columns, *J. Constructional Steel Research*, 59, 427-452, 2003

Hasançebi O., Çarbas S., Dogan E., Erdal F., Saka M.P., Performance evaluation of metaheuristic search techniques in the optimum of real size pin jointed structures. *Computers and structures*, 87, 284-302, 2009

Heppner F., Grenander U., a stochastic nonlinear model for coordinated bird flocks. In S. Krasner, Ed., *The Ubiquity of Chaos*, AAAS Publications, Washington DC, 1990

Holland J.H., *Adaptation in natural and artificial systems*, The MIT Press, 1992

Hömmö E., *Design methods for console joint of the composite column and WQ-beam,* MSc. Thesis, Tampere, 2008

Ingberg S.H., Test of Severity of Building Fires. *Quarterly, National Fire Association*, vol.22, 1928

ISO-834 Fire Resistance Tests-Elements—Elements of building construction. International Standard, ISO 834, Geneva, 1975

Jalkanen J.: *Tubular truss optimization using heuristic algorithms*, Doctoral Thesis, Tampere University of Technology, Publication 706, Tampere, 2007

Juang, D.-S. Effects of semi-rigid joints and P-□. forces on the optimum design of seismic steel frames, *Proc. of Structures Congress '89*, ASCE, 586-595, 1989

Jármai K., Rodrigues J.P.C., Farkas J., Optimization of steel structures for fire resistance using PSO, *6th World Congresses of Structural and Multidisciplinary Optimization*, Rio de Janeiro, 2005

Johansson B., *Buckling Resistance of Structures of High Strength Steel, in Use and Application of High-Performance Steel for Steel Structures*, Structural Engineering Documents 8, IABSE, 2005

Kameshki, E.S., Saka, M.P., Optimum design of nonlinear steel frames with semi-rigid joints using a genetic algorithm, *Computers & Structures*, 79, 1593-1604, 2001

Kawagoe, K., *Fire Behaviour in Rooms*. Building research Institute, Japan, Report No. 27, 1958

Kennedy J., Eberhart R., Particle Swarm Optimization, *IEEE*, 1942-1948, 1995

Kirkpatrick S., Gelatt C.D.,. Vecchi M.P.: Optimization by simulated annealing, *Science*, New Series, Vol. 220, No. 4598. (May 13, 1983), pp. 671-680.

Klanšek, U., Kravanja, S., Cost estimation, optimization and competitiveness of different composite floor systems-Part 2: Optimization based competitiveness between the composite I beams, channel-section and hollow-sections trusses, *J. Constructional Steel Research*, 62, 449-462, 2006

Kodur V.K.R., Performance based fire resistance design of concrete-filled steel columns, *J. Constructional Steel Research*, 51, 21-36, 1999

Law M., Arnault P., Fire Loads, Natural Fires and Standard Fires. *International Conference on Planning and Design of Tall Buildings Preprints*: Reports Vol. 1b-8, 1972,

Li L.J., Huang Z.B., Liu F., A heuristic particle swarm optimization method for truss structures with discrete variables. *Computers and structures*, 87, 435-443, 2009

Ma Z., Mäkelainen P., *Modern fire safety design methods*, Helsinki University of Technology, Espoo, 2007

Machaly, E.S.B., Optimum weight analysis of steel frames with semi-rigid joints, *Computers & Structures*, 23, 565-574, 1986

Malhotra H.L., Design of Fire-resisting Structures. *Surrey University Press*, 1982

Mamaghani I.H.P., Seismic design of concrete-filled steel box columns, *Proceedings of 6th European Conference on Steel and Composite Structures*, 1059-1064, Budapest, 2011

Mao C.J., Chiou Y.J., Hsiao P.A., Ho M.C., Fire response of steel semi-rigid beam-column moment joints, *J. Constructional Steel Research*, 65, 1290-1303, 2009

Matlab® ver. 7.8.0.347 (R2009a), The MathWorks™ , 2009

Metropolis N., Rosenbluth A., Rosenbluth M., Teller A., Teller E., *J.Chem.Phys.* 21. 1087, 1953

Mäkelainen P., Ma Z., Fire resistance of composite slim floor beams, *J. Constructional Steel Research*, 54, 345-363, 2000

Monforton G.R., Wu T.S., Matrix analysis of semi-rigidly connected frames, *Journal of Structural Division*, V.89, N.6, 1963

Nyman S., Virdi K., Fire response of concrete filled hollow steel sections, *Proceedings of EUROSTEEL 2011 6th European Conference on Steel and Composite Structures*, pp. 1575-1580, ECCS European Convention for Constructional Steelwork, Brussels, 2011

Ove Arup & Partners, *Design Guide for Fire Safety of Bare Exterior Structural Steel*. Technical Reports, American Iron and Steel Institute, London, 1977

Paulsen O.R., Hadvig, S., Heat Transfer in Fire Test Furnaces, *Journal of Fire and flammability*, vol.8, 423-442, 1977

Pettersson O., Magnusson S.E., Thor, J., *Fire Engineering Design of Steel Structures*, Swedish Institute of Steel Construction, Publication 50, Stockholm, 1976

Poitras G, et al., Optimization of steel floor systems using particle swarm optimization, *Journal of Constructional Steel Research (2011)*, doi:10,1016/j.jcrs.2011.02.016

Reynolds C.W., Flocks, herds and schools: a distributed behavioural model, *Computer Graphics*, 21, 25-34, 1987

Ruukki, www.ruukki.com, 2011

Salminen M., Bzdawka K., Catenary action and strains in WQ-beam in office building during fire, *Proceedings of the METNET seminar 2011 in Aarhus*, 37-49, 2011

SBN, Swedish Building Regulations, SBN 1967

Simões da Silva L., Optimization of frames with semi-rigid joints, *Computers & Structures Vol. 60*, 4, 531-539, 1996

Tahir MMd, *Structural and economic aspects of the use of semi-rigid joints in steel frames*, Ph.D. thesis, University of Warwick, 1997

Takkula P., *WQ-palkin palosuojamaalauksen optimointi* (in Finnish), MSc. Thesis, Tampere, 2007

TNO Building and construction research, TNO report 2002-CVB-R06144, Netherlands Organization for Applied Scientific Research, 2002

TRY, *Teräsnormikortti N:o 17/2005, Kävelystä aiheutuvat välipohjien värähtelyt* (in Finnish), Helsinki, 2005

TRY, *Teräsnormikortti N:o 18/2007, Palkkeihin tuetun ontelolaataton suunnittelu* (in Finnish), Helsinki, 2007

TRY, *Teräsnormikortti N:o 21/2009, WQ-palkin poikkileikkauksen mitoitus normaali- ja palotilanteessa* (in Finnish), Helsinki, 2009

TRY, *Betonitäytteisen teräsliitopilarin suunnitteluohje* (in Finnish), Julkaisumonistamo Eteläranta Oy, Helsinki, 2004

Vulcan Solutions Limited (VSL). [Online] [cited 25 August 2011] http://www.vulcan-solutions.com

Wald F., Simões da Silva L., Moore D.B., Lennon T., Chladna M., Santiago A., Benes M., Borges L., Experimental behaviour of a steel structure under natural fire, *Fire Safety Journal 41*, 2006, pp. 509-522

Wald F., Kallerova P., Chlouba J., Sokol Z., Strejcek M., Pospisil J., Stroner M., Krement T., Smitka V., *Fire Test on Administrative Building in Mokrsko*, Printing house Ceska technika, Czech Technical University in Prague, 2010

Wang, J.-F., Li, G.-Q., A practical design method for semi rigid composite frames under vertical loads, *J. Constructional Steel Research*, 64, 176-189, 2008

Wang P., Li G-Q., Wang Y., Behaviour and design of restrained steel column in fire, Part 3: Practical design method, *J. Constructional Steel Research*, 66, 1422-1430, 2010

Wang Y.C., A simple method for calculating the fire resistance of concrete-filled CHS column, *J. Constructional Steel Research*, 54, 365-386, 2000

Wang Y.C., Davies J.M., An experimental study of non-sway loaded and rotationally restrained steel column assemblies under fire conditions: analysis of the test results and design calculations, *J. Constructional Steel Research*, 59, 291-313, 2003

Wilson E.O., *Sociobiology: The new synthesis*, Belknap Press, Cambridge, MA, 1975

Wolpert D.H., Macready W.G., No free lunch theorems for optimization, *IEEE Transactions on Evolutionary Computation*, Vol. 1, No. 1, 1997

Wong Y.L., Yu T., Chan S.L., A simplified analytical method for unbraced composite frames with semi-rigid joints, *J. Constructional Steel Research*, 63, 961-969, 2007

Yin Y.Z., Wang Y.C., A numerical study of large deflection behaviour of restrained steel beams at elevated temperatures, *J. Constructional Steel Research*, 60, 1029-1047, 2004

Yin Y.Z., Wang Y.C., Analysis of catenary action in steel beams using a simplified hand calculation method, Part 1: theory and validation for uniform temperature distribution, *J. Constructional Steel Research*, 61, 183-211, 2005

Yin Y.Z., Wang Y.C., Analysis of catenary action in steel beams using a simplified hand calculation method, Part 2: validation for non-uniform temperature distribution, *J. Constructional Steel Research*, 61, 213-234, 2005

APPENDIX A

The following appendix presents a detailed calculation of the loads acting on the example structure considered in subchapter 2.3.

DISTRIBUTED LOADS

The vertical loads acting on the structure are calculated following Eurocode 1, Part 1-1 [EN 1991-1-1, 2004] for the normal design situation and Eurocode 1, Part 1-2 [EN 1991-1-2, 2002] for the fire design situation. The imposed load on the floor is $q_k = 3.0\ \mathrm{kN/m^2}$.

The true length of the HC slab is shorter than the length measured between the axes (X) by half the beam width (b_{nom}), and the 50 mm filling between the beam and the slab at both ends, as presented in Eq. A.1.

$$slab\_length = X - \frac{b_{nom}}{2} - 50\mathrm{mm} - \frac{b_{nom}}{2} - 50\mathrm{mm} \tag{A.1}$$

$$slab_{length} = 14000\mathrm{mm} - \frac{300\mathrm{mm}}{2} - 50\mathrm{mm} - \frac{300\mathrm{mm}}{2} - 50\mathrm{mm} = 13.60\mathrm{m}$$

In the case of the edge beam, the live load on the beam is taken from half of the slab length (since the slabs are simply supported) plus the beam's nominal width, plus the 50 mm of concrete filling between the beam web and the slab, plus 20 mm (the small cantilever), as presented in Eq. A.2.

$$Q_k = \left(\frac{slab_{length}}{2} + b_{nom} + 50\mathrm{mm} + c\right) * q_k \tag{A.2}$$

$$Q_k = \left(\frac{13.60\mathrm{m}}{2} + 0.30\mathrm{m} + 0.05\mathrm{m} + 0.02\mathrm{m}\right) * 3.0\frac{\mathrm{kN}}{\mathrm{m^2}} = 21.51\ \mathrm{kN/m}$$

The dead load is the sum of three elements: the concrete slab, the covering concrete on the slab and the concrete filling around the WQ-beam. The dead load of the beam itself is automatically taken into account in the calculations. The weight of the beam per meter is the density of the steel (7850 kg/m^3) times the cross-section area, times the safety factor 1.15. The dimensions used in the dead load calculation are shown in Figure A1.

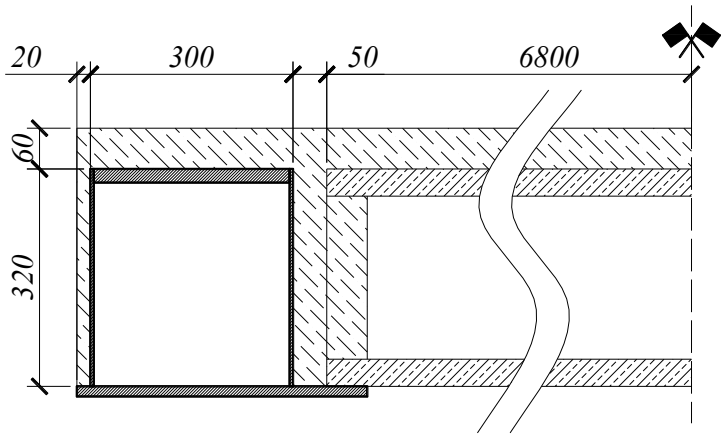

Figure A1. Dimensions used for the load calculation

The mass of P32 is taken as g_{slab} = 400 kg/m^2. The weight of the covering concrete is taken from Annex A of Eurocode 1, Part 1-1 [EN 1991-1-1, 2004] as being 24.0 kN/m^3. This is increased by 1.0 kN/m^3 to take account of the reinforcing steel. Thus γ_{con} = 25.0 kN/m^3.

The dead load on the beam is calculated with Eq. A.3.

$$G_k = \frac{slab\_length}{2} * g_{slab} * g + \frac{slab\_length}{2} * cover * \gamma_{con} + A_{con} * \gamma_{con} \quad \text{(A.3)}$$

where:

$cover$ is 60 mm,

A_{con} is the area of the cross-section of the concrete around the beam,

$A_{con} = (20\text{mm} + 50\text{mm}) * 320\text{mm} + 60\text{mm} * (20\text{mm} + 300\text{mm} + 50\text{mm}) = 44600\text{mm}^2$,

$\frac{slab\_length}{2} = 6.800\text{m}$,

$g = 9.81 \frac{\text{m}}{\text{s}^2}$ is gravitational acceleration,

$G_k = 6.800\text{m} * 0.4\,\text{T/m}^2 * 9.81\,\text{m/s}^2 + 6.800\text{m} * 0.06\text{m} * 25\,\text{kN/m}^3 + 0.0446\text{m}^2 * 25\,\text{kN/m}^3$,

$G_k = 38.00\,\text{kN/m}$.

LOAD COMBINATIONS AND LOAD CASES FOR THE AMBIENT DESIGN SITUATION

For static calculations at ambient temperature the load combinations are made according to Eurocode 0, Annex A1 [EN 1990, 2002]. The load combinations are expressed in Eq. A.4.

$$\Sigma\gamma_{G.j} * G_{k.j} + \gamma_{Q.1} * Q_{k.1} + \Sigma\gamma_{Q.i} * \Psi_{0.i} * Q_{k.i} \quad \text{(A.4)}$$

where:

$G_{k.j}$ is the characteristic value of the dead load,
$Q_{k.1}$ is the characteristic value of the main live load,
$Q_{k.i}$ is the characteristic value of the accompanying live loads,
$\gamma_{G.j}$ is the partial safety factor for the dead load,
$\gamma_{Q.1}$ is the partial safety factor for the main live load,
$\gamma_{Q.i}$ is the partial safety factor for the accompanying live loads,
$\Psi_{0.i}$ is the combination factor for the accompanying live loads.

Since there is only one live load considered in this study, there will be only one upper and one lower load combination. The upper and lower values of the design loads are calculated using the partial safety factors of Finnish National Annex A1 to EN 1990:

$$Q_{sup} = Q_k * \gamma_{Q.sup} = 21.51\,\text{kN/m} * 1.50 = 32.27\ \text{kN/m} \quad \text{(A.5)}$$

$$Q_{inf} = Q_k * \gamma_{Q.inf} = 21.51\,\text{kN/m} * 0.00 = 0.00\ \text{kN/m} \quad \text{(A.6)}$$

$$G_{sup} = G_k * \gamma_{G.sup} = 38.00\,\text{kN/m} * 1.15 = 43.70\ \text{kN/m} \quad \text{(A.7)}$$

$$G_{inf} = G_k * \gamma_{G.inf} = 38.00\,\text{kN/m} * 0.90 = 34.20\ \text{kN/m} \quad \text{(A.8)}$$

The upper and lower values of the distributed forces follow Eq. A.9 and A.10, respectively.

$$Sup = Q_{sup} + G_{sup} = 32.3\,\mathrm{kN/m} + 43.7\,\mathrm{kN/m} = 76.0\,\mathrm{kN/m} \quad \text{(A.9)}$$

$$Inf = Q_{inf} + G_{inf} = 0.0\,\mathrm{kN/m} + 34.2\,\mathrm{kN/m} = 34.2\,\mathrm{kN/m} \quad \text{(A.10)}$$

LAOD COMBINATIONS FOR FIRE DESIGN SITUATION

For static calculations in fire design situation the load combinations are made according to Eurocode 0, Annex A1 [EN 1990, 2002]. The load combinations are expressed with Eq. A.11.

$$\Sigma\gamma_{GA.j} * G_{k.j} + A_d + \Psi_{2.1} * Q_{k.1} + \Sigma\gamma_{Q.i} * \Psi_{2.i} * Q_{k.i} \quad \text{(A.11)}$$

where:

$\gamma_{GA.j}$ is the partial safety factor for the dead load in accidental design situation, according to Eurocode 0, Annex A1, Point A1.3.2(1) [EN 1990, 2002],
$G_{k.j}$ is the characteristic value of the dead load,
A_d is additional indirect action caused by the fire,
$Q_{k.1}$ is the characteristic value of the main live load,
$Q_{k.i}$ is the characteristic value of the accompanying live loads,
$\gamma_{Q.i}$ is the partial safety factor for the accompanying live loads,
$\Psi_{2.1}$ is a combinatorial factor for the main live load,
$\Psi_{2.i}$ is a combinatorial factor for the accompanying live loads.

According to Eurocode 1 Part 1-2 Point 4.3.1 [EN 1991-1-2, 2003] and Eurocode 0, Annex A, Table A1.1 [EN 1990, 2002], the $\Psi_{2.1}$ factor for fire situation is 0.3. Thus the distributed load on the beam can be calculated with Eq. A.12.

$$Fire = \Psi_{2.1} * Q_k + G_k = 0.3 * 21.5\,\mathrm{kN/m} + 38.0\,\mathrm{kN/m} = 44.5\,\mathrm{kN/m} \quad \text{(A.12)}$$

CONCENTRATED MOMENT

The problem of eccentric loading causing additional moments in the columns occurs only in TYPE 1A and TYPE 1C frames. Both of these types are considered to have only two outer frames. The problem of uncertainty about which eccentricity is more unfavourable is solved by using two contrary arrangements of the imperfections for the two frames of the structure. The principal for a single storey frame is schematically presented in Figure A2.

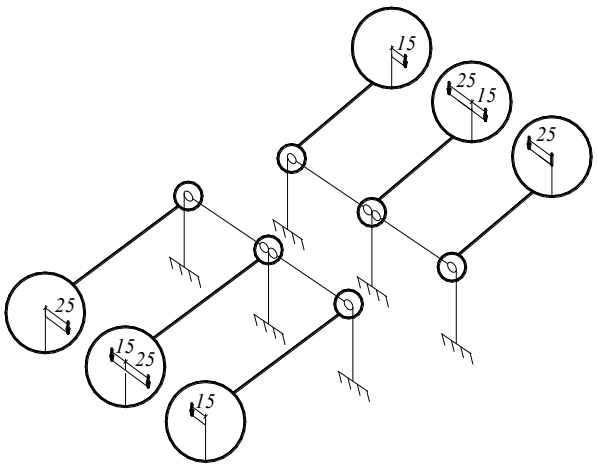

Figure A2. Scheme of additions to column loading eccentricity

Let us consider one of the middle columns – the one with the 25 mm extra on the left side and 15 mm on the right. For the first load case, the distributed load on the beams on both sides of the column is $Supreme = 76.0\,\mathrm{kN/m}$.

The concentrated load on both consoles of the column (d_l and d_r) will be the same, taken from half the span length of the beam as in Eq. A.13.

$$R_{l.sup} = R_{r.sup} = Sup * \frac{Y}{2} = 76.0\,\mathrm{kN/m} * \frac{12\mathrm{m}}{2} = 456.0\mathrm{kN} \quad \text{(A.13)}$$

The bending moment coming onto the column from the left console is shown in Eq. A.14.

$$M_{Ed.col.l} = R_{l.sup} * \left(\frac{col}{2} + 25\mathrm{mm}\right) \quad \text{(A.14)}$$

$$M_{Ed.col.l} = 456.0\mathrm{kN} * \left(\frac{0.25\mathrm{m}}{2} + 0.025\mathrm{m}\right) = 68.4\mathrm{kNm}$$

and from the right console in Eq. A.15.

$$M_{Ed.col.r} = R_{r.sup} * \left(\frac{col}{2} + 15\mathrm{mm}\right) \quad \text{(A.15)}$$

$$M_{Ed.col.r} = 456.0\mathrm{kN} * \left(\frac{0.25\mathrm{m}}{2} + 0.015\mathrm{m}\right) = 63.8\mathrm{kNm}$$

To remain consistent with the directions of the axes, in *frame3D* the moments turning to the left are positive while those turning to the right are negative. Thus, the total concentrated bending moment applied to that particular column, for the first load case, is shown in Eq. A.16.

$$M_{Ed.col} = M_{Ed.col.l} - M_{Ed.col.r} \quad \text{(A.16)}$$

$$M_{Ed.col} = 68.4\mathrm{kNm} - 63.8\mathrm{kNm} = 4.6\mathrm{kNm}$$

The bending moment applied to the column opposite to the one under consideration will have the opposite sign.

This method of calculation is more suitable for other load cases. For example, when the load on the beam left of the column is $Supreme$ and on the right $Infime$.

$$R_{r.inf} = Inf * \frac{Y}{2} = 34.2\,\mathrm{kN/m} * \frac{12\mathrm{m}}{2} = 205.2\mathrm{kN} \quad \text{(A.17)}$$

$$M_{Ed.col.r} = R_{r.inf} * \left(\frac{col}{2} + 15\mathrm{mm}\right) \quad \text{(A.18)}$$

$$M_{Ed.col.r} = 205.2\mathrm{kN} * \left(\frac{0.25\mathrm{m}}{2} + 0.015\mathrm{m}\right) = 28.7\mathrm{kNm}$$

The total concentrated bending moment applied to the top of the column is as shown in Eq. A.19.

$$M_{Ed.col} = M_{Ed.col.l} - M_{Ed.col.r} \quad \text{(A.19)}$$

$$M_{Ed.col} = 68.4\mathrm{kNm} - 28.7\mathrm{kNm} = 39.7\mathrm{kNm}$$

While the right side moment for the column on the opposite side of the building follows Eq. A.20.

$$M_{Ed.col.r} = R_{r.inf} * \left(\frac{col}{2} + 25\mathrm{mm}\right) \quad \text{(A.20)}$$

$$M_{Ed.col.r} = 205.2\text{kN} * \left(\frac{0.25\text{m}}{2} + 0.025\text{m}\right) = 30.8\text{kNm}$$

And the total moment for that column is shown in Eq. A.21.

$$M_{Ed.col} = M_{Ed.col.l} - M_{Ed.col.r} \tag{A.21}$$

$$M_{Ed.col} = 63.8\text{kNm} - 30.8\text{kNm} = 33.0\text{kNm}$$

The bending moment from the eccentricities for the edge columns is calculated in a similar way, but the load on the side where no beam is resting is zero.

The ratio of permanent to total loading, required for the calculation of composite columns, is as in Eq. A.22.

$$PTratio = \frac{mean(G_d)}{mean(G_d + Q_d)} \tag{A.22}$$

where:

G_d is the matrix of all the dead loads acting on the beams for all the load cases,

Q_d is the matrix of all the live loads acting on the beams for all the load cases.

In the example structure:

$$PTratio = \frac{38.0\text{kN/m}}{59.5\text{kN/m}} = 0.639.$$

APPENDIX B

The following appendix presents detailed resistance check of example beam WQ 320-5-20x300-15-430/20. The cross-section of the considered beam is presented Figure B1. The dimensions used for the calculation are as follows:

- $h_{nom} = 320\text{mm}$ - nominal beam height,
- $t_w = 5\text{mm}$ - beam web thickness,
- $t_{f1} = 22\text{mm}$ - top flange thickness,
- $b_{f1} = 300\text{mm}$ - top flange width (nominal beam width),
- $t_{f2} = 15\text{mm}$ - bottom flange thickness,
- $b_{f2} = 430\text{mm}$ - bottom flange width,
- $c = 20\text{mm}$ - short cantilever of the bottom flange.

To avoid problems in calculating the bending resistance of the beam, some other notations are introduced and used throughout the calculation process:

- $b = 290\text{mm}$ - width of the top flange plate,
- $h_w = 298\text{mm}$ - web height,
- $h = 335\text{mm}$ - total beam height.

The length of the considered beam is:

- $L = 12.0\ \text{m}.$

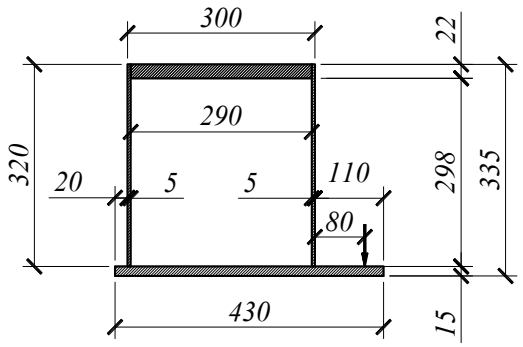

Figure B1. Dimensions of the cross-section of the example beam [mm]

STIFFNESS

First, the area of the beam cross-section is calculated from Eq. B.1.

$$A_{section} = 2 * t_w * h_w + t_{f1} * b_{f1} + t_{f2} * b_{f2} \quad \text{(B.1)}$$

$$A_{section} = 2 * 5\text{mm} * 298\text{mm} + 22\text{mm} * 300\text{mm} + 15\text{mm} * 430\text{mm} = 16030\text{mm}^2$$

The centre of gravity, measured in the vertical direction from the bottom of the beam, and thus the location of the horizontal elastic neutral axis, is calculated from Eq. B.2.

$$z_{0.y} = \left(b_{f2}/2 * {t_{f2}}^2 + 2 * t_w * h_w * (h_w/2 + t_{f2}) + t_{f1} * b_{f1} * \left(t_{f1}/2 + h_w + b_{f2}\right)\right)/A_{section} \quad \text{(B.2)}$$

All substitutions are in [mm]:

$$z_{0.y} = \left(430/2 * 15^2 + 2 * 5 * 298 * (298/2 + 15) + 22 * 300 * (22/2 + 298 + 15)\right)/16030 =>$$

$$z_{0.y} = 166.9\text{mm} = 0.1669\text{m}.$$

From Steiner's equation the second moment of area with respect to the neutral axis is calculated for all the elements separately and summarised at the end.

$$I_{y.f1} = b_{f1} * {t_{f1}}^3/12 + b_{f1} * t_{f1} * \left(z_{0.y} - h + t_{f1}/2\right)^2 \quad \text{(B.3)}$$

$$I_{y.f1} = 300 * 22^3/12 + 300 * 22 * (166.9 - 335 + 22/2)^2 = 1.631 * 10^8$$

$$I_{y.f2} = b_{f2} * {t_{f2}}^3/12 + b_{f2} * t_{f2} * \left(z_{0.y} - t_{f2}/2\right)^2 \quad \text{(B.4)}$$

$$I_{y.f2} = 430 * 15^3/12 + 430 * 15 * (166.9 - 15/2)^2 = 1.640 * 10^8$$

$$I_{y.w} = t_w * {h_w}^3/12 + h_w * t_w * \left(z_{0.y} - t_{f2} - h_w/2\right)^2 \quad \text{(B.5)}$$

$$I_{y.w} = 5 * 298^3/12 + 5 * 298 * (166.9 - 15 - 298/2)^2 = 0.110 * 10^8$$

$$I_y = I_{y.f1} + I_{y.f1} + 2 * I_{y.w} \quad \text{(B.6)}$$

$$I_y = (1.631 + 1.640 + 2 * 0.110) * 10^8 = 3.491 * 10^8\text{mm}^4 = 3.491 * 10^{-4}\text{m}^4$$

The centre of gravity in the horizontal direction and the second moment of area with respect to vertical neutral axis are calculated from Eq. B.7 – B.12.

$$z_{0.z} = \begin{pmatrix} {b_{f2}}^2 * t_{f2}/2 + t_w * h_w * (c + t_w/2) + t_w * h_w * \left(c + b_{f1} - t_w/2\right) \\ +t_{f1} * b_{f1} * \left(c + b_{f1}/2\right) \end{pmatrix} \Big/ A_{section} \quad \text{(B.7)}$$

$$z_{0.z} = \begin{pmatrix} 430^2 * 15/2 + 5 * 298 * (20 + 5/2) + 5 * 298 * (20 + 300 - 5/2) \\ +22 * 300 * (20 + 300/2) \end{pmatrix} /16030 =>$$

$$z_{0.z} = 188.1\text{mm} = 0.1881\text{m}$$

$$I_{z.f1} = t_{f1} * {b_{f1}}^3/12 + b_{f1} * t_{f1} * \left(z_{0.z} - b_{f1}/2 - c\right)^2 \quad \text{(B.8)}$$

$$I_{z.f1} = 22 * 300^3/12 + 300 * 22 * (188.1 - 300/2 - 20)^2 = 0.517 * 10^8$$

$$I_{z.f2} = t_{f2} * {b_{f2}}^3/12 + b_{f2} * t_{f2} * \left(z_{0.z} - b_{f2}/2\right)^2 \quad \text{(B.9)}$$

$$I_{z.f2} = 15 * 430^3/12 + 430 * 15 * (188.1 - 430/2)^2 = 1.041 * 10^8$$

$$I_{z.w1} = h_w * {t_w}^3/12 + h_w * t_w * (z_{0.z} - c - t_w/2)^2 \quad \text{(B.10)}$$

$$I_{z.w1} = 298 * 5^3/12 + 298 * 5 * (188.1 - 20 - 5/2)^2 = 0.409 * 10^8$$

$$I_{z.w2} = h_w * {t_w}^3/12 + h_w * t_w * \left(z_{0.z} - c - b_{f1} + t_w/2\right)^2 \quad \text{(B.11)}$$

$$I_{z.w2} = 298 * 5^3/12 + 298 * 5 * (188.1 - 20 - 300 + 5/2)^2 = 0.250 * 10^8$$

$$I_z = I_{z.f1} + I_{z.f1} + I_{z.w1} + I_{z.w2} \quad \text{(B.12)}$$

$$I_z = (0.517 + 1.041 + 0.409 + 0.250) * 10^8 = 2.217 * 10^8 \text{mm}^4 = 2.217 * 10^{-4} \text{m}^4$$

According to Eurocode 3, Part 1-1 [EN 1993-1-1, 2005], Young's modulus for steel is $E = 210\text{GPa}$. The beam stiffness used in the static calculation is shown in Eq. B.13 – B.15.

$$EA_{beam} = E * A_{section} \quad \text{(B.13)}$$

$$EA_{beam} = 210 \frac{\text{GN}}{\text{m}^2} * 0.01603 \text{m}^2 = 3.366 \text{ GN} = 3366 \text{MN}$$

$$EI_{beam.y} = E * I_y \quad \text{(B.14)}$$

$$EI_{beam.y} = 210 \frac{\text{GN}}{\text{m}^2} * 3.491 * 10^{-4} \text{m}^4 = 73.31 \text{MNm}^2$$

$$EI_{beam.z} = E * I_z \quad \text{(B.15)}$$

$$EI_{beam.z} = 210 \frac{\text{GN}}{\text{m}^2} * 2.217 * 10^{-4} \text{m}^4 = 46.56 \text{MNm}^2$$

The beam is prevented from rotation so there is no torsion considered. The beam's torsional stiffness, needed for the static analysis is assumed to be:

$GI_{beam.v} = 10^9 \text{Nm}^4$.

Since the beam is fire protected and the beam temperature in fire situation is assumed not to increase significantly, the beam stiffness calculated above is used in all ambient and fire design situations.

FORCES IN THE BEAM

Case 1 – forces in 11 cross-sections along the beam:

$$\begin{bmatrix} N \\ Q_y \\ Q_z \\ M_v \\ M_y \\ M_z \end{bmatrix} = \begin{bmatrix} -331.9 & -331.9 & -331.9 & -331.9 & -331.9 & -331.9 & -331.9 & -331.9 & -331.9 & -331.9 & -331.9 \\ -000.0 & -000.0 & -000.0 & -000.0 & -000.0 & -000.0 & -000.0 & -000.0 & -000.0 & -000.0 & -000.0 \\ +454.6 & +361.8 & +268.9 & +176.1 & +083.2 & -009.6 & -102.5 & -195.4 & -288.2 & -381.1 & -473.9 \\ +000.0 & +000.0 & +000.0 & +000.0 & +000.0 & +000.0 & +000.0 & +000.0 & +000.0 & +000.0 & +000.0 \\ -634.0 & -144.1 & +234.3 & +501.3 & +656.9 & +701.0 & +633.7 & +455.0 & +164.9 & -236.7 & -749.7 \\ +000.0 & +000.0 & +000.0 & +000.0 & +000.0 & +000.0 & +000.0 & +000.0 & +000.0 & +000.0 & +000.0 \end{bmatrix} * \begin{bmatrix} \text{kN} \\ \text{kN} \\ \text{kN} \\ \text{kNm} \\ \text{kNm} \\ \text{kNm} \end{bmatrix}'$$

Case 2 – forces in 11 cross-sections along the beam:

$$\begin{bmatrix} N \\ Q_y \\ Q_z \\ M_v \\ M_y \\ M_z \end{bmatrix} = \begin{bmatrix} -258.5 & -258.5 & -258.5 & -258.5 & -258.5 & -258.5 & -258.5 & -258.5 & -258.5 & -258.5 & -258.5 \\ -000.0 & -000.0 & -000.0 & -000.0 & -000.0 & -000.0 & -000.0 & -000.0 & -000.0 & -000.0 & -000.0 \\ +467.0 & +374.1 & +281.3 & +188.4 & +095.5 & +002.7 & -090.2 & -183.0 & -275.9 & -368.8 & -461.6 \\ +000.0 & +000.0 & +000.0 & +000.0 & +000.0 & +000.0 & +000.0 & +000.0 & +000.0 & +000.0 & +000.0 \\ -640.4 & -135.8 & +257.5 & +539.3 & +709.6 & +768.6 & +716.1 & +552.2 & +276.8 & -110.0 & -608.2 \\ +000.0 & +000.0 & +000.0 & +000.0 & +000.0 & +000.0 & +000.0 & +000.0 & +000.0 & +000.0 & +000.0 \end{bmatrix} * \begin{bmatrix} \text{kN} \\ \text{kN} \\ \text{kN} \\ \text{kNm} \\ \text{kNm} \\ \text{kNm} \end{bmatrix}'$$

RESISTANCE CHECK

All six kinds of cross-sectional forces (axial, shear in two directions, torsion and bending in two directions) are obtained from the static analysis. The results are written in the form of a matrix i.e. $N_{amb}(i,j,k)$. The indices (i,j,k) mean:

i is the index of the element number,

j is the index of the cross-section for which the forces are presented,

k is the index denoting the load case.

The matrices for other loads are presented in a similar way: Qy_{amb}, Qz_{amb}, Mv_{amb}, My_{amb}, Mz_{amb}. The loads in fire situation are presented with $fire$ index instead of amb and k denotes the individual fire cases.

The evaluation of the beam's resistance is conducted separately for each element, cross-section and load case.

MATERIAL

The material factors of the S 355 grade steel used in the structure conform to Eurocode 3, Part 1-1, Section 3.2.6 [EN 1993-1-1, 2005] and they are:

$E = 210.0\text{GPa},$

$\nu = 0.30,$

$G = 80.77\text{GPa},$

$f_y = 355.0\text{MPa},$

$f_y = 510.0\text{MPa}.$

The material safety factors according to Section 6.1 of [EN 1993-1-1, 2005] are:

$\gamma_{M0} = 1.00,$

$\gamma_{M1} = 1.00,$

$\gamma_{M2} = 1.25.$

ε following table 5.2 of [EN 1993-1-1, 2005] for grade S 355 is:

$$\varepsilon = \sqrt{\frac{235\text{MPa}}{fy}} = \sqrt{\frac{235\text{MPa}}{355\text{MPa}}} = 0.814 \qquad \text{(B.16)}$$

and

$\eta = 1.0$ for $f_y < 460\text{MPa}.$

CROSS-SECTION CLASS

Since there is a non-zero hogging moment at the support of the beam. This necessitates the determination of the cross-section class for all the beam plates: the top and bottom flanges and the webs. The web has to be checked for both sagging and hogging moments since the beam cross-section is not symmetrical.

- The top flange is cross-section class 1:

$$\frac{b}{t_{f1}} \quad < \quad 33 * \varepsilon \tag{B.17}$$

$$\frac{290\text{mm}}{22\text{mm}} = 13.2 \quad < \quad 33 * 0.814 = 26.8.$$

- The inner part of the bottom flange is cross-section class 1:

$$\frac{b}{t_{f2}} \quad < \quad 33 * \varepsilon \tag{B.18}$$

$$\frac{290\text{mm}}{15\text{mm}} = 19.3 \quad < \quad 33 * 0.814 = 26.8.$$

- The outer part of the bottom flange is cross-section class 2:

$$\frac{b_{f2}-b_{f1}-c}{t_{f2}} \quad > \quad 9 * \varepsilon \tag{B.19}$$

$$\frac{430\text{mm}-300\text{mm}-20\text{mm}}{15\text{mm}} = 7.33 \quad > \quad 9 * 0.814 = 7.33$$

$$\frac{b_{f2}-b_{f1}-c}{t_{f2}} \quad < \quad 10 * \varepsilon \tag{B.20}$$

$$\frac{430\text{mm}-300\text{mm}-20\text{mm}}{15\text{mm}} = 7.33 \quad < \quad 10 * 0.814 = 8.14.$$

- The beam web for the sagging moment

  The beam's horizontal plastic neutral axis measured from the bottom of the beam is:

$$z_{pl.y} = \left(A_{section}/2 - t_{f2} * b_{f2}\right)/(2 * t_w) + t_{f2} \tag{B.21}$$

$$z_{pl.y} = (16030\text{mm}^2/2 - 15\text{mm} * 430\text{mm})/(2 * 5\text{mm}) + 15\text{mm} =>$$

$$z_{pl.y} = 171.5\text{mm} = 0.1715\text{m}.$$

  In accordance with table 5.2 of [EN 1993-1-1, 2005], the ratio α_{span} between the height of the tensioned and compressed parts of the beam's web in the span is calculated from Eq. B.22.

$$\alpha_{span} = \left(h_w - \left(z_{pl.y} - t_{f2}\right)\right)/h_w = \left(298\text{mm} - (175.1\text{mm} - 15\text{mm})\right)/298\text{mm} \tag{B.22}$$

$$\alpha_{span} = 0.4628$$

  Thus the beam web class in the span as specified in table 5.2 of [EN 1993-1-1, 2005] is calculated from Eq. B.23.

$$\frac{h_w}{t_w} \quad < \quad 36 * \varepsilon/\alpha_{span} \tag{B.23}$$

$$\frac{298\text{mm}}{5\text{mm}} = 59.6 \quad < \quad 36 * 0.814/0.4628 = 63.3$$

- The beam web for the hogging moment

  The ratio α_{sup} between the height of the tensioned and compressed parts of the beam's web at the support is calculated from Eq. B.24.

$$\alpha_{sup} = 1 - \alpha_{span} = 1 - 0.4628 = 0.5372 \tag{B.24}$$

  Thus the beam web class at the support, as specified in table 5.2 of [EN 1993-1-1, 2005], is 2.

$$\frac{h_w}{t_w} \quad > \quad 396 * \varepsilon/(13 * \alpha_{sup} - 1) \tag{B.25}$$

$$\frac{298\text{mm}}{5\text{mm}} = 59.6 \quad > \quad 396 * 0.814/(13 * 0.5372 - 1) = 53.9$$

$$\frac{h_w}{t_w} \quad < \quad 456 * \varepsilon/(13 * \alpha_{sup} - 1) \tag{B.26}$$

$$\frac{298\text{mm}}{5\text{mm}} = 59.6 \quad < \quad 456 * 0.814/(13 * 0.5372 - 1) = 62.0$$

BOTTOM FLANGE IN LATERAL BENDING

Since the load from the slab is applied to the outer part of the bottom flange the flange is in bending. The resistance of the flange to bending has to be verified, as does its influence on the resistance of the whole beam cross-section in bending. In the example structure, all the beams only have load on one side. Thus, to simplify matters it can be assumed that the maximal total load on the beam ($Supreme$) is the same as the load on the flange.

$$Supreme = 76.0\,\text{kN/m}$$

The greatest moment in the flange will occur at the outer side of the web. The distance between that place and the applied load is the 50 mm gap plus half of the beam support width. So e equals:

$$e = 50\text{mm} + \frac{60\text{mm}}{2} = 80\text{mm}. \tag{B.27}$$

And the flange bending moment follows Eq. B.28.

$$M_{p.Ed} = e * Supreme \tag{B.28}$$

$$M_{p.Ed} = 0.080\text{m} * 76.0\,\text{kN/m} = 6.08\text{kNm/m}$$

The plastic resistance of the bottom flange per 1 meter of width is:

$$M_{p.pl.Rd} = {t_{f2}}^2/4 * \frac{f_y}{\gamma_{M0}} \tag{B.29}$$

$$M_{p.pl.Rd} = (0.015\text{m})^2/4 * \frac{355*10^6\text{Pa}}{1.00} = 20.0\text{kNm/m}.$$

The resistance utilisation in this example is:

$$\frac{M_{p.Ed}}{M_{p.pl.Rd}} = \frac{6.08\text{kNm/m}}{20.0\text{kNm/m}} = 0.304.$$

The utility ratio of the bottom flange in lateral bending is less than 0.5, so there is no reduction of the beam bending resistance. If the utility ratio were greater than 0.5 and a reduction were necessary there are two ways to do it. For flange class 1 or 2 it is possible to use the effective width of the bottom flange for the calculation of the plastic bending resistance of the beam. The effective width is then calculated following Eq. B.30.

$$b_{f2.eff} = b_{f2} * \sqrt{1 - \left(\frac{M_{p.Ed}}{M_{p.pl.Rd}}\right)^2} \tag{B.30}$$

If the bottom flange is class 3, the effective yield strength of the bottom flange should be calculated following Eq. B.31.

$$y_{f2.eff} = y_{f2} * \sqrt{1 - \left(\frac{M_{p.Ed}}{M_{p.pl.Rd}}\right)^2} \tag{B.31}$$

SHEAR RESISTANCE

The example calculation will be conducted at 3 cross-sections along the beam. The loads for those sections are:

$Q_{z.left} = 467.0\text{kN}$,

$Q_{z.middle} = 2.7\text{kN} \approx 0.0\text{kN}$,

$Q_{z.right} = -461.6\text{kN}$.

According to Eurocode 3, Part 1-1, Section 6.2.6(3) [EN 1993-1-1, 2005], the shear area of a welded box profile can be derived from Eq. B.32.

$$A_v = \eta \sum (h_w * t_w) \tag{B.32}$$

$A_v = 1.2 * 2 * (298\text{mm} * 5\text{mm}) = 3576\text{mm}^2 = 0.00358\text{m}^2$

And the design plastic shear resistance from Eq. B.33.

$$V_{pl.Rd} = \frac{A_v(f_y/\sqrt{3})}{\gamma_{M0}} \tag{B.33}$$

$$V_{pl.Rd} = \frac{0.00358\text{m}^2\left(355 * 10^6\text{Pa}/\sqrt{3}\right)}{1.0} = 732930\text{N} = 732.9\text{kN}$$

Since the torsion in the beam is zero, by definition, the design value of the shear force is $\text{V}_{\text{Ed}} = 467.0\text{kN}$.

According to [TRY, 2009] the resistance to shear buckling has to be verified if:

$$\frac{h_w}{t_w} > \frac{72*\varepsilon}{\eta} \tag{B.34}$$

$$\frac{298\text{mm}}{5\text{mm}} = 59.6 > \frac{72*0.814}{1.2} = 48.8.$$

In that case, the design resistance of unstiffened webs for shear should conform to Eurocode 3, Part 1-5, Section 5.2 [EN 1993-1-1, 2005]:

$$V_{b.Rd} = V_{bw.Rd} + V_{bf.Rd} \leq \frac{2*\eta*f_y*h_w*t_w}{\sqrt{3}*\gamma_{M1}}. \quad \text{(B.35)}$$

The web contribution $V_{bw.Rd}$ is calculated from Eq. B.36, following Section 5.3 of [EN 1993-1-5, 2006].

$$V_{bw.Rd} = \frac{2*\chi_w*f_y*h_w*t_w}{\sqrt{3}*\gamma_{M1}} \quad \text{(B.36)}$$

where:

$\chi_w = 0.83/\bar{\lambda}_w$ according to table 5.1 of [EN 1993-1-5, 2006], (B.37)

$\bar{\lambda}_w = 0.76\sqrt{\frac{f_{yw}}{\tau_{cr}}}$ according to Section 5.3(3) of [EN 1993-1-5, 2006], (B.38)

$\tau_{cr} = k_\tau * \sigma_E$ according to Section 5.3(3) of [EN 1993-1-5, 2006], (B.39)

$\sigma_E = \frac{\pi^2*E*t^2}{12*(1-\nu^2)*b^2}$ according to Annex A.1, Section (2) of [EN 1993-1-5, 2006]. (B.40)

In this example case σ_E is equal to:

$$\sigma_E = \frac{\pi^2*210*10^9\text{Pa}*(5\text{mm})^2}{12*(1-0.3^2)*(298\text{mm})^2} = 53430 * 10^3\text{Pa} = 53.43\text{MPa}.$$

The shear buckling coefficient k_τ can be obtained by referring to Annex A.3 of [EN 1993-1-5, 2006]. Section (1) gives two equations for the calculation of k_τ depending on the ratio of the distance between the stiffeners and the web height $\frac{a}{h_w}$. In the structure in question, the WQ-beams do not have any stiffeners except for the end plates located at the ends of the beam. Thus the stiffener interval a is taken as equal to L.

$$a = L = 12.00\text{m} \quad \text{(B.41)}$$

And the $\frac{a}{h_w}$ ratio will be always greater than one. Thus, for a web without longitudinal stiffeners, k_τ follows Eq. B.42.

$$k_\tau = 5.34 + 4.00(h_w/a)^2 \quad \text{(B.42)}$$

$$k_\tau = 5.34 + 4.00(0.298\text{m}/12.00\text{m})^2 = 5.34.$$

τ_{cr}, $\bar{\lambda}_w$, χ_w, are calculated from equations B.43 – B.45

$$\tau_{cr} = k_\tau * \sigma_E = 5.34 * 53.43\text{MPa} = 285\text{MPa} \quad \text{(B.43)}$$

$$\bar{\lambda}_w = 0.76\sqrt{\frac{f_{yw}}{\tau_{cr}}} = 0.76\sqrt{\frac{355\text{MPa}}{285\text{MPa}}} = 0.848 \quad \text{(B.44)}$$

$$\chi_w = 0.83/\bar{\lambda}_w = 0.83/0.848 = 0.979. \quad \text{(B.45)}$$

The web contribution derived from Eq. B.36 is equal to:

$$V_{bw.Rd} = \frac{2*0.979*355\text{MPa}*298\text{mm}*5\text{mm}}{\sqrt{3}*1.0} = 598570\text{N} = 598.6\text{kN}.$$

As a simplification, it can be assumed that $V_{bf.Rd} = 0.0$. $V_{b.Rd}$ is lower than the limit.

$$V_{b.Rd} = V_{bw.Rd} = 598.6\text{kN} \quad < \quad \frac{2*\eta*f_y*h_w*t_w}{\sqrt{3}*\gamma_{M1}} = \frac{2*1.2*355\text{MPa}*298\text{mm}*5\text{mm}}{\sqrt{3}*1.0} = 732.9\text{kN}$$

The beam's shear resistance is validated from Eq. B.46.

$$\frac{\mathrm{V_{Ed}}}{V_{pl.Rd}} = \frac{467.0\mathrm{kN}}{732.9\mathrm{kN}} = 0.637 \tag{B.46}$$

The beam's shear buckling is validated from Eq. B.47.

$$\frac{\mathrm{V_{Ed}}}{V_{b.Rd}} = \frac{467.0\mathrm{kN}}{598.6\mathrm{kN}} = 0.780 \tag{B.47}$$

BENDING RESISTANCE

The bending resistance of the cross-section is determined according to Eurocode 3, Part 1-1, Section 6.2.5 [EN 1993-1-1, 2005].

There are three methods for calculating the bending resistance depending on the cross-section class of the individual components of the beam.

1. Flanges class 1-2, webs class 1-2

   The plastic bending resistance of the cross-section is calculated following Eurocode 3, Part 1-1, Section 6.2.5, equation (6.13) [EN 1993-1-1, 2005]. The principle of the calculation is presented in Figure B2 and expressed by equation B.48.

$$\mathrm{M_{c.Rd}} = \mathrm{M_{pl.Rd.y}} = \frac{\mathrm{W_{pl} * f_y}}{\gamma_{\mathrm{M0}}} \tag{B.48}$$

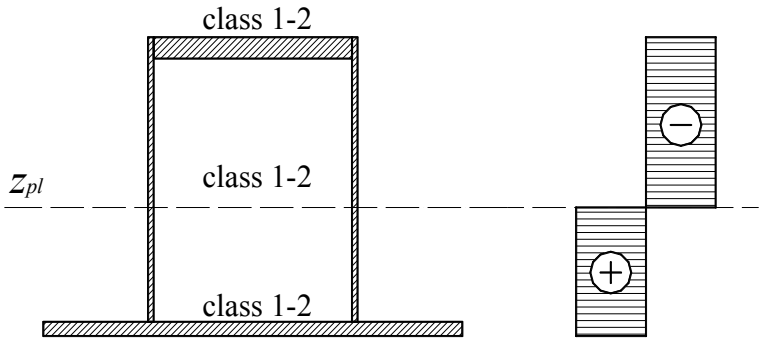

Figure B2. Plastic resistance for class 1-2 section

2. Flanges class 1-2, webs class 3

   The plastic bending resistance of the cross-section is calculated in accordance with Eurocode 3, Part 1-1, Section 6.2.5, equation (6.13) [EN 1993-1-1, 2005]. This procedure uses the effective cross-section of the web that is in class 3 as specified in Section 6.2.2.4 of [EN 1993-1-1, 2005]. The principle of the calculation is presented in Figures B3 and B4, and expressed by equation B.49.

$$\mathrm{M_{c.Rd}} = \mathrm{M_{pl.Rd.y.eff}} = \frac{\mathrm{W_{pl.eff} * f_y}}{\gamma_{\mathrm{M0}}} \tag{B.49}$$

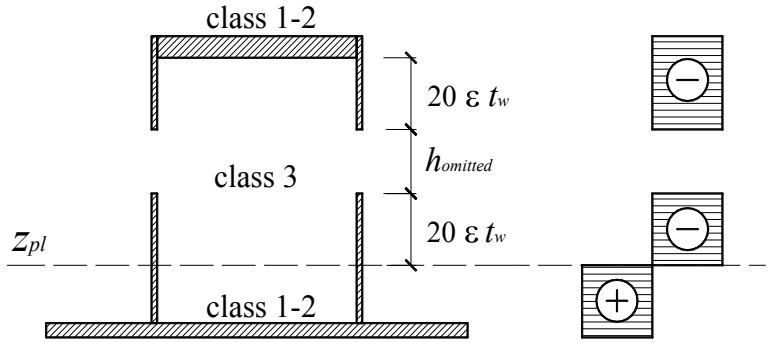

Figure B3. Plastic resistance of the effective area of class 3 section in sagging moment

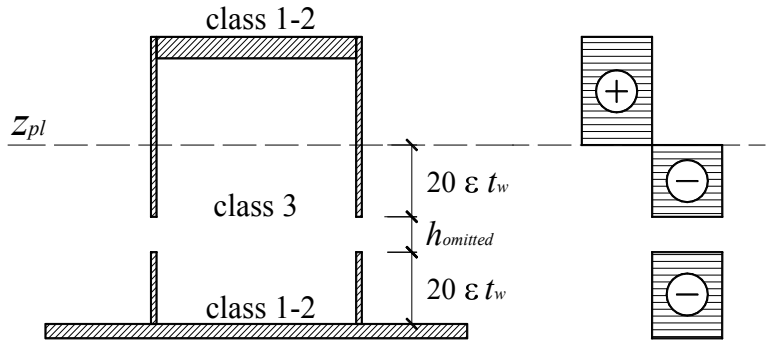

Figure B4. Plastic resistance of the effective area of class 3 section in hogging moment

3. Flanges class 3, webs class 1-3

   The elastic bending resistance of the cross-section is calculated following Eurocode 3, Part 1-1, Section 6.2.5, equation (6.14) [EN 1993-1-1, 2005]. Here, this is given by equation B.50. The principle of the calculation is presented in Figure B5 and expressed by equation B.50.

$$M_{c.Rd} = M_{el.Rd.y} = \frac{W_{el} * f_y}{\gamma_{M0}} \quad \text{(B.50)}$$

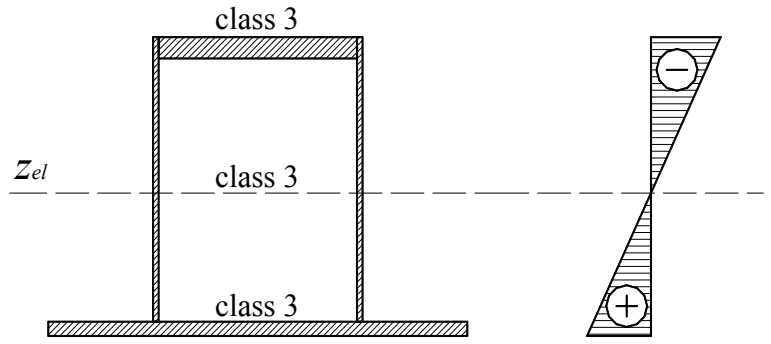

Figure B5. Elastic resistance for class 3 section

The example structure has class 2 beams so the first fully plastic procedure will be used to determine the bending resistance. At this moment, the shear force in the beam has to be taken into account. The interaction of shear and bending in the beam's cross-section is

taken into account as specified in Section 6.2.8 of [EN 1993-1-1, 2005]. If the utility ratio in shear is greater than 0.5, the design resistance of the cross-section is calculated using reduced yield strength. The reduced yield strength of the web is calculated from eq. B.51.

$$f_{y_{web}} = \left(1 - \left(\frac{2*\mathrm{V_{Ed}}}{V_{pl.Rd}} - 1\right)^2\right) * f_y \quad \text{(B.51)}$$

For the example case it is:

$$f_{y_{web}} = \left(1 - \left(2 * \frac{467000\mathrm{N}}{732900\mathrm{N}} - 1\right)^2\right) * 355 * 10^6\mathrm{Pa} = 328.3\mathrm{MPa}.$$

Since the beam cross-section is class 2, the bending resistance of the beam will be calculated as fully plastic resistance. To do this, the plastic neutral axis of the cross-section is required:

$z_{ply} = 171.5\mathrm{mm} = 0.1715\mathrm{m}$

The plastic bending modulus is calculated separately for the flanges and the webs (Esq. B.52 and B.53 respectively). The following calculations are in mm:

$$W_{ply_f} = \left(b_{f2} * t_{f2} * \left(z_{ply} - t_{f2}/2\right)\right) + \left(b_{f1} * t_{f1} * \left(h - z_{ply} - t_{f1}/2\right)\right) \quad \text{(B.52)}$$

$W_{ply_f} = \left(430 * 15 * (171.5 - 15/2)\right) + \left(300 * 22 * (335 - 171.5 - 22/2)\right)$ =>

$W_{ply_f} = 2064300\mathrm{mm}^3 = 0.002064\mathrm{m}^3$

$$W_{ply_w} = 2 * \begin{pmatrix} t_w * \left(z_{ply} - t_{f2}\right) * \left(z_{ply} - t_{f2}\right)/2 + \\ t_w * \left(h_w - z_{ply} + t_{f2}\right) * \left(h_w - z_{ply} + t_{f2}\right)/2 \end{pmatrix}. \quad \text{(B.53)}$$

After simplification, W_{ply_w} is equal to:

$$W_{ply_w} = t_w \left(\left(z_{ply} - t_{f2}\right)^2 + \left(h_w - z_{ply} + t_{f2}\right)^2\right).$$

$W_{ply_w} = 5 * ((171.5 - 15)^2 + (298 - 171.5 + 15)^2) = 222570\mathrm{mm}^3 = 0.000223\mathrm{m}^3$

The plastic bending resistance at the support equals:

$$M_{plRdy_{sup}} = W_{ply_w} * f_y + W_{ply_f} * f_{y_{web}} \quad \text{(B.54)}$$

$M_{plRdy_{sup}} = 0.002064\mathrm{m}^3 * 355.0 * 10^6\mathrm{Pa} + 0.000223\mathrm{m}^3 * 328.3 * 10^6\mathrm{Pa} = 805900\mathrm{Nm}.$

The difference in the shear force values between the two ends of the beam is negligible in terms of its influence on the bending resistance. Thus, the bending resistance at both beam ends is the same. All the intermediate values were calculated for the selected sections along the beam. The maximum bending resistance is in the middle of the beam span. This is where the shear force is practically zero and the bending moment reaches its maximum. The bending resistance in the middle cross-section of the beam is calculated from Eq. B.55.

$$M_{plRdy_{span}} = W_{ply_f} * f_y + W_{ply_w} * f_y \quad \text{(B.55)}$$

$$M_{plRdy_{span}} = 0.002064\text{m}^3 * 355 * 10^6\text{Pa} + 0.000223\text{m}^3 * 355 * 10^6\text{Pa} = 811880\text{Nm}$$

The utilisation ratio for a beam in bending at the end of the beam, where the bending moment is greater, follows Eq. B.56.

$$\frac{M_{Edy_{sup}}}{M_{plRdy_{sup}}} = \frac{640.4\text{kNm}}{805.9\text{kNm}} = 0.795 \quad \text{(B.56)}$$

The utilisation at the cross-section in the middle of the beam span follows Eq. B.57.

$$\frac{M_{Edy_{span}}}{M_{plRdy_{span}}} = \frac{768.5\text{kNm}}{811.9\text{kNm}} = 0.947 \quad \text{(B.57)}$$

AXIAL RESISTANCE

The axial resistance of the beam is calculated using the effective area of the cross-section. The effective area as specified in Eurocode 3, Part 1-1, Section 4.4 of [EN 1993-1-1, 2005] is expressed with Eq. B.58.

$$A_{e.eff} = \rho * A_c \quad \text{(B.58)}$$

where:

A_c is the area of the unreduced cross-section of the plate,

ρ is the reduction factor for plate buckling.

For internal compression elements ρ is calculated from Eq. B.59.

$$\rho = \frac{\overline{\lambda_p} - 0.055(3+\Psi)}{\overline{\lambda_p}^2} \quad \text{if} \quad \overline{\lambda_p} > 0.673 \quad \text{and} \quad (3+\Psi) \geq 0 \quad \text{(B.59)}$$

$$\rho = 1.0 \quad \text{if} \quad \overline{\lambda_p} \leq 0.673$$

For outstanding compression elements ρ is calculated from Eq. B.60.

$$\rho = \frac{\overline{\lambda_p} - 0.188}{\overline{\lambda_p}^2} \quad \text{if} \quad \overline{\lambda_p} > 0.748 \quad \text{(B.60)}$$

$$\rho = 1.0 \quad \text{if} \quad \overline{\lambda_p} \leq 0.748$$

where:

Ψ is the stress ratio according to tables 4.1 and 4.2 of [EN 1993-1-1, 2005],

$$\overline{\lambda_p} = \frac{\bar{b}/t}{28.4\varepsilon\sqrt{k_\sigma}} \quad \text{(B.61)}$$

where:

$\bar{b}$ is the appropriate width of the considered element,

k_σ is the buckling factor as specified in tables 4.1 and 4.2 of [EN 1993-1-1, 2005].

The reduction factor for all the plates of the beam under axial compression is calculated as follows:

- For the beam webs, due to stress distribution under axial load:

  $k_\sigma = 4.0$ and $\Psi = 1.0$,

  $$\overline{\lambda_p} = \frac{h_w/t_w}{28.4\varepsilon\sqrt{k_\sigma}} = \frac{298\text{mm}/5\text{mm}}{28.4*0.814*\sqrt{4}} = 1.290, \quad \text{(B.62)}$$

  $$\rho_w = \frac{\overline{\lambda_p} - 0.055(3+\Psi)}{\overline{\lambda_p}^2} = \frac{1.290 - 0.055(3+1)}{1.290^2} = 0.643. \quad \text{(B.63)}$$

- For the top flange, due to stress distribution under axial load:

  $k_\sigma = 4.0$ and $\Psi = 1.0$,

  $$\overline{\lambda_p} = \frac{h_w/t_w}{28.4\varepsilon\sqrt{k_\sigma}} = \frac{290\text{mm}/22\text{mm}}{28.4*0.814*\sqrt{4}} = 0.285, \quad \text{(B.64)}$$

  $\rho_{f1} = 1.0$.

- For the inner part of the bottom flange, due to stress distribution under axial load:

  $k_\sigma = 4.0$ and $\Psi = 1.0$,

  $$\overline{\lambda_p} = \frac{h_w/t_w}{28.4\varepsilon\sqrt{k_\sigma}} = \frac{290\text{mm}/15\text{mm}}{28.4*0.814*\sqrt{4}} = 0.418, \quad \text{(B.65)}$$

  $\rho_{f2.i} = 1.0$.

- For the protruding part of the bottom flange, due to stress distribution under axial load:

  $k_\sigma = 0.43$ and $\Psi = 1.0$,

  $$\overline{\lambda_p} = \frac{h_w/t_w}{28.4\varepsilon\sqrt{k_\sigma}} = \frac{110\text{mm}/15\text{mm}}{28.4*0.814*\sqrt{0.43}} = 0.484, \quad \text{(B.66)}$$

  $\rho_{f2.o} = 1.0$.

Since only the web cross-sectional area is reduced, the reduced area of the whole cross-sectional area is calculated from Eq. B.67.

$$A_{e.eff.section} = 2 * \rho_w * t_w * h_w + t_{f1} * b_{f1} + t_{f2} * b_{f2} \quad \text{(B.67)}$$

$A_{e.eff.section} = 2 * 0.643 * 5\text{mm} * 298\text{mm} + 22\text{mm} * 300\text{mm} + 15\text{mm} * 430\text{mm}$ =>

$A_{e.eff.section} = 14966\text{mm}^2 = 0.01497\text{m}^2$

Thus, the resistance of the beam in pure compression is calculated from Eq. B.68.

$$N_{Rd} = A_{e.eff.section} * f_y \quad \text{(B.68)}$$

$N_{Rd} = 0.01497\text{m}^2 * 355 * 10^6\text{Pa} = 5.314 * 10^6\text{N} = 5314\text{kN}$

The compressive force in the beam in load case 2 equals:

$N_{Ed} = 258.5\text{kN}$.

The beam's utility in compression is calculated from Eq. B.69.

$$\frac{N_{Ed}}{N_{Rd}} = \frac{258.5\text{kN}}{5314\text{kN}} = 0.049 \quad \text{(B.69)}$$

Due to the web reduction, the neutral axis of the cross-section changes. The axial force in the beam acting along the new axis of the beam gives additional bending moment, and this has to be taken into account when calculating the bending resistance.

The new elastic neutral axis of the beam is:

$$z_{0.y} = \begin{pmatrix} b_{f2}/2 * {t_{f2}}^2 + t_{f1} * b_{f1} * \left(t_{f1}/2 + h_w + t_{f2}\right) \\ +2 * t_w * (\rho_w h_w/2)\left(\left(\rho_w h_w/4 + t_{f2}\right) + \left(h_w - \rho_w h_w/4 + t_{f2}\right)\right) \end{pmatrix} \Big/ A_{e.eff.section}. \quad \text{(B.70)}$$

Substituting all the dimensions in [mm] gives:

$$z_{0.y} = \begin{pmatrix} 430/2 * 15^2 + 22 * 300 * (22/2 + 298 + 15) \\ +2 * 5 * (0.643 * 298/2)\left(\left(0.643 * \frac{298}{4} + 15\right) + (298 - 0.643 * 298/4 + 15)\right) \end{pmatrix} \Big/ 14966$$

$$z_{0.y} = 167.1\text{mm} = 0.1671\text{m}.$$

The additional moment coming from the eccentric axial force in the beam follows Eq. 3.71.

$$M_{Edy_{addition}} = N_{Ed} * \left(z_{pl.y} - z_{0.y}\right) \quad \text{(B.71)}$$

$$M_{Edy_{addition}} = 258.5 * 10^3\text{N} * (0.1715\text{m} - 0.1671\text{m}) = 1137\text{Nm} = 1.14\text{kNm}.$$

Since the neutral axis for the reduced cross-section is higher than the plastic axis with respect to which the bending resistance was calculated, the additional bending moment increases the values in the span and decreases the values at the supports. In this case the bending utility in the span is:

$$\frac{M_{Edy_{span}} + M_{Edy_{addition}}}{M_{plRdy_{span}}} = \frac{768.5\text{kNm} + 1.1\text{kNm}}{811.9\text{kNm}} = 0.948. \quad \text{(B.72)}$$

FLANGE INDUCED BUCKLING

Buckling of the flange that is in compression in the plane of the web is prevented by fulfilling the criterion specified in Eurocode 3, Part 1-5, Section 8(1) [EN-1993-1-5, 2006]. The criterion is expressed with Eq. B.73.

$$\frac{h_w}{t_w} \leq k \frac{E}{f_{yf}} \sqrt{\frac{A_w}{A_{fc}}} \quad \text{(B.73)}$$

where:

A_w is the area of the web,

A_{fc} is the area of the flange in compression,

f_{yf} is the yield strength of the flange in compression,

$k = 0.4$ for the cross-section class 2, in accordance with Section 8(1) of [EN-1993-1-5, 2006].

The criterion is verified for both situations, when either the bottom or top flange is in compression.

- $\frac{0.298\text{m}}{0.005\text{m}} \leq 0.4 \frac{210*10^9\text{Pa}}{355*10^6\text{Pa}} \sqrt{\frac{2*0.298\text{m}*0.005\text{m}}{0.300\text{m}*0.022\text{m}}}$

  $59.6 \leq 160.8$ The requirement is met for the top flange in compression.

- $\frac{0.298\text{m}}{0.005\text{m}} \leq 0.4 \frac{210*10^9\text{Pa}}{355*10^6\text{Pa}} \sqrt{\frac{2*0.298\text{m}*0.005\text{m}}{0.430\text{m}*0.015\text{m}}}$

  $59.6 \leq 159.0$ The requirement is met for the bottom flange in compression.

BEAM AMBIENT CALCULATION SUMARY

Another requirement imposed on the WQ-beam is that the webs are at least class 3. The Eurocode requirement for class 3 parts subjected to bending and compression is used to create $Class_{requirement}$ constraint. The requirement is expressed with equation B.74.

$$Class_{requirement} = \frac{c/t}{\frac{42\varepsilon}{0.67+0.33\Psi}} \leq 1.0 \quad \text{when} \quad \Psi > -1$$

$$Class_{requirement} = \frac{c/t}{62\varepsilon(1-\Psi)\sqrt{(-\Psi)}} \leq 1.0 \quad \text{when} \quad \Psi \leq -1 \qquad \text{(B.74)}$$

In a similar way, all the requirements, including flange induced buckling, are written as the $utility$ vector following Eq. B.75.

$$utility = \left[Class_{requirement}, \frac{M_{p.Ed}}{M_{p.pl.Rd}}, \frac{\text{V}_{\text{Ed}}}{V_{pl.Rd}}, \frac{\text{V}_{\text{Ed}}}{V_{b.Rd}}, \frac{N_{Ed}}{N_{Rd}}, \frac{M_{Edy_{span}}}{M_{plRdy_{span}}}, \frac{N_{Ed}}{N_{Rd}} + \frac{M_{Edy_{span}}}{M_{plRdy_{span}}}, \frac{\frac{h_w}{t_w}}{k\frac{E}{f_{yf}}\sqrt{\frac{A_w}{A_{fc}}}} \right] \leq 1.0 \qquad \text{(B.75)}$$

For the example beam at the end and in the middle of the span the $utility$ vectors are:

$utility_{sup} = [0.00,\ 0.304,\ 0.637,\ 0.780,\ 0.049,\ 0.793,\ 0.842,\ 0.371] \leq 1.0,$

$utility_{span} = [0.00,\ 0.304,\ 0.004,\ 0.005,\ 0.049,\ 0.948,\ 0.997,\ 0.371] \leq 1.0.$

For each beam element the highest utilities of the cross-section are recorded. For the example beam in load case 2 the utility vector describing the whole beam would be:

$utility_2 = [0.00,\ 0.304,\ 0.637,\ 0.780,\ 0.049,\ 0.948,\ 0.997,\ 0.371] \leq 1.0.$

The same beam in the first load case has a utility ratio of 0.992 at the support over the middle column. The shear utility at the support is calculated from Eq. B.76.

$$\frac{\text{V}_{\text{Ed}}}{V_{pl.Rd}} = \frac{473.9\text{kN}}{732.9\text{kN}} = 0.647 \qquad \text{(B.76)}$$

So the reduced yield strength of the web is:

$$f_{y_{web}} = \left(1 - \left(\frac{2*\text{V}_{\text{Ed}}}{V_{pl.Rd}} - 1\right)^2\right) * f_y = (1 - (2 * 0.647 - 1)^2) * 355\text{MPa} = 324.3\text{MPa}. \qquad \text{(B.77)}$$

The plastic bending resistance at the support is then:

$$M_{plRdy_{sup}} = W_{ply_w} * f_y + W_{ply_f} * f_{y_{web}} \quad \text{(B.78)}$$

$$M_{plRdy_{sup}} = 0.002064\text{m}^3 * 355.0 * 10^6\text{Pa} + 0.000223\text{m}^3 * 324.3 * 10^6\text{Pa} = 805.0\text{kNm}.$$

The bending utility is calculated from Eq. B.79:

$$\frac{M_{Edy_{sup}}}{M_{plRdy_{sup}}} = \frac{749.7\text{kNm}}{805.0\text{kNm}} = 0.930. \quad \text{(B.79)}$$

The utilisation of axial compression is calculated from equation B.80.

$$\frac{N_{Ed}}{N_{Rd}} = \frac{331.9\text{kN}}{5314\text{kN}} = 0.062 \quad \text{(B.80)}$$

And together, axial compression and bending give $0.930 + 0.062 = 0.992$.

The maximal utility ratios for the example beam in load case 1 are:

$$utility_1 = [0.00,\ 0.304,\ 0.647,\ 0.792,\ 0.062,\ 0.930,\ 0.992,\ 0.371] \leq 1.0.$$

APPENDIX C

The following appendix presents detailed resistance check of two example columns in three different design situations:

- normal design situation;
- fire design situation at elevated temperature;
- fire design situation at ambient temperature.

For the static analysis of the frame the column stiffnesses are required. Due to the composite construction the column stiffness varies in all 3 design situations. The column stiffness changes along with the change in temperature.

In this example, the fire resistance class of the structure is R 60, meaning that the structure is required to withstand 60 minutes of ISO fire [EN 1991-1-2, 2003]. The distribution of temperature in the column cross-section is taken from [TRY, 2004]. Depending on the temperature, the Young's modulus of all three materials of which the column is composed is reduced according to Tables C1-C3.

Table C1. Table 3.2 of Eurocode 4, Part 1-2 [EN 1994-1-2, 2006] presenting reduction factors k_θ for stress-strain relationships of structural steel at elevated temperatures.

Steel Temperature θ_a[°C]	$k_{E,\theta} = \frac{E_{a,\theta}}{E_a}$	$k_{p,\theta} = \frac{f_{ap,\theta}}{f_{ay}}$	$k_{y,\theta} = \frac{f_{ay,\theta}}{f_{ay}}$	$k_{u,\theta} = \frac{f_{au,\theta}}{f_{ay}}$
20	1,00	1,00	1,00	1,25
100	1,00	1,00	1,00	1,25
200	0,90	0,807	1,00	1,25
300	0,80	0,613	1,00	1,25
400	0,70	0,420	1,00	
500	0,60	0,360	0,78	
600	0,31	0,180	0,47	
700	0,13	0,075	0,23	
800	0,09	0,050	0,11	
900	0,0675	0,0375	0,06	
1000	0,0450	0,0250	0,04	
1100	0,0225	0,0125	0,02	
1200	0	0	0	

Table C2. Table 3.3 of Eurocode 4, Part 1-2 [EN 1994-1-2, 2006] presenting values for the two main parameters of the stress-strain relationships of concrete at elevated temperatures.

Concrete Temperature θ_c [°C]	$k_{c,\theta} = f_{c,\theta}/f_c$		$\varepsilon_{cu,\theta} \cdot 10^3$
	NC	LC	NC
20	1	1	2,5
100	1	1	4,0
200	0,95	1	5,5
300	0,85	1	7,0
400	0,75	0,88	10,0
500	0,60	0,76	15,0
600	0,45	0,64	25,0
700	0,30	0,52	25,0
800	0,15	0,40	25,0
900	0,08	0,28	25,0
1000	0,04	0,16	25,0
1100	0,01	0,04	25,0
1200	0	0	-

Table C3. Table 3.4 of Eurocode 4, Part 1-2 [EN 1994-1-2, 2006] presenting reduction factors k_θ for stress-strain relationships of cold work reinforcing steel at elevated temperatures.

Steel Temperature θ_s [°C]	$k_{E,\theta} = \frac{E_{s,\theta}}{E_s}$	$k_{p,\theta} = \frac{f_{sp,\theta}}{f_{sy}}$	$k_{y,\theta} = \frac{f_{sy,\theta}}{f_{sy}}$
20	1,00	1,00	1,00
100	1,00	0,96	1,00
200	0,87	0,92	1,00
300	0,72	0,81	1,00
400	0,56	0,63	0,94
500	0,40	0,44	0,67
600	0,24	0,26	0,40
700	0,08	0,08	0,12
800	0,06	0,06	0,11
900	0,05	0,05	0,08
1000	0,03	0,03	0,05
1100	0,02	0,02	0,03
1200	0	0	0

It should be noted that due to the nature of Table C2, Young's modulus for the concrete is not the same for 20 ˚C in fire situation as it is in the ambient one. Because of this, and also the fact that in fire situation only parts of the columns are subjected to temperature increase, there are three different column stiffnesses that need to be calculated.

Let us consider the column of a cross-section presented in Figure C1.

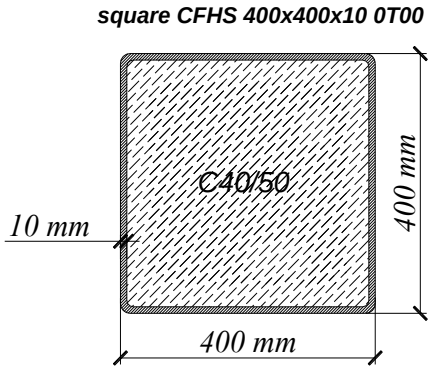

Figure C1. Cross-sections of the considered example column

The dimensions used for the calculation are as follows:

- $col = 400\text{mm}$ - steel tube width,
- $t = 10\text{mm}$ - steel tube wall thickness,
- $L_{eff} = 3600\text{mm}$ - effective length of the column.

The stiffness of a CFHS is composed of 3 elements. The nominal stiffness of each material (Young's modulus) is multiplied by the corresponding material cross-section area and the second moment of area to calculate the axial and bending stiffnesses respectively. For the bending stiffness, the composite action of the elements is also taken into account by using the correction and calibration factors. The material notations follow those of EN 1994-1-2 [EN 1994-1-2, 2006]: a – steel, c – concrete, s – reinforcement. In order to simplify matters, all the roundings of the steel profile are omitted in the calculation of the geometric characteristics of the column cross-section.

The area and the second moment of the area of the steel section are calculated by Esq. C.1 – C.2.

$$A_a = 4 * (col - t) * t \tag{C.1}$$

$$A_a = 4 * (400\text{mm} - 10\text{mm}) * 10\text{mm} = 15600\text{mm}^2 = 0.0156\text{m}^2$$

$$I_a = 4 * (col - t) * t \tag{C.2}$$

$$I_a = 4 * (400\text{mm} - 10\text{mm}) * 10\text{mm} = 3.957 * 10^8\text{mm}^4 = 3.957 * 10^{-4}\text{m}^4$$

The geometric characteristics of the uncracked concrete gross cross-sectional area follow Esq. C.3 – C.4.

$$A_{c.gross} = (col - 2 * t)^2 \tag{C.3}$$

$$A_{c.gross} = (400\text{mm} - 2 * 10\text{mm})^2 = 144400\text{mm}^2 = 0.1444\text{m}^2$$

$$I_{c.gross} = \frac{(col - 2*t)^4}{12} \tag{C.4}$$

$$I_{c.gross} = \frac{(400\text{mm} - 2*10\text{mm})^4}{12} = 1.738 * 10^9\text{mm}^4 = 1.738 * 10^{-3}\text{m}^4$$

Since there is no reinforcement in this column, the net area of the concrete cross-section and the net second moment of area of the concrete cross-section are the same as for the gross cross-section.

$$A_c = A_{c.gross} = 0.1444\mathrm{m}^2 \quad \text{(C.5)}$$

$$I_c = I_{c.gross} = 1.738 * 10^{-3}\mathrm{m}^4 \quad \text{(C.6)}$$

COLUMN STIFFNESS AT AMBIENT TEMPERATURE

The axial stiffness of the column is shown in Eq. C.7.

$$EA = E_a A_a + E_{cm} A_c + E_s A_s \quad \text{(C.7)}$$

$$EA = 210 * 10^9\mathrm{Pa} * 0.0156\mathrm{m}^2 + 35.0 * 10^9\mathrm{Pa} * 0.1444\mathrm{m}^2 = 8.330 * 10^9\mathrm{N} = 8330\mathrm{MN}.$$

According to Section 6.7.3.3 of Eurocode 4, Part 1-1 [EN 1994-1-1, 2004], the characteristic value of the effective flexural stiffness used for the determination of the relative slenderness is shown by Eq. C.8.

$$EI_{eff} = E_a I_a + K_e * E_{cm} I_c + E_s I_s \quad \text{(C.8)}$$

where:

K_e is a correction factor equal to 0.6.

So, the effective flexural stiffness is:

$$EI_{eff} = 210 * 10^9\mathrm{Pa} * 3.957 * 10^{-4}\mathrm{m}^4 + 0.6 * 35.0 * 10^9\mathrm{Pa} * 1.738 * 10^{-3}\mathrm{m}^4 =>$$

$$EI_{eff} = 119.60 * 10^6\mathrm{Nm}^2 = 119600\ \mathrm{kNm}^2.$$

The design value of the effective flexural stiffness that is used to determine the sectional forces according to point 6.7.3.4 of Eurocode 4, Part 1-1 [EN 1994-1-1, 2004] is Eq. C.9.

$$EI_{eff.II} = K_o * (E_a I_a + K_{e.II} * E_{cm} I_c + E_s I_s) \quad \text{(C.9)}$$

where:

$K_{e.II}$ is a correction factor equal to 0.5,

K_o is a calibration factor equal to 0.9.

So the design value of effective flexural stiffness is derived from Eq. C.10.

$$EI_{eff.II} = 0.9 * (E_a I_a + 0.5 * E_{cm} I_c + E_c I_c) \quad \text{(C.10)}$$

$$EI_{eff.II} = 0.9 * (210 * 10^9\mathrm{Pa} * 3.957 * 10^{-4}\mathrm{m}^4 + 0.5 * 35.0 * 10^9\mathrm{Pa} * 1.738 * 10^{-3}\mathrm{m}^4) =>$$

$$EI_{eff.II} = 102.20 * 10^6\mathrm{Nm}^2 = 102200\ \mathrm{kNm}^2$$

For the ambient design situation it is necessary to determine whether the long term effect needs to be taken into account. According to [TRY, 2004] the long term effect has to be taken into account if the dimensionless column slenderness $\bar{\lambda}$ is smaller than the comparative slenderness λ_{vert}. Comparative slenderness is expressed with Eq. C.11.

$$\lambda_{vert} = \frac{0.8}{1-\delta} \quad \text{(C.11)}$$

where:

δ is the steel tube contribution ratio – the ratio of the plastic axial resistance of the steel tube and the plastic resistance of the composite cross-section and follows Eq. C.12,

$$\delta = \frac{A_a * f_{yd}}{N_{plRd}} \quad \text{(C.12)}$$

where:

N_{plRd} is the design plastic axial resistance of the composite section expressed with Eq. C.13,

$$N_{plRd} = A_a * f_{yd} + A_c * f_{cd} + A_s * f_{sd} \quad \text{(C.13)}$$

where the design values of the materials follow Esq. C.14 – C.16.

Structural steel $$f_{yd} = \frac{f_a}{\gamma_a} = \frac{355\text{MPa}}{1.10} = 322.7\text{MPa}. \quad \text{(C.14)}$$

Concrete $$f_{cd} = \frac{f_{ck}}{\gamma_c} = \frac{40\text{MPa}}{1.35} = 29.6\text{MPa}. \quad \text{(C.15)}$$

Reinforcing steel $$f_{sd} = \frac{f_{sk}}{\gamma_s} = \frac{500\text{MPa}}{1.15} = 434.8\text{MPa}. \quad \text{(C.16)}$$

$$N_{plRd} = 0.0156\text{m}^2 * 322.7 * 10^6\text{Pa} + 0.1444\text{m}^2 * 29.6 * 10^6\text{Pa} = 9308\text{kN}.$$

Thus:

$$\delta = \frac{0.0156\text{m}^2 * 322.7 * 10^6\text{Pa}}{9308 * 10^3\text{N}} = 0.541,$$

so the comparative slenderness equals:

$$\lambda_{vert} = \frac{0.8}{1-0.541} = 1.74.$$

The dimensionless column slenderness has to be lower than 2.0 and is calculated from:

$$\bar{\lambda} = \sqrt{\frac{N_{plR}}{N_{cr}}}, \quad \text{(C.17)}$$

where:

N_{plR} is the characteristic plastic axial resistance of the composite section,

$$N_{plR} = 0.0156\text{m}^2 * 355.0 * 10^6\text{Pa} + 0.1444\text{m}^2 * 40.0 * 10^6\text{Pa} =>$$

$$N_{plR} = 11.31 * 10^6\text{N} = 11310\text{kN}$$

N_{cr} is Euler critical force calculated for l_e equal to single storey height - 3.6 m:

$$N_{cr} = \frac{\pi^2}{l_e{}^2} EI_{eff} = \frac{\pi^2}{(3.6\text{ m})^2} 119.6 * 10^6\text{Nm}^2 = 91.0 * 10^6\text{N} = 91000\text{kN}. \quad \text{(C.18)}$$

$$\bar{\lambda} = \sqrt{\frac{11.31 * 10^6\text{N}}{91.99 * 10^6\text{N}}} = 0.351$$

$$\bar{\lambda} = 0.35 < \lambda_{vert} = 1.74.$$

The column's dimensionless slenderness is below the limit, so the long term effects do not have to be taken into account in this example. However, if this factor were to be taken into account, the Young's modulus of the concrete affected by the long term effect should be calculated using Eq. C.19.

$$E_{c.eff} = E_{cm} * \frac{1}{1+\left(\frac{N_{g.Sd}}{N_{Sd}}\right)*\phi_t} \quad \text{(C.19)}$$

where:

$\frac{N_{g.Sd}}{N_{Sd}}$ is equal to $PTratio$,

ϕ_t is the creep coefficient according to Eurocode 4, Part 1-1 [EN 1994-1-1, 2004] point 3.1.4. This is calculated for relative humidity of 80%, loading time of 30 days, and concrete C40/50. It would have a value of 1.50.

In the event of second order effects being taken into account, $E_{c.eff}$ is used to calculate axial stiffness, flexural stiffness and the design flexural stiffness.

COLUMN STIFFNESS IN FIRE AT 20 °C.

The axial stiffness of the column is:

$$EA_{\theta.20} = E_{a.\theta.20}A_a + E_{c.\theta.20}A_c + E_{s.\theta.20}A_s \quad \text{(C.20)}$$

$$EA_{\theta.20} = 210 * 10^9\text{Pa} * 0.0156\text{m}^2 + 16.0 * 10^9\text{Pa} * 0.1444\text{m}^2 = 5.586 * 10^9\text{N} = 5586\text{MN}.$$

According to point 6.7.3.3 of Eurocode 4, Part 1-1 [EN 1994-1-1, 2004] the characteristic value of the effective flexural stiffness used for determination of the relative slenderness follows Eq. C.21.

$$EI_{eff.\theta.20} = E_{a.\theta.20}I_a + K_e * E_{cm.\theta.20}I_c + E_{c.\theta.20}I_c \quad \text{(C.21)}$$

where:

K_e is a correction factor equal to 0.8.

So, the effective flexural stiffness is:

$$EI_{eff.\theta.20} = 210 * 10^9\text{Pa} * 3.957 * 10^{-4}\text{m}^4 + 0.8 * 16.0 * 10^9\text{Pa} * 1.738 * 10^{-3}\text{m}^4 =>$$

$$EI_{eff.\theta.20} = 105.30 * 10^6\text{Nm}^2 = 105300\ \text{kNm}^2.$$

The design value of the effective flexural stiffness that is used to determine the sectional forces as in point 6.7.3.4 of Eurocode 4, Part 1-1 [EN 1994-1-1, 2004] follows Eq. C.22.

$$EI_{eff.\theta.20.II} = K_o * (E_{a.\theta.20}I_a + K_{e.II} * E_{c.\theta.20}I_c + E_{s.\theta.20}I_s) \quad \text{(C.22)}$$

where:

$K_{e.II}$ is a correction factor equal to 0.5,

K_o is a calibration factor equal to 0.9.

So the design value of effective flexural stiffness is:

$$EI_{eff.\theta.20.II} = 0.9 * (E_{a.\theta.20} I_a + 0.5 * E_{c.\theta.20} I_c + E_{c.\theta.20} I_c) \quad \text{(C.23)}$$

$EI_{eff.\theta.20.II} = 0.9 * (210 * 10^9\text{Pa} * 3.957 * 10^{-4}\text{m}^4 + 0.5 * 16.0 * 10^9\text{Pa} * 1.738 * 10^{-3}\text{m}^4)$ =>

$EI_{eff.\theta.20.II} = 87.30 * 10^6\text{Nm}^2 = 87300\ \text{kNm}^2.$

The long term effects in fire situation have not been taken into account.

COLUMN STIFFNESS IN FIRE SITUATION AT ELEVATED TEMPERATURE

The temperatures for the 400x400x10 0T00 column after 60 minutes taken from [TRY, 2004] are:

- 889 ˚C – steel tube temperature,
- 335 ˚C – concrete filling temperature.

The reduction factors for the stress-strain relation ratio for all three materials used in columns (in general) are presented in Tables C1-C3. Therefore, Young's modulus for the steel tube and the concrete filling used in the example column are calculated from Esq. C.24 – C.25.

- Young's modulus of the steel tube:

$$E_{a.\theta} = E_a * k_{Ea.\theta} \quad \text{(C.24)}$$

where:

$k_{Ea.\theta}$ is the reduction factor for the tube's Young's modulus at the temperature of 889 ˚C calculated from Table C1,

$k_{Ea.\theta} = \frac{889^\circ\text{C} - 800^\circ\text{C}}{900^\circ\text{C} - 800^\circ\text{C}} * (0.0675 - 0.0900) + 0.0900 = 0.0700.$

$E_{a.\theta} = 210.0GPa * 0.0700 = 14.70GPa.$

- Young's modulus of the concrete filling:

$$E_{csec.\theta} = k_{c.\theta} * \frac{f_{ck}}{\varepsilon_{cu.\theta}} \quad \text{(C.25)}$$

where:

$\varepsilon_{cu.\theta}$ is the reduction factor for concrete Young's modulus at the temperature of 335 ˚C calculated from Table C2,

$\varepsilon_{cu.\theta} = \frac{335^\circ\text{C} - 300^\circ\text{C}}{400^\circ\text{C} - 300^\circ\text{C}} * (0.010 - 0.007) + 0.007 = 0.0080$

$k_{c.\theta}$ is the strength reduction factor for concrete at the temperature of 335 ˚C calculated from Table C2,

$k_{c.\theta} = \frac{335^\circ\text{C} - 300^\circ\text{C}}{400^\circ\text{C} - 300^\circ\text{C}} * (0.75 - 0.85) + 0.085 = 0.815.$

$E_{csec.\theta} = 0.815 * \frac{0.040\text{GPa}}{0.0080} = 4.08\text{GPa}.$

Using these material properties, the column stiffness in fire can be calculated.

The axial stiffness of the column follows Eq. C.26.

$$EA_\theta = E_{a.\theta}A_a + E_{c.\theta}A_c + E_{s.\theta}A_s \quad \text{(C.26)}$$

$$EA_\theta = 14.70 * 10^9\text{Pa} * 0.0156\text{m}^2 + 4.08 * 10^9\text{Pa} * 0.1444\text{m}^2 = 8.185 * 10^8\text{N} = 818\text{MN}$$

According to Section 6.7.3.3 of Eurocode 4, Part 1-1 [EN 1994-1-1, 2004] the characteristic value of the effective flexural stiffness used for determination of the relative slenderness is calculated from Eq. C.27.

$$EI_{eff.\theta} = K_{ea} * E_{a.\theta}I_a + K_{ec} * E_{csec.\theta}I_c + K_{es} * E_{s.\theta}I_s \quad \text{(C.27)}$$

where:

K_{ea} is a correction factor, for steel tube equal to 0.9,

K_{ec} is a correction factor, for concrete filling equal to 0.8,

K_{es} is a correction factor, for reinforcement equal to 0.9.

So, the effective flexural stiffness is:

$$EI_{eff.\theta} = 0.9 * 14.70 * 10^9\text{Pa} * 3.957 * 10^{-4}\text{m}^4 + 0.8 * 4.08 * 10^9\text{Pa} * 1.738 * 10^{-3}\text{m}^4 \Rightarrow$$

$$EI_{eff.\theta} = 10.91 * 10^6\text{Nm}^2 = 10910\ \text{kNm}^2.$$

The design value of the effective flexural stiffness that is used to determine the sectional forces specified in Section 6.7.3.4 of Eurocode 4, Part 1-1 [EN 1994-1-1, 2004] follows Eq. C.28.

$$EI_{eff.\theta.II} = K_o * (E_{a.\theta}I_a + K_{e.II} * E_{c.\theta}I_c + E_{s.\theta}I_s) \quad \text{(C.28)}$$

where:

$K_{e.II}$ is a correction factor equal to 0.5,

K_o is a calibration factor equal to 0.9.

So the design value of effective flexural stiffness for the example column follows Eq. C.29.

$$EI_{eff.\theta.II} = 0.9 * (E_{a.\theta}I_a + 0.5 * E_{c.\theta}I_c + E_{c.\theta}I_c) \quad \text{(C.29)}$$

$$EI_{eff.\theta.II} = 0.9 * (14.70 * 10^9\text{Pa} * 3.957 * 10^{-4}\text{m}^4 + 0.5 * 4.08 * 10^9\text{Pa} * 1.738 * 10^{-3}\text{m}^4) \Rightarrow$$

$$EI_{eff.\theta.II} = 8.43 * 10^6\text{Nm}^2 = 8430\ \text{kNm}^2$$

The long term effects in fire situation are not taken into account.

FORCES IN THE COLUMN

The cross-sectional forces for the corner column of the example structure are presented below. The matrices show the critical cross-sectional forces for the three chosen columns. The locations of the chosen columns are shown in Figure C2.

Critical loads for the edge column on the top floor (no. 13): case 2 and fire respectively:

$$\begin{bmatrix} N_{case2} \\ Q_{y.case2} \\ Q_{z.case2} \\ M_{v.case2} \\ M_{y.case2} \\ M_{z.case2} \end{bmatrix} = \begin{bmatrix} -486.6 & -467.0 \\ -000.0 & -000.0 \\ -258.5 & -258.5 \\ +000.0 & +000.0 \\ +187.6 & -743.0 \\ +000.0 & +000.0 \end{bmatrix} * \begin{bmatrix} \text{kN} \\ \text{kN} \\ \text{kN} \\ \text{kNm} \\ \text{kNm} \\ \text{kNm} \end{bmatrix}' \qquad \begin{bmatrix} N_{\theta} \\ Q_{y.\theta} \\ Q_{z.\theta} \\ M_{v.\theta} \\ M_{y.\theta} \\ M_{z.\theta} \end{bmatrix} = \begin{bmatrix} -290.1 & -270.5 \\ -000.0 & -000.0 \\ -192.2 & -192.2 \\ +000.0 & +000.0 \\ +253.4 & -438.4 \\ +000.0 & +000.0 \end{bmatrix} * \begin{bmatrix} \text{kN} \\ \text{kN} \\ \text{kN} \\ \text{kNm} \\ \text{kNm} \\ \text{kNm} \end{bmatrix}'$$

Critical loads for edge column on the bottom floor (no. 1): case 1 and fire respectively:

$$\begin{bmatrix} N_{case1} \\ Q_{y.case1} \\ Q_{z.case1} \\ M_{v.case1} \\ M_{y.case1} \\ M_{z.case1} \end{bmatrix} = \begin{bmatrix} -1435.8 & -1416.2 \\ -000.0 & -000.0 \\ -147.6 & -147.6 \\ +000.0 & +000.0 \\ -178.9 & +352.3 \\ +000.0 & +000.0 \end{bmatrix} * \begin{bmatrix} \text{kN} \\ \text{kN} \\ \text{kN} \\ \text{kNm} \\ \text{kNm} \\ \text{kNm} \end{bmatrix}' \qquad \begin{bmatrix} N_{\theta} \\ Q_{y.\theta} \\ Q_{z.\theta} \\ M_{v.\theta} \\ M_{y.\theta} \\ M_{z.\theta} \end{bmatrix} = \begin{bmatrix} -876.7 & -857.1 \\ -000.0 & -000.0 \\ -016.9 & -016.9 \\ +000.0 & +000.0 \\ +020.9 & -040.0 \\ +000.0 & +000.0 \end{bmatrix} * \begin{bmatrix} \text{kN} \\ \text{kN} \\ \text{kN} \\ \text{kNm} \\ \text{kNm} \\ \text{kNm} \end{bmatrix}'$$

Critical loads for middle column on the bottom floor (no. 2): case 1 and fire respectively:

$$\begin{bmatrix} N_{case1} \\ Q_{y.case1} \\ Q_{z.case1} \\ M_{v.case1} \\ M_{y.case1} \\ M_{z.case1} \end{bmatrix} = \begin{bmatrix} -2840.0 & -2831.9 \\ -000.0 & -000.0 \\ -000.2 & -000.2 \\ +000.0 & +000.0 \\ -000.1 & +000.8 \\ +000.0 & +000.0 \end{bmatrix} * \begin{bmatrix} \text{kN} \\ \text{kN} \\ \text{kN} \\ \text{kNm} \\ \text{kNm} \\ \text{kNm} \end{bmatrix}' \qquad \begin{bmatrix} N_{\theta} \\ Q_{y.\theta} \\ Q_{z.\theta} \\ M_{v.\theta} \\ M_{y.\theta} \\ M_{z.\theta} \end{bmatrix} = \begin{bmatrix} -1689.9 & -1681.9 \\ -000.0 & -000.0 \\ +000.0 & +000.0 \\ +000.0 & +000.0 \\ +000.0 & +000.0 \\ +000.0 & +000.0 \end{bmatrix} * \begin{bmatrix} \text{kN} \\ \text{kN} \\ \text{kN} \\ \text{kNm} \\ \text{kNm} \\ \text{kNm} \end{bmatrix}'$$

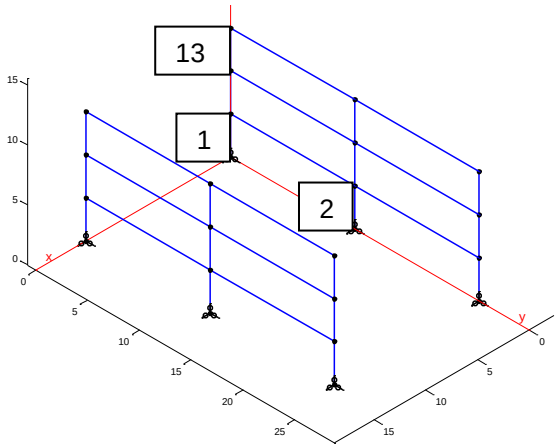

Figure C2. Columns for which the results are presented.

GEOMETRIC CHARACTERISTICS OF THE EDGE COLUMN CROSS-SECTION

Steel tube:

$A_a = 15600\text{mm}^2 = 0.0156\text{m}^2$,

$I_a = 3.957 * 10^8\text{mm}^4 = 3.957 * 10^{-4}\text{m}^4$,

$$W_{pa} = \frac{col^3}{4} - \frac{(col-2*t)^3}{4} \qquad \text{(C.30)}$$

$W_{pa} = \frac{(400\text{mm})^3}{4} - \frac{(400\text{mm}-2*10\text{mm})^3}{4} = 2.282 * 10^6\text{mm}^3 = 2.282 * 10^{-3}\text{m}^3.$

Concrete:

$A_c = 144400\text{mm}^2 = 0.1444\text{m}^2,$

$I_c = 1.715 * 10^9\text{mm}^4 = 1.715 * 10^{-3}\text{m}^4$,

$W_{pc} = \frac{(col-2*t)^3}{4} - W_{ps}$ (C.31)

$W_{pc} = \frac{(400\text{mm}-2*10\text{mm})^3}{4} - 0.0\text{mm}^3 = 13.72 * 10^6\text{mm}^3 = 1.372 * 10^{-2}\text{m}^3.$

The requirement of [TRY, 2004], Section 2.5.1 is that the longitudinal reinforcement level of the concrete core should be in the range of 1-6 %. The upper limit comes from Eurocode 4, Part 1-1, Section 6.7.3.1(3) [EN 1994-1-1, 2004]. If this is exceeded, the reinforcement included in the resistance calculation is limited to 6 %. The lower limit is the borderline between concrete that is considered as reinforced (>1 %) and plain (<1 %). The core of the example column is considered to be pure concrete.

AMBIENT DESIGN - BENDING RESISTANCE

The maximum design bending resistance of the cross-section is given by the equation:

$M_{max.Rd} = W_{pa} * f_{ad} + W_{ps} * f_{sd} + 0.5 * W_{pc} * f_{cd}$ (C.32)

where:

f_{ad} is the design yield strength of the steel tube,

f_{sd} is the design yield strength of the reinforcing bars,

f_{cd} is the design resistance of the concrete.

The maximum design bending resistance for the example column is:

$M_{max.Rd} = 2.282 * 10^{-3}\text{m}^3 * 322.7 * 10^6\text{Pa} + 0.5 * 1.372 * 10^{-2}\text{m}^3 * 29.6 * 10^6\text{Pa} =>$

$M_{max.Rd} = 939500\text{Nm} = 939.5\text{kNm}.$

In the calculation of M_{max} only half of the concrete core is taken into account. This means that the forces in the cross-section are not in equilibrium. This state can be achieved only when the missing force is applied from the outside – when the column is under compression the force equilibrium is maintained and the maximum design bending resistance of the column can be achieved. It's a different situation when the column is under pure bending. In that case, it is necessary to find the neutral axis of the cross-section as shown in Figure C3.

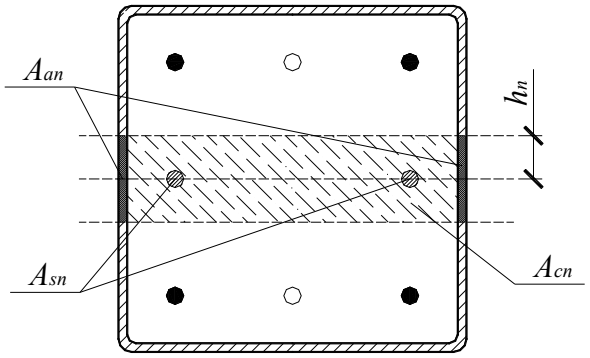

Figure C3. Symbols used in calculation of the neutral axis for column in pure bending

The design resistance of the concrete core is:

$$N_{pmRd} = A_c * f_{cd} = 0.1444\text{m}^2 * 29.6 * 10^6 * \text{Pa} = 4274240\text{N} = 4274\text{kN}. \quad \text{(C.33)}$$

The equilibrium equation of the forces in the cross-section is calculated from Eq. C.34.

$$0.5 * N_{pmRd} - A_{cn} * f_{cd} = A_{sn} * f_{sd} + A_{an} * f_{ad} \quad \text{(C.34)}$$

where:

A_{an} is the area of the steel tube cross-section that is within the distance h_n from the centre-line of the column cross-section,

A_{cn} is the area of the concrete core that is within the distance h_n from the centre-line of the column cross-section,

A_{sn} is the area of the reinforcement cross-section that is within the distance h_n from the centre-line of the column cross-section, in this example column $A_{sn} = 0$.

From the equilibrium equation the distance h_n is calculated with Eq. C.35.

$$h_n = \frac{N_{pmRd} - A_{sn}(2f_{sd} - f_{cd})}{2\left((col - 2t)f_{cd} + 4t * f_{ad}\right)} \quad \text{(C.35)}$$

$$h_n = \frac{4274240\text{N} - 0\text{m}^2 * \left(2 * 434.8 * 10^6\text{Pa} - 29.6 * 10^6\text{Pa}\right)}{2 * \left((0.400\text{m} - 2 * 0.010\text{m}) * 29.6 * 10^6\text{Pa} + 4 * 0.010\text{m} * 322.7 * 10^6\text{Pa}\right)} = 0.0885\text{m} = 88.5\text{mm}.$$

According to [TRY, 2004] the difference between the maximum plastic bending resistance and the plastic resistance in pure bending is equal to the plastic resistance of the material that is within h_n distance from the centre-line. Thus, the bending resistance of the cross-section is calculated from Eq. C.36.

$$M_{pl.Rd} = M_{max.Rd} - W_{pan} * f_{ad} - W_{psn} * f_{sd} - 0.5 * W_{pcn} * f_{cd} \quad \text{(C.36)}$$

where:

W_{pan} is the section modulus of the steel tube that is within h_n distance from the centre-line:

$$W_{pan} = 2 * \frac{\text{t} * (2 * \text{h}_\text{n})^2}{4} = 2 * \frac{0.010\text{m} * (2 * 0.0885\text{m})^2}{4} = 1.566 * 10^{-4}\text{m}, \quad \text{(C.37)}$$

W_{pcn} is the section modulus of the concrete core that is within the distance h_n from the centre-line of the column cross-section:

$$W_{pcn} = \frac{(col-2t)*(2*h_n)^2}{4} = \frac{(0.400\text{m}-2*0.010\text{m})*(2*0.0885\text{m})^2}{4} = 2.976 * 10^{-3}\text{m}, \quad \text{(C.38)}$$

W_{psn} is the section modulus of the reinforcement cross-section that is within the distance h_n from the centre-line of the column cross-section, in this example column $W_{psn} = 0$.

$$M_{pl.Rd} = 939500\text{Nm} - 1.566 * 10^{-4}\text{m} * 322.7 * 10^{6}\text{Pa} - 0.5 * 2.976 * 10^{-3}\text{m} * 29.6 * 10^{6}\text{Pa}$$

$$M_{pl.Rd} = 844920\text{Nm} = 844.9\text{kNm}$$

AMBIENT DESIGN - BUCKLING RESISTANCE

The axial resistance of the column is calculated in accordance with Eurocode 1994, Part 1-1, Section 6.7.3.5 [EN 1994-1-1, 2004], from equation C.39.

$$N_{Rd} = \chi * N_{pl.Rd} \quad \text{(C.39)}$$

where:

$N_{pl.Rd} = 9308\text{kN}$,

χ is the reduction factor for the relevant buckling mode, in terms of relative slenderness $\bar{\lambda} = 0.351$. Following Eurocode 1993, Part 1-1, Section 6.3.1.2 [EN 1993-1-1, 2005], if $\bar{\lambda} \leq 0.2$ or if $N_{Sd}/N_{cr} \leq 0.1$ then $\chi = 1.0$.

$$\chi = \frac{1}{\Phi+\sqrt{\Phi^2-\bar{\lambda}^2}} \text{ but } \chi \leq 1.0 \quad \text{(C.40)}$$

where:

$$\Phi = 0.5\left[1 + \alpha\left(\bar{\lambda} - 0.2\right) + \bar{\lambda}^2\right], \quad \text{(C.41)}$$

where:

$\alpha = 0.49$ is the imperfection factor read from table 6.1 of [EN 1993-1-1, 2005] for buckling curve C, since the steel tubes of CFHS columns are cold-formed.

$$\Phi = 0.5 * [1 + 0.49 * (0.351 - 0.200) + 0.351^2] = 0.599.$$

$$\chi = \frac{1}{0.599+\sqrt{0.599^2-0.351^2}} = 0.922.$$

Since $N_{cr} = 91000\text{kN}$ and the maximal axial force for the considered column is $N_{Sd} = 486.3\text{kN}$, the ratio $486\text{kN}/91000\text{kN} = 0.0053$ is smaller than 0.1. In this case $\chi = 1.0$.

The buckling resistance of the considered edge column is:

$$N_{Rd} = 1.00 * 9308\text{kN} = 9308\text{kN}.$$

The utilization in axial compression is:

$$\frac{N_{Sd}}{N_{Rd}} = \frac{486.6\text{kN}}{9308.0\text{kN}} = 0.052. \quad \text{(C.42)}$$

AMBIENT DESIGN - TRANSVERSE SHEAR

In most used in Finland type of framing system the shear resistance of the columns is never the crucial one. Because of that [TRY, 2004] does not provide any information about the shear resistance calculation for CFHS columns. In this study the shear resistance of the column cross-section is calculated as the sum of the resistance of the steel tube and the reinforced concrete core. The shear calculation for the steel tube follows Eurocode 3, Part 1-1 [1993-1-1, 2005] and the shear calculation for the core follows Eurocode 2, Part 1-1 [EN 1992-1-1, 2004]. No composite action has been taken into account. A limitation has been imposed on the utilization of shear resistance so that it stays below 0.9. The influence of shear on the axial and bending resistance is not taken into account. The resistance of stirrups used to hold the longitudinal bars in place is taken into account when calculating shear resistance. The 0.9 limitation on the utility factor for shear was used in order to maintain some margin of safety.

The shear area of the steel tube is calculated according to Eurocode 3, Part 1-1, Section 6.2.6(3) [EN 1993-1-1, 2005]. It is expressed with Eq. C.43.

$$A_v = A_a * col/(col + col) = A_a/2 = 15600\text{mm}^2/2 = 7800\text{mm}^2 = 0.0078\text{m}^2 \quad \text{(C.43)}$$

And the shear resistance of the tube follows Eq. C.44.

$$V_{plaRds} = \frac{A_v * f_{ad}}{\sqrt{3}} \quad \text{(C.44)}$$

$$V_{plaRds} = \frac{0.0078\text{m}^2 * 322.7 * 10^6\text{Pa}}{\sqrt{3}} = 1.453 * 10^6\text{N} = 1453\text{kN}$$

Since there is no reinforcement in the column, the design value of the shear resistance of pure concrete is calculated according to Section 6.2.2 of [EN 1992-1-1, 2004].

$$V_{Rdc} = \left[C_{Rdc}\left[\left(min(\rho_1 \quad 2.00\%)\right)^{\frac{1}{3}}\right] + k_1 * \sigma_{cp}\right] * b_w * \text{d} \quad \text{(C.45)}$$

Due to the fact that $\rho_1 = 0.0$, equation C.45 can be simplified to the form:

$$V_{Rdc} = \left[k_1 * \sigma_{cp}\right] * b_w * \text{d}. \quad \text{(C.46)}$$

With the minimum value of:

$$V_{Rdcmin} = \left[v_{min} + k_1 * \sigma_{cp}\right] * b_w * \text{d}. \quad \text{(C.47)}$$

The value of the shear resistance of the concrete will be calculated as V_{Rdcmin}.

where:

$$v_{min} = 0.035 * k^{\frac{3}{2}} * \left(\frac{f_{ck}}{MPa}\right)^{0.5} \quad \text{(C.48)}$$

where:

$$k = min\left[1 + \left(\frac{200\text{mm}}{d}\right)^{0.5} \quad 2\right] = min\left[1 + \left(\frac{200\text{mm}}{380\text{mm}}\right)^{0.5} \quad 2\right] = 1.726. \quad \text{(C.49)}$$

$$v_{min} = 0.035 * 1.726^{\frac{3}{2}} * \left(\frac{40\text{MPa}}{\text{MPa}}\right)^{0.5} = 0.502,$$

$k_1 = 0.15$ is taken as the recommended value, as in [EN 1992-1-1, 2004],

σ_{cp} is the compressive stress in concrete due to the axial loading. The part of the axial load that is coming onto the concrete is proportional to the concrete plastic resistance to the plastic resistance of the whole column cross-section. The value used in the calculation should be in MPa.

$$\sigma_{cp} = \frac{N_{pm.Rd}}{N_{pl.Rd}} \frac{N_{Sd}}{A_c} = \frac{4274*10^3\text{N}}{9308*10^3\text{N}} * \frac{486.3*10^3\text{N}}{0.1444\text{m}^2} = 1.56 * 10^6\text{Pa} = 1.55\text{MPa}\,, \quad \text{(C.50)}$$

b_w is the width of the concrete core in millimetres,

$$b_w = col - 2t = 400\text{mm} - 2 * 10\text{mm} = 380\text{mm}, \quad \text{(C.51)}$$

$d = b_w$ is the depth of the concrete core in millimetres. (C.52)

The concrete shear resistance is:

$$V_{Rdc} = V_{Rdcmin} = \left[v_{min} + k_1 * \sigma_{cp}\right] * b_w * \text{d}, \quad \text{(C.53)}$$

$$V_{Rdc} = [0.502 + 0.15 * 1.55] * 380 * 380 = 106000\text{N} = 106.0\text{kN}.$$

Finally, the shear resistance of the whole composite cross-section is calculated from Eq. C.54.

$$V_{Rd} = V_{Rdc} + V_{plaRds} \quad \text{(C.54)}$$

$$V_{Rd} = 106\text{kN} + 1453\text{kN} = 1559\text{kN}$$

Utilization in shear in the top column, including the 0.9 factor, gives:

$$\frac{V_{Sd}}{0.9*V_{Rd}} = \frac{258.5\text{kN}}{0.9*1559.0\text{kN}} = 0.184. \quad \text{(C.55)}$$

AMBIENT DESIGN - SECOND ORDER EFFECTS

The second order effects can be accounted for, in accordance with Eurocode 3, Part 1-1, Section 6.7.3.4 [EN 1993-1-1, 2005], by multiplying the larger of the end values by a factor k. The biggest of the absolute values of the moments in the example column is $M_{Sd} = 743.0\text{kNm}$.

The factor k is expressed with equation C.56.

$$k = \frac{\beta}{1-\frac{N_{Sd}}{N_{cr.eff}}} \quad \text{but greater than 1.0} \quad \text{(C.56)}$$

where:

$N_{cr.eff}$ is the effective critical force,

$$N_{cr.eff} = \frac{\pi^2}{l_e^{\,2}} EI_{eff.II} = \frac{\pi^2}{(3.6\text{ m})^2} 102.2 * 10^6\text{Nm}^2 = 77.75 * 10^6\text{N} = 77750\text{kN}, \quad \text{(C.57)}$$

β is an equivalent moment factor as specified in table 6.4 of [EN 1994-1-1, 2004],

$$\beta = max\left[\left[0.66 + 0.44\left(\frac{M_{Sd2}}{M_{Sd1}}\right)\right] \quad 0.44\right] \quad \text{(C.58)}$$

where:

$M_{Sd1} = 743.0\text{kNm}$ is the greater of the end bending moments in the column, the absolute value being taken for the calculations,

$M_{Sd2} = -187.6\text{kNm}$ is the smaller of the end bending moments in the column, positive if it is on the same side as M_{Sd1}, negative if otherwise.

$$\beta = max\left[\left[0.66 + 0.44\left(\frac{-187.6\text{kNm}}{743.0\text{kNm}}\right)\right] \quad 0.44\right] = 0.549.$$

$k = \frac{0.549}{1-\frac{486.6\text{kN}}{77750\text{kN}}} = 0.553$ so $k = 1.0.$

The bending moment, including second order effects, is calculated from Eq. C.59.

$$M_{Sd} = k * M_{Sd1} = 1.0 * 743.0\text{kNm} = 743.0\text{kNm} \quad \text{(C.59)}$$

AMBIENT DESIGN - BENDING RESISTANCE UNDER AXIAL LOAD

The calculation of the column bending resistance under axial load follows Eurocode 4, Part 1-1, Section 6.7.3.3 [1994-1-1, 2004]. The bending resistance is calculated from Eq. C.60.

$$M_{Rd} = \alpha_M * \mu * M_{plRd} \quad \text{(C.60)}$$

where:

$\alpha_M = 0.9$ is the coefficient for S 355 steel,

μ is a coefficient accounting for the influence of the axial force on the bending resistance. The coefficient is calculated using the graphical method presented in Figure C4.

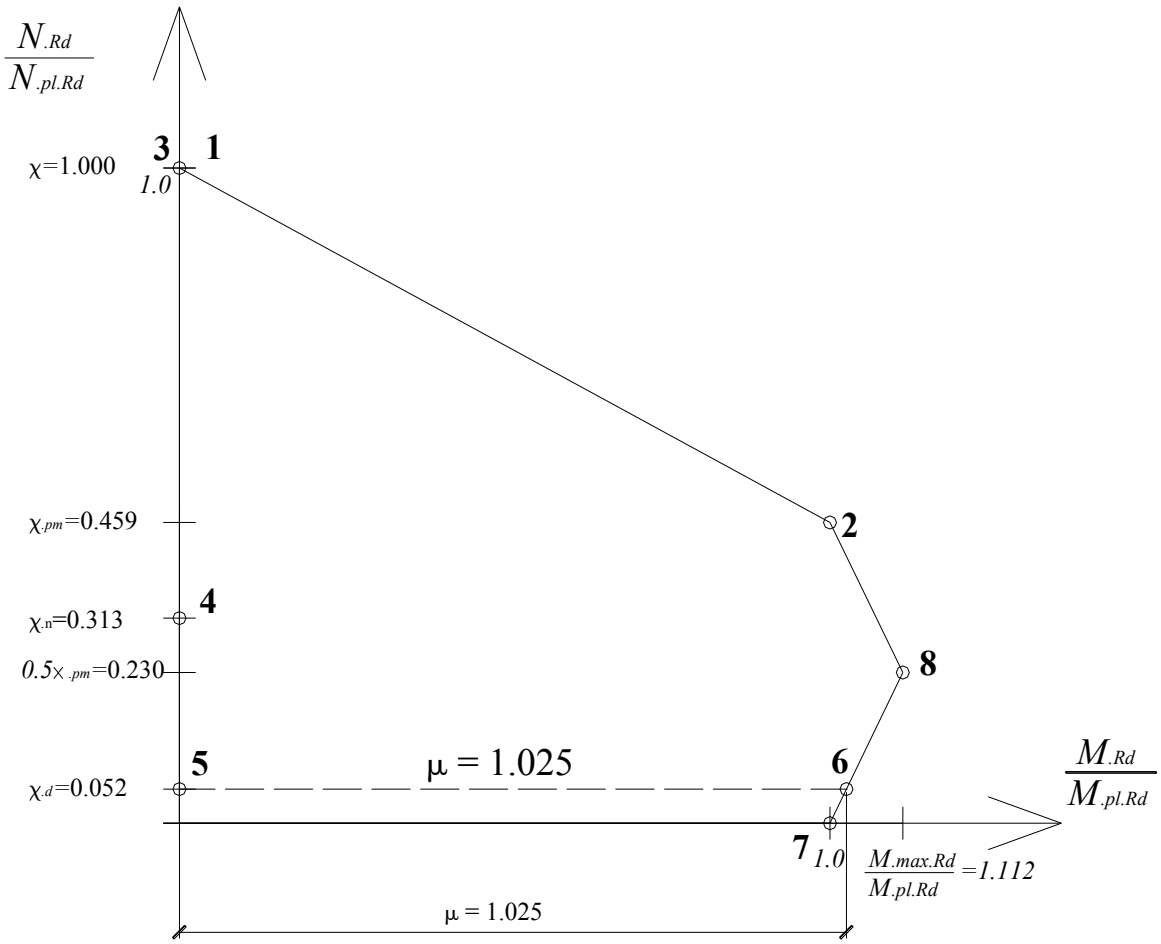

Figure C4. Graphical method for calculating μ.

Figure C4 presents the calculation of μ step by step. The calculation of the coordinates of all the points is presented below. The horizontal axis represents the moments in relation to the plastic moment resistance under pure bending. The vertical axis represents the axial force in relation to the full plastic axial resistance of the column cross-section. The coordinates of the points are presented in brackets, [moment axis, axial force axis]:

1. $[0.0 \quad 1.0]$,
2. $[1.0 \quad \chi_{pm}]$,
3. $[- \quad \chi]$ this point is on the line connecting points 1 and 2,
4. $[0.0 \quad \chi_n]$,
5. $[- \quad \chi_d]$ this point is on the line connecting points 3 and 4,
6. $[- \quad \chi_d]$ this point is on the line connecting points 1 and 2.

The distance between points 5 and 6 is the searched for value of μ. If the coefficient μ is greater than one it can only be used when the design cross-section bending moment M_{Ed} is a direct result of eccentric axial load N_{Ed}. Otherwise, the axial force causing the increase in

the bending resistance should be decreased by 20%. $\gamma_F = 0.80$ in accordance with [EN 1994-1-1, 2004], Section 6.7.1(7).

If the value of χ_d is lower than χ_{pm} (point 5 is located lower than point 2) points 7 and 8 have to be added to the graph:

7. $[1.0 \quad 0.0]$,
8. $\left[\frac{M_{maxRd}}{M_{plRd}} \quad 0.5\chi_{pm}\right]$.

In such a case, point 6 would be on the line connecting points 2 and 8 or 7 and 8, depending on whether the χ_d is higher or lower than $0.5\chi_{pm}$ - respectively.

The values of all the coordinates necessary to draw the plot for the example column are calculated below.

$$\chi_{pm} = \frac{N_{pm}}{N_{plRd}} = \frac{4274.0\text{kN}}{9308.0\text{kN}} = 0.459 \tag{C.61}$$

$$\chi = \frac{N_{Rd}}{N_{plRd}} = \frac{9308.0\text{kN}}{9308.0\text{kN}} = 1.000 \tag{C.62}$$

$$\chi_n = \chi\frac{\left(1-\frac{M_{Sd2}}{M_{Sd1}}\right)}{4} = 1.000\frac{\left(1-\frac{-187.6\text{kNm}}{743.0\text{kNm}}\right)}{4} = 0.313 \tag{C.63}$$

$$\chi_d = \frac{N_{Sd}}{N_{plRd}} = \frac{486.6\text{kN}}{9308.0\text{kN}} = 0.052 \tag{C.64}$$

$$\frac{M_{maxRd}}{M_{plRd}} = \frac{939.5\text{kNm}}{844.9\text{kNm}} = 1.112 \tag{C.65}$$

As shown in Figure C4, the graphical method of calculation gave $\mu = 1.025$. The value of χ_d is lower than $0.5\chi_{pm}$ meaning that an increase in the axial force causes an increase in μ and consequently in the bending resistance. Because of this, the value of μ should be reduced using equation C.66.

$$\mu_{reduced} = 0.8(\mu - 1) + 1 = 0.8 * (1.025 - 1.000) + 1.000 = 1.020 \tag{C.66}$$

As a result the bending resistance of the column under axial load is:

$$M_{Rd} = 0.9 * 1.020 * 844.9\text{kNm} = 775.6\text{kNm}. \tag{C.67}$$

And the utilisation of bending resistance is calculated from Eq. C.68.

$$\frac{M_{Sd}}{M_{Rd}} = \frac{743.0\text{kNm}}{775.6\text{kNm}} = 0.958 \tag{C.68}$$

The $utility$ vector for the column is written as such in the form presented in Eq. C.69.

$$utility = \left[\frac{N_{Sd}}{N_{Rd}}, \frac{M_{Sd}}{M_{Rd}}, \frac{V_{Sd}}{0.9*V_{Rd}}\right] \leq 1.0 \tag{C.69}$$

For the example edge column on the top floor, in load case 2, it is equal to:

$$utility_2 = [0.052,\ 0.958,\ 0.184] \leq 1.0.$$

The requirement is met.

FIRE DESIGN – BENDING RESISTANCE

For the calculation of column resistance the reduced yield strength of steel and the reduced compressive strength of concrete are required. Reduction factors are taken from Tables C1-C3.

- Yield strength of the steel tube

$$f_{a.\theta} = f_y * k_{y.\theta} \quad \text{(C.70)}$$

where:

$k_{y.\theta}$ is the reduction factor for the tube's yield strength at the temperature of 889 ˚C calculated from Table C1,

$$k_{y.\theta} = \frac{889^{\circ}\mathrm{C} - 800^{\circ}\mathrm{C}}{900^{\circ}\mathrm{C} - 800^{\circ}\mathrm{C}} * (0.06 - 0.11) + 0.11 = 0.0655.$$

$$f_{a.\theta} = 355.0\mathrm{MPa} * 0.0655 = 23.25\mathrm{MPa}.$$

- The compressive strength for the concrete filling

$$f_{c.\theta} = f_{ck} * k_{c.\theta} \quad \text{(C.71)}$$

where:

$k_{c.\theta}$ is the reduction factor for the concrete's compressive strength at the temperature of 335 ˚C calculated from Table C2,

$$k_{c.\theta} = \frac{335^{\circ}\mathrm{C} - 300^{\circ}\mathrm{C}}{400^{\circ}\mathrm{C} - 300^{\circ}\mathrm{C}} * (0.75 - 0.85) + 0.85 = 0.815.$$

$$f_{c.\theta} = 40.0\mathrm{MPa} * 0.815 = 32.60\mathrm{MPa}.$$

Most of the characteristics and resistances of the cross-section are the same as in the ambient design situation but calculated using different material properties. And thus:

the maximum bending resistance is:

$$M_{max.Rd.\theta} = W_{pa} * f_{a.\theta} + W_{ps} * f_{s.\theta} + 0.5 * W_{pc} * f_{c.\theta} \quad \text{(C.72)}$$

$$M_{max.Rd.\theta} = 2.282 * 10^{-3}\mathrm{m}^3 * 23.25 * 10^{6}\mathrm{Pa} + 0.5 * 1.372 * 10^{-2}\mathrm{m}^3 * 32.60 * 10^{6}\mathrm{Pa} =>$$

$$M_{max.Rd.\theta} = 276690\mathrm{Nm} = 276.7\mathrm{kNm}.$$

The design resistance to compression of the concrete core is:

$$N_{pmRd.\theta} = A_c * f_{c.\theta} = 0.1444\mathrm{m}^2 * 32.6 * 10^{6} * \mathrm{Pa} = 4707000\mathrm{N} = 4707\mathrm{kN}. \quad \text{(C.73)}$$

The neutral axis is located at:

$$h_n = \frac{N_{pmRd} - A_{sn}|2f_{s.\theta} - f_{c.\theta}|}{2\left((col - 2t)f_{c.\theta} + 4t * f_{a.\theta}\right)} \quad \text{(C.74)}$$

$$h_n = \frac{4707000\mathrm{N}}{2*\left((0.400\mathrm{m} - 2*0.010\mathrm{m})*32.6*10^{6}\mathrm{Pa} + 4*0.010\mathrm{m}*23.25*10^{6}\mathrm{Pa}\right)} = 0.1767\mathrm{m} = 176.7\mathrm{mm}.$$

The column resistance to pure bending is:

$$M_{pl.Rd.\theta} = M_{max.Rd.\theta} - W_{pan} * f_{a.\theta} - W_{psn} * f_{s.\theta} - 0.5 * W_{pcn} * f_{c.\theta} \quad \text{(C.75)}$$

where:

$$W_{pan} = 2 * \frac{t*(2*h_n)^2}{4} = 2 * \frac{0.010\text{m}*(2*0.1767\text{m})^2}{4} = 6.245 * 10^{-4}\text{m}, \quad \text{(C.76)}$$

$$W_{pcn} = \frac{(col-2t)*(2*h_n)^2}{4} = \frac{(0.400\text{m}-2*0.010\text{m})*(2*0.1767\text{m})^2}{4} = 11.865 * 10^{-3}\text{m}, \quad \text{(C.77)}$$

$$W_{psn} = 0. \quad \text{(C.78)}$$

$$M_{pl.Rd.\theta} = 276700\text{Nm} - 6.245 * 10^{-4}\text{m} * 23.25 * 10^{6}\text{Pa} - 0.5 * 1.187 * 10^{-2}\text{m} * 32.6 * 10^{6}\text{Pa}$$

$$M_{pl.Rd.\theta} = 68699\text{Nm} = 68.7\text{kNm}.$$

FIRE DESING – BUCKLING RESISTANCE

The buckling resistance of the column is:

$$N_{Rd.\theta} = \chi_\theta * N_{pl.Rd.\theta} \quad \text{(C.79)}$$

where:

$$N_{pl.R.\theta} = A_a * f_{a.\theta} + A_c * f_{c.\theta} + A_s * f_{s.\theta}, \quad \text{(C.80)}$$

$$N_{pl.R.\theta} = 0.0156\text{m}^2 * 23.25 * 10^{6}\text{Pa} + 0.1444\text{m}^2 * 32.6 * 10^{6}\text{Pa} = 5.070 * 10^{6}\text{N},$$

$$\chi_\theta = \frac{1}{\Phi_\theta + \sqrt{\Phi_\theta{}^2 - \overline{\lambda_\theta}^2}} \text{ but } \chi_\theta \leq 1.0 \quad \text{(C.81)}$$

where:

$$\overline{\lambda_\theta} = \sqrt{\frac{N_{pl.R.\theta}}{N_{cr.\theta}}} \quad \text{(C.82)}$$

where:

$$N_{pl.R.\theta} = N_{pl.Rd.\theta} = 5070\text{kN}, \quad \text{(C.83)}$$

$$N_{cr.\theta} = \frac{\pi^2}{l_{e.\theta}{}^2} EI_{eff.\theta} \quad \text{(C.84)}$$

where:

$l_{e.\theta}$ is the effective column length in fire situation equal to half of the column height on an intermediate floor and 0.7 of the column height on the top floor, which is in accordance with Eurocode 4, Part 1-2, Section 4.3.5.1(10) [EN-1994-1-2, 2006]. In this case:

$$l_{e.\theta} = 0.5 * 3.6\text{m} = 1.8\text{m}, \quad \text{(C.85)}$$

$$EI_{eff.\theta} = K_{e.\theta.a} * E_{a.\theta} I_a + K_{e.\theta.c} * E_{csec.\theta} I_c + K_{e.\theta.s} * E_{s.\theta} I_s \quad \text{(C.86)}$$

where:

$K_{e.\theta.a}$ is a correction factor for the steel tube equal to 0.9,

$K_{e.\theta.c}$ is a correction factor for the concrete core equal to 0.8,

$K_{e.\theta.s}$ is a correction factor for the reinforcement equal to 0.9

$$EI_{eff.\theta} = 0.9 * 14.7 * 10^9\text{Pa} * 3.957 * 10^{-4}\text{m}^4 + 0.8 * 4.08 * 10^9\text{Pa} * 1.738 * 10^{-3}\text{m}^4 = 1.0908 * 10^7\text{N} = 10.91\text{MN},$$

$$N_{cr.\theta} = \frac{\pi^2}{(1.8\text{m})^2} 1.0908 * 10^7\text{N} = 33.19 * 10^6\text{N} = 33.19\text{MN},$$

$$\overline{\lambda_\theta} = \sqrt{\frac{5070\text{kN}}{33190\text{kN}}} = 0.391,$$

$$\Phi_\theta = 0.5\left[1 + \alpha\left(\overline{\lambda_\theta} - 0.2\right) + \overline{\lambda_\theta}^2\right] \quad \text{(C.87)}$$

$$\Phi_\theta = 0.5 * [1 + 0.49 * (0.391 - 0.200) + 0.391^2] = 0.623,$$

$$\chi_\theta = \frac{1}{0.623 + \sqrt{0.623^2 - 0.391^2}} = 0.9025 \quad \text{but} \quad \frac{N_{Sd.\theta}}{N_{cr.\theta}} = \frac{874\text{kN}}{33190\text{kN}} = 0.026 < 0.1 \quad \text{so} \quad \chi_\theta = 1.0.$$

The buckling resistance of the column is:

$N_{Rd.\theta} = 1.0 * 5070\text{kN} = 5070\text{kN}.$

And the utilization in axial compression is calculated using equation C.88.

$$\frac{N_{Sd.\theta}}{N_{Rd.\theta}} = \frac{876.7\text{kN}}{5070.0\text{kN}} = 0.173 \quad \text{(C.88)}$$

FIRE DESIGN - SHEAR RESISTANCE

The shear resistance of the steel tube in fire situation is calculated from Eq. C.89.

$$V_{plaRds.\theta} = \frac{A_v * f_{a.\theta.20}}{\sqrt{3}} \quad \text{(C.89)}$$

$$V_{plaRds.\theta} = \frac{0.0078\text{m}^2 * 23.25 * 10^6\text{Pa}}{\sqrt{3}} = 1.047 * 10^5\text{N} = 104.7\text{kN}$$

The shear resistance of the steel tube alone is already two times greater than the maximal shear force, so no further calculation need be presented here. The shear force is 17.0 kN.

FIRE DESIGN - SECOND ORDER EFFECTS

The biggest absolute value of moment in the example column is $M_{Sd.\theta} = 40.0\text{kNm}.$

The factor k_θ is expressed with equation C.90.

$$k_\theta = \frac{\beta_\theta}{1 - \frac{N_{Sd.\theta}}{N_{cr.eff.\theta}}} \quad \text{but greater than 1.0} \quad \text{(C.90)}$$

where:

$$N_{cr.eff.\theta} = \frac{\pi^2}{l_e^2} EI_{eff.\theta.II} = \frac{\pi^2}{(1.8\text{ m})^2} 8.40 * 10^6\text{Nm}^2 = 25.56 * 10^6\text{N} = 25560\text{kN}, \quad \text{(C.91)}$$

$$\beta_\theta = max\left[\left[0.66 + 0.44\left(\frac{M_{Sd2.\theta}}{M_{Sd1.\theta}}\right)\right] \quad 0.44\right] \quad \text{(C.92)}$$

where:

$M_{Sd1.\theta} = 40.0\text{kNm},$

$$M_{Sd2.\theta} = -20.9\text{kNm}.$$

$$\beta_\theta = max\left[\left[0.66 + 0.44\left(\frac{-20.9\text{kNm}}{40.0\text{kNm}}\right)\right] \quad 0.44\right] = 0.440,$$

$$k_\theta = \frac{0.440}{1-\frac{876.7\text{kN}}{25589\text{kN}}} = 0.456 \quad \text{so} \quad k_\theta = 1.0.$$

The bending moment in the column is not increased.

$$M_{Sd.\theta} = k_\theta * M_{Sd1.\theta} = 1.0 * 40.0\text{kNm} = 40.0\text{kNm} \tag{C.93}$$

FIRE DESIGN - BENDING RESISTANCE UNDER AXIAL LOAD

The bending resistance follows equation C.94.

$$M_{Rd.\theta} = \alpha_M * \mu_\theta * M_{plRd.\theta} \tag{C.94}$$

where:

μ_θ is a coefficient calculated using the graphical method presented in Figure C5.

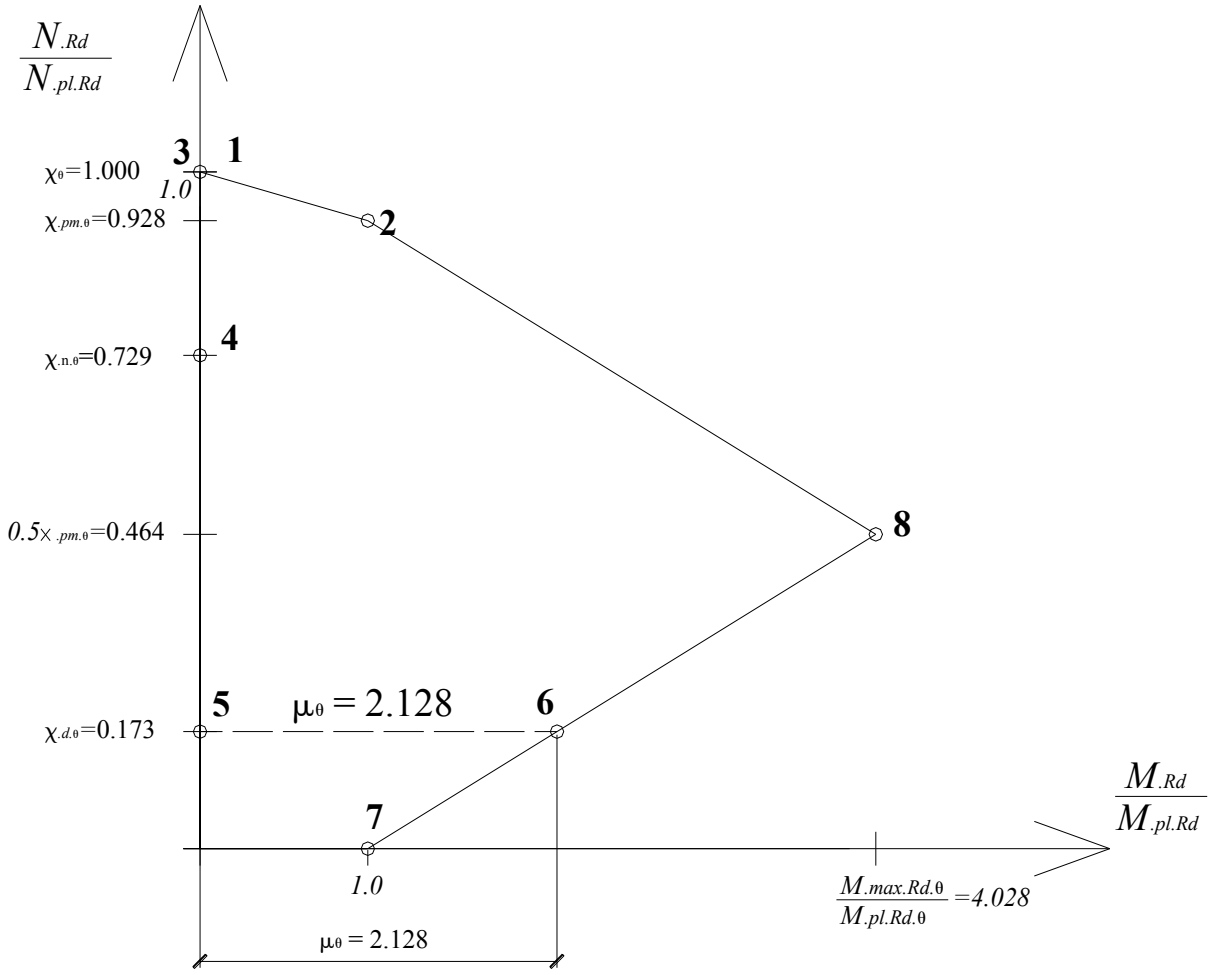

Figure C5. Graphical method of calculating μ_θ.

The values of all the coordinates necessary to draw the plot presented in Figure C5 for the example column are calculated below.

$$\chi_{pm.\theta} = \frac{N_{pm.\theta}}{N_{plRd.\theta}} = \frac{4707.4\text{kN}}{5070.2\text{kN}} = 0.928 \quad \text{(C.95)}$$

$$\chi_{\theta} = \frac{N_{Rd.\theta}}{N_{plRd.\theta}} = \frac{5070.2\text{kN}}{5070.2\text{kN}} = 1.000 \quad \text{(C.96)}$$

$$\chi_{n.\theta} = \chi_{\theta}\frac{\left(1-\frac{M_{Sd2.\theta}}{M_{Sd1.\theta}}\right)}{4} = 1.000\frac{\left(1-\frac{-40.0\text{kNm}}{20.9\text{kNm}}\right)}{4} = 0.729 \quad \text{(C.97)}$$

$$\chi_{d.\theta} = \frac{N_{Sd.\theta}}{N_{plRd.\theta}} = \frac{876.7\text{kN}}{5070.0\text{kN}} = 0.173 \quad \text{(C.98)}$$

$$\frac{M_{maxRd.\theta}}{M_{plRd.\theta}} = \frac{276.7\text{kNm}}{68.7\text{kNm}} = 4.028 \quad \text{(C.99)}$$

The factor reduced following clause 6.7.1(7) of Eurocode 4, Part 1-1 [EN 1994-1-1, 2004] is:

$$\mu_{\theta.reduced} = 0.8(\mu_{\theta} - 1) + 1 = 0.8 * (2.128 - 1.000) + 1.000 = 1.902. \quad \text{(C.100)}$$

As a result the bending resistance of the column under axial load is:

$$M_{Rd.\theta} = 0.9 * 1.902 * 68.7\text{kNm} = 117.6\text{kNm}.$$

And the utilisation of the bending resistance is:

$$\frac{M_{Sd.\theta}}{M_{Rd.\theta}} = \frac{40.0\text{kNm}}{117.6\text{kNm}} = 0.340. \quad \text{(C.101)}$$

For the example edge column on the bottom floor, in fire situation it is:

$$utility_{fire} = \left[\frac{N_{Sd.\theta}}{N_{Rd.\theta}}, \frac{M_{Sd.\theta}}{M_{Rd.\theta}}, \frac{V_{Sd.\theta}}{0.9*V_{Rd.\theta}}\right] = [0.173,\ 0.340,\ 0.083] \leq 1.0. \quad \text{(C.102)}$$

The requirement is met.

APPENDIX D

This appendix presents the detailed example of calculation of cost of the example structures that was considered in the main text. The unit prices for all the main elements are taken from a Finnish building construction cost data book [Haahtela, 2005].

BEAMS

The cost of a WQ-beam consists of two elements:

- The welded steel beam
- Fire protection

The cost of a non-fire-protected WQ-beam is the beam's weight times the price given in [Haahtela, 2005] measured in €/kg. The given price per kilogram is dependent on the beam's weight per meter. The unit price of the beam for price level "75" is presented in Table D1. The values of the unit price ($PRICE_{beam}$) for beam weights between 120 and 150 kg/m are interpolated in between 1.4 and 1.7 €/kg. The heavier the beam, the lower the unit price.

Table D1. WQ-beam unit prices for price level "75".

Beam weight	Unit price
[kg/m]	[€/kg]
< 120	1.70
120-150	1.40-1.70
> 150	1.40

The weight of the beam per meter, which is used to determine the unit price, is calculated from equation D.1.

$$WEIGHT_{beam\_per\_meter} = A_{section} * \rho_{steel} \quad \text{(D.1)}$$

where:

$\rho_{steel} = 7850 \frac{\text{kg}}{\text{m}^3}$ is the density of the steel.

The cost of the whole beam is calculated from Eq. D.2.

$$COST_{beam\_unprotected} = WEIGHT_{beam\_per\_meter} * L_0 * 1.02 * \left(PRICE_{beam} + ADD_{office}\right) \quad \text{(D.2)}$$

where:

L_0 is the length of the beam taking the joint stiffness into account. If the joint is completely rigid, the beam length is measured between the column axes. If it is completely hinged, the length corresponds to the simply supported beam that lies between columns. The length of a simply supported beam is calculated from Eq. D.3.

$$L_{hinged} = L - \frac{col_{edge}}{2} - \frac{col_{mid}}{2} - 2 * 20\text{mm} \quad \text{(D.3)}$$

col_{edge} and col_{mid} are the heights of the edge and middle column cross-sections respectively, and 20 mm is the space required by the column console.

$$L_{hinged} = 12000\text{mm} - \frac{400\text{mm}}{2} - \frac{250\text{mm}}{2} - 2 * 20\text{mm} = 11635\text{mm}$$

If the joint is semi-rigid the additional material needed to make the joint is taken into account in the beam length. The length of the beam is between the length of a simply supported one and a fully rigidly connected one. The intermediate values are taken as being proportional to the joint stiffness S, and the beam length is expressed by Eq. D.4.

$$L_0 = S * \left(L - L_{hinged}\right) + L_{hinged} \quad \text{(D.4)}$$

$$L_0 = 0.70 * (12.00\text{m} - 11.64\text{m}) + 11.64\text{m} = 11.89\text{m},$$

1.02 is a factor adding two percent to the weight of the beam irrespective of the joint stiffness. This accounts for the end plates at the ends of the beam,

$ADD_{office} = 0.3\,€/\text{kg}$ is an addition to the beam price for beams used in office buildings [Haahtela, 2005].

So for the example beam, the total weight is:

$$WEIGHT_{beam\_per\_meter} = 0.01603\text{m}^2 * 7850\frac{\text{kg}}{\text{m}^3} = 125.84\frac{\text{kg}}{\text{m}}.$$

$PRICE_{beam}$ read from Table D1 is:

$$PRICE_{beam} = \frac{125.84\frac{\text{kg}}{\text{m}} - 120.00\frac{\text{kg}}{\text{m}}}{150.00\frac{\text{kg}}{\text{m}} - 120.00\frac{\text{kg}}{\text{m}}} * (1.40\,€/\text{kg} - 1.70\,€/\text{kg}) + 1.70\,€/\text{kg} = 1.642\,€/\text{kg}.$$

The cost of the whole unprotected beam is equal to:

$$COST_{beam\_unprotected} = 125.84\frac{\text{kg}}{\text{m}} * 11.89\text{m} * 1.02 * (1.642\,€/\text{kg} + 0.300\,€/\text{kg}) = 2963.80€.$$

The price of the fire protection for the beam depends on the area of the surface that is exposed to fire and the unit price of the paint. The Finnish extension of the Eurocode regarding the design of WQ-beams covers fire protection by coating in intumescent paint in a range of between 0.8 and 1.4 mm thick. The paint layer thickness was not calculated. For the cost calculation, the fire paint thickness was taken to be equal to 1.0 mm. This simplification does not significantly influence the results of the analyses for the total cost of the structure.

The unit price of the 1.0 mm thick fire protection layer ($PRICE_{paint}$) is taken as being equal to 15.0 €/m^2, in accordance with [Takkula, 2007]. The paint cost includes 2 % extra.

$$COST_{paint} = SURFACE * PRICE_{paint} * 1.02 \quad \text{(D.5)}$$

where:

$SURFACE$ is the surface area of the bottom flange to be painted times the length of the beam

$$SURFACE = \left(b_{f2} + 2t_{f2}\right) * L_0 = (0.430\text{m} + 2 * 0.015\text{m}) * 11.89\text{m} = 5.469\text{m}^2. \quad \text{(D.6)}$$

$$COST_{paint} = 5.469\text{m}^2 * 15\,€/\text{m}^2 * 1.02 = 83.68€$$

So the total cost of a single beam is the sum of the cost of the steel and the cost of the paint, as in Eq. D.7.

$$COST_{beam} = COST_{beam\_unprotected} + COST_{paint} \quad \text{(D.7)}$$

$$COST_{beam} = 2963.80€ + 83.68€ = 3047.5€$$

The fire paint cost is about 2.7 % of the beam cost in this case.

COLUMNS

The cost of a CFHS column consists of three elements:

- Cold formed hollow section,
- Concrete filling,
- Reinforcement.

The prices of the cold formed hollow section (tube) are taken from [Haahtela, 2005] at the regional price level "75". The prices are expressed in € per kilogram of steel and depend on the weight of the steel tube per meter of length. The prices used in the calculation are presented in Table D2. The values of the unit price for tubes between 30 and 150 kg/m are interpolated, so that the heavier the beam is, the lower its unit price.

Table D2. Cold formed hollow section unit prices for price level "75" [Haahtela, 2005].

Tube weight [kg/m]	Unit price [€/kg]
< 30	2.30
30-60	1.90-2.30
60-90	1.60-1.90
90-120	1.60
120-150	1.40-1.60
> 150	1.40

The weight of the 400 mm steel tube used for the edge columns is calculated from equation D.8.

$$WEIGHT_{tube400\_per\_meter} = A_a * \rho_{steel} \quad \text{(D.8)}$$

$$WEIGHT_{tube400\_per\_meter} = 0.01560\text{m}^2 * 7850\,\frac{\text{kg}}{\text{m}^3} = 122.46\,\frac{\text{kg}}{\text{m}}$$

The price read from Table D2 is:

$$PRICE_{tube400} = \frac{122.46\frac{\text{kg}}{\text{m}} - 120.00\frac{\text{kg}}{\text{m}}}{150.00\frac{\text{kg}}{\text{m}} - 120.00\frac{\text{kg}}{\text{m}}} * (1.40\,€/\text{kg} - 1.60\,€/\text{kg}) + 1.60\,€/\text{kg} = 1.5836\,€/\text{kg}.$$

The final cost of the tube is increased by 5 % to account for the consoles on which the beams rest. For the edge column, the tube cost is presented in Eq. D.9.

$$COST_{tube400} = WEIGHT_{tube400_{per_{meter}}} * L_0 * 1.05 * PRICE_{tube400} \quad \text{(D.9)}$$

where:

$L_0 = 3.60\text{m}$ is the column height measured between floors.

$$COST_{tube400} = 122.46\frac{\text{kg}}{\text{m}} * 3.60\text{m} * 1.05 * 1.5836\,€/\text{kg} = 733.05€$$

According to [Haahtela, 2005] the price of the concrete filling for the column (including casting on site) is 121.0 €/m^2. Together with 5 % extra, for a 3.6 m high column the column cost is calculated from Eq. D.10.

$$COST_{filling400} = PRICE_{filling} * A_c * L_0 * 1.05 \quad \text{(D.10)}$$

$$COST_{filling400} = 121.0\,€/\text{m}^3 * 0.1444\text{m}^2 * 3.60\text{m} * 1.05 = 66.05€$$

So the total cost of the edge column is:

$$COST_{edge} = COST_{tube400} + COST_{filling400} = 733.05€ + 66.05€ = 799.10€. \quad \text{(D.11)}$$

For the middle column the calculations are as follows.

$$WEIGHT_{tube250\_per\_meter} = A_a * \rho_{steel} \quad \text{(D.12)}$$

where:

$$A_a = 4 * (col - 2t) * t = (0.250\text{m})^2 - (0.250\text{m} - 2 * 0.006\text{m})^2 = 0.005856\text{m}^2. \quad \text{(D.13)}$$

$$WEIGHT_{tube250\_per\_meter} = 0.00586\text{m}^2 * 7850\frac{\text{kg}}{\text{m}^3} = 45.97\frac{\text{kg}}{\text{m}}$$

$$PRICE_{tube250} = \frac{45.97\frac{\text{kg}}{\text{m}} - 30.00\frac{\text{kg}}{\text{m}}}{60.00\frac{\text{kg}}{\text{m}} - 30.00\frac{\text{kg}}{\text{m}}} * (1.90\,€/\text{kg} - 2.30\,€/\text{kg}) + 2.30\,€/\text{kg} = 2.0871\,€/\text{kg}$$

$$COST_{tube250} = 45.97\frac{\text{kg}}{\text{m}} * 3.60\text{m} * 1.05 * 2.0871\,€/\text{kg} = 362.69€$$

$$COST_{filling250} = PRICE_{filling} * A_c * L_0 * 1.05 \quad \text{(D.14)}$$

where:

$$A_c = (col - 2t)^2 - A_s \quad \text{(D.15)}$$

where:

$$A_s = n * \pi * \phi^2/4 \quad \text{(D.16)}$$

where:

$n = 5$ is the number of longitudinal reinforcing bars,

$\phi = 25\text{mm}$ is the diameter of the longitudinal reinforcing bars,

$$A_s = 4 * \pi * (0.025\text{m})^2/4 = 0.00196\text{m}^2,$$

$$A_c = (col - 2t)^2 - A_s = (0.250\text{m} - 2 * 0.006\text{m})^2 - 0.00196\text{m}^2 = 0.05468\text{m}^2,$$

$$COST_{filling250} = 121.0\,€/\text{m}^3 * 0.05468\text{m}^2 * 3.60\text{m} * 1.05 = 25.01€.$$

The price of the A 500 HW reinforcing steel used in the middle column is 1.25 €/kg. The weight of the longitudinal reinforcement per meter of column length is:

$$WEIGHT_{longitudinal} = A_s * \rho_{steel} = 0.00196\text{m}^2 * 7850\frac{\text{kg}}{\text{m}^3} = 15.39\frac{\text{kg}}{\text{m}}. \quad \text{(D.17)}$$

The weight of the stirrups joining the longitudinal bars is calculated from Eq. D.18.

$$WEIGHT_{stirrups} = LENGTH_{single\_stirrup} * \left(\pi * {\phi_s}^2/4\right) * \rho_{steel}/s \quad \text{(D.18)}$$

where:

$\phi_s = 8\text{mm}$ is the diameter of the stirrup,

$s = 0.375\text{m}$ is the spacing of the stirrups,

$$LENGTH_{single\_stirrup} = 4 * (col - 2t - 2u_s) * 1.2 \quad \text{(D.19)}$$

where:

1.2 is a factor accounting for 20 % extra length for the joint,

$$LENGTH_{single\_stirrup} = 4 * (0.250\text{m} - 2 * 0.006\text{m} - 2 * 0.035\text{m}) * 1.2 = 0.806\text{m}.$$

$$WEIGHT_{stirrups} = 0.806\text{m} * (\pi * 0.008\text{m}^2/4) * 7850\frac{\text{kg}}{\text{m}^3}/0.375\text{m} = 0.848\frac{\text{kg}}{\text{m}}$$

The cost of the reinforcement is calculated with 5 % extra to account for the joints in accordance with Eq. D.20.

$$COST_{reinf} = \left(WEIGHT_{longitudinal} + WEIGHT_{stirrups}\right) * PRICE_{reinf} * L_0 * 1.05 \quad \text{(D.20)}$$

$$COST_{reinf} = \left(15.39\frac{\text{kg}}{\text{m}} + 0.85\frac{\text{kg}}{\text{m}}\right) * 1.25\,€/\text{kg} * 3.60\text{m} * 1.05 = 76.73€$$

And the total cost of the middle column is the sum of the costs of all three elements as in Eq. D.21.

$$COST_{middle} = COST_{tube250} + COST_{filling250} + COST_{reinf} \quad \text{(D.21)}$$

$$COST_{middle} = 362.69€ + 25.01€ + 76.73€ = 464.43€$$

The total cost of the frame, i.e. 12 beams, 12 edge columns and 6 middle columns is:

$$COST_{frame} = \sum_{beams} COST_{beam} + \sum_{edge\_columns} COST_{edge} + \sum_{middle\_columns} COST_{middle} \quad \text{(D.22)}$$

$$COST_{frame} = 12 * 3047.50€ + 12 * 799.10€ + 6 * 464.43€ = 48940€.$$

FLOORS

To get the total cost of the structure, which is the objective function for the optimization algorithm, the cost of the HC slabs together with covering concrete has to be included. The cost of all the HC slabs used in the building depends on their true length, the total width of the slabs used and the unit price. The unit price of HC slabs taken from [Haahtela, 2005] for price level “75” and used in this study are presented in Table D3. The prices shown are for simple floors with easy shapes, (no openings, etc.).

Table D3. Slab data used for cost calculation

HC slab symbol	Unit price [€/m^2]	Concrete cover [mm]
P20	46.0	60
P27	54.0	60
P32	55.0	60
P40	63.0	100
P50	90.0	100

The total cost of the HC slab floors consists of three elements:

- pre-stressed hollow core slab,
- concrete cover on top of the HC slab, including reinforcement,
- concrete filling of the gaps between the slab and the beam web and the cover on top of the beam.

Some data used in the calculation of costs have already been calculated in the subchapter on load calculation. These are:

$cover = 60\text{mm}$ is the thickness of the concrete cover on the slab,

$A_{con} = 0.0446\text{m}^2$ is the area of the cross-section of the concrete around the beam,

$slab_{length} = 13.60\text{m}$ is the true length of the HC slab.

The reference area of a single floor of the building is:

$$A_{floor} = 2 * X * Y = 2 * 12.0\text{m} * 14.0\text{m} = 336.0\text{m}^2. \quad \text{(D.23)}$$

The cost of the HC slab for a single floor, with 5 % extra, is calculated using Eq. D.24.

$$COST_{slab} = 2 * slab_{length} * Y * PRICE_{slab} * 1.05 \quad \text{(D.24)}$$

$$COST_{slab} = 2 * 12.0\text{m} * 13.60\text{m} * \frac{55.0€}{\text{m}^2} * 1.05 = 18850€$$

The cost of the concrete cover on top of the slab is shown by Eq. D.25.

$$COST_{cover} = 2 * Y * slab_{length} * cover * PRICE_{cover} * 1.05 + COST_{reinf\_cover} \quad \text{(D.25)}$$

where:

$PRICE_{cover} = 121€/\text{m}^3$ is the unit price of the covering concrete taken from [Haahtela, 2005],

$COST_{reinf\_cover}$ is the cost of the reinforcement of the covering concrete.

An assumption has been made that the reinforcement of the covering concrete is maximal for this kind of slab [Parma, 2009]. This means that there are 9 12-mm bars per meter. Only the reinforcement spanning the HC slabs is taken into account in the cost calculation. In the example case, reinforcement for the covering concrete of a single floor, with 5 % extra, is calculated from equation D.26,

$$COST_{reinf\_cover} = 9 * (\pi * \phi^2/4) * \rho_{steel} * PRICE_{reinf} * A_{floor} * 1.05 \quad \text{(D.26)}$$

$$COST_{reinf\_cover} = 9 * (\pi * (0.012\text{m})^2/4) * 7850\frac{\text{kg}}{\text{m}^3} * 1.25\,€/\text{kg} * 336.0\text{m}^2 * 1.05 =>$$

$$COST_{reinf\_cover} = 3521.90€.$$

$$COST_{cover} = 2 * 12.0\text{m} * 13.60\text{m} * 0.06\text{m} * \frac{121€}{\text{m}^3} * 1.05 + 3521.90€ = 6010.00€$$

And the cost of the concrete filling around 4 beams on a single floor, with 5 % extra, is shown by Eq. D.27.

$$COST_{beam\_cover} = 4 * Y * A_{con} * PRICE_{cover} * 1.05 \quad \text{(D.27)}$$

$$COST_{beam\_cover} = 4 * 12.0\text{m} * 0.0446\text{m}^2 * \frac{121€}{\text{m}^3} * 1.05 = 271.99€$$

The total cost of the HC slab floor is the sum of all the elements, as shown in Eq. D.28.

$$COST_{floor} = COST_{slab} + COST_{cover} + COST_{beam\_cover} \quad \text{(D.28)}$$

$$COST_{floor} = 18850€ + 6010€ + 272€ = 25132€$$

The total cost of the structure: the frame + the floors, is calculated from Eq. D.29.

$$COST_{structure} = COST_{frame} + 3 * COST_{floor} \quad \text{(D.29)}$$

$$COST_{structure} = 48940€ + 3 * 25132€ = 124336€$$

And the cost for one square meter of the building is:

$$COST_{structure/m^2} = \frac{COST_{structure}}{3 * A_{floor}} = \frac{124336€}{3 * 336\text{m}^2} = 123.35€/\text{m}^2. \quad \text{(D.30)}$$

APPENDIX E

This appendix presents the calculation of the first natural frequency of a slim floor. The fundamental natural frequency is calculated according to [TRY, 2005] and is expressed with Eq. E.1:

$$f_0 = \frac{1}{\sqrt{\frac{1}{(f_{0,b})^2} + \frac{1}{(f_{0,s})^2}}} \tag{E.1}$$

where:

$f_{0,b}$ is the fundamental frequency of the WQ-beam,

$f_{0,s}$ is the fundamental frequency of the HC slab.

First, the natural frequency of the WQ-beam is calculated. Let us consider a one span beam with rotational springs at both ends, presented in Figure E1.

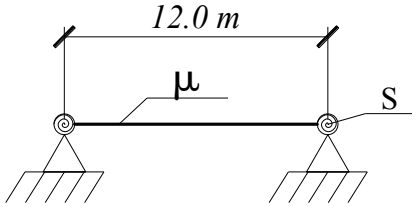

Figure E1. Beam scheme for the dynamic analysis

The joint fixity ratio S is in the range 0.00–1.00 with 0.00 meaning a hinged joint and 1.00 a fully rigid one. Taking the first extreme, we have a simply supported beam with a natural frequency that can be calculated using Eq. E.2:

$$f_{hinged} = \frac{k^2 * \pi}{2L^2}\sqrt{\frac{EI}{\mu}} \tag{E.2}$$

where:

k is number of the natural frequency, for the fundamental frequency $k = 1$,

L is the beam length,

EI is the beam bending stiffness,

μ is the uniformly distributed mass of the beam.

The natural frequency for a beam that is fully fixed at both ends is given by Eq. E.3:

$$f_{rigid} = \left(\frac{2k+1}{2}\right)^2 \frac{\pi}{2L^2}\sqrt{\frac{EI}{\mu}}. \tag{E.3}$$

So there is a fixed ratio between the first natural frequencies of a beam with hinges at the ends and one with rigid joints (eq. E.4).

$$\frac{f_{rigid}}{f_{hinged}} = \frac{\left(\frac{2k+1}{2}\right)^2 \frac{\pi}{2L^2}\sqrt{\frac{EI}{\mu}}}{\frac{k^2*\pi}{2L^2}\sqrt{\frac{EI}{\mu}}} = \frac{\left(\frac{2k+1}{2}\right)^2}{k^2} = \frac{\left(\frac{2*1+1}{2}\right)^2}{1^2} = 2.25 \tag{E.4}$$

The first natural frequencies of all the beams with intermediate joint stiffness are in between the natural frequency of a hinged beam and a fixed beam. Therefore, this ratio can be used to calculate the frequencies of all the beams with semi-rigid joints. The natural frequency ratio as a function of joint stiffness was calculated using *frame3D.* The results are presented in Figure E2.

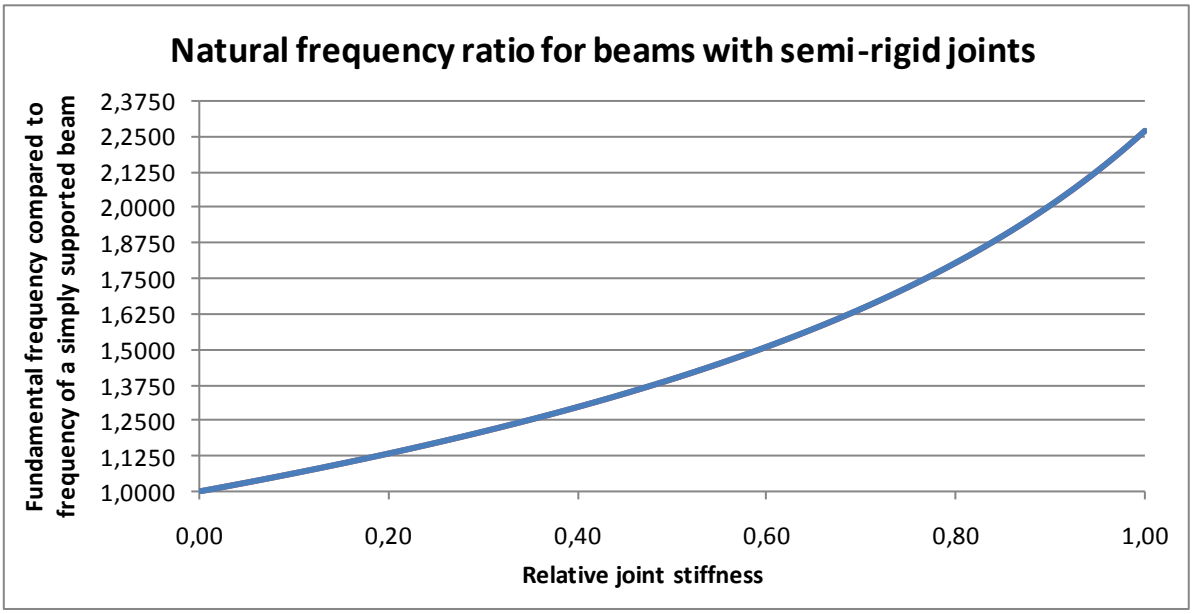

Figure E2. Plot of fundamental frequency of a beam with semi-rigid joints in relation to fundamental frequency of a simply supported beam.

The data necessary for the frequency calculation are:

- the upper dead load on the beam in normal situation, load case 1,

  $G_k = 38.0\,\mathrm{kN/m}$,

- the weight of the beam,

  $WEIGHT_{beam\_per\_meter} = 125.84\frac{\mathrm{kg}}{\mathrm{m}}$,

- the axial stiffness of the beam,

  $EA_{beam} = 3366\mathrm{MN}$,

- the axial compressive force in the beam in normal situation, load case 1 (the value used here is taken for the beam on the top floor),

  $N = 331.9\mathrm{kN}$,

- the bending stiffness of the beam,

  $EI_{beam.y} = 73.31\mathrm{MNm}^2$.

The Euler critical force for a beam with hinges at the ends is:

$$P_{cr} = \frac{\pi^2 * EI_{beam.y}}{L^2} = \frac{\pi^2 * 733100000\mathrm{Nm}^2}{(12\mathrm{m})^2} = 50246000\mathrm{N} = 50246\mathrm{kN}. \quad \text{(E.5)}$$

Compared to the Euler critical force, the axial force in the beam is very small and will not be taken into account in the calculation of the natural frequency:

$$\frac{N}{P_{cr}} = \frac{331.9\,\text{kN}}{50246\text{kN}} = 0.0066 = 0.66\%. \quad \text{(E.6)}$$

The mass distributed along the beam when calculating vibration is calculated from equation E.7:

$$\mu_{beam} = \left(G_k + WEIGHT_{beam_{per_{meter}}} * g + Q_{30kg}/g\right) \quad \text{(E.7)}$$

where:

G_k is the characteristic value of the dead load applied to the beam,

$WEIGHT_{beam_{per_{meter}}}$ is the characteristic beam weight,

g is the gravitational acceleration,

Q_{30kg} is the live load applied to the beam,

$$Q_{30kg} = 30\frac{\text{kg}}{\text{m}^2} * \left(\frac{slab_{length}}{2} + b_{nom} + 50\text{mm} + c\right) * g,$$

where the expression in the brackets is the width from which the beam collects the live load (see subchapter 2.3.2) and 30 kg/m^2 is the live load value taken for the vibration calculation in accordance with [TRY, 2005].

$$Q_{30kg} = 30\frac{\text{kg}}{\text{m}^2} * \left(\frac{13.60\text{m}}{2} + 0.30\text{m} + 0.05\text{m} + 0.02\text{m}\right) * 9.81\frac{\text{m}}{\text{s}^2} = 2110\frac{\text{N}}{\text{m}} = 2.1\frac{\text{kN}}{\text{m}}.$$

$$\mu_{beam} = \left(38000\,\text{N/m} + 125.84\frac{\text{kg}}{\text{m}} * 9.81\frac{\text{m}}{\text{s}^2} + 2110\frac{\text{N}}{\text{m}}\right)/\text{g} = 4215\frac{\text{kg}}{\text{m}}.$$

The first natural frequency of a simply supported beam is calculated from Eq. E.8.

$$f_{1.hinged} = \frac{k^2 * \pi}{2(L)^2}\sqrt{\frac{EI}{\mu}} = \frac{1^2 * \pi}{2(12\text{m})^2}\sqrt{\frac{73310000\text{Nm}^2}{4215\frac{\text{kg}}{\text{m}}}} \quad \text{(E.8)}$$

$$f_{1.hinged} = 1.896\ \text{Hz}$$

For a clamped beam it can simply be calculated from Eq. E.9.

$$f_{1.rigid} = 2.25 * f_{1.hinged} = 2.25 * 1.896\ \text{Hz} = 4.266\text{Hz} \quad \text{(E.9)}$$

For a beam with semi-rigid joints with relative rotational stiffness $S = 0.70$, according to Figure E2 the calculation is:

$$f_{1.S-R} = 1.6415 * f_{1.hinged} = 1.6415 * 1.896\ \text{Hz} = 3.112\text{Hz}. \quad \text{(E.10)}$$

Of course, in reality the beam is not supported on a fixed base but it is attached to elastic columns. However, in the example frame the stiffness of the columns is high in relation to the beam bending stiffness.

Let us use the Cross method to compare the beam and the column stiffness. The static layout of the substructure in question is presented in Figure E3. The beam-column joint is assumed to be rigid and the columns are assumed to be simply supported by the floors above and below the floor under consideration.

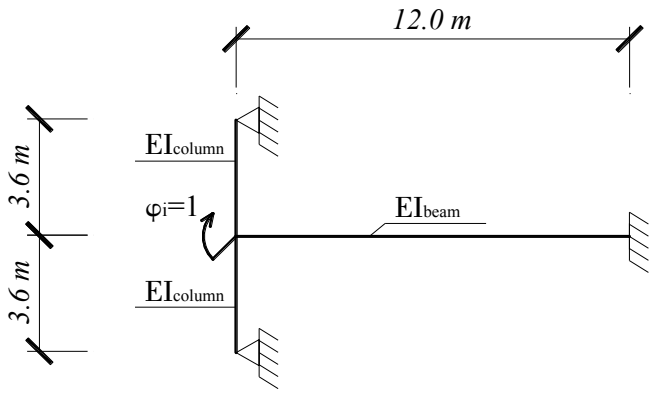

Figure E3. Static layout for the stiffness comparison

If a unit rotation (φ_i) is applied to the beam-column joint it causes a bending moment that gets distributed between the three elements. The proportions of the distribution come from the stiffnesses of the three elements. The moments developed in the columns, at the ends where rotation is applied, are calculated using the transformation equation for elements fixed at one end and hinged at the other: $3EI/L$. The moment in the beam is calculated from the equation for a doubly fixed element: $4EI/L$. Using these two, we can compare the stiffness of the elements in question. The stiffness of two columns compared to the stiffness of one beam is expressed with equation E.11.

$$\frac{2*\left(\frac{3EI_{eff.II}}{L_{column}}\right)}{\frac{4EI_{beam.y}}{L_{beam}}} = \frac{2*\left(\frac{3*102200\ \mathrm{kNm^2}}{3.6\mathrm{m}}\right)}{\frac{4*73310\mathrm{kNm^2}}{12.0\mathrm{m}}} = 6.97 \qquad \text{(E.11)}$$

The column stiffness is almost 7 times greater than the beam stiffness if the beam has rigid joints at the ends. If the joints are semi-rigid this ratio will be even greater. Because of this, and the fact that the mass distributed on the beams is much larger than the mass distributed on columns, the stiffness and mass of the columns were not taken into account in the calculation of the beam's natural frequency.

The fundamental frequency of the beam $f_{0,b}$ is presented in equation E.12:

$$f_{0,b} = f_{1.S-R} = 3.112\mathrm{Hz}. \qquad \text{(E.12)}$$

As a simplification, the natural frequency of the HC slab with covering concrete is calculated on the assumption that the slab is simply supported on the beams. Moreover, the slab and covering concrete are assumed to act as one. The geometrical characteristics of the HC slab cross-section can be obtained from [TRY, 2007]. The necessary data are listed below.

- Cross-section area of the hollow core slab. The slab is 1.2 m wide.

  $A_{hc} = 187.4 * 10^3\ \mathrm{mm^2}$

- Second moment of area of the hollow core slab. The slab is 1.2 m wide.

  $I_{hc} = 2.498 * 10^{-3}\ \mathrm{m^4}$

- Distance between the horizontal neutral axis and the bottom of HC slab.

  $z_{0.hc} = 160\ \mathrm{mm}$

The concrete covering is class C25/30 while the HC slab is made of C50/60. Therefore, the calculation of the neutral axis of the floor should take into account using different Young's modules for both types of concrete. The Young's modules were taken from Eurocode 2, Part 1-1, Section 3.1.3 [EN 1992-1-1, 2004] and they are $E_{C25/30} = 31\ \mathrm{GPa}$ and $E_{C50/60} = 37\ \mathrm{GPa}$ for the cover and the slab respectively. The stiffness of the reinforcement had been omitted in the vibration analysis.

The neutral axis is calculated from Eq. E.13:

$$z_{0.floor} = \frac{A_{hc} * E_{C50/60} * z_{0.hc} + cover * 1.2\ \mathrm{m} * E_{C25/30} * (h_{nom} + cover/2)}{A_{hc} * E_{C50/60} + cover * 1.2\ \mathrm{m} * E_{C25/30}} \quad \text{(E.13)}$$

where:

$cover$ is the thickness of the covering concrete layer,

$1.2\ \mathrm{m}$ is the width of the considered part of floor.

$$z_{0.floor} = \frac{0.1874 * \mathrm{m}^2 * 37 * 10^9\mathrm{Pa} * 0.160\mathrm{m} + 0.060\mathrm{m} * 1.2\ \mathrm{m} * 31 * 10^9\mathrm{Pa} * (0.320\mathrm{m} + 0.060/2)}{0.1874 * \mathrm{m}^2 * 37 * 10^9\mathrm{Pa} + 0.060\mathrm{m} * 1.2\ \mathrm{m} * 31 * 10^9\mathrm{Pa}} = 0.2069\mathrm{m}$$

The bending stiffness of the floor is calculated using Steiner's equation in a form shown in Eq. E.14:

$$EI_{floor} = \left(I_{hc} + A_{hc} * \left(z_{0.floor} - z_{0.hc}\right)^2\right) * E_{C50/60} + \left(\frac{cover^3 * 1m}{12} + cover * 1.2m * \left(z_{0.floor} - (h_{nom} + cover/2)\right)^2\right) * E_{C25/30} \quad \text{(E.14)}$$

$$EI_{floor} = (2.498 * 10^{-3}\ \mathrm{m}^4 + 0.1874 * \mathrm{m}^2 * (0.2069\mathrm{m} - 0.160\mathrm{m})^2) * 37\ 10^9\mathrm{Pa} + \left(\frac{(0.060\mathrm{m})^3 * 1.2\mathrm{m}}{12} + 0.060\mathrm{m} * 1.2\mathrm{m} * \left(0.2069\mathrm{m} - (0.320\mathrm{m} + 0.060\mathrm{m}/2)\right)^2\right) * 31\ 10^9\mathrm{Pa} =>$$

$$EI_{floor} = 107.68 * 10^6\mathrm{Nm}^2 + 46.38 * 10^6\mathrm{Nm}^2 = 154.06 * 10^6\mathrm{Nm}^2 = 154.06\mathrm{MNm}^2.$$

The distributed mass of the HC slab floor takes into account the self weight of the slab, the covering concrete and the 30 kg/m^2 live load applied to the slab (eq. E.15):

$$\mu_{slab} = g_{slab} * 1.2\mathrm{m} + cover * \gamma_{con}/g * 1.2\mathrm{m} + 30\frac{\mathrm{kg}}{\mathrm{m}^2} * 1.2\mathrm{m} \quad \text{(E.15)}$$

where:

$1.2\mathrm{m}$ is the width of the HC slab,

γ_{con} is the weight of the covering concrete layer,

g is the gravitational acceleration.

$$\mu_{slab} = 400\frac{\mathrm{kg}}{\mathrm{m}^2} * 1.2\ \mathrm{m} + 0.060\mathrm{m} * 1.2\ \mathrm{m} * 25000\frac{\mathrm{N}}{\mathrm{m}^3}/9.81\frac{\mathrm{m}}{\mathrm{s}^2} + 30\frac{\mathrm{kg}}{\mathrm{m}^2} * 1.2\ \mathrm{m} = 699\ \frac{\mathrm{kg}}{\mathrm{m}}$$

The fundamental frequency of the slab vibration is calculated from equation E.16:

$$f_{0,s} = \frac{\pi}{2{L_{slab}}^2}\sqrt{\frac{EI_{floor}}{\mu_{slab}}} \quad \text{(E.16)}$$

where:

$L_{slab} = 14\text{m}$ is the slab span measured between the beam axes.

$$f_{0,s} = \frac{\pi}{2*(14m)^2}\sqrt{\frac{154.06*10^6\text{Nm}^2}{699\,\frac{\text{kg}}{\text{m}}}} = 3.763\text{Hz}$$

The fundamental frequency of the whole floor as in Eq. E.17 is equal to:

$$f_0 = \frac{1}{\sqrt{\left(\frac{1}{3.112\text{Hz}}\right)^2+\left(\frac{1}{3.763\text{Hz}}\right)^2}} = 2.398\text{Hz}. \quad \text{(E.17)}$$

Tampereen teknillinen yliopisto
PL 527
33101 Tampere

Tampere University of Technology
P.O.B. 527
FI-33101 Tampere, Finland

ISBN 978-952-15-2808-8
ISSN 1459-2045